

Novel Technology for Hydrogen Separation from Natural Gas using Pressure Swing Adsorption

A thesis submitted in total fulfillment for the
TU Delft degree of Master Mechanical Engineering

conducted at the
Department of Chemical Engineering
THE UNIVERSITY OF MELBOURNE

to be defended on 24 November 2020.

Author:

[I.A.E. Burgers](#)

Supervisors:

| | |
|-----------------------|--------------------------------|
| Prof. E.L.V. Goetheer | Delft University of Technology |
| Prof. P.A. Webley | University of Melbourne |
| Dr. P. Xiao | University of Melbourne |
| Dr. G. Li | University of Melbourne |

Preface

This thesis is submitted as partial fulfillment of the master degree Mechanical Engineering of the TU Delft, the Netherlands. The research is conducted at the University of Melbourne, Australia, within the department of Chemical Engineering. It will be defended on 24 November 2020. The committee consists out of the following members: Prof. Earl Goetheer, Prof. Paul Webley, Dr. Penny Xiao, Prof. Wiebren de Jong, and Dr. Mahinder Ramdin.

The thesis is part of the research project at the University of Melbourne with the Future Fuels CRC, which aims at the decarbonisation of Australia's energy network. Woodside Energy, Australia's largest natural gas producer, is involved as the industrial partner and funds the project at Melbourne University through the Future Fuels CRC.

Acknowledgements

Writing my master thesis has been a great journey. I have learned so much in the past months and I am grateful that I have been able to contribute my part to this project. It really encouraged me to continue working on contributing to a more sustainable world.

This year turned out very differently for all of us, but I am very happy that I was able to finish my thesis here in Australia and I would like to express my thanks and appreciation to everyone who supported me. First and foremost, I would like to thank Prof. Paul Webley for giving me the opportunity to come to the University of Melbourne to conduct this research for my master thesis. Thank you for your support through out the project and your wise and helpful insights during our many zoom meetings. Special thanks to Penny Xiao for always being supportive and helpful during my thesis and for being available to answer any of my questions or doubts.

Furthermore, I would like to thank Kevin Gang Li for supervising my project after Paul moved to Monash University. My thanks go to Leila Dehdari, for supporting me during the project and showing me around in the lab the few times that it was possible.

I would like to thank Prof. Earl Goetheer for all the early morning meetings. Thanks for always showing enthusiasm about my work and for supporting me all the way through. In addition, thanks to Prof. Wiebren de Jong and Dr. Mahinder Ramdin for being part of my committee.

Lastly, I want to thank my parents and sister for their endless support and encouragement. Many thanks to Luuk for your unconditional interest and support every time I needed to vent about my project. It has been a tough year, but I am very grateful to have you by my side.

I.A.E. Burgers

Abstract

Australia has a high potential for production of renewable energy, such as wind and solar. Due to the stochastic operating conditions, excessively produced energy can be used to produce hydrogen by electrolysis to store the energy, known as power-to-gas. This hydrogen can be injected into the existing natural gas pipeline network, providing both storage and transport of hydrogen. There are many applications for hydrogen, however, this thesis focuses on the use of hydrogen for fuel cell cars. In order to use the hydrogen blended with the natural gas, a gas separation is required. Pressure swing adsorption is a commonly used technology to produce pure hydrogen, which exploits the adsorption of gases at high partial pressures. In this thesis, a PSA system is designed to separate a feed of 5 vol% and 10 vol% hydrogen mixed with natural gas at a pressure of 20 bar, and the economic feasibility of hydrogen supplied by a PSA system at a refuelling station is assessed and compared with other alternatives.

The PSA separation is achieved with a 6 bed system, which consists of 4 pressure equalisation steps, to increase the product recovery, and repressurises the bed with the pure hydrogen product, to increase the purity. The adsorbent material is key in the design of a PSA system, which determines the operation performance and cost. Due to the large amount of gas components present in natural gas, a three layered bed is designed. Activated carbon is selected as the main adsorbent layer, adsorbing methane, which is the main component in the gas mixture. Heavy hydrocarbons and CO₂ adsorb very strongly on activated carbon, therefore, a pre-layer of silica gel is used to prevent accumulations of these gases. Silica gel has a linear isotherm for heavy hydrocarbons and CO₂, which means the gas components will desorb at the desorption pressure. Lastly, a zeolite LiLSX layer is used for the adsorption of nitrogen. Process simulations are performed, focusing on the thickness of the pre-layer. No pre-layer results in accumulations of the heavy hydrocarbons on the activated carbon main layer, and thus reduces the available sites for methane to adsorb. This results in a low purity hydrogen product. When the pre-layer is too long, the total amount of activated carbon is reduced and thus not enough adsorbent is available for the methane to adsorb. A thickness of 0.2 meter in a bed of 1.2 meter height is concluded to be ideal.

It is concluded that an economically feasible design for a refuelling station with hydrogen supplied by a PSA system is proposed. Hydrogen can be dispensed to a fuel cell vehicle in the best case scenario for \$14.79 with hydrogen originally produced by electrolysis, and for \$12.14 for hydrogen originally produced by SMR without CCS. The final hydrogen price (including hydrogen supply, compression, storage, and dispensing) is compared to two other hydrogen supply methods: on-site electrolysis and tube-trailer transported hydrogen. Currently, PSA supplied hydrogen is a more economical option,

especially if the hydrogen is produced from fossil fuel based resources. On-site electrolysis can become a more economical option in the future with improved cell efficiencies and reduced electricity prices. Tube-trailer transported hydrogen is highly influenced by the distance travelled. If the hydrogen originates from electrolysis, tube-trailer transported hydrogen will always be more expensive. For different fossil fuel based hydrogen technologies, a break-even distance is calculated.

Contents

| | |
|---------------------------------------------------------------|-------------|
| Preface | iii |
| Acknowledgements | iv |
| Abstract | v |
| List of Figures | ix |
| List of Tables | xi |
| Abbreviations | xiii |
| Symbols | xv |
| 1 Introduction | 1 |
| 1.1 Power-to-Gas | 1 |
| 1.2 Energy Market in Australia | 3 |
| 1.3 Hydrogen Strategy in Australia | 5 |
| 1.4 Fuelling Strategy | 6 |
| 1.5 Objective and Scope | 10 |
| 1.6 Outline | 12 |
| 2 Literature Review | 13 |
| 2.1 Introduction | 13 |
| 2.2 Gas Separation Methods | 14 |
| 2.3 Adsorption Technology | 16 |
| 2.4 Pressure Swing Adsorption Process | 23 |
| 2.5 Other Adsorption Processes | 27 |
| 2.6 PSA Applications | 29 |
| 2.7 Separation of Hydrogen from Natural Gas | 31 |
| 2.8 Pressure Swing Adsorption Simulation | 34 |
| 2.9 Hydrogen Refuelling Stations | 38 |
| 2.10 Summary | 44 |
| 3 Methodology | 47 |
| 3.1 Introduction | 47 |
| 3.2 Adsorption Material Selection | 47 |
| 3.3 Process Simulations | 49 |
| 3.4 Refuelling Station Design | 52 |
| 3.5 Economic Refuelling Station | 54 |
| 3.6 Comparison of Different Hydrogen Supply Methods | 56 |
| 3.7 Summary | 57 |
| 4 Process Analysis | 59 |
| 4.1 Introduction | 59 |
| 4.2 Results Adsorbents Screening | 59 |
| 4.3 Simulation Results | 68 |

| | | |
|----------|-----------------------------------------------------------|------------|
| 4.4 | Summary | 79 |
| 5 | Techno-Economic Analysis | 81 |
| 5.1 | Introduction | 81 |
| 5.2 | Design Hydrogen Refuelling Station | 82 |
| 5.3 | Techno-Economic Analysis | 86 |
| 5.4 | Comparison of Different Hydrogen Supply Methods | 90 |
| 5.5 | Summary | 98 |
| 6 | Conclusion and Recommendations | 101 |
| 6.1 | Conclusion | 101 |
| 6.2 | Recommendations | 104 |
| A | Natural Gas composition | 107 |
| B | Material Isotherms | 109 |
| C | Simulation Results | 113 |
| D | HRSAM Model Results | 135 |
| E | Final Hydrogen Cost Calculations | 145 |
| | Bibliography | 149 |

List of Figures

| | | |
|------|---------------------------------------------------------------------------------------------------------------------------------------------------------------------------|----|
| 1.1 | Schematic overview of possible applications of hydrogen in Australia. . . . | 2 |
| 1.2 | Map of Australia's non-renewable and renewable energy sources. | 3 |
| 1.3 | Jemena's Power to Gas project. | 5 |
| 1.4 | Components of a typical refuelling station. | 7 |
| 1.5 | Schematic depicting the project overview. | 11 |
| | | |
| 2.1 | Flow diagram literature review. | 13 |
| 2.2 | Homogeneous and composite microporous adsorbent particle. | 17 |
| 2.3 | Brunauer classifications of adsorption isotherms. | 18 |
| 2.4 | Working capacity represented for the isotherm of methane on activated carbon. | 21 |
| 2.5 | Schematic structure of (a) zeolite A, and (b) zeolite X and Y. | 22 |
| 2.6 | Breakthrough curve for non-ideal system. | 23 |
| 2.7 | Schematic of the Skarstrom cycle | 25 |
| 2.8 | Schematic of the Guerin-Domine cycle | 25 |
| 2.9 | Dual reflux PSA half cycle. | 29 |
| 2.10 | HylyPure process concept. | 32 |
| 2.11 | Process design with a second high pressure membrane in the recycle stream. | 32 |
| 2.12 | Development of an adsorption wave front through the bed. | 35 |
| 2.13 | Site plan for a hydrogen refuelling station, combined with a gasoline station. | 38 |
| 2.14 | Pressure profile during the fuelling of a fuel cell car, according to the SAE J2601 protocol. | 41 |
| 2.15 | Schematic of Jemena pipeline distribution network in New South Wales. | 43 |
| | | |
| 3.1 | Schematic overview of the 6 bed, 12 step PSA process used for the separation of hydrogen and natural gas. | 49 |
| 3.2 | Bed pressure profile during the designed 12 step PSA cycle. | 50 |
| 3.3 | Overview of the three different hydrogen supply methods considered in the comparison. | 56 |
| | | |
| 4.1 | Adsorption isotherms of different gases on CuBTC at 298 K. | 61 |
| 4.2 | Adsorption isotherms of different gases on activated carbon at 298K. | 61 |
| 4.3 | Working capacity and selectivity for selected gases on activated carbon represented as function of the feed pressure, assuming blow down to atmospheric pressure. | 62 |
| 4.4 | Adsorption isotherms of different gases on silica gel at 298K. Dual site Langmuir curves plotted. | 64 |
| 4.5 | Adsorption isotherms of nitrogen on various types of zeolite at 298 K. | 65 |
| 4.6 | Solid loading of the heavy hydrocarbons at the end of the adsorption step for a 5 vol% hydrogen feed input. | 72 |
| 4.7 | Gas concentration of the heavy hydrocarbons at the end of the adsorption step for a 5 vol% hydrogen feed input. | 72 |
| 4.8 | Solid loading of the methane at the end of the adsorption step for a 5 vol% hydrogen feed input. | 73 |
| 4.9 | Gas concentration of the methane at the end of the adsorption step for a 5 vol% hydrogen feed input. | 73 |
| 4.10 | Solid loading of the heavy hydrocarbons at the end of the adsorption step for a 10 vol% hydrogen feed input. | 74 |

| | | |
|------|----------------------------------------------------------------------------------------------------------------------------------------------------------------------------------------------------------|----|
| 4.11 | Gas concentration of the heavy hydrocarbons at the end of the adsorption step for a 10 vol% hydrogen feed input. | 74 |
| 4.12 | Solid loading of the methane at the end of the adsorption step for a 10 vol% hydrogen feed input. | 75 |
| 4.13 | Gas concentration of the methane at the end of the adsorption step for a 10 vol% hydrogen feed input. | 75 |
| 4.14 | Solid loading of the heavy hydrocarbons at the end of the adsorption step, end of desorption step, and the end of the pressure equalisation steps for a 5 vol% hydrogen feed input. | 76 |
| 4.15 | Gas concentration of the heavy hydrocarbons at the end of the adsorption step, end of desorption step, and the end of the pressure equalisation steps for a 5 vol% hydrogen feed input. | 76 |
| 4.16 | Gas flows in the separation of hydrogen and natural gas by a PSA process using a 10 vol% hydrogen input feed and a pre-layer of 0.2 meter. | 77 |
| | | |
| 5.1 | Schematic overview of a hydrogen refuelling station where a PSA process is used to separate the hydrogen from the natural gas mixture, transported in the natural gas pipeline network. | 81 |
| 5.2 | Variations in the demand per hour during a day for a gasoline station in the US. | 84 |
| 5.3 | Best case operating cost of the PSA as a function of the lifetime, for different production methods of hydrogen assuming an electricity price of 5c/kWh and a natural gas price of \$9.50/GJ. | 87 |
| 5.4 | Worst case operating cost of the PSA as a function of the lifetime, for different production methods of hydrogen assuming an electricity price of 25c/kWh and a natural gas price of \$15.00/GJ. | 88 |
| 5.5 | Best case scenario for PSA separated hydrogen assuming a natural gas price of \$9.50/GJ and an electricity price of 5c/kWh. | 91 |
| 5.6 | Worst case scenario for PSA separated hydrogen assuming a natural gas price of \$15.00/GJ and an electricity price of 25c/kWh. | 91 |
| 5.7 | Hydrogen production cost by electrolysis as a function the electricity price. | 93 |
| 5.8 | Current hydrogen price for on-site electrolysis, assuming various electricity prices for both PEM and AE electrolyser cells. | 94 |
| 5.9 | Prospect of hydrogen price for on-site electrolysis, assuming various electricity prices for both PEM and AE electrolyser cells. | 94 |
| 5.10 | Best case scenario for tube-trailer transported hydrogen over a distance of 200 km, assuming an electricity price of 5c/kWh. | 96 |
| 5.11 | Worst case scenario for tube-trailer transported hydrogen over a distance of 1000 km, assuming an electricity price of 25c/kWh. | 97 |

List of Tables

| | | |
|-----|-------------------------------------------------------------------------------------------------------------------------------------------------------------------------------------------------------------------------------------------------------|----|
| 1.1 | Hydrogen purity requirements in fuel cell electric vehicles specified by ISO 14687-2 (Type I & II Grade D). | 10 |
| 1.2 | Constant values defining the scope. | 11 |
| 2.1 | Classification of commercial adsorbents. | 20 |
| 2.2 | Different types of high pressure hydrogen storage tanks. | 39 |
| 3.1 | Partial pressure ranges in which the different gas components operate, representing the adsorption pressure and desorption pressure during the cycle, respective to the concentration of the different gas components in the mixture (see Table A.2). | 48 |
| 3.2 | Summary table of cyclic 6 bed 12 step PSA cycle used in the process analysis. | 50 |
| 3.3 | Parameters used in MINSA for the 6 bed 12 step process cycle based on the lab scale PSA design. | 51 |
| 3.4 | Overview of different simulations performed in the process analysis. | 51 |
| 3.5 | Different scenarios for a hydrogen refuelling station. | 52 |
| 3.6 | Production factors used for the feedstock price calculation of the natural gas and hydrogen mixture. | 55 |
| 4.1 | Working capacity and material properties of selected materials for methane adsorption. | 60 |
| 4.2 | Selectivity of methane on CuBTC and activated carbon. | 60 |
| 4.3 | Working capacity and material properties of selected materials for nitrogen adsorption. | 65 |
| 4.4 | Selectivity of N ₂ over various gases on zeolite LiLSX. | 66 |
| 4.5 | Molecular dipole moments of various components. | 67 |
| 4.6 | Overview of the simulation results for a hydrogen input feed of 5 vol%, for a varying silica gel pre-layer thickness. | 69 |
| 4.7 | Overview of the simulation results for a hydrogen input feed of 10 vol%, for a varying silica gel pre-layer thickness. | 69 |
| 4.8 | Gas concentrations and adsorption amount of heavy hydrocarbons at different location in the bed, at the end of the adsorption, pressure equalisation, and desorption step. | 77 |
| 5.1 | Dimensions PSA columns for a different hydrogen product demand, representing different sizes of hydrogen refuelling station. | 82 |
| 5.2 | Input values for scale up PSA process, producing 350 kg of hydrogen per day. | 83 |
| 5.3 | Results of the Aspen HYSYS compressor design. | 83 |
| 5.4 | Main variables in HRSAM model design for a hydrogen refuelling station. | 85 |
| 5.5 | Equipment cost for the pressure swing adsorption process. | 86 |
| 5.6 | Overview table of capital and operational and maintenance costs for a hydrogen refuelling station with varying daily demand. | 89 |
| 5.7 | Cost breakdown for hydrogen compression, storage and dispensing (CS&D) at a refuelling station expressed in \$/kg H ₂ , assuming an electricity price of 25c/kWh. | 89 |
| 5.8 | Best case scenario, hydrogen production price assuming electricity price of 5c/kWh and a natural gas price of \$9.50/GJ. The fixed PSA costs include the capital cost for a 10 year lifetime and the maintenance cost. | 90 |

| | | |
|------|-----------------------------------------------------------------------------------------------------------------------------------------------------------------------------------------------------------------------------------|----|
| 5.9 | Worst case scenario, hydrogen production price assuming electricity price of 25c/kWh and a natural gas price of \$15.00/GJ. The fixed PSA costs include the capital cost for a 10 year lifetime and the maintenance cost. | 90 |
| 5.10 | Constants used for the different electrolyser cells. | 92 |
| 5.11 | Final hydrogen price for on-site electrolysis with a PEM cell and an AE cell. | 93 |
| 5.12 | Best case scenario for tube-trailer transported hydrogen for varying distances travelled, assuming an electricity price of 5c/kWh. | 96 |
| 5.13 | Worst case scenario for tube-trailer transported hydrogen for varying distances travelled, assuming an electricity price of 25c/kWh. | 96 |
| 5.14 | Break-even distance with hydrogen cost price compared to PSA refuelling station, for the best case and worst case scenario. | 97 |

Abbreviations

| | |
|-----------------|------------------------------------------------------|
| AE | Alkaline Electrolyser |
| ARENA | Australian Renewable Energy Agency |
| CAPEX | Capital Expenditures |
| CCS | Carbon Capture and Storage |
| CMSM | Carbon Molecular Sieves Membranes |
| COF | Covalent Organic Framework |
| CRC | Cooperate Research Centre |
| CS&D | Compression, Storage, and Dispensing |
| CSS | Cyclic Steady State |
| CSTR | Continuous Stirred Tank Reactor |
| DPM | Discretised Pellet model |
| EHC | Electrochemical Hydrogen Compressor |
| FCEV | Fuel Cell Electric Vehicle |
| GHG | Green House Gas |
| HRS | Hydrogen Refuelling Station |
| HRSAM | Hydrogen Refuelling Station Analysis Model |
| IAST | Ideal Adsorbed Solution Theory |
| LDF | Linear Driving Force |
| MINSA | Monash Integrated Numerical Simulator for Adsorption |
| NG | Natural Gas |
| NIST | Natural Institute of Standards and Technology |
| O&M | Operational & Maintenance |
| OPEX | Operational Expenditures |
| PEM | Proten Exchange Membrane |
| PSA | Pressure Swing Adsorption |
| PV | Photovoltaic |
| RPSA | Rapid Pressure Swing Adsorption |
| SMR | Steam Methane Reformer |
| TSA | Temperature Swing Adsorption |
| VSA | Vacuum Swing Adsorption |

Symbols

| | | |
|---------------|------------------------------|----------------------------------------|
| b | Langmuir adsorption constant | [bar ⁻¹] |
| D | diffusion coefficient | [m ² s ⁻¹] |
| d | diameter | [m] |
| E | internal energy | [J] |
| H | Henry's constant | [bar mol kg ⁻¹] |
| H | enthalpy | [J mol ⁻¹] |
| k | mass transfer coefficient | [s ⁻¹] |
| p | pressure | [bar] |
| q | amount adsorbed | [mol kg ⁻¹] |
| r | radius | [m] |
| R | gas constant | [J K ⁻¹ mol ⁻¹] |
| T | temperature | [K] |
| t | time | [s] |
| u | interstitial velocity | [m s ⁻¹] |
| ε | bed voidage | [-] |
| ρ | density | [kg m ⁻³] |

Superscripts

| | |
|---|-------------|
| * | equilibrium |
| - | average |

Subscripts

| | |
|-------|------------|
| i | component |
| ads | adsorption |
| p | pellet |
| sat | saturated |

Chapter 1

Introduction

1.1 Power-to-Gas

Global warming is a great threat to the environment and is challenging the world we live in today. With increasing amounts of anthropogenic Green House Gasses (GHG) emitted into the atmosphere, resulting in rising temperatures and sea levels, and with a constant growth of the total energy demands, a structural change in the energy system is required to cope with these challenges. To keep supplying the increasing energy demand and reduce environmental risks, fossil fuels must be replaced with renewable energy sources, which is known as the energy transition. Hydrogen can play a key role in this, as it is a remarkably clean fuel, which only produces water during oxidation [1]. Furthermore, it is one of the most efficient energy fuels, containing an energy yield of 122 kJ/g, which is 2.75 times higher compared to fossil fuels [2, 3].

Hydrogen is not naturally found, but can be produced in several ways. Common ways of producing hydrogen are through coal gasification and steam methane reforming (SMR), which both emit CO₂ as by-product. This form of hydrogen is known as *grey* hydrogen, which can be compensated for by using Carbon Capture and Storage (CCS), classifying the hydrogen as *blue*. Green hydrogen, produced without emitting any GHG, is generated from renewable energy sources by electrolysis, which is an electrochemical process of decomposing water into hydrogen and oxygen [3].

Hydrogen has many different applications in Australia, which are depicted in Figure 1.1. Like natural gas, hydrogen can be used for heating purposes, both domestically and industrially. In industry, hydrogen can serve as chemical feedstock to form ammonia, which is today the most common application of hydrogen. Both pure hydrogen and ammonia form a great potential as export products for Australia.

Hydrogen can be used as a fuel to generate electricity, by means of a fuel cell, and power fuel cell cars, buses, trucks, or trains, creating a new market for the transport sector. The Hyundai Nexa was the first fuel cell car on the market, which requires one kilogram of hydrogen to drive up to 100 km [1]. This triggered other car manufacturers like Toyota, Honda, and Daimler to compete in the development of hydrogen cars [4].

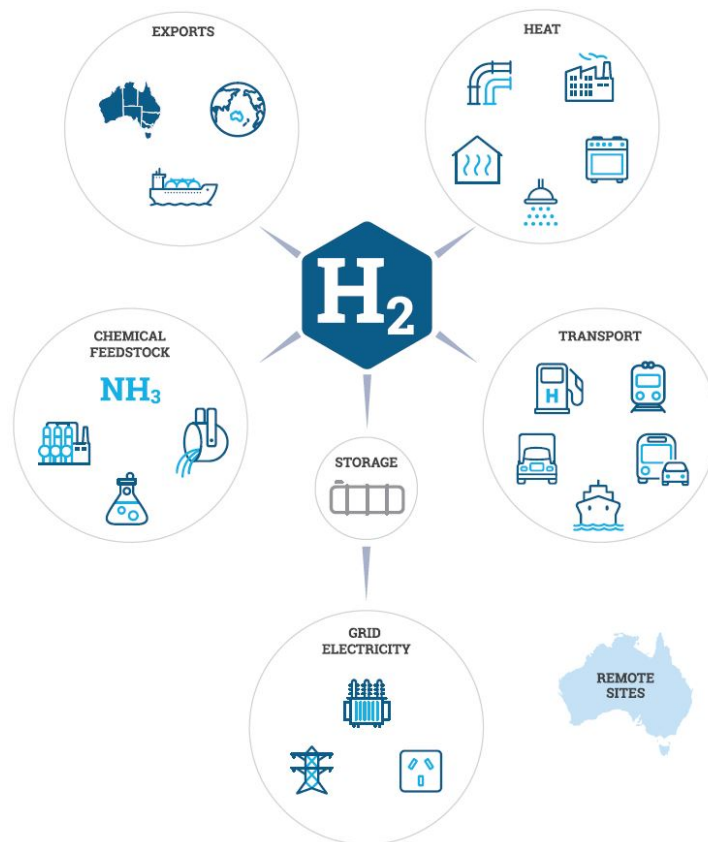


FIGURE 1.1: Schematic overview of possible applications of hydrogen in Australia [1].

Currently three commercial cars are on the market: Hyundai Tucson, Toyota Mirai, and Honda Clarity [5]. All have a storage tank capacity of 5 kg of hydrogen, stored at 700 bar.

Lastly, hydrogen can be used to store excess amounts of renewable energy. As the inexhaustible wind and solar resources have stochastic operating conditions, an uneven generation of electricity is produced. Excessively produced electricity can be stored, to be able to supply the energy demand when the electricity production does not meet the demand. One way of doing that is by storing the energy in the form of hydrogen through electrolysis. This process is known as power-to-gas. The gas, hydrogen, now serves as an energy carrier. The energy can be released by reversing the electrolysis process, forming water by combining hydrogen and oxygen.

Power-to-gas is an efficient way of both storing and transporting energy in the form of hydrogen [6]. The natural gas distribution network can be utilised for the transportation of hydrogen, as hydrogen can be added to the natural gas network. The grid offers a large network for distributing hydrogen and simultaneously serves as storage of the excess renewable energy in the form of hydrogen gas. At any point in the network the hydrogen can be separated from the natural gas and either used directly as a fuel, for transportation for example, or as a feedstock for producing electricity by means of a fuel cell, or for other industrial applications. This creates great opportunities for linking the electrical and the natural gas systems [7].

1.2.2 Renewable Energy Sources

Next to fossil fuels, Australia has a very high potential for the production of renewable energy, as can be seen from Figure 1.2(B). Different to fossil fuels as energy producers, the availability of renewable energy resources can only be given as estimates of potential sources, since these forms of energy rely on the availability of the source. Another way to report the potential of renewable energy is by the installed capacity, which is the maximum power output of the installed generators. Wind and solar energy have the highest potential in Australia as renewable energy sources. Since 2001 the Renewable Energy Target, which is a federal government policy, is operating. According to this target, at least 33 000 GWh of electricity produced in Australia by 2020 must come from renewable energy. This goal has been reached in 2019 already [9]. Unfortunately, there is no federal policy at the moment to replace the previous Renewable Energy Target, which is a concerning prospect for achieving a decarbonisation of Australia's economy [10]. States are taking more initiatives individually to encourage investment in renewable energy projects and thereby filling up the voids [11].

For example, Tasmania is producing an outstanding amount of renewable energy already, which covers over 95% of the electricity used on the island. Most of the energy comes from hydro-power and some is produced from wind power. The current 2500 MW capacity is meant to double according to the *Battery of the Nation plan*, which will make Tasmania an exporter of renewable energy to the mainland of Australia [11]. Part of the plan includes a new interconnector, connecting Victoria and Tasmania.

Victoria only produced 20% of the electricity from renewable energy by the end of 2018 [11]. They target to reach 40% of the total electricity produced to be from renewable resources by 2025 and a net zero emission target is set for 2050. The Solar Homes program must ensure support for the investment of solar panels for eligible households, where they receive a rebate on the investment and an interest-free loan for the remainder to be paid back in four years.

In Queensland only 9.5% of the electricity produced came from renewable energy sources by 2018 [11]. This is in high contrast with the number of investments made in the construction of renewable energy plants. Across the world, the highest potential of solar radiation per square meter can be found in Australia. The number of installed rooftop photovoltaic (PV) systems, both large scale and small scale, is rapidly increasing. A total of 8132.83 MW of installed solar capacity was achieved by 2018, of which mainly situated in Queensland [11]. By 2030, half of the electricity is projected to come from renewable energy, which they are well on their way for, as more small-scale solar systems are being installed and new wind farms are under construction.

1.2.3 Energy Consumption

With a population of 25 million people, the total energy consumption of Australia in 2017-2018 was estimated at 6172 PJ of which fossil fuels provided almost all energy [12]. The transport sector is the dominant consumer of energy, where an increase in diesel for



FIGURE 1.3: Jemena's Power to Gas demonstration [13].

road transport and an increase for jet fuel was identified. The Australian Energy Update 2019 [12], provides a detailed summary of the energy used and produced in Australia. The main conclusions drawn from this report related to the energy consumption, are that oil takes the largest share in the primary energy mix, followed by coal and natural gas. The total energy produced in 2017-2018 is estimated at 18 603 PJ, of which two-third is exported. As resources are being exploited, Australia becomes more dependent on imports of especially refined products and crude oil, which resulted in a total amount of energy imported of 2454 PJ.

1.3 Hydrogen Strategy in Australia

As described above, there is a lot of potential for wind and solar power to be extracted from the extensive amount of land that Australia is rich of. In order to use the potentially available renewable energy and to make export possible, hydrogen comes into play. A National Hydrogen Strategy was initiated by Australia's Chief Scientist Dr Alan Finkel in December 2018, aiming at *"the development of a clean, innovative, and competitive hydrogen industry that benefits all Australians and [to be] a major player by 2030"* [1]. A Working Group, lead by Dr Alan Finkel, is established to coordinate the developments. The main goal of the strategy is to build a supply and demand, where all market barriers are removed, such that a global cost-competitive market is accelerated. The idea is to achieve this by creating hydrogen hubs, where on a smaller scale the various industries are connected and innovation is fostered. This will provide the possibility to integrate hydrogen into the current electricity network in such a way that reliability is enhanced.

The Australian Renewable Energy Agency (ARENA) was established in 2012 with the aim *"to improve the competitiveness of renewable energy technologies and increase the supply of renewable energy in Australia"* [14]. Next to supporting research, ARENA is also involved in informing in policy decision making. A total of AU\$22.1 million is funded for 16 research projects [11]. Several projects around the country are currently being realised. One of those projects is the *Jemena Power to Gas Demonstration* [15], depicted in Figure 1.3, which is a 5 year trial project in Western Sydney. Wind and

solar energy is converted into hydrogen by a 500 kW electrolyser on-site. Most of the hydrogen is injected into the Jemena gas pipeline network, which is connected to 250 homes. This is used to demonstrate and test the feasibility of hydrogen transport in the current gas pipeline network. The rest of the hydrogen is stored underground in large tanks for refuelling stations, where hydrogen vehicles can fill up. A similar project is running in Adelaide, *Hydrogen Park SA*, which connects 710 properties with the gas network in which up to 5% hydrogen is blended in. Both projects are important stepping stones in demonstrating a long term storage solution for the Australian energy market with hydrogen.

1.4 Fuelling Strategy

Hydrogen used as a fuel in fuel cell electric vehicles (FCEV) emits nothing but water. Therefore, hydrogen can be a large contributor in decarbonising Australia's transport sector. Consumers are encouraged to drive FCEVs, but this can only be achieved if hydrogen is readily available to refuel those vehicles. Therefore, a fuelling strategy is required which ensures a reliable network of hydrogen refuelling stations is operating throughout the country [16]. The early phase development is the most crucial phase, as only few vehicles are used and refuelling station utilization is low.

Several models are developed which can predict the hydrogen refuelling infrastructure requirements [17]. These focus on where refuelling stations should be placed, how many, and what types of stations there are required in each specific region. Small stations will have a production capacity of around 350 kg of hydrogen per day, whereas a large station is defined as producing over 1000 kg of hydrogen per day [18]. One of these models is the Scenario Evaluation and Regionalization Analysis (SERA) model [18], developed by the National Renewable Energy Laboratory (NREL) in the US. In California, a significant hydrogen refuelling stations infrastructure is already operational. The expected growth modelled with the SERA model predicts up to 21 000 stations across the US by 2050, supporting 61 million FCEVs, and providing access to 215 million people [18]. This can only be achieved by a national expansion strategy, where state and national policy are combined to strongly coordinate and plan the build of a hydrogen refuelling strategy. The total number of refuelling stations in the US today is 42 [19], of which most are centered around Los Angeles and San Francisco. Australia currently has no commercially operational hydrogen refuelling station throughout the country and is therefore in the preface of developing an hydrogen refuelling infrastructure.

1.4.1 Refuelling Station

A hydrogen refuelling station is typically made up of various storage tanks, compressors, heat exchangers and a dispenser, which is schematically depicted in Figure 1.4. Typical pressures of hydrogen tanks in cars is 700 bar, whereas buses typically have a storage tank at 350 bar. The dispenser must safely inject the high pressure hydrogen into the tank for which a fuelling protocol (J 2601) is developed by the Society of Automotive

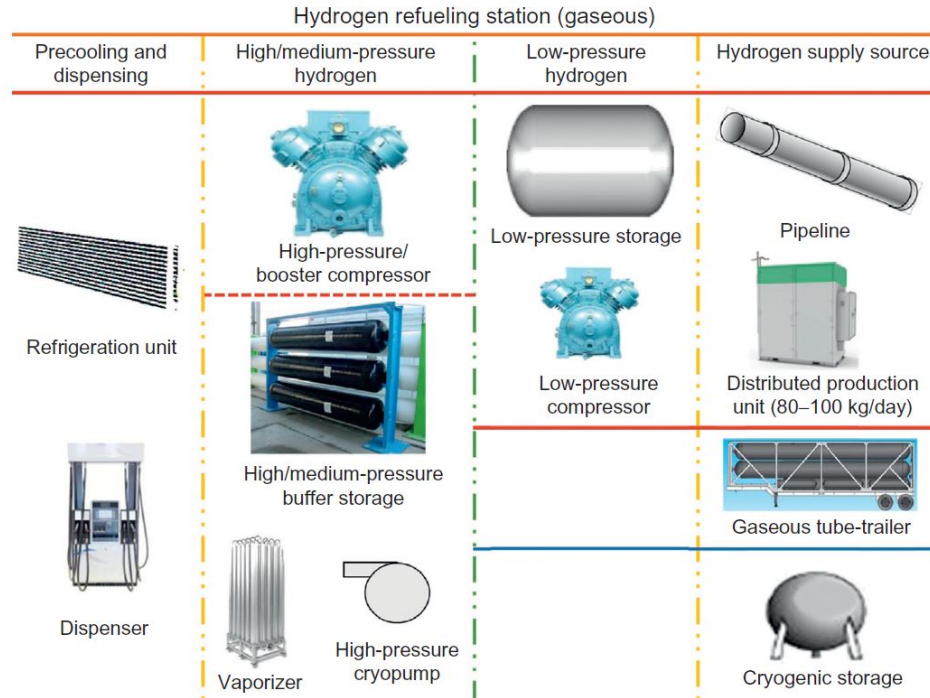


FIGURE 1.4: Components of a typical refuelling station [20].

Engineers (SAE) [20]. According to these safety standards, the temperature of the hydrogen may never exceed $85\text{ }^{\circ}\text{C}$. Therefore, at the end of the fill, the vehicle tank pressure cannot exceed 875 bar. The fuelling rate must be limited to 3.6 kg/min at any time and the target fuelling time is 3 minutes [20].

To ensure the temperature of the hydrogen does not exceed the limit during dispensing, a heat exchanger is installed prior to the dispenser, in which it is precooled to a temperature in between $-33\text{ }^{\circ}\text{C}$ and $-40\text{ }^{\circ}\text{C}$. A refrigeration unit is used for the gaseous hydrogen, whereas a vaporiser is used for the liquefied hydrogen.

In order to continuously meet the refuelling demand, a cascade storage tank is typically used to store the hydrogen. This cascade consists of different tanks storing hydrogen at different pressure in order to dispense the hydrogen to a vehicle at 700 bar. For hydrogen produced on-site or delivered by a pipeline, the hydrogen is supplied at a low pressure of 20-35 bar. Therefore, an extra low pressure storage tank is used to store the hydrogen, which is then further compressed to the cascade system. The size of the storage tanks is controlled by the hydrogen demand at the refuelling station. Underground storage of hydrogen could be a possibility to reduce the land use at refuelling station. This does however also complicate inspection and maintenance [21].

1.4.2 Transport of Hydrogen

Before being able to fuel any vehicle at a refuelling station, hydrogen must first be produced and transported to the specific station. Due to the low volumetric energy density of hydrogen, efficient storage of large quantities is crucial. The main forms of

hydrogen storage are as compressed gas or cryogenic liquid. Pressurised hydrogen is the easiest method, with typical storage pressures of 250 bar to 500 bar for transportation in tube-trailers [22]. Liquid hydrogen can be stored at a larger energy density, compared to pressurised hydrogen. The liquefaction process, which is operated at 21 K, does require a high amount of energy and is therefore very costly [23]. The pressurised or liquefied hydrogen is then transported by tube-trailer or train to the refuelling stations [20].

Another way of transporting and storing hydrogen is through a pipeline network, which provides a cheap and safe alternative for long distance transport of hydrogen with minimum energy loss [24]. The development of a new network for the transportation of hydrogen is very expensive and will not outweigh the transportation cost by pressurisation or liquefying hydrogen. Therefore, currently much research is being undertaken to investigate the possibilities of transporting hydrogen mixed within the natural gas pipeline network as an alternative, intermediate solution. The existing natural gas network is extensive and therefore provides access to a large transport network for hydrogen. Numerous studies provide a review on the safety and technical feasibility of blending hydrogen into the natural gas pipeline network [24–29]. The risk of ignition and/or explosion due to leakage is identified as the main risk, which increases with increasing hydrogen concentration added to the gas mixture. The maximum amount of hydrogen injection remains a topic of debate, as it influences both the structure of the pipelines and the applications of the end users. An injection of up to 10% of hydrogen by volume in Australian natural gas pipeline network has been reviewed by Bruce et al. [30], and it is concluded that there are no significant safety or risk aspects, neither any significant implications with state legislation's [31]. This provides great opportunities to investigate the possibilities of using the hydrogen transported in the natural gas grid.

1.4.3 Gas Separation Methods

Blending hydrogen into the natural gas network adds the need for separating the hydrogen from the natural gas to be able to use it as a fuel in FCEVs. There are several existing technologies that can be used for this separation, namely: absorption, cryogenic separation, membrane separation, or adsorption. Gas absorption uses a liquid solvent to purify a gas stream. No selective solvent for hydrogen exist, which makes absorption not suitable for the separation of hydrogen and natural gas. Cryogenic separation is the most costly separation method, as it operates at very low temperatures and high pressures [32]. The gases are separated by distillation as partial condensation of the gases occurs at the operating condition. Membrane separation is a very simple, low cost, and energy efficient process typically used for bulk separation. It is driven by a pressure gradient and therefore produces a low pressure product. PSA is the most commonly used hydrogen purification method used in industry, which exploits the adsorption of gases on adsorbent material at high partial pressures. PSA is able to produce a product with high purity and high recovery.

For the separation of hydrogen from natural gas, to be used at a refuelling station, it is very important to produce a high purity hydrogen product (for specifications see Section 1.4.4). Furthermore, the capital cost of the process must be economical for

implementing at small scale. Therefore, PSA separation is chosen as the best option for the separation required. Additionally, the gas feed mixture used at the refuelling station is supplied at a high pressure directly suitable as feed stream for the PSA. This diminishes the need for compression, which is the main operational cost for a PSA process. The pressure of the product is also already at elevated pressures, which reduces the total compression required after the separation before the hydrogen can be fueled to a fuel cell vehicle.

The PSA separation process can be used in different cases for the separation of hydrogen and natural gas. In the first case, the pure hydrogen is the product, which can be used as fuel for fuel cell vehicles. The methane is regarded as a waste stream and the purity is therefore not considered. In the second case, the pure methane is the product, which can be applied for applications connected to the natural gas grid that do not tolerate hydrogen, such as turbines. The purity of the hydrogen is not taken into consideration. In the third case, the aim is to produce both a pure hydrogen and pure methane which can be used for their respective applications. This thesis focuses on the production of a high purity hydrogen product to feed fuel cell vehicles.

Refuelling stations will be placed at strategic locations, which is determined by the accessibility of the stations for the consumers and required operating conditions for the selected separation system. The natural gas pipeline network available in these areas determine the pressure at which the gas mixture is extracted. In this thesis, a pressure of 20 bar is assumed to be supplied as feed to the PSA as case study. Other pressures (30 bar and 50 bar) are considered by other members of the research group at the University of Melbourne.

1.4.4 Fuel Cell Quality Hydrogen

The hydrogen separated from the natural gas mixture will in this thesis be used for the fuelling of fuel cell vehicles. Hydrogen used in fuel cell vehicles requires high purity, as impurities damage the fuel cell membrane. Therefore, the ISO 14687-2 is established, to set a boundary for the quality of the hydrogen, which is listed in Table 1.1.

The types of impurities present in the mixture are determined by the source of the natural gas and the hydrogen. The composition of the natural gas from different sources in Australia is tabulated in Table A.1 in the Appendix. The main component in the natural gas mixture is methane. Furthermore, natural gas consists of several heavy hydrocarbons, CO₂, and N₂. To separate all these different gases to produce a pure hydrogen product, multiple adsorbent materials are required in the PSA process, in which each layer different gases are adsorbed.

Other components can be present in trace elements in the natural gas mixture as well, such as CO, sulphur components and water, which can be harmful for the fuel cell [33]. Each component has a different impact on the membrane of the fuel cell. CO binds to the platinum sites of the catalyst, reducing the available sites for the hydrogen adsorption and oxidation and thus degrading the membrane [34]. It is possible for the CO molecules

TABLE 1.1: Hydrogen purity requirements in fuel cell electric vehicles specified by ISO 14687-2 (Type I & II Grade D) [35].

| Component | Limit | Unit |
|-----------------------------|--------------|-------------|
| Helium | 300 | ppm |
| Nitrogen | 100 | ppm |
| Argon | 100 | ppm |
| Water | 5 | ppm |
| Oxygen | 5 | ppm |
| Hydrocarbons | 2 | ppm |
| Carbon dioxide | 2 | ppm |
| Carbon monoxide | 0.2 | ppm |
| Formic acid | 0.2 | ppm |
| Ammonia | 0.1 | ppm |
| Total halogenated compounds | 50 | ppb |
| Formaldehyde | 10 | ppb |
| Sulphur components | 4 | ppb |
| Particulate concentration | 1 | mg/kg |

to desorb from the membrane, by increasing the concentration or the temperature. This makes the degradation of the membrane reversible. Sulphur components adsorb to the membrane in a similar way as CO molecules. This process is, however, known to be irreversibly and damages the fuel cell irreparably [33]. Furthermore, CO₂ is known to form CO through the reverse water gas shift reaction. Therefore, the concentration of CO₂ must be limited in order to reduce the amount of CO formed. The sulphur components consist mainly of hydrogen sulphide, H₂S, and mercaptans, which are added to the gas mixtures as odourant. Sulphur adsorbs to the platinum sites of the catalyst, just like CO does, resulting in a reduced number of sites available for hydrogen and oxygen to react [34]. Lastly, water does not significantly effect the fuel cell membrane, however it does lower the efficiency [35].

In this project, the main focus is on the adsorption of the main gas components in natural gas, which are methane, heavy hydrocarbons, nitrogen, and CO₂. The adsorption characteristics of the trace elements is studied based on literature.

1.5 Objective and Scope

In Australia there are currently no hydrogen refuelling station operating and thus the infrastructure has yet to be developed. In this thesis the feasibility of a hydrogen refuelling station where a PSA system is to supply the hydrogen is assessed. The hydrogen is produced at a central production plant, which can be by electrolysis or by fossil fuel based methods. Two different mixtures of hydrogen and natural gas are used in the analysis, where 5 vol% and 10 vol% of hydrogen is added to the natural gas and distributed by the existing pipeline network to the refuelling station. At the station the hydrogen is separated, compressed, stored, and finally dispensed to the vehicle. The natural gas produced as waste stream from the PSA system is either supplied directly

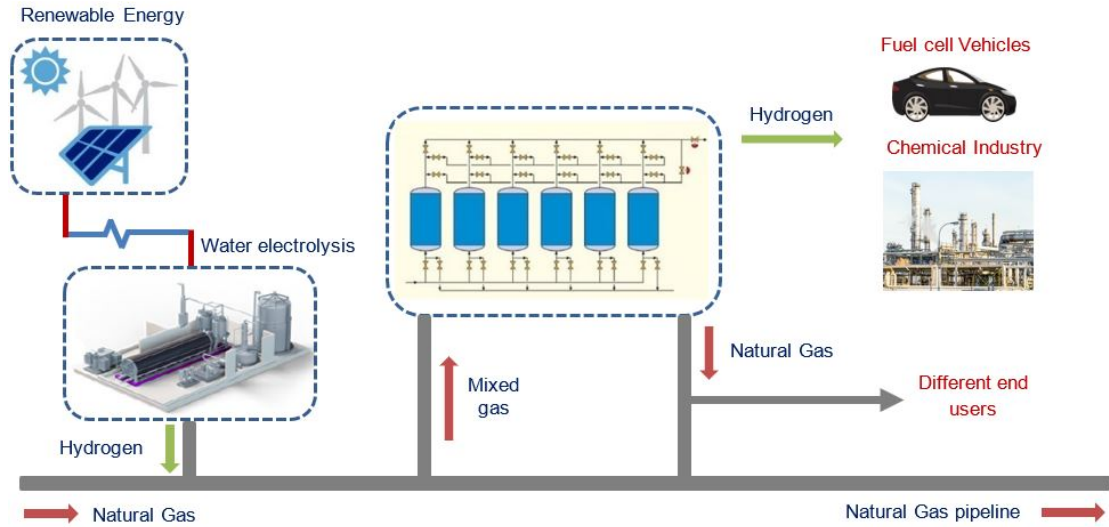


FIGURE 1.5: Schematic depicting the project overview. Hydrogen is produced at a centralised location, then injected in the natural gas pipeline network and transported to decentralised locations where the hydrogen is separated from the natural gas by a PSA system. The hydrogen can directly be used for fuel cell cars or in the chemical industry, the natural gas can be supplied back to the grid or supplied to different other end users.

to the end user or compressed back to the natural gas pipeline. An overview of the project is schematically depicted in Figure 1.5.

In this thesis, the separation is achieved by a PSA system operating at 20 bar and 298 K. Within the project, other operating pressures are evaluated as well, focusing on 30 and 50 bar. Higher pressures are not considered as this significantly increases the capital cost of the PSA system. Operating the system at pressures below 20 bar is not considered relevant, due to the lower adsorption amount possible. The temperature is fixed at 298 K as initial temperature for the analysis of the PSA system. Further research focusing on a temperature range relevant for Australia will give a better understanding of the temperature influence on the PSA separation, but is not considered in this study.

The gas composition used is that of the natural gas from Moomba in South Australia. The amount of hydrogen added to the natural gas mixture (5 or 10 vol%) represents

TABLE 1.2: Constant values defining the scope.

| Constants | Value | Unit |
|-------------------------------|----------------|--------|
| Pressure | 20 | bar |
| Temperature | 298 | K |
| Hydrogen | 5, 10 | vol% |
| Trace components hydrocarbons | ≤ 2 | ppm |
| Trace components N_2 | ≤ 100 | ppm |
| Trace compents CO_2 | ≤ 2 | ppm |
| Trace compents sulphur | ≤ 4 | ppb |
| Natural gas composition | Moomba, SA | - |
| Hydrogen demand | 350, 700, 1000 | kg/day |

the early stage of hydrogen injection in Australia, and is therefore chosen to be most relevant in this early stage feasibility study. The system is designed for three different sizes of hydrogen demand at a refuelling station, representing a small, medium, and large station. The compression and storage required after the separation process in order to supply the fuel cell vehicle at the specified pressure of 700 bar is optimised according to the demand. The boundary limits that define the scope of this thesis are listed in Table 1.2.

This master thesis aims at effectively designing a pressure swing adsorption system for the separation of hydrogen from natural gas, which is blended and transported in the existing pipeline network, for the use of hydrogen at refuelling stations for fuel cell vehicles.

The object of this master thesis twofold;

- (a) Design a PSA system to separate a feed of either 5 vol% or 10 vol% hydrogen mixed with natural gas at 20 bar.
- (b) Asses the economic feasibility of the PSA system at a refuelling station and compare with alternative solutions.

1.6 Outline

In Chapter 2, the literature review of this thesis is provided. The review is presented in two parts. The first part focuses on the gas separation, exploring the different separation methods possible for the separation of hydrogen from natural gas. Adsorption is selected as the separation method in this thesis, which will be used in a pressure swing adsorption system. In the second part, the main components of a hydrogen refuelling station are reviewed, as well as a detailed discussion on the transportation of hydrogen in the natural gas network in Australia.

Chapter 3 provides the methodology used. The approach for the process design, focusing on the selection of adsorbent materials, and the process analyses, based on MINSA simulations, are explained. Furthermore, the design approach of the refuelling station, focusing on the PSA system and the compression and storage separately, is provided. Lastly, the methodology for the techno-economic analysis for the refuelling station presented.

Then, Chapter 4 presents the results and discussion of the material selection and the process simulations. Chapter 5 presents the results and discussion of the techno-economic analysis.

Lastly, Chapter 6 offers conclusions and recommendations for future work.

Chapter 2

Literature Review

2.1 Introduction

In this chapter, the literature review performed for this thesis is summarised. It is split up in two different parts. The first part is schematically depicted in a flow diagram in Figure 2.1. Various gas separation methods are discussed, which are possible for the separation of natural gas and hydrogen, such as absorption, cryogenic distillation, membrane separation, and adsorption. Then the application of adsorption in various processes is further evaluated, where pressure swing adsorption, temperature swing adsorption, vacuum swing adsorption, and the dual reflux process are examined. Pressure swing adsorption is the most widely used form of adsorption process, of which the common applications, like hydrogen purification and CO₂ capture are explained. Finally, the literature available on methods for separation of hydrogen from natural gas is provided, given a state-of-the-art of the research conducted in this thesis.

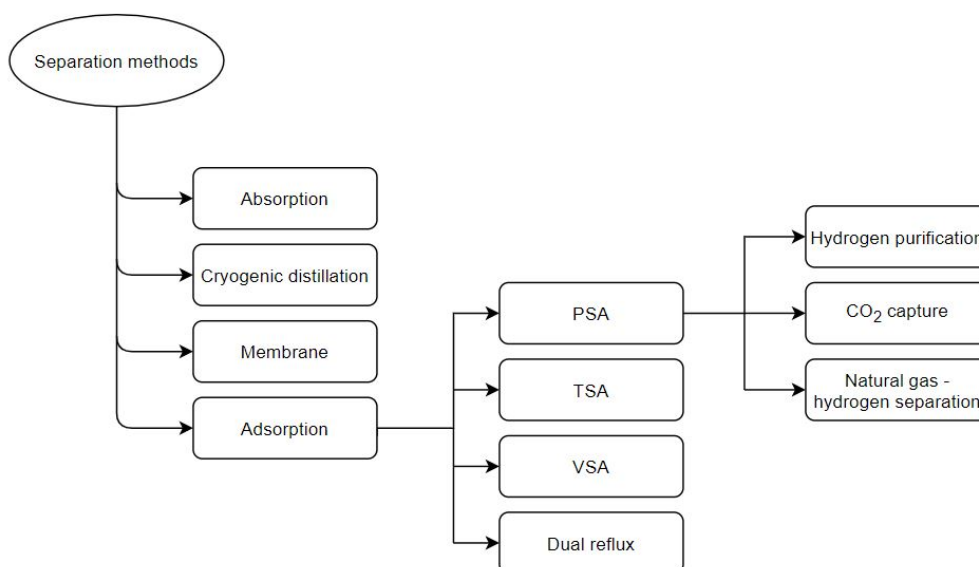


FIGURE 2.1: Flow diagram literature review.

The second part of the literature review focuses on the hydrogen refuelling station. A review of the main components present at a hydrogen refuelling station is provided, as well as a discussion on the safety issues to be considered. Lastly, it reviews the implications and challenges of transporting hydrogen in the existing natural gas pipeline network to a refuelling station.

2.2 Gas Separation Methods

Different separation technologies exist that are suitable for gas separation. However, not all are directly suitable for the separation of hydrogen and natural gas at a hydrogen refuelling station. First of all, the hydrogen product must be of high purity, to be able to use as fuel for fuel cell cars. Furthermore, a high recovery is preferable. Lastly, the cost of the system must be economical at a small scale, such that it can be directly installed at a refuelling station. This section provides an overview of several common separation methods with both their advantages and disadvantages for the required application.

2.2.1 Absorption

In gas absorption, gas is absorbed by a liquid solvent to purify gas streams or to recover a product. The product leaves the absorption column at feed pressure. To regenerate the liquid solvent, a thermochemical process is required, to release the absorbed gases again at high temperatures [36]. This is a very energy intensive process and therefore significantly increases the cost of the separation.

Typical gas purification processes include the removal of CO₂ from hydrogen in ammonia production and the purification of natural gas by removing acid gases [37]. Currently no absorption processes are developed yet for the separation of hydrogen and natural gas. There is no selective solvent for hydrogen, so therefore a solvent capable of absorbing all components in natural gas is required to achieve a pure hydrogen product [38].

2.2.2 Cryogenic Separation

Cryogenic separation is the partial condensation of gas mixtures at very low temperatures and high pressures, where the gases are separated by distillation [36]. This process is known to be highly energy intensive and thus costly. It is, therefore, only cost-effective at a large industrial scale. Furthermore, it has the advantage of producing the product as a liquid, which can be stored easily at large quantities [32].

In the case of hydrogen separation at a refuelling station, large scale options are not suitable. Therefore, cryogenic separation of hydrogen and natural gas will not be economically feasible as smaller wide spread units at refuelling stations.

2.2.3 Membrane Separation

Membrane separation is a pressure gradient driven process, producing a low pressure product output. This is disadvantageous for the use of hydrogen as a fuel for fuel cell cars, as a high pressure is required, and thus increases the costs for compression. Membrane separation is, however, a very simple, low cost, and energy efficient process [36]. Membranes are generally considered most suitable for bulk separation processes since only moderate purity is attained [39].

There are numerous different membranes suitable for the purification of hydrogen. The main three membranes are porous membranes, dense membranes and protonic membranes [32]. There is a wide range of porous membranes available for hydrogen purification, such as zeolites or alumina-based ceramics, however none are commercially feasible yet [32].

Dense metal membranes are currently the most advanced technology used for hydrogen purification, of which palladium membranes are most commonly used in industry, providing an excellent hydrogen selectivity. A good purity is therefore achievable, which is an important constraint for the hydrogen use as a fuel. A recovery of around 85% can be achieved [36]. Palladium is however a scarce and expensive material, which does not make it suitable for a large scale industrial application. Furthermore, it is prone to hydrogen embrittlement, specifically at low temperatures. Therefore, a high temperature operation is required (400 - 500 °C) [36].

2.2.4 Adsorption

Adsorption is the binding of a gas molecule on a solid surface by forming attractive forces [40]. These attractive forces are a result of the reduction in potential energy, due to the interaction of atoms and molecules in the adsorbent material and adsorbate gas or fluid. This results in an increased molecular density in the proximity of the surface compared to the free phase [41]. Adsorption is an exothermic process, whereas the reverse process, desorption or regeneration, is endothermic. It is achieved by reducing the pressure or by raising the temperature, and allows for recovery of the adsorbent. Adsorption is a dynamic equilibrium of adsorbed and desorbed particles.

The state-of-the-art hydrogen purification technology used in industry is pressure swing adsorption, in which gases adsorb to an adsorbent material at high partial pressures [32]. There is no adsorbent material which is able to adsorb hydrogen efficiently, due to the characteristics of the hydrogen molecule being very small and relatively inert. The purification of hydrogen in a PSA process therefore relies on the adsorption of the other gases, leaving the hydrogen out at the top of the column.

A high pressure is required to adsorb the gases in the mixture to the adsorbent, which is achieved by using a high pressure input feed. The gas mixture taken from the natural gas pipeline at a refuelling station will have a sufficiently high pressure to ensure a good separation. This diminishes the need for compressing the gas mixture, which is

usually the most power consuming process, and thus the operational cost are very much reduced. The capital costs for a PSA system are low compared to the capital costs for cryogenic distillation [42]. PSA process can obtain very high hydrogen purity product, which is required for the use of hydrogen as a fuel.

2.2.5 Hybrid System

A significant amount of research has been undertaken in combining membrane separation and PSA separation process, in which the advantageous characteristics of both process are exploited [38, 39, 42–44]. Two configurations can be classified, in which a membrane separation is either followed by a PSA process or follows up after the PSA. In the first configurations, the membrane performs the bulk separation after which the PSA ensures the purity of the product is achieved. In the second configuration, the waste stream of the PSA process is used as feed stream for the membrane, to increase the recovery.

Several studies show the potential of using a hybrid system for separation hydrogen and natural gas, which will be further elaborated on in Section 2.7.

2.3 Adsorption Technology

The gas separation method used in this thesis is adsorption technology, because of the high purity hydrogen that can be obtained, the high recovery, and the high product pressure obtained. The process used is pressure swing adsorption (PSA), which exploits the adsorption of gases on adsorbent materials in a cyclic process. The adsorbent material is key in the design of a PSA system, which determines the operation performance, design, and cost. This section discusses the principles of adsorption in detail, starting with the adsorption kinetics. This is followed by a review on the adsorption isotherms and the selecting criteria of adsorbent material. Then a number of common adsorbent materials and the adsorption in a fixed bed are discussed.

2.3.1 Adsorption Kinetics

The adsorption of a solute onto a porous surface incorporates a four step process [40]. Firstly, an external mass transfer of the solute from the bulk fluid to the outer solid surface of the adsorbent occurs. Then, the solute diffuses from the outer solid surface to the inner solid surface known by means of internal mass transfer. Next, it diffuses along the porous surface, and lastly it adsorbs onto the porous surface. All steps are reversed during desorption. The internal mass transfer is generally dominating the diffusion and thus controls the adsorption rate.

Adsorbents can be subdivided into two classes: homogeneous and composite microporous adsorbents, as illustrated in Figure 2.2. Homogeneous adsorbents are made up of a persisting pore network throughout the particle, whereas composite adsorbents have a pore network formed by aggregation of small microporous microparticles. The

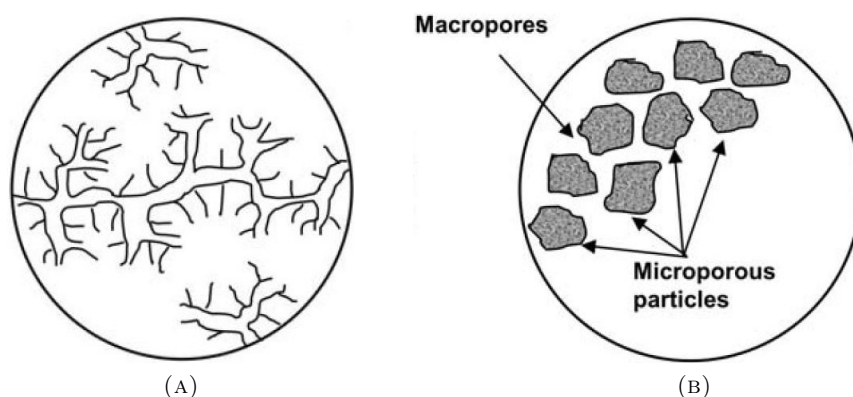


FIGURE 2.2: Homogeneous and composite microporous adsorbent particle [40].

macropores within the pellets connect to the micropores in the microparticle, creating a bimodal character of the pore size distribution because of the two different forms of carriers. Typically, micropores are characterised by a diameter of less than 2 nm and macropores by diameters of more than 50 nm [41].

The transport in the macropores can result through multiple forms of diffusion. Bulk molecular diffusion dominantly occurs in liquid phase systems, whereas Knudsen diffusion and surface diffusion dominate in vapour phase systems. Knudsen diffusion only occurs in the gas phase, as the molecules collide with the surface more frequently than with each other, because the mean free path of the molecules is larger than the pore size. In the liquid phase the mean free path of a molecule is generally very small, similar to the diameter of the molecule itself, and thus Knudsen diffusion does not apply. Macropores generally serve as superhighways for molecules to diffuse into the interior pores of the adsorbent [40].

In the micropores, the molecules never escape the force field of the wall and therefore no Knudsen diffusion can apply. In these very small pores, it no longer makes sense to distinguish molecules as adsorbed or free. Therefore, generally all molecules are regarded as adsorbed in the micropores.

Surface diffusion occurs by jumps from site to site on the surface, where temperature and concentration play an important role in the diffusivity. Only in relatively large pores and at relatively large pressure, the flux from Poiseuille flow contributes to the diffusivity. All contributions add up directly to the combined diffusivity.

2.3.2 Adsorption Isotherms

The adsorption characteristics of an adsorbate on a specific adsorption material are represented in an isotherm. This is a graph representing the amount of adsorbed gas for increasing pressure or concentration at fixed temperature. Brunauer classified five different types of isotherms, which are depicted in Figure 2.3. Type I and II isotherms are most favourable, because both have strong initial adsorption, even at low pressure or

concentration, and thus a large working capacity can be achieved. This will be further elaborated on in Section 2.3.3.

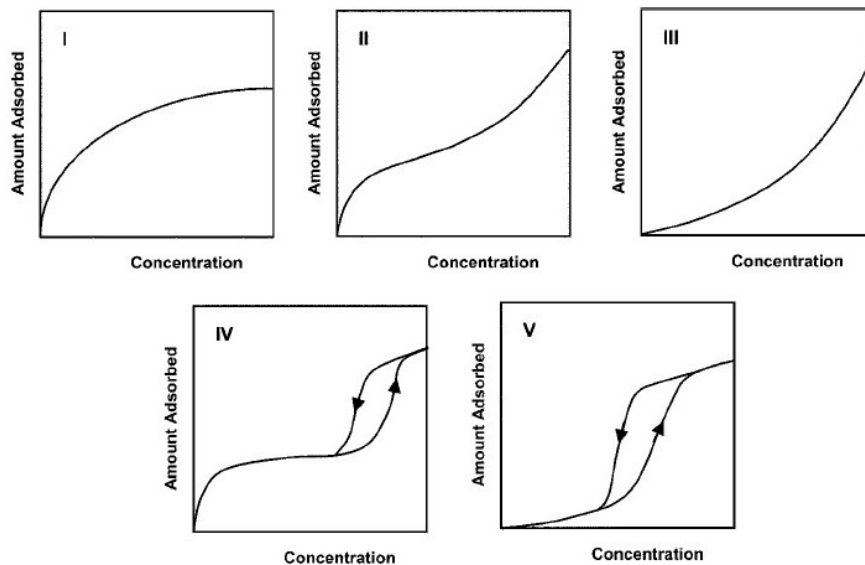


FIGURE 2.3: Brunauer classifications of adsorption isotherms [40].

The isotherms can be represented by different models. The simplest model follows Henry's Law and assumes a linear isotherm profile,

$$q_i = H_i p_i \quad (2.1)$$

Here q is the amount of adsorbed species i , H is Henry's constant [bar mol/kg] and p is the partial pressure of gas i . A linear profile can be assumed for adsorption on a surface at sufficiently low concentrations [41].

The type I isotherm is very well modeled with the Langmuir isotherm, which approaches Henry's Law at low concentrations and reaches the saturation limit at high concentrations,

$$\frac{q_i}{q_{sat,i}} = \frac{b_i p_i}{1 + b_i p_i} \quad (2.2)$$

Where b_i is the Langmuir constant [bar⁻¹]. The Langmuir model is simple, but provides a qualitative representation of the adsorption behaviour in many systems. It is therefore a commonly used and can be simply extended for multiple components.

Another variation of the Langmuir isotherm is the dual-site Langmuir isotherm, which is two Langmuir isotherm equations summed together,

$$q_i = \frac{q_{max,B} B p}{1 + B p} + \frac{q_{max,D} D p}{1 + D p} \quad (2.3)$$

$$B = b_0 \exp \frac{-Q_B}{RT} \quad (2.4)$$

$$D = d_0 \exp \frac{-Q_D}{RT} \quad (2.5)$$

Where Q_B and Q_D represent the heat of adsorption for the adsorption on two different types of sites.

The Langmuir model can also be extended for multi-components which is applicable for the adsorption of mixtures. In that case the isotherm is presented as,

$$\frac{q_A}{q_{sat,A}} = \frac{b_{APA}}{1 + b_{APA} + b_{BPB} + \dots} \quad (2.6)$$

The more different gases in the mixture, the smaller the adsorption of each component due to the decrease in respective partial pressure, compared to single gas adsorption.

The Freundlich isotherm is another representation of the type I isotherm and regarded as an empirical expression. In contrast to the Langmuir isotherm, it does not comply with Henry's Law at low concentrations,

$$q_i = b_i p_i^{1/n}, \quad n > 1.0 \quad (2.7)$$

A combination of the Langmuir and Freundlich isotherm provides greater flexibility. It should be noted that this is a purely empirical expression [41],

$$\frac{q_i}{q_{sat,i}} = \frac{b_i p_i^{1/n}}{1 + b_i p_i^{1/n}}. \quad (2.8)$$

The Langmuir-Freundlich isotherm can also be extended for multicomponent gas mixtures in the same way as the Langmuir isotherm as represented by Equation 2.6.

Lastly, the type II and type IV isotherm are commonly represented by the BET isotherm [45],

$$\frac{q_i}{q_{sat,i}} = \frac{b_i (p_i/p_{sat,i})}{(1 - p_i/p_{sat,i})(1 - p_i/p_{sat,i} + b_i p_i/p_{sat,i})} \quad (2.9)$$

2.3.3 Selection Criteria for Adsorption Materials

The design of a PSA cycle is largely dominated by the selection of the ideal adsorption material [46]. There exist many different types of adsorbent materials, of which the main ones are listed in Table 2.1. A classification can be made between equilibrium selective

TABLE 2.1: Classification of commercial adsorbents [40].

| Equilibrium Selectivite | | Kinetic Selectivite | |
|---------------------------------------------------|-------------------------------------------------------------------|-------------------------|---------------------|
| Hydrophylic | Hydrophobic | Amorphous | Crystalline |
| Activated Alumina | Activated Carbon | Carbon Molecular Sieves | Small-pore zeolites |
| Silica gel | Microporous silica | | |
| Al-rich zeolites | Silicalite, dealuminated mordenite and other silica rich zeolites | | |
| Polymeric resins containing -OH groups or cations | Other polymeric resins | | |

and kinetic selective materials, where equilibrium selective materials form the dominating group and are controlled by the physical adsorption equilibrium. These materials again can be subdivided into hydrophylic (polar) and hydrophobic (non-polar) surfaces, of which hydrophylic surface attract water much more strongly than hydrophobic surfaces. Polar molecules are attracted much more strongly by polar surfaces, but non-polar molecules are attracted by polar and non-polar surfaces similarly [41]. Kinetic selectivity is controlled by the pore size distribution of the adsorbent material and therefore functions as a molecular sieve. The adsorbents are either amorphous, non-crystalline structures, and crystalline structures.

The literature on adsorbent materials is very extensive. In order to select a material for a specific a PSA process, a screening of the different materials based on their working capacity, working selectivity, and heat of adsorption can be made. PSA is a cyclic process in which the gas is adsorbed at a high pressure, the adsorption pressure, and desorbed at the low pressure, desorption pressure, in the cycle. The working capacity is defined as the difference in the loading of the adsorbent at the adsorption pressure and the desorption pressure. In Figure 2.4 the isotherm for methane adsorbed on activated carbon at three different temperatures is represented [47]. The difference in the amount of methane adsorbed at the adsorption pressure, here 16 bar, and the desorption pressure, in this case 4 bar, is the working capacity. The pressure range is the working pressure at which the adsorption cycle operates. The working capacity can be represented as follows,

$$\Delta q_i = q_i(p, T)_{ads} - q_i(p, T)_{des} \quad (2.10)$$

The working selectivity of the material is defined as the affinity of the adsorbent for the adsorption of gas i over gas j , in the case of multicomponent gas adsorption. The selectivity is therefore the working capacity of gas i over the working capacity of gas j . This can be represented as,

$$\frac{\Delta q_i}{\Delta q_j} = \frac{q_i(p, T)_{ads} - q_i(p, T)_{des}}{q_j(p, T)_{ads} - q_j(p, T)_{des}} \quad (2.11)$$

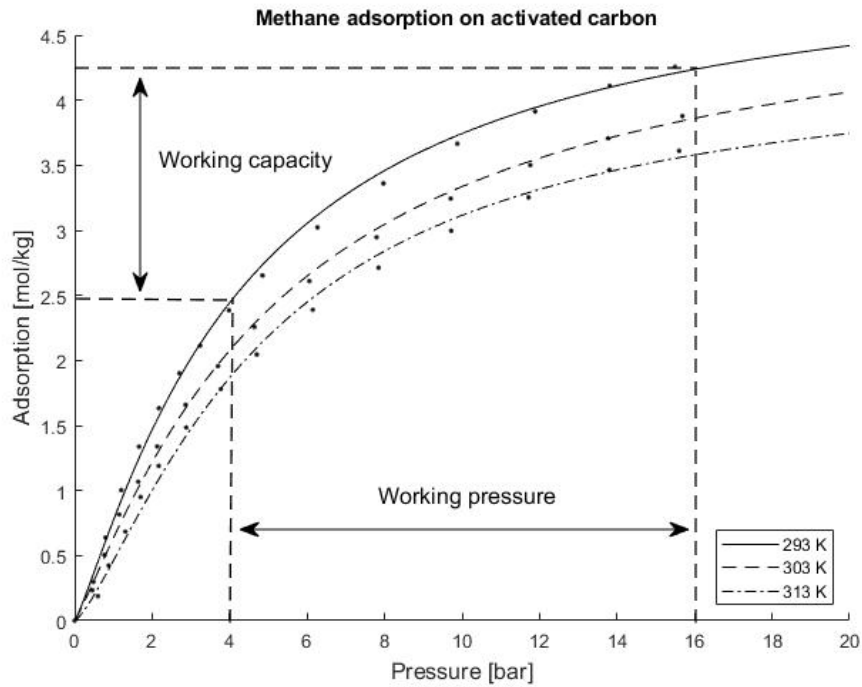


FIGURE 2.4: Isotherm of methane on activated carbon for different temperatures. Working capacity is the total amount adsorbed between the adsorption and desorption pressure, represented here as 16 and 4 bar respectively. The isotherms are presented by the Langmuir-Freundlich isotherm for three different temperatures. As the temperature increases, the total adsorption amount decreases. Data used from [47].

The heat of adsorption provides insight in the heat released during adsorption, where a high heat of adsorption relates to a strong adsorption. This can be calculated using the Clausius-Clapeyron equation,

$$\frac{\partial \ln p}{\partial T} = \frac{\Delta H_{vap}}{RT^2} \quad (2.12)$$

Furthermore, the physical strength of the adsorbent is important as well when selecting a material for the adsorption bed in the PSA process. Due to reoccurring pressurisation and depressurisation of the bed, the adsorption material erodes and thus loses strength. It is costly and time consuming if the adsorbent bed needs replacement frequently while the PSA process is operational.

2.3.4 Adsorbent Materials

There is a wide range of adsorbent materials available, each having different characteristics for gas adsorption. Some of the common adsorbents frequently used in industry are reviewed in this section.

Activated carbon is a well known adsorbent material, first used in an industrial application in the mid-19th century as filter in a ventilation system [48]. It has been

used in many different adsorption processes both for liquid and gas adsorption and is very suitable in industry, as it contains a well-developed pore structure, high surface area and good mechanical characteristics [49]. The characteristics of the activated carbons depend on the starting material and the activation procedure. Activated carbons are produced from coal or petroleum, but more recently from lignocellulosic materials, which is an abundant and low cost material. Examples can be hardwood, palm seeds, coconut shell, or even date stones [48, 49]. The pore size distribution and surface polarity can vary widely and influence the performance of the activated carbon. Activated carbons are mainly used for the removal of hydrophobic organic species.

Zeolites have a crystalline structure which acts as a sieve. The diameter of the channels formed in the framework determines the size of the molecules that can enter. Common zeolites are type A, X, and Y zeolites, of which a schematic framework structure is depicted in Figure 2.5. The frameworks are a tetrahedrally connected assemblage of SiO_2 and AlO_2 units [41]. The first use of zeolites was in the 1950s for gas chromatography [50]. Today, zeolites have been used for air separation and purification, hydrocarbon separation and purification, and natural gas upgrading, to name a few. The thermal stability and low cost of the natural zeolites are favourable characteristics for their use [51].

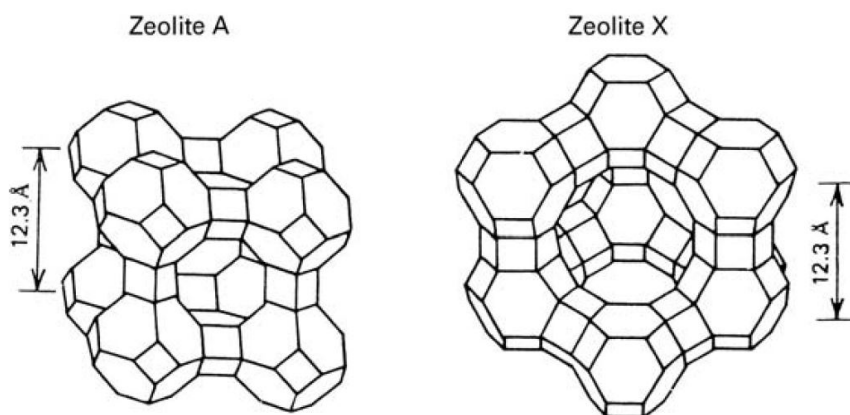


FIGURE 2.5: Schematic structure of (a) zeolite A, and (b) zeolite X and Y [40].

Silica gel is mainly made of SiO_2 and is mostly used for the removal of water, as it has a large capacity for water and can easily be regenerated [52]. If hydroxyl groups are present, the surface shifts to hydrophilic, because the hydroxyl groups make it possible for hydrogen bonds to form at the surface. Therefore, the silica surface is an intermediate between hydrophilic and hydrophobic material [41].

2.3.5 Adsorption in Fixed Bed

The adsorption behaviour of an adsorbent material in a fixed bed is represented with a breakthrough curve. A breakthrough curve is a representation of the adsorption concentration at the adsorption bed as a function of time, starting from the start of the flow.

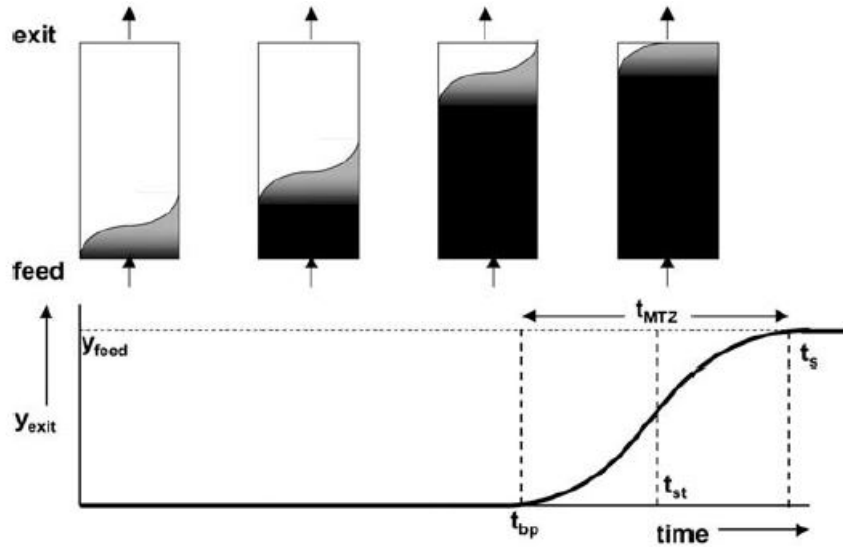


FIGURE 2.6: Breakthrough curve for non-ideal system [40].

In an ideal fix-bed, the breakthrough curve is a sharp wave. Behind the wave front, the adsorbent bed is saturated with the adsorbate and the concentration of the input fluid is that of the feed. Ahead of the wave front and in the exit fluid, the adsorbent is adsorbate free. The wave reaches the breakthrough point if the input fluid reaches the outlet of the bed. In the ideal system the adsorbent is fully saturated with adsorbate. This is known as the breakthrough point.

In a non-ideal system, internal and external transport resistances influence the fluid flow, as well as the axial dispersion within the adsorption material. This results in a S-shaped concentration front in the breakthrough curve, which is depicted in Figure 2.6. At the break-point time, t_{bp} , the wave front reaches the outlet of the bed. The run continues until the whole bed is saturated at t_{sat} and the outlet concentration is equal to the inlet concentration. The region in between the break-point time and the saturation time is defined as the mass transfer zone where the adsorption takes place. The steepness of the curve is a representation of how much of the capacity of the adsorption bed can actually be exploited and can decrease or increase with time, depending on the adsorption isotherm [40].

2.4 Pressure Swing Adsorption Process

Adsorption is used in a pressure swing adsorption (PSA) process. The principle function of PSA is to separate or purify gasses within a mixture, by means of the adsorption of one or more gasses on an adsorption material. The adsorbed gasses are regenerated by reducing the partial pressure. It is a low-cost and energy efficient separation technology frequently used in industry [41].

In the following sections, various PSA process designs are explained, starting with the Skarstrom cycle and the Guerin-Domine cycle, which mark the start of the development

of the PSA process. The initial practical use of the PSA cycle by Skarstrom focused on the drying of air. Other early applications are the separation of air, either for the generation of O₂ or N₂ [53]. Then, the fundamental design parameters that should be considered when designing and optimising a PSA process, purity and recovery, are discussed. Lastly, a review on layered bed adsorption is given.

2.4.1 Basic Process Cycles

The Skarstrom cycle, which dates back to 1958 [54], is known as the introduction to the PSA process. The cycle is developed for an equilibrium separation process and is schematically depicted in Figure 2.7. The design consists of two connected beds, which follow a four step cycle,

1. Pressurisation
2. Adsorption
3. Countercurrent blowdown
4. Countercurrent purge

The two connected beds follow the sequence of steps in such a way that there is a continuous flow of product gas. In the first step, column A is pressurised with the feed gas while column B is depressurised to atmospheric pressure, also known as the countercurrent blowdown. Once column A is pressurised, the adsorption step starts. A small gas flow of the generated product is fed countercurrently, with respect to the feed, into column B to purge the bed. Once the purge step is finished, the bed is ready for a new adsorption cycle. Bed B is now pressurised with the feed stream while bed A is depressurised to atmospheric pressure and the cycle can be repeated.

During adsorption, a continuous flow of feed gas is entering the column. The feeding time depends on the breakthrough of the most strongly adsorbing gas. As soon as the impurity of the output gas stream increases above a predefined acceptable limit, the adsorption phase is finished and the flow of feed gas stops. After the adsorption step, the bed is saturated with the strongly adsorbing specie. It is recovered in the two consecutive steps: countercurrent blowdown and countercurrent purge. The countercurrent flow ensures the regeneration of the product end, such that in the following adsorption step the impurity of the product gas is minimised. The blowdown serves as an initial desorption and decreases the amount of purge required to regenerate the bed. The purge is used to flush the void spaces in the adsorbent material. A trade off has to be made between the decrease in product recovery, as part of the product is used during the purge step, and the degree of product purity. The Skarstrom cycle was initially designed for the separation of air, and is widely used for air-drying [53].

Skarstrom defined some basic rules for the design of a PSA cycle. First of all, the heat of adsorption produced during the cycle should be controlled by using a short cycle

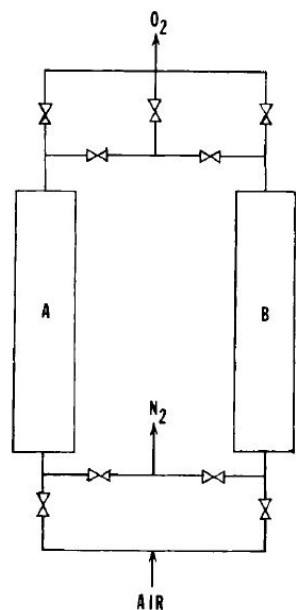


FIGURE 2.7: Skarstrom cycle [53].

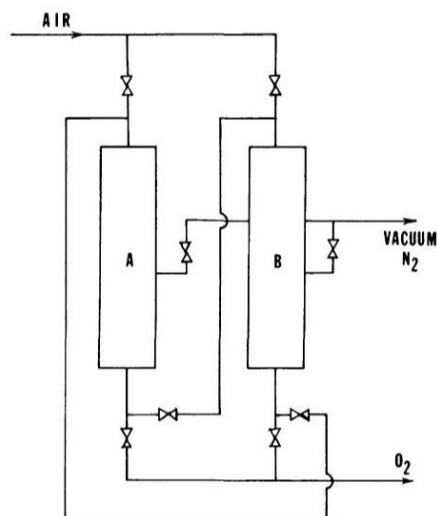


FIGURE 2.8: Guerin-Domine cycle [53].

with a low throughput per cycle, in order to maintain an isothermal operation. Secondly, for an increased product purity, the amount of purge used must comply the 1:1 volume ratio of purge to feed, which ensures a complete displacement of the gas in the bed and thus enhances the product purity achieved. Thirdly, purity is also controlled by the absolute pressure ratio, which should be greater than the reciprocal of the mole fraction of product in the feed stream [53, 55].

The Guerin-Domine cycle, which is schematically depicted in Figure 2.8 as a two column cycle, was approximately filed at the same time as the Skarstrom cycle [53]. Each bed follows a three step cycle: pressurisation, depressurisation, and evacuation. Similar to the Skarstrom cycle, bed A is pressurised with the feed stream entering the top of the bed. Once the required pressure is reached, the top of the bed is closed and bed A is depressurised cocurrently, by connecting the bottom of bed A with the top of bed B, while the effluent is recovered as the raffinate product, O_2 . When the intermediate pressure is achieved, the bottom of the bed is closed and bed A is evacuated by the vacuum line which is connected to the middle of the bed. By lowering the pressure in the bed to a vacuum, the bed is regenerated, removing all the adsorbed N_2 . A significant improvement of product recovery can be achieved compared to the Skarstrom cycle which utilises a purge step for the regeneration of the bed. The same steps are performed by bed A and B consecutively, providing a constant product output flow.

The main disadvantage of this vacuum swing adsorption (VSA) cycle is the low pressure at which the product is delivered. Furthermore, the extra mechanical costs required to achieve a vacuum should be outweighed against the increase in product recovery.

2.4.2 PSA Separation Performance

The performance of a PSA process is primarily determined by the product purity and recovery [56]. Both can be calculated for the light top product or the heavy bottom product. The equations for the top product purity and recovery are as follows,

$$\text{Purity} = \frac{C_i^{top} Q_i^{top}}{\sum_{i=0}^N C_i^{top} Q_i^{top}} \quad (2.13)$$

$$\text{Recovery} = \frac{\int_0^t C_i^{top} Q_i^{top} - C_i^{purge} Q_i^{purge} dt}{C_i^{feed} Q_i^{feed}} \quad (2.14)$$

If the process is designed to generate a high purity product at the bottom, the concentration C_i^{top} and flow rate Q_i^{top} should represent the bottom product, instead of the top product.

There will always be a trade-off between the purity and recovery. The purity is enhanced by using more purge, as this will desorb all the components left in the column, starting off the new cycle with a cleaner bed. This does require the use of more product, which leaves the column at the bottom after the purge step, and thus decrease the recovery. A higher recovery can be achieved by using more pressure equalisation steps. As the beds are connected, energy is conserved and the losses in the final blowdown step will reduce, due to the smaller pressure difference.

2.4.3 Layered Bed Adsorption

In the case of separating hydrogen and natural gas in a pressure swing adsorption process, there are many different gases in the mixture that must be adsorbed in order to reach a high purity hydrogen product at the top of the column. Therefore, it is necessary to utilise different adsorbent materials layered in the bed for a good separation [57]. This does, however, add an extra challenge to the separation process, that is breakthrough constraints. All gases have different adsorption isotherms for each material, as discussed in Section 2.3.2. The main layer of the bed in the PSA cycle for separating hydrogen from the natural gas mixture will predominantly adsorb methane, which is the main component in the gas mixture. Other gases such as the heavy hydrocarbons tend to adsorb very strongly to this main layer, which can cause accumulation of these gases on the adsorbent material. To prevent accumulation of these gases they must be prevented from breaking through into the main adsorbent layer. This is achieved by using a pre-layer, which is capable of adsorbing the heavy hydrocarbons, but is also capable of desorbing the gases at their respective desorption partial pressures. Furthermore, the methane and the nitrogen should not breakthrough the entire bed, as this will increase the impurity in the hydrogen product.

In multicomponent adsorption, rollup is a common phenomenon. This effect is described as a hump on the breakthrough curve, which surpasses the inlet concentration

of the component. In an equilibrium driven separation, this hump is caused due to the light component being displaced by the heavy component on the adsorbent [58, 59]. The length of each layer is therefore crucial for an optimal performance of the process. Park et al. [58] evaluated that the optimal length of each layer is determined by the feed composition and feed velocity. All gases should breakthrough simultaneous in all layers in order to maximally exploit the adsorbent material. It is therefore important not only to choose the right adsorbent material, but also to determine the required length of each layer.

2.5 Other Adsorption Processes

This section starts with the explanation of various other adsorption cycles, namely the temperature, vacuum, and rapid pressure swing adsorption cycles. Then, the dual reflux PSA cycle, which is a combination of the pressure and vacuum swing adsorption cycle is discussed.

2.5.1 Temperature Swing Adsorption

Other than PSA, temperature swing adsorption (TSA) utilises temperature for the adsorption of gases, in which the adsorption occurs at the lower temperature and at higher temperature the bed is regenerated. The main use of a TSA is for the purification of gas streams, rather than the separation of gases [60]. Temperature swing is a very slow cycle, due to the time required to heat the entire bed to a specific temperature. Common cycle times are several hours up to several days. Therefore, the TSA cycle requires a high amount of energy and usually the columns are of significantly large size, which increases the amount of adsorbent required [61].

Another possible use of the TSA cycle is to regenerate very strongly adsorbed species that do not desorb during the PSA cycle. To prevent the accumulation of the trace elements, a TSA cycle can be used after a certain number of cycles. This is particularly useful for the desorption of the trace elements elaborated on in Section 4.2.4 and common practice in industry to ensure the adsorption capacity is kept at its maximum.

2.5.2 Vacuum Swing Adsorption

The conventional PSA system, based on the Skarstrom cycle, produces a light product, which is the weakly adsorbing gas, at a high purity. The strongly adsorbed gas, the heavy product, is stripped of the gas mixtures by adsorbing onto the adsorbent at high pressure. This cycle is therefore referred to as the stripping cycle. In some applications, however, the heavy product is required at high purity, for example, in CO₂ capture. This can be achieved by regenerating the adsorbent bed at vacuum pressure [62]. This process is also known as the enriching PSA cycle.

The heavy components adsorb very strongly onto the adsorbent, meaning the initial slope of the isotherm is very steep. In order to regenerate all of this product, atmospheric pressure is not sufficient. When the pressure is reduced to a vacuum pressure, the amount of heavy component regenerated increases. This is known as vacuum swing adsorption (VSA) and commonly used for CO₂ recovery [62]. There is, however, a trade-off between the power consumption required to reach the vacuum pressure and the recovery of the heavy product [63].

2.5.3 Rapid Pressure Swing Adsorption

A way to increase the process productivity of the PSA cycle is to speed up the cycle times. In rapid pressure swing adsorption (RPSA), the cycle times are reduced from minutes to seconds [64]. If the cycle time is below 30 seconds, the process is typically a RPSA process. The decrease of the cycle time does cause kinetic limitations, which results in longer mass transfer zones [56]. A lower purity and recovery are achieved compared to conventional PSA cycles and RPSA cycles have an increased energy consumption [65]. Rotary valves are commonly used, which are capable of controlling multiple ports of the different beds at the same time, such that all beds switch between steps at the exact same time.

Application of the RPSA is mainly in medical oxygen units, which are preferably smaller in size and thus portable. By reducing the cycle time, the productivity is increased and thus the PSA unit can be made smaller [56].

2.5.4 Dual Reflux Pressure Swing Adsorption

Both the stripping cycle and the enriching cycle have the disadvantage that only one of the product streams is at high purity. The dual reflux PSA combines both cycles into one unit such that both the heavy and the light product output streams are at a high purity. A conventional dual reflux PSA consists of two columns. The feed stream enters one of the two columns at an intermediate position, which divides the tank into a stripping section and an enriching section. Both beds are at a different pressure, so the pure products leave the columns at opposite ends. Both pure product streams are partially used to reflux the other bed, after passing a compressor to either increase or decrease the pressure of the stream. As the feed enters bed 1, bed 2 is being purged with the product stream of bed 1. In the second step, the two beds are connected in a pressure equalisation step. Once the equilibrium pressure is reached, the gas stream is compressed until the high pressure bed is repressurised to the high pressure while the other bed is blown down to the low pressure. The other half of the cycle repeats the same steps, but for the reversed beds [66, 67]. A half cycle of the dual reflux PSA process is depicted in Figure 2.9.

A dual reflux PSA has 4 possible configurations, depending on the bed through which the feed gas enters and the pressure transfer mode used [68]. The feed gas can either enter the high pressure bed or to the low pressure bed. For each of those configurations,

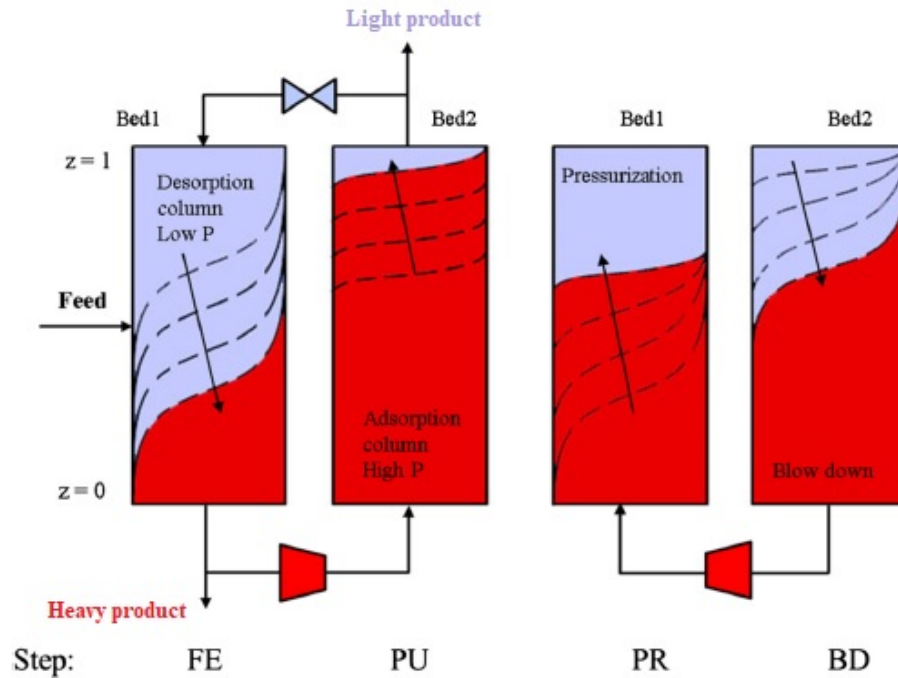


FIGURE 2.9: Dual reflux PSA half cycle [66].

the pressure transfer can be performed with the heavy product stream or the light product stream, resulting in 4 different configurations.

For the separation of hydrogen from natural gas, different applications are possible. This research focuses on the production of a high purity hydrogen product such that it can be used for fuel cell cars. However, it is also possible to design a PSA system in which both product streams are of high purity, such that both can be used for respective applications. Applications for high purity methane can be found in industry, where any hydrogen present in the mixture is harmful for certain equipment, such as turbines. Therefore, for further research, it could be interesting to investigate the possibility of using a dual reflux cycle.

2.6 PSA Applications

PSA is mostly used for air separation and hydrogen purification. There are, however, more applications of the PSA cycle possible. In recent years, with more focus on climate change, people reported more on the use of PSA systems for the adsorption of CO_2 . This section discusses the use of a PSA in hydrogen purification first. Then, the adsorption of CO_2 from post-combustion gas streams is discussed. Finally, adsorption for the upgrading of natural gas, by adsorbing CO_2 , is reviewed.

2.6.1 Hydrogen Purification

The most extensively used application of the PSA process cycle is for the purification of hydrogen from steam methane reformers or refinery off-gas streams. The off-gas streams are commonly at pressures between 8 and 28 bar at 21-38 °C. A typical SMR off-gas stream composition contains 70-80% H₂, with CO₂ as main impurity and traces of CH₄, CO, and N₂. Refinery off-gas streams are typically composed of 65-90% H₂, containing CH₄ as main impurity and only traces of C₂H₆, C₃H₈ [69]. Both streams are generally saturated with water, which must be removed as well in order to produce a dry hydrogen product of 98-99.999% purity with a recovery of 70-90%.

In order to purify hydrogen, a mixture of multiple other gases must be adsorbed in the PSA process to ensure a pure product. Selectivity over hydrogen is very high, which makes hydrogen very suitable for PSA separation. There is not one specific material capable of adsorbing all gases equally strongly to produce a pure product. A combination of multiple adsorbent materials is therefore used in each column. This has the advantage of selectively adsorbing each gas, in which the order of the layers is very important. Some gases have very high selectivity on certain adsorbent materials, which can cause accumulation of these gases on the material. This reduces the working capacity of the material and thus reduces the performance of the overall PSA process. Commonly activated carbon and zeolites are used as materials for hydrogen purification by PSA.

2.6.2 Post Combustion CO₂ capture

Recent increased environmental concerns have advanced the development of CO₂ adsorption by PSA systems. PSA process are reported to capture CO₂ from post combustion flue gas, in order to reduce the emissions of the plants. However, considering the capture cost, a lot of research is currently being undertaken into the development of better adsorbents, with high CO₂ selectivity [70]. Both PSA and TSA processes are possible for this operation, where PSA has the big advantage of faster cycle times and thus smaller beds. However, the pressure of flue gas after combustion is low, creating a need for compression. VSA is therefore the preferred operating cycle, for which zeolite 13X and activated carbon are the most commonly used adsorbents [61].

2.6.3 Removal of CO₂ from Natural Gas

Furthermore, natural gas gained increased attention as a more sustainable alternative for fossil fuels. It is less costly and has a more complete combustion resulting in less air pollution [71]. Wells with high CO₂ content become more interesting if the natural gas can be purified, which can be achieved with a VSA process.

Another source of methane can come from landfill gas, which is a mixture of 45-65% CH₄ balanced with CO₂ and some trace elements. Due to increased demand for methane, landfill gas can be purified by VSA to meet the pipeline methane specifications

[72]. Upgrading of landfill gas is not only beneficial for reduction of methane emissions, but also creates an energy market in countries that do not have natural gas resources.

2.7 Separation of Hydrogen from Natural Gas

This thesis focuses on the separation of hydrogen from natural gas transported in the existing gas grid. Several authors have researched the possibilities to separate hydrogen from natural gas, such that it can be used as fuel for hydrogen fuel cell cars. Liemberger et al. [38] investigated the use of a hybrid system with a membrane and PSA system to achieve the separation. Grainger et al. [73], Nayebossadri et al. [74], and Nordio et al. [75] focused on using a membrane only to separate the hydrogen. This section provides a review of the published literature available. There is no literature published yet on the use of a PSA alone to achieve the separation of hydrogen from natural gas, such that is usable as a fuel for fuel cell vehicles.

2.7.1 NaturalHy project

NaturalHy is a project with multiple European partners, investigating several critical issues concerning blending of hydrogen with natural gas in the existing pipeline network. Grainger and Hägg [76] conducted a research focused on the separation of hydrogen from natural gas by a carbon molecular sieve. The sieve is made from wood pulp, which creates a nanoporous carbon film, which is suitable only for hydrogen molecules to pass through and thus filtering the gas mixture.

Experiments were conducted for a mixture with 30 vol% and 5 vol% hydrogen at a pressure of 40 bar and 8 bar and a temperature of 25 °C and 90 °C. For the case where a pressure of 40 bar, temperature of 25 °C, and hydrogen concentration of 30% is assumed, the purity achieved is above 99.6% with a recovery of 90%. The recovery drastically drops (to 10%) when the purity is further increased to 99.9%. Furthermore, it was concluded that at higher temperatures the selectivity of the membrane is lower and thus the purity is not achieved anymore.

2.7.2 HylyPure Project

Liemberger et al. [77] published several papers on the separation of hydrogen from natural gas with a hybrid system of a membrane and PSA, which is called HylyPure. The membrane is used for the hydrogen enrichment of the gas mixture. Then a PSA process is employed for the purification of hydrogen to the required fuel cell quality. A schematic process overview is presented in Figure 2.10.

Separate experiments for the membrane separation and the PSA process were performed [38]. A polyimide membrane is used and tested with a feed mixture of 2-4% H₂, 1% CO₂, and methane entering at 51 bar. The hydrogen is enriched to 15-22% (v/v) at a pressure of 5-6 bar. Lower pressures result in higher enrichment. However, the PSA

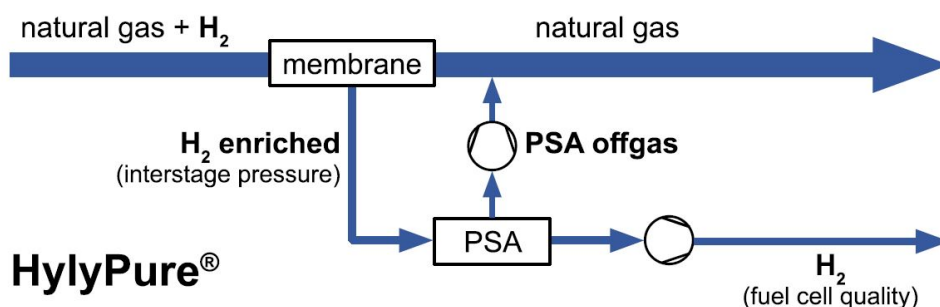


FIGURE 2.10: HylyPure process concept [77].

cycle requires a high pressure, so the enrichment is stopped when the hydrogen rich stream reaches 5-6 bar. CO₂ is known to plasticise the polyimide membrane, which reduces the efficiency or can even damage the membrane irreversibly. Other components in the natural gas mixture that are known for plasticising as well are heavy hydrocarbons. However, the partial pressures of these gases are low and thus are the permeabilities.

The PSA cycle is designed as a 4 bed 6 step process, including an adsorption step, blow down step, purge step, two cleaning steps for the pipes, and a pressurisation step. Materials used are silica gel as a pre-layer for the adsorption of water and heavy hydrocarbons, followed by an activated carbon layer for the adsorption of CH₄ and CO₂ and a final layer of zeolite 5A for the removal of N₂ and CO. A 20% hydrogen mixture with CH₄ is used for the experimental evaluation of the cycle in a bed with only one adsorbent layer of activated carbon. A purity of more than 98% is reached with a recovery of 55-65% is achieved for the single bed PSA cycle [38].

In a follow up paper, seven different process designs are investigated [78]. Various configurations are proposed including a second membrane and several variations of recompression. The one presented in Figure 2.11 is concluded to be the most energy

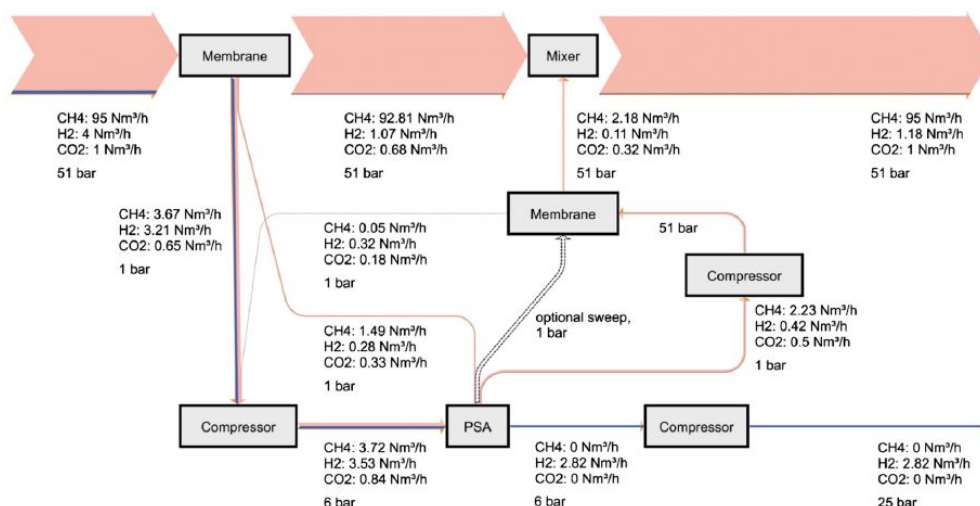


FIGURE 2.11: Process design with a second high pressure membrane in the recycle stream as proposed by Liemberger et al. [78].

efficient, with a decrease in energy demand by 60% and a reduction of 20% of the total membrane area and 50% of the PSA size compared to the initial HylyPure design. The cycle includes a second membrane, which is used to recycle the hydrogen present in the PSA waste stream, reducing the total energy demand. All results are based on simulations which investigated several influential parameters, such as the feed gas composition and pressure, and membrane selectivity.

2.7.3 Palladium-based Membranes

Nayebossadri et al. [74] studied the use of three different Palladium-based membranes, Pd, PdCu₅₃, and PdAg₂₄ membranes, for the separation of hydrogen from natural gas where the concentration of hydrogen is varied from 91% to 15%, operated at 400 °C with a 5 bar pressure differential. All three membranes showed an effective separation of hydrogen and natural gas, up to 15% hydrogen in the mixture. No exact product concentrations were provided, hence it is unclear if the hydrogen is suitable for fuel cell cars. Due to the high pressure gradient and elevated temperatures required for an efficient Pd-based membrane operation, the use of these membranes will be only cost effective in the high pressure transmission pipelines. Furthermore, Pd-membranes are highly sensitive to especially sulphur components present in natural gas. Further research is recommended to study the long-term effects of this on the separation.

The concentrations of hydrogen in the natural gas mixture research by [74] are quite high, at least 15% is required for the hydrogen to permeate through the membrane. The feasibility of adding hydrogen to the natural gas is currently being researched for an addition of 5-10% hydrogen, in Australia. The Palladium-based membranes will therefore only be relevant in a later stage if more hydrogen will be added. For the use of hydrogen as a fuel for fuel cell cars, the quality of the hydrogen is also an important aspect. No data is provided in by the authors, so it is unclear if the separation with a palladium-membrane can provide sufficiently pure hydrogen.

2.7.4 Hybrid Membrane System

Nordio et al. [75] studied the use of Pd-membranes and carbon molecular sieves membranes (CMSM) in different hybrid systems. Additionally, an electrochemical hydrogen compressor (EHC) is used for further purification of the membrane retentate outlet, separating the remaining hydrogen out of the gas stream before supplying it back to the grid. A temperature swing adsorption (TSA) technology is used optionally when sweep gas is used at the permeate side of the membrane. In that case the hydrogen stream must be further purified, removing the remaining water.

The various hybrid systems are designed for a hydrogen production of 25 kg/day. Configuration A consists of one membrane module and an EHC. Configuration B is made up of 2 Pd-membrane modules with a compressor in between, and an EHC are combined. The first membrane is used for an initial purification, whereas the second membrane further purifies the hydrogen. Configuration C is similar to configuration B,

however, now the membranes are placed in series, with no compressor in between. The types of membranes (Pd-based or CMSM) and permeate pressure are varied within this configuration, resulting in 5 sub-configurations. The last configuration, configuration D, consists of 2 membranes in series, where a sweep gas is used in the first membrane module, an EHC and a TSA unit.

The Pd-membranes require an operation temperature of 400 °C and the CMSM operates at 70 °C. The pressure of the gas mixture of hydrogen and natural gas is considered at 40 bar and 8 bar, representing a high pressure and low pressure grid connection. In terms of energy consumption, configuration C is the best configuration for a low pressure grid, with a purity achieved of 99.92%. Configuration B can increase the final hydrogen product to 99.99%, however this increases the energy consumption as well. CMSM achieve a lower purity, compared to Pd-based membranes, but have a lower energy consumption and capital cost as well. When using a high pressure input feed at 40 bar, configuration C provides a very high purity (99.99%). Comparing the purity and production cost, the authors conclude that their proposed systems are competitive with conventional separation methods, such as PSA.

The authors are very critical on the use of a PSA system in the introduction of their article. The main reason being that the cost for compression required in a PSA system are very high and have a high energy consumption. This is true if the feed gas has to be pressurised. However, the feed gas can directly be used at the pressure available in the pipeline. The only compression required then is the compression of the natural gas back into the grid. The membranes used in the study require elevated temperatures of either 70 °C or 400 °C, which also requires a lot of energy. Furthermore, the hydrogen product achieved with a membrane separation is at atmospheric pressure. When the hydrogen is used as fuel for fuel cell cars, the hydrogen must be compressed as well. The comparison of a PSA system used in industry for hydrogen purification cannot directly be compared with a PSA used for the separation of hydrogen and natural gas.

2.8 Pressure Swing Adsorption Simulation

To analyse the PSA system that will be designed in this study, PSA simulations will be used. It is not always possible to do experimental work on pressure swing adsorption processes, therefore simulations are a highly valuable tool to analyse processes. Experiments can be very costly and time consuming, so if no experimental facility is available or time is limited, simulations are commonly used to assess PSA processes.

The adsorption process within the PSA cycle is complex due to the large amount of variables within the system. This section provides a brief explanation of the equilibrium theory, which is the simplest way of representing the adsorption dynamics within the bed, and the linear driving force model, a more comprehensive model representing the intra-particle mass transfer. To represent the full PSA process, a more extensive model is required. In this thesis, MINSA is used as the process simulator, which is a simulator developed at Monash University and has been used for over 20 years in research on the

PSA process. The main working principles of MINSA will be explained at the end of this section.

2.8.1 Models used for PSA Process Simulation

To understand the dynamics within the adsorption column, the equilibrium theory can be applied. This theory assumes that there is a constant equilibrium between the fluid phase and the adsorbed phase, implying an infinite fast mass transfer [40, 41]. It is a useful theory for a first approximation of the breakthrough curve, and thus the length of the bed. The velocity of the solute concentration in the concentration wave front v_c is given in terms of the interstitial velocity of the fluid through the bed u and the slope of the adsorption isotherm $\frac{dq}{dc}$ at a specified concentration,

$$v_c \equiv \left. \frac{\partial z}{\partial t} \right|_c = \frac{u}{\varepsilon_{bed} + (1 - \varepsilon_{bed})\rho_{part} \left. \frac{dq}{dc} \right|_c} \approx \frac{u}{(1 - \varepsilon_{bed})\rho_{part} \left. \frac{dq}{dc} \right|_c} \quad (2.15)$$

This approximation can be made, because usually $\varepsilon_{bed} \ll (1 - \varepsilon_{bed}) \cdot \rho_{part} \cdot dq/dc$. For the equilibrium case of an adsorption and desorption process, Equation 2.15 can be used to analyse the development of the adsorption wave front. In Figure 2.12, three wave front scenarios are depicted for three types of isotherm: unfavourable, linear, and favourable. The development of the concentration gradient for the unfavourable isotherm is dispersive, as it increases the adsorption zone as it moves through the bed. The linear isotherm results in a steady, unchanged adsorption zone through the full length of the bed. Lastly, the favourable isotherm shows a wave front of which the gradient increases as it moves through the bed, since high concentrations move more rapidly through the bed. It is not physically possible for the high concentrations to move ahead of the low concentrations.

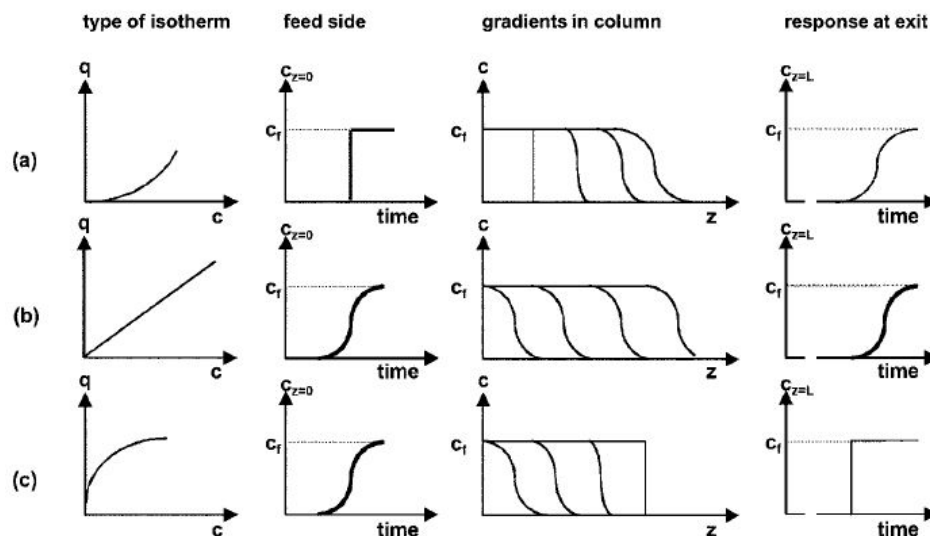


FIGURE 2.12: Development of an adsorption wave front through the bed for (a) unfavourable, (b) linear, and (c) favourable isotherm [40].

The equilibrium theory provides a good first insight in the adsorption dynamics, however, it does not consider temperature changes in the bed, nor particle kinetics. Especially, when the time scale of the process reaches a similar time scale as a gas molecule requires to move from an adsorption site to the bulk gas phase or the other way around, representing the mass transfer is increasingly important [79]. The Linear Driving Force model (LDF) is a frequently used mass transfer model for gas adsorption kinetics in PSA simulation. It is an analytical, simple, and physically consistent model [80]. It was first introduced by Glueckauf and Coates [81] in 1947 for adsorption chromatography, where a linear relation for the mass transfer driving force was assumed between the amount adsorbed of species i in equilibrium with the bulk flow q^* , and the average amount adsorbed, \bar{q} , of species i ,

$$\frac{\delta q_i}{\delta t} = k_i(q_i^* - \bar{q}_i) \quad (2.16)$$

Where k is the mass transfer coefficient [s^{-1}], defined as,

$$k_i = \frac{15D_i}{r_p^2} \quad (2.17)$$

This was first validated by Glueckauf and has been confirmed for many different initial and boundary conditions [55]. Furthermore, r_p is the pellet radius of the adsorbent material [m] and D_i is the diffusion coefficient of the component i [m^2s^{-1}], which is calculated in MINSA. The LDF model is very simple, but nevertheless works very well for process analysis. In the estimation of the separation, the kinetic properties described at the particle, column, and overall system are averaged several times. Therefore, detailed information of the adsorption at a local level is often lost and thus the LDF model proves a sufficiently detailed model [80].

2.8.2 Monash Integrated Numerical Simulator for Adsorption

In this thesis, the PSA process simulations are performed with the Monash Integrated Numerical Simulator for Adsorption (MINSA), developed by R.S. Todd, J. He and P.A. Webley at Monash University in 2001 [82, 83]. It is a flexible and fast model that can handle a large range of boundary conditions and can be used as a numerical simulation of experiments.

MINSA is a PSA process simulator, which uses the finite volume method to discretise the coupled partial differential equation, for the conservation of mass and energy, in space. This is done with the quadratic upstream interpolation scheme (QUICK). The resulting ordinary differential equations are then solved in time by a first-order, backward difference integrator (DVODE). This successive substitution is continued until cyclic steady state (CSS) is achieved. Despite the robustness of this method, it is a slow method to use to converge to CSS. In order to accelerate it, successive node refinement is used.

The Ergun equation is used to represent the pressure drop within the bed, which is a commonly used model as it models both laminar and turbulent flows through the bed. The heat of adsorption is calculated with the Clausius-Clapeyron equation (see Equation 2.12). The mass transfer is modelled with the linear driving force model (LDF), as explained in Section 2.8.1. The transport mechanism of the gas molecules is assumed to be controlled by molecular diffusion in the macropores. The void volume at the bottom and top of the bed can be included and are modelled as continuous stirred tank reactors with non-isothermal conditions. Isotherms can be presented in different forms, of which the extended dual-site Langmuir model was used in the simulations in this thesis.

Only one bed is simulated performing all steps in the cycle, as the other bed consecutively go through the same steps. The main equations used by MINSA in the simulation are presented below.

Extended dual-site Langmuir isotherm:

$$q_i = \frac{q_{max,iB} B_i p_i}{1 + \sum_{j=1}^{j=n} B_j p_j} + \frac{q_{max,iD} D_i p_i}{1 + \sum_{j=1}^{j=n} D_j p_j} \quad (2.18)$$

$$B_i = b_{i0} \exp \frac{-Q_{iB}}{RT} \quad (2.19)$$

$$D_i = d_{i0} \exp \frac{-Q_{iD}}{RT} \quad (2.20)$$

Conservation of Mass:

$$y \frac{\partial p}{\partial t} + p \frac{\partial y}{\partial t} - \frac{py}{T} \frac{\partial T}{\partial t} = -\frac{\varepsilon_b T}{\varepsilon_t} \frac{\partial}{\partial z} \left(\frac{vpy}{T} \right) - \frac{\rho_b RT}{\varepsilon} \frac{\partial n_i}{\partial t} \quad (2.21)$$

Conservation of Energy:

$$\rho_b \frac{\partial U_{solid}}{\partial t} + \varepsilon_t \frac{\partial (\rho_{gas} U_{gas})}{\partial t} = -\varepsilon_t \frac{\partial}{\partial z} (v \rho_{gas} H_{gas}) - \frac{4h_w l_0}{D_{v_0}} (T - T_W) \quad (2.22)$$

Ergun Equation:

$$-\frac{\partial P}{\partial z} = \frac{1.75(1-\varepsilon)\rho_g}{\varepsilon d_p} u^2 + \frac{12\mu(1-\varepsilon)^2}{\varepsilon^2 d_p^2} u \quad (2.23)$$

2.9 Hydrogen Refuelling Stations

The second part of this literature review focuses on hydrogen refuelling stations. Refuelling stations can have varying layouts, depending on where they are located, what their capacity is, and how the hydrogen is delivered to the station. To illustrate what a hydrogen refuelling station, where the hydrogen is delivered by a pipeline at 20 bar, could look like, a schematic site plan is depicted in Figure 2.13. There are a few main components which are required for each refuelling station, such as the dispenser, storage tanks, and compressors. This section discusses these components, as well as a general discussion on the safety of a hydrogen refuelling station. Finally, a review on the challenges of blending hydrogen into the existing natural gas network is provided.

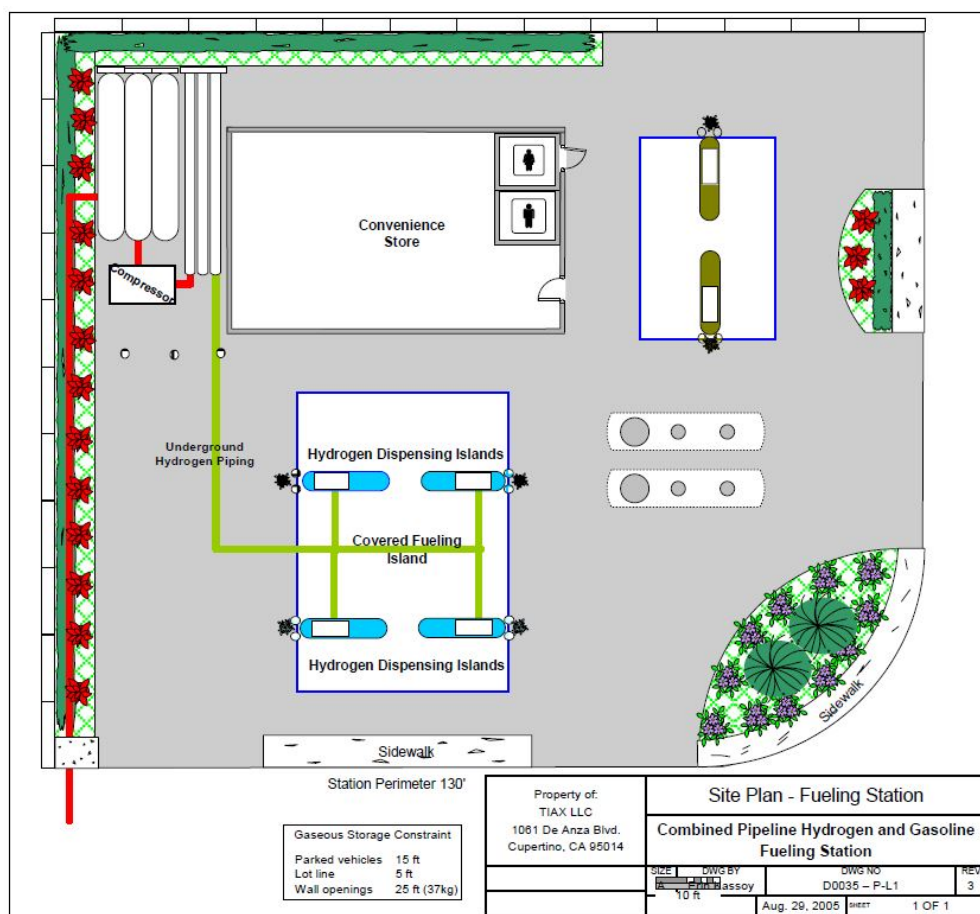


FIGURE 2.13: Site plan for a hydrogen refuelling station, combined with a gasoline station [84].

2.9.1 Dispenser

The main component is the dispenser, which injects the hydrogen into the hydrogen car. The fuelling protocol (J 2601) made by the Society of Automotive Engineers (SAE) ensures the hydrogen entering the car does not exceed 875 bar and 85 °C [20]. The dispenser must be able to withstand high pressure hydrogen. Especially the hose is a

challenging component, as it also requires to be flexible [85]. Therefore, the dispenser is a very expensive component, which will be addressed later in Section 3.5.

2.9.2 Heat exchanger

The temperature of the hydrogen can be controlled by a heat exchanger before the high pressure gas enters the dispenser. This is an essential step to ensure the safety of the dispenser. During compression of the hydrogen into the tank of the fuel cell car, the temperature of the hydrogen increases substantially [86]. The temperature of hydrogen before entering the dispenser must therefore be reduced to between $-33\text{ }^{\circ}\text{C}$ and $-40\text{ }^{\circ}\text{C}$ as defined by the fuelling protocol (J 2601). Only with sufficient cooling, the fast refuelling of a fuel cell car can be achieved [87].

2.9.3 Storage tanks

Hydrogen must be stored as compressed gas, to increase the energy density and decrease the size of the tanks and total size of the refuelling station. There are four types of pressure vessels that are suitable for hydrogen storage, which are listed in Table 2.2. Type I pressure vessel is the oldest, dating back to the end of the 19th century and is till today the most widely used type [88]. It can store hydrogen at pressures of 150 to 300 bar. For higher pressures, Type II pressure vessels are used in stationary applications. Type III and IV are typically used in portable applications, where weight is an important restraint on the design. The pressures can reach up to 450 to 900 bar [85]. These type of vessels are used in the current hydrogen cars. The choice of pressure vessel is a balance between the tank volume, storage pressure, size, and cost [85].

TABLE 2.2: Different types of high pressure hydrogen storage tanks [88].

| | |
|-----------------|-----------------------------------------------------------------------|
| Type I | All-metal vessel |
| Type II | Metal vessel, hoop wrapped with a fiber-resin composite |
| Type III | Metal vessel, axial and hoop wrapped with a fiber-resin composite |
| Type IV | Polymeric vessel, axial and hoop wrapped with a fiber-resin composite |

For hydrogen refuelling stations, different configurations of low, medium, and high pressure storage is possible. Depending on the size of the refuelling station, a preferred configuration must be selected. For low pressure hydrogen storage, Type I pressure vessels are commonly used [87]. Cascade vessels, which store hydrogen at pressures between 400 and 500 bar, are either of Type I or II. Type IV pressure vessels are required for high pressure storage of hydrogen up to 900 bar. The advantage of a high pressure vessel is that it can store more hydrogen per volume, however it is not always necessary to store hydrogen at such a high pressure. First of all, the costs of a high pressure vessel are significantly higher. Furthermore, a medium pressure hydrogen can be used to start the fuelling of a fuel cell car, followed by high pressure hydrogen supplied from

a high pressure storage tank. This reduces the total amount of hydrogen that must be compressed to fuel a car, and thus reducing the energy costs of compression [87].

Parks et al. [87] suggest two refuelling station configurations. In the first configuration, two compression steps are used. First, hydrogen is compressed to a medium pressure of 172-250 bar, which is used to start the refuelling of the fuel cell car. The second compression partially compresses the medium pressure hydrogen to a high pressure of 875 bar. This hydrogen is used to top off the fuel cell cars. Two medium pressure vessels storing 367 and 200 kg of hydrogen, and three high pressure vessels, each storing 43 kg of hydrogen, are used.

The second configuration also utilises a hybrid cascade system [87]. The two medium pressure vessels are replaced by one large vessel storing 400 kg of hydrogen at 500 bar, and the total high pressure hydrogen storage capacity is reduced to only one vessel, containing 50 kg of hydrogen at 950 bar. The optimal size and number of pressure vessels depends on the layout of the refuelling station and affect the performance and costs of the total system. Optimisation is therefore key in the design of a refuelling station.

Furthermore, two extra tanks must be considered in the final design of the refuelling station. One tank for the feed gas pumped out of the natural gas pipeline before it is fed into the PSA system. And one tank for the downstream product of the PSA cycle, which will be compressed back into the natural gas grid.

2.9.4 Compressors

The compression of hydrogen is the largest contributor to the costs of a refuelling station. Parks et al. [87] conducted a research to the technical status and costs of hydrogen refuelling stations where they compared different refuelling configurations. Compression of hydrogen to 900 bar or more can only be achieved in multistage compression. Compression of hydrogen generates heat, thus compression must always be combined with intercooling technologies for safety reasons [86]. Furthermore, it is important that the compressor does not contaminate the hydrogen with lubricants, as these affect the fuel cell performance. Lastly, the compressor must have a high reliability [85].

The reciprocating piston compressor and the diaphragm compressor are most commonly used. Diaphragm compressors are mainly used for small-scale application and are able to remove heat generated during compression more effectively [86]. This is accomplished by the large surface area of the diaphragm, the cooled compression oil, and a cooling system added to the cover of the compressor. Controlling the heat generated during compression is an important issue which has a large influence on both safety and efficiency.

In the refuelling station design, compressors are required for the storage of the pure hydrogen in pressure vessels, and for the repressurisation of the heavy down stream product before injecting it back into the natural gas grid.

2.9.5 Safety

An important aspect of the hydrogen refuelling station is safety. First of all, sensors able to detect any leaking hydrogen are very important for both safety and economic aspects [85]. Hydrogen sensors must be in place to monitor any leak near the dispenser, storage tank, or pipeline network. Furthermore, the quality of the hydrogen to be dispensed into the vehicle should be regularly checked to ensure the hydrogen is not in any way contaminated with other gases. If the hydrogen quality does not meet the ISO 14687-2 standard (see Table 1.1), it can be harmful for the fuel cell operating in the car.

The dispenser is one of the main components of concern with regards to customer safety. To ensure the hydrogen can be dispensed safely from the dispenser into the car, a safety protocol is developed. In Figure 2.14 the pressure is represented as a function of the fuelling time. In the startup time the nozzle is connected to the vehicle, and a connection pulse is performed. An initial leak check is performed before the start of the fuelling as well. The hydrogen is supplied from three different storage tanks at three different pressures. The switch between the tanks happens during the bank switching, which results in a short term fuelling pause [89]. All the while, fuel leak checks may be performed by temporally pausing the fuelling and measuring the pressure. If the pressure drops, a leak is present and the fuelling is stopped. Next to regulating the pressure during the dispensing, the temperature and flow rate are also regulated to ensure a safe filling of the vehicle tank.

The storage of a large amount of hydrogen at high pressures is also important to consider when designing a refuelling station. The main hazards with hydrogen storage

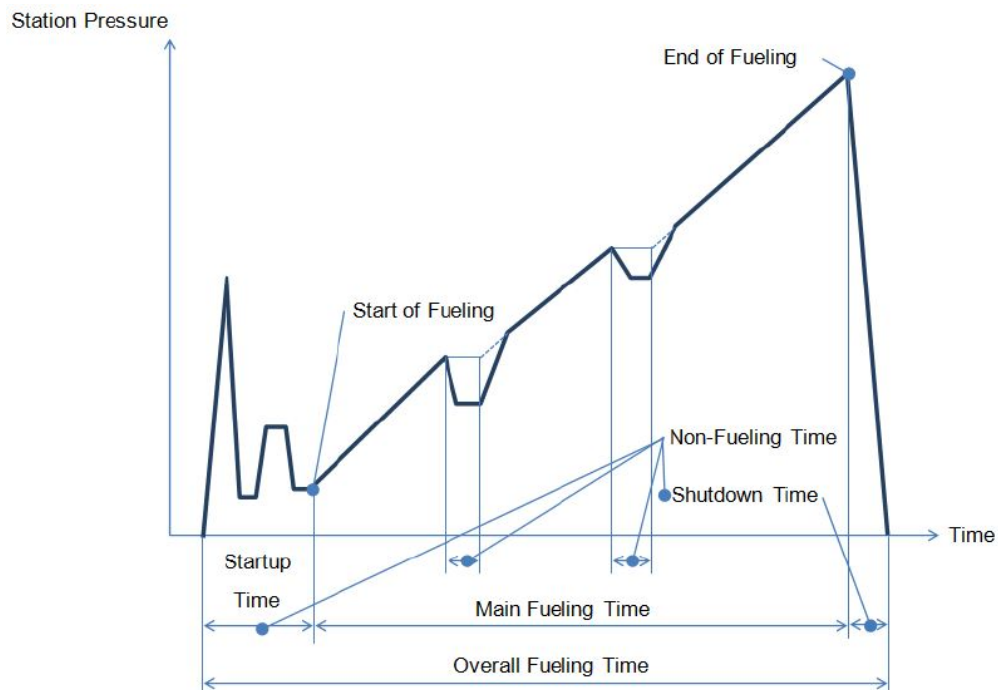


FIGURE 2.14: Pressure profile during the fuelling of a fuel cell car, according to the SAE J2601 protocol [89].

is a breakage or leakage which may cause the hydrogen to suddenly erupt with great pressure [90]. Underground storage of hydrogen can be considered to increase safety and to reduce the area footprint of the refuelling station [91].

2.9.6 Hydrogen Transportation

Hydrogen can be transported to a hydrogen refuelling station in different ways. At the moment, hydrogen refuelling stations are most commonly supplied by compressed hydrogen delivered by tube-trailers. The pressure in the tanks varies from 250 bar to around 500 bar. The higher the pressure at which the hydrogen is supplied, the smaller the compression and storage required at the refuelling station. The hydrogen can be directly used to start filling or can be compressed to higher pressure vessels [92]. The return pressure of the tube-trailers is a trade-off between the cost of compression and storage at the refuelling station and the cost for the delivery of the hydrogen to the station. A common return pressure is between 150 and 50 bar, depending on the configuration of the station.

Another way is transporting hydrogen through a pipeline network. This is a very efficient way of transporting gas, but it does require the construction of a new pipeline network suitable for the transport of hydrogen.

Hydrogen can also be transported by injections in the already existing natural gas pipeline network. The network can be used to store (excess) renewable energy in the form of gas, known as the power-to-gas concept [93]. The addition of hydrogen to the natural gas is a way to decarbonise the gas network. Hydrogen can however not be added without any challenges.

The natural gas distribution network is build up of several consecutive pipelines, in which the pressure gradually decreases. The Jemena pipeline network in New South Wales (NSW) is depicted in Figure 2.15. All transmission pipelines, transporting the natural gas at high pressures, are steel pipes. The APA group owned gas pipeline and the Eastern Gas Pipeline (EGP) transport the natural gas from the gas fields to the custody transfer station in NSW at a pressures of 62 and 149 bar, respectively. The trunk main pipeline operates at around 69 bar and delivers the gas to large industrial customers. Primary main lines serve large industrial customers with gas at pressures of 35 bar, whereas the secondary mains connect industrial and commercial customers with gas at 10.5 bar.

The distribution pipelines connect domestic customers to the grid, which are typically plastic pipelines. There is a medium pressure main line, operating between 1 and 4 bar, and a low pressure main line, which provides natural gas at vacuum pressures (30-2 kPa).

An extensive review identifying the commercial, technical, and regulatory issues for the injection of hydrogen into the natural gas network in Australia is published by Smith and Coates [25]. The main risk of blending hydrogen with natural gas and transporting it in the existing gas network is the risk of leakage resulting in ignition and/or explosion.

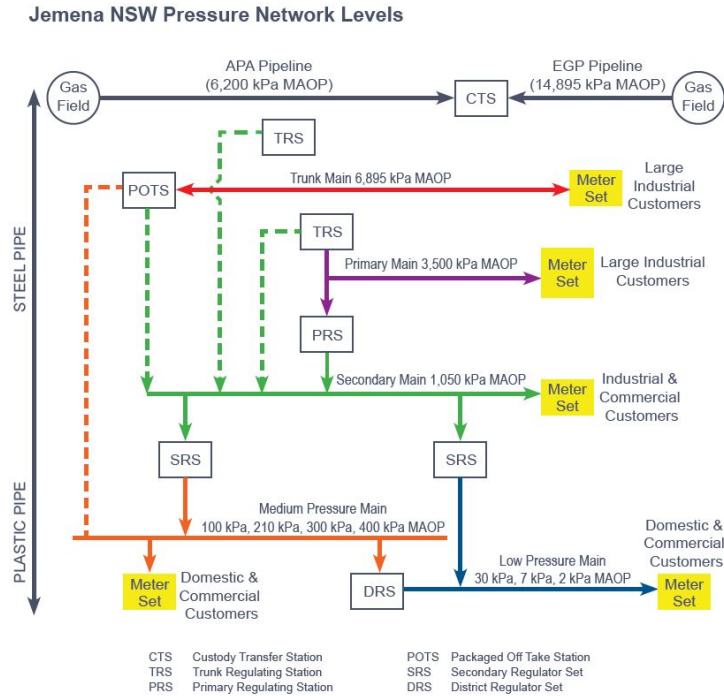


FIGURE 2.15: Schematic the Jemena pipeline distribution network in New South Wales [31].

Uncontrolled release of hydrogen is also acknowledged by Messaoudani et al. [24] as the principle hazard. Burning hydrogen does not emit visible light nor smoke, which makes detection of a fire more challenging as well. The risk increases as the percentage of hydrogen added to the natural gas mixture increases.

Steel pipelines can be prone to hydrogen embrittlement, affected by hydrogen concentration, pressure and temperature conditions [24]. The severeness of the embrittlement is hard to predict, as the history of the pipeline plays a major role in this [27]. Plastic pipelines can cause leakage of hydrogen due to the permeability of plastics to hydrogen, which accounts for the main gas loss in the system [26]. This is however considered an insignificant small amount [25].

Jo and Ahn [29] derived an equation which estimates the size of the area which is potentially affected by a malfunctioning of a transmission pipeline carrying hydrogen. This hazard distance is proportional to the diameter of the pipeline and to the square root of the operating pressure. The lack of experimental data on the safety issues of hydrogen injection in the natural gas pipelines remains the largest knowledge gap in the feasibility [24].

The heating value of the gas mixture decreases with increasing amount of hydrogen added. This requires larger volumes of gas supply at a higher velocity to provide the same energy delivered as the density of the gas is decreased. Consequently, the pressure drop increases as well. Domestic gas appliances are capable of operating with a 5% hydrogen addition, but will need additional testing for larger quantities [25]. de Vries et al. [28] assessed the impact of hydrogen addition in natural gas for end-use appliances, as the

combustion properties change. The Wobbe Index, an indicator of the heat released at specific pressure and valve setting, decreases with the addition of hydrogen in the mixture, causing flame instability or flashback [25, 28].

The limit of hydrogen allowed in the natural gas pipelines remains an open question. Up to 20% hydrogen addition should not cause any severe problems according to Melaina et al. [26], whereas Haeseldonckx and William [27] limits the total amount of hydrogen to be added to 17%. An injection of up to 10% of hydrogen by volume in Australian natural gas pipeline network is reviewed by Bruce et al. [30], and they concluded that there are no significant safety or risk aspects, neither any significant implications with state legislation's. However, Smith and Coates [25], Melaina et al. [26], and Haeseldonckx and William [27] all emphasize in their reviews that it should not be forgotten that many countries used to distribute *city gas*, which consisted of 30-50% hydrogen, in the gas network before switching to natural gas, thereby indicating that it is technically possible to transport higher amounts of hydrogen without significantly increasing safety issues.

In order to get a better understanding of the above mentioned implication related to blending hydrogen into the natural gas pipeline network, there are four pilot projects currently running in Australia to get a better understanding of the implications [31]. One of the trial projects is the Hydrogen Park SA, located in Tonsley Park, Adelaide. A 1.25 MW electrolyser produces hydrogen, of which up to 5 vol% is injected into the existing Tonsley gas network. Similar projects are currently running in Western Sydney, Canberra, and Perth.

2.10 Summary

In this chapter, the literature review is summarised. Different gas separation methods were reviewed, resulting in the selection of adsorption for the separation of hydrogen from natural gas. Adsorption is the adhesion of gas molecules on a solid surface at elevated pressure, which can be used in different processes. Adsorbent materials are characterised by adsorption isotherms, which represents the adsorption characteristics of gases on adsorbent materials. A high working capacity and working selectivity are the main criteria for a good adsorbent material.

Pressure swing adsorption is a process cycle which exploits the adsorption of gases at high pressure and desorption at low pressure, which will be used in this thesis. Other cycles are possible as well, but not further considered. Currently, the main application of PSA system is for hydrogen purification. There is no literature available on the use of a PSA alone to separate hydrogen from natural gas, which is transported through a natural gas pipeline. Several authors looked at the separation of hydrogen from natural gas using a hybrid system of a membrane and PSA, or using only a membrane.

Lastly, a review of the different components on a hydrogen refuelling station are discussed. The main components are the compressors, storage tanks, and dispenser. The safety at a refuelling station is very important, as hydrogen is dispensed at high

pressure. Safety protocols exist which should ensure a safe dispensing. The options for hydrogen transport are reviewed, including the transport of hydrogen through the natural gas pipeline for the New South Wales gas network. Safety issues are concerned for the transport as well, as hydrogen can easily leak or cause embrittlement.

Chapter 3

Methodology

3.1 Introduction

This chapter provides the methodology used in this thesis. It is divided into a process analysis part and an economic analysis part. In the first part, the PSA process is designed. A screening of numerous adsorbent materials is performed to find the most suitable materials for the designed PSA process. Then, the PSA process is analysed using the MINSA process simulator. The thickness of the pre-layer (for the adsorption of heavy hydrocarbons, to protect the main bed) is evaluated for both a 5 vol% and 10 vol% hydrogen mixture with natural gas. In the second part, a techno-economic analysis is performed for the building and operation of a PSA process at a hydrogen refuelling station, including the compression, storage and dispensing of the hydrogen. The refuelling station is design for three different demand sizes of hydrogen per day, representing a small, medium, and large scale refuelling station. An economical analysis has been performed based on the capital cost and the operating cost for both the PSA process and the compression, storage, and dispensing to get an insight in the feasibility of the proposed refuelling station design. Finally, the proposed hydrogen supply system is compared to two other configurations: one at which the hydrogen is produced on-site through electrolysis; and one at which centrally produced hydrogen is transported by a tube-trailer to the refuelling station.

3.2 Adsorption Material Selection

An extensive amount of adsorption isotherms is available in literature. The National Institute of Standards and Technology (NIST) provides a comprehensive database with isotherm data [94], which has been used to study the different types of materials available and to select the ones suitable for the separation of hydrogen from natural gas. When selecting a suitable adsorbent material, firstly the different gas components and in which concentration they are present in the mixture must be considered. Co-adsorption effects and desorption behaviour of the material must be evaluated, and finally, physical properties and the economics play a role in the decisive material selection [95].

The composition of natural gas in the pipeline used in this thesis is based on the Moomba natural gas in New South Wales (see Table A.2). The main components are methane, ethane, nitrogen, propane, carbon dioxide, and heavy hydrocarbons, which are all non-polar gases. The concentration of the different gas components is related to their respective partial pressures, which should be taken into account when analysing the adsorption isotherms. Table 3.1 provides an overview of the partial pressure operating range for each gas component, assuming a maximum total pressure of 20 bar during adsorption and the minimum total pressure is atmospheric during desorption in the cycle.

TABLE 3.1: Partial pressure ranges in which the different gas components operate, representing the adsorption pressure and desorption pressure during the cycle, respective to the concentration of the different gas components in the mixture (see Table A.2).

| Gas | Adsorption pressure [bar] | Desorption pressure [bar] |
|-------------------------------|----------------------------------|----------------------------------|
| CH ₄ | 20 | 1 |
| N ₂ | 2 | 0.1 |
| C ₂ H ₆ | 0.8 | 0.03 |
| C ₃ H ₈ | 0.08 | 0.003 |
| CO ₂ | 0.08 | 0.003 |
| C ₄ + | 0.006 | 0.0002 |

Additionally, trace elements can be present in the gas mixture, which must be removed in order to achieve high purity hydrogen which can be used for fuel cell cars. The main trace elements that will be considered are sulphur components (mercaptans and hydrogen sulphide) and very small amounts of water (typically 40-70 mg/m³). The adsorption characteristics of these components on the selected adsorbent materials will be evaluated based on a literature study.

A large number of adsorbent materials is studied by evaluating their single component adsorption isotherms of the different gases in the mixture. Only a rough screening of the materials is required, therefore no mixture adsorption isotherms are evaluated. Hydrogen is a very small and light gas which does not adsorb significantly on any known material at standard temperature and pressure. Therefore, for this separation, all other gases in the mixture must be adsorbed such that pure hydrogen can leave the top of the bed.

It is not possible to find one adsorbent material to perform the separation. One adsorbent material might be able to adsorb all gas components in the mixture, however, it is very important that the gas components can be desorbed as well, in order to regenerate the bed. Therefore, a three layered adsorption column is designed in which each layer adsorbs a different gas or group of gases. As methane is the predominant component of the gas mixture, the main adsorbent layer must adsorb methane. Ethane is the second largest component, followed by nitrogen, propane, carbon dioxide and heavy hydrocarbons.

An ideal adsorbent has a high working capacity and high working selectivity. A high working capacity results in a smaller amount of adsorbent required, whereas a high

selectivity increases the purity of the product. Therefore, the initial screening of the materials is based on the working capacity in the operating pressure range for each gas type and the working selectivity.

In this screening only isothermal working capacity is calculated, assuming the temperature is constant at the adsorption and desorption pressure. Adiabatic working capacity does include this temperature difference and will thus result in a lower working capacity. It is decided not necessary to include the adiabatic conditions as this is a rough screening only based on literature data. The working capacity is calculated according to Equation 2.10. The selectivity of the different materials is calculated for isothermal conditions as well, for the same reasoning, and is calculated according to Equation 2.11.

In order to have an idea of the heat produced during adsorption, the heat of adsorption is calculated at a constant adsorption loading using the Clausius Clapeyron equation (Equation 2.12). This also gives insight in the affinity between the adsorbents and the adsorbates, as heat produced increases with a stronger adsorption.

Additionally, the material must be stable, non-hazardous, and preferably commercially available as this significantly reduces the overall costs.

3.3 Process Simulations

Based on the adsorbent materials selected, the adsorption process cycle is designed. In this thesis, a 6 bed PSA process is designed with 12 steps in each cycle. A large number of beds is required to facilitate the pressure equalisation steps, which ensures a high hydrogen recovery. Therefore, the cycle design consists of an adsorption step, four pressure equalisation steps, a blow down step, and a repressurisation step with the pure hydrogen product, schematically depicted in Figure 3.1. A continuous product output

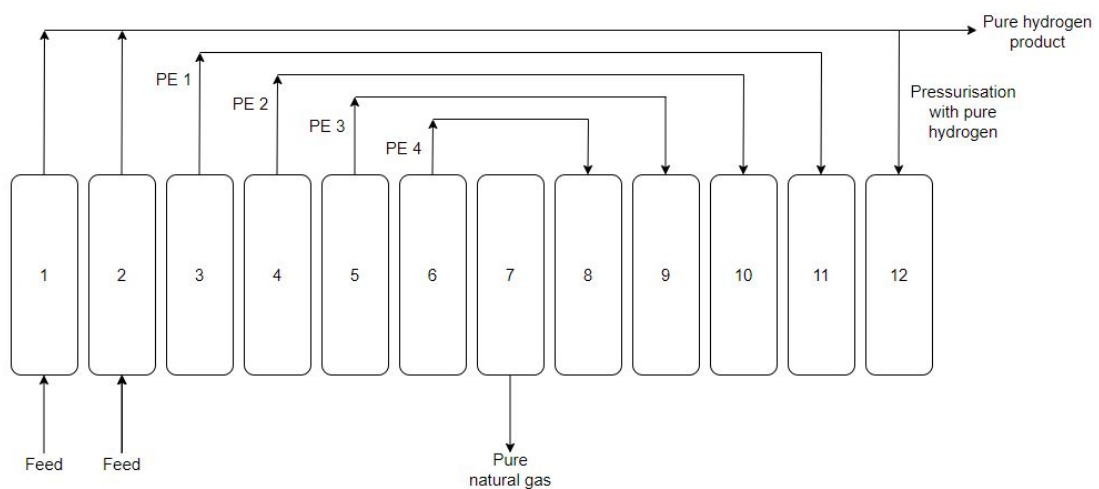


FIGURE 3.1: Schematic overview of the 6 bed, 12 step PSA process used for the separation of hydrogen and natural gas. The four pressure equalisation (PE) steps conserve energy of the total process and increase the hydrogen recovery.

at the top of the column is achieved, as there is always one bed going through the adsorption step. For all process cycle designs a trade-off must be made between product recovery and product purity. Therefore, in this design, four equalisation steps are chosen to increase the product recovery. No purge step is used, but instead the repressurisation is done counter-currently using the pure hydrogen product. In the presence of the high purity hydrogen, the remained adsorbed gas components in the void space desorb, providing a cleaner bed at the start of the following adsorption step in the new cycle, resulting in a higher hydrogen purity product without decreasing the recovery.

A summary of the steps during the cyclic process are represented in Table 3.2. The pressure profile during a full cycle is represented in Figure 3.2. As can be seen from the figure, after the adsorption step, 4 pressure equalisation steps are performed where pressure is provided to another bed. After the blowdown, the column receives a pressure equalisation, building up the pressure in the bed again. The final pressure is achieved using the pure hydrogen product, ensuring the bed is ready for the next cycle. The choice for a 6 bed system is based on the operating pressure and the required pressure equalisation steps to ensure a high hydrogen recovery.

The process analysis is performed using the adsorption simulator MINSA, of which the main principles and underlying equations used are covered in Section 2.8. The design parameters used in the simulation for the PSA system are listed in Table 3.3. The

TABLE 3.2: Summary table of cyclic 6 bed 12 step PSA cycle used in the process analysis.

| | | | | | | | | | | | | |
|-----|---------|--------|---------|--------|---------|--------|---------|--------|---------|--------|---------|--------|
| Bed | | | | | | | | | | | | |
| A | ADS | | EQI ↑ | EQII ↑ | EQIII ↑ | EQIV ↑ | BD | EQIV ↓ | EQIII ↓ | EQII ↓ | EQI ↓ | RP ↓ |
| B | EQI ↓ | RP ↓ | ADS | | EQI ↑ | EQII ↑ | EQIII ↑ | EQIV ↑ | BD | EQIV ↓ | EQIII ↓ | EQII ↓ |
| C | EQIII ↓ | EQII ↓ | EQI ↓ | RP ↓ | ADS | | EQI ↑ | EQII ↑ | EQIII ↑ | EQIV ↑ | BD | EQIV ↓ |
| D | BD | EQIV ↓ | EQIII ↓ | EQII ↓ | EQI ↓ | RP ↓ | ADS | | EQI ↑ | EQII ↑ | EQIII ↑ | EQIV ↑ |
| E | EQIII ↑ | EQIV ↑ | BD | EQIV | EQIII | EQII | EQI | RP ↓ | ADS | | EQI ↑ | EQII ↑ |
| F | EQI ↑ | EQII ↑ | EQIII ↑ | EQIV ↑ | BD | EQIV | EQIII | EQII | EQI | RP ↓ | ADS | |

EQ - Equalisation, BD - Blowdown, RP - Repressurisation, ↓ - countercurrent flow, ↑ - cocurrent flow

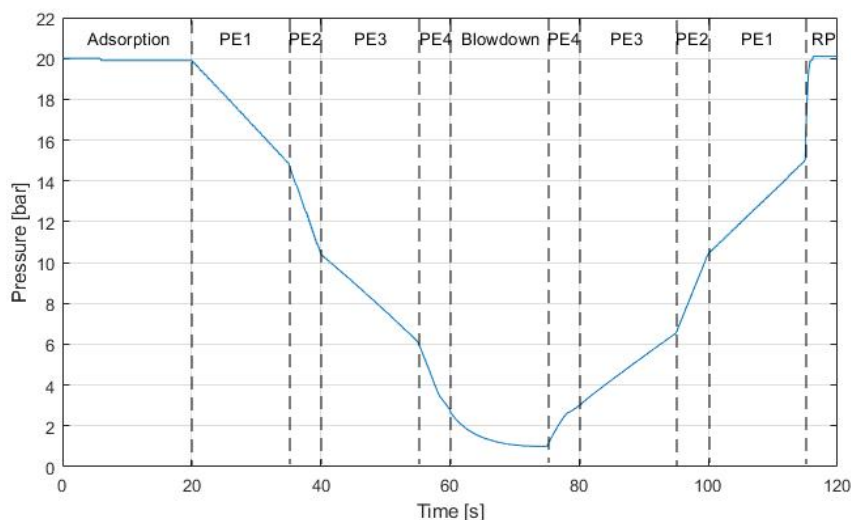


FIGURE 3.2: Bed pressure profile during the designed 12 step PSA cycle.

TABLE 3.3: Parameters used in MINSA for the 6 bed 12 step process cycle based on the lab scale PSA design.

| Parameter | Value | Unit |
|----------------|-------|---------------------|
| Flow rate | 100 | nm ³ /hr |
| Pressure | 20 | bar |
| Temperature | 298 | K |
| Column height | 1.2 | m |
| Inner diameter | 0.3 | m |

simulation is based on the lab scale PSA column operating at the University of Melbourne, which operates with a flow rate of 100 nm³/hr for the mentioned dimensions. The process design evaluates two different input flow rates, containing 5 vol% and 10 vol% hydrogen. MINSA can only manage 5 different components in the simulation, therefore some components are grouped together, based on the similarity in the adsorption isotherms. Methane, nitrogen, and hydrogen each represent a single component. Ethane and carbon dioxide are grouped together as well as the heavy hydrocarbons (C₃₊), defining the fourth and fifth component in the mixture. The concentrations of the mixtures are tabulated in the Appendix in Table A.2.

In total, a set of 162 discretised time ordinary differential equations are being solved by the first-order, backward difference integrator (DVIDE). PID loops are used to help find the solution. The simulations run multiple cycles, until cyclic steady state (CSS) is achieved. The tolerance allowed between the current and the previous cycle is set to 0.01 for the pressure [bar], adsorption loading [gmol kg⁻¹], and temperature [K]. Only when this is achieved, the final results can be used. The adsorption time steps vary for the hydrogen concentration in the feed gas stream, and decrease as the concentration decreases. The purity and recovery of the hydrogen product stream are calculated using Equation 2.13.

TABLE 3.4: Overview of different simulations performed in the process analysis. Analysing the hydrogen concentration in the input feed gas and the influence of thickness of the silica gel pre-layer.

| # | H ₂ input concentration [vol%] | Adsorption Material | | | Layer thickness [m] | | | Dimensions [m] | |
|----|-------------------------------------------|---------------------|------|-------|---------------------|------|-----|----------------|-----|
| | | Bottom | Main | Top | Bottom | Main | Top | Height | ID |
| 1 | | Silica gel | AC | LiLSX | 0.0 | 1.1 | 0.1 | 1.2 | 0.3 |
| 2 | | Silica gel | AC | LiLSX | 0.1 | 1.0 | 0.1 | 1.2 | 0.3 |
| 3 | | Silica gel | AC | LiLSX | 0.2 | 0.9 | 0.1 | 1.2 | 0.3 |
| 4 | | Silica gel | AC | LiLSX | 0.3 | 0.8 | 0.1 | 1.2 | 0.3 |
| 5 | | Silica gel | AC | LiLSX | 0.4 | 0.7 | 0.1 | 1.2 | 0.3 |
| 6 | | Silica gel | AC | LiLSX | 0.0 | 1.1 | 0.1 | 1.2 | 0.3 |
| 7 | | Silica gel | AC | LiLSX | 0.1 | 1.0 | 0.1 | 1.2 | 0.3 |
| 8 | | Silica gel | AC | LiLSX | 0.2 | 0.9 | 0.1 | 1.2 | 0.3 |
| 9 | | Silica gel | AC | LiLSX | 0.3 | 0.8 | 0.1 | 1.2 | 0.3 |
| 10 | | Silica gel | AC | LiLSX | 0.4 | 0.7 | 0.1 | 1.2 | 0.3 |

3.3.1 Pre-layer Thickness

The process analysis evaluates the influence of the silica gel pre-layer for the adsorption of contaminants for the main bed. Five thicknesses are assessed: 0, 0.1, 0.2, 0.3, and 0.4 meter. The total height of the column is kept constant at 1.2 meter. The zeolite LiLSX post-layer is kept at a fixed thickness of 0.1 meter. The goal is to find the optimal pre-layer thickness in the 6 bed 12 step process cycle. The constraint for simulation results is to produce a hydrogen product with a purity of at least 99%. All results are then compared, evaluating the hydrogen recovery, methane purity, and total hydrogen product output per day. The best performing pre-layer thickness can then be selected. The simulations are performed for a hydrogen concentration of 5 vol% and 10 vol% in the feed gas stream. In Table 3.4 an overview of the different simulations that are analysed is provided.

3.4 Refuelling Station Design

The second part of this thesis focuses on the design and economic analysis of a hydrogen refuelling station, where a PSA system supplies the hydrogen. For this design, a total of 10 vol% hydrogen is assumed in the feed mixture, supplied through the existing pipeline network at a pressure of 20 bar. The design of the refuelling station will be analysed for the PSA and for the storage, compression, and dispensing design for three different scenarios. The first scenario represents a small refuelling station, with a hydrogen demand of 350 kg of H₂ per day. The second scenario is a medium sized refuelling station, producing 700 kg of H₂ per day, and the third scenario produces 1000 kg of H₂ per day, depicting a large scale hydrogen station [18]. The storage tank of a fuel cell car is 5 kg of hydrogen at 700 bar, which results in a maximum number of cars refuelling per day of 70, 140, and 200, for the small, medium, and large refuelling station respectively. In Table 3.5 an overview of the different parameters for the three scenarios is provided.

TABLE 3.5: Different scenarios for a hydrogen refuelling station.

| | Scenario I | Scenario II | Scenario III |
|-------------------------------------------|------------|-------------|--------------|
| Size refuelling station | Small | Medium | Large |
| Hydrogen product [kg H ₂ /day] | 350 | 700 | 1000 |
| Max. number of cars per day | 70 | 140 | 200 |

3.4.1 PSA Design

The PSA process is the fundamental part of the refuelling station which determines the hydrogen production per day. The dimensions of the PSA columns in the initial simulations are based on the lab setup available at the University of Melbourne. This setup is not able to produce the amount of hydrogen needed for a refuelling station, and therefore requires a scale up design.

In an ideal scaling design, the height of the bed is kept constant, such that the pressure drop does not increase. Therefore, the diameter of the bed is increased until the same velocity is obtained for the increased input flow rate, ensuring the same pressure drop. In this case, with a height of just 1.2 meter, the diameter has to increase significantly to ensure the same velocity. With an increased diameter, the heat generated during adsorption will be disproportionately divided over the bed diameter, as the heat can only be transferred through the walls. Furthermore, the design of the column is influenced by the operating pressure during the PSA process. If a very wide and short column is designed, the wall thickness and thus the cost of the column increases. For a narrow and tall column, the pressure is more evenly distributed over the walls of the column and thus a thinner wall can be used. Therefore, in hydrogen purification PSA systems, the columns are very thin and tall.

In the scaling of the PSA system in this study for the different hydrogen demands per day, the flow rate of the feed stream is scaled linearly with the height of the column ($Q \sim H$), and with the square root of the inner diameter ($Q \sim \sqrt{ID}$). The ratio between the height and the inner diameter of the column are commonly 3:1 or 4:1 [96].

In order to confirm if the scaling method described above provides the expected hydrogen product, an extra simulation is performed. This is done for a hydrogen demand of 350 kg/day only, as this will provide sufficient insight in the accuracy of the scaling method.

3.4.2 Compression and Storage Design

The Hydrogen Refuelling Station Analysis Model (HRSAM) will be used to find the optimum design of the compression and storage at the refuelling station [92]. This model is developed by Argonne National Laboratory, along with the National Renewable Energy Laboratory and the Pacific Northwest National Laboratory [92]. It is developed to find the optimum size for the compression and cascade storage tanks, while minimizing the refuelling costs. The optimisation can be done for a user set daily hydrogen demand and for two different gaseous hydrogen delivery methods: as compressed gas by tube-trailers or as a pure gas at 20 bar delivered by a pipeline.

The model assumes a cascade of three pressure vessels (type IV), which are equal in size. Each vessel has a volume of 255 L, and a capacity of 12 kg of hydrogen at 95 MPa, 298 K. All three vessels have a different minimum pressure threshold representing a low, medium, and high pressure storage tank. The filling of the vehicle is assumed to start with the hydrogen from the lowest pressure vessel, followed by the medium pressure vessel, and ends with the hydrogen from the high pressure vessel [92]. A flow rate of 0.1 kg/min is assumed as the threshold for switching to the consecutive pressure vessel, to be able to fill the vehicle with a maximum of 5 kg of hydrogen at 70 MPa, 298 K. Furthermore, it is assumed that the hydrogen flow is adiabatic, quasi steady and compressible. For each 250 kg of hydrogen demand per day, a dispenser with a single hose is required. The compressor is assumed to have an adiabatic efficiency of 65% and keeps the cascade vessels at their required operating pressures. The model is

validated by Reddi et al. [92] and used in various hydrogen refuelling station analyses [20, 84, 87, 97].

3.5 Economic Refuelling Station

The economics of the refuelling station is analysed for the initial capital costs and the operational costs. The initial investment costs are dominated by the capital expenditures (CAPEX) for the compression and storage of the hydrogen and the PSA separation system. Furthermore, the operational expenditures (OPEX) will be analysed for the total operation of the refuelling station.

3.5.1 Economics Compression and Storage

The capital costs for the compression and storage of the hydrogen on the refuelling station is analysed using the HRSAM model, described previously in Section 3.4.2. This model also estimates the equipment costs of the different components for the compression, storage, and dispensing, as well as the operating costs. The total capital investment costs are split up into initial capital investment and other capital investment costs. Initial investment costs comprise the different equipment required at the station, such as the compressors, storage tanks, dispenser, and refrigeration unit. The other capital investment costs include the site preparation, engineering & design, project contingency, one-time licensing fees, and up-front permitting costs. All prices are based on 2016 US dollars. The final prices provided in this thesis are all converted to 2020 Australian dollars.

The operating costs for the refuelling station are calculated, estimating the labour costs, electricity costs for all different components, and various other fixed costs such as insurance, property taxes, operating, maintenance, and repair costs, and land rental. In Appendix D, an overview of all the constants used by the HRSAM model are listed. Both the capital and operating costs are evaluated for the three different refuelling stations as defined in Table 3.5.

3.5.2 Economics PSA

Additional to the compression and storage costs, the PSA separation system must be included in the analysis of the refuelling station. A selective design analysis will be performed, in which only the critical components of the system are analysed. The main components are the adsorbent vessels, the adsorbent material, the valves, and the compressor for compressing the methane off gas stream back into the pipeline network. To get to the final capital investment costs, usually the Lang factors are used in industrial analysis [98]. Since this is not an industrial scale PSA process, these factors are significantly too high for this scenario. Therefore, an estimation will be made based on previous experience combined with elaborate discussions with Prof. Paul Webley. This

method provides sufficient detail to obtain an order-of-magnitude cost estimation, which is the goal of this first economic analysis of a hydrogen refuelling station where a PSA process is used for the separation of hydrogen. The accuracy of this method is +/- 30% to 40% [98].

All equipment costs are gathered by online research and quotations, except for the compressor, which is calculated using Aspen HYSYS. The Peng-Robinson equation of state is used for the gas properties. The build-in economic analyser tool of Aspen HYSYS is used to evaluate the equipment costs of the compressor.

The operational cost for the PSA process is calculated based on the operational cost of the compressor for compressing the natural gas back into the pipeline network, the maintenance cost of the PSA equipment, the capital cost of the PSA, and the feedstock price of the natural gas hydrogen mixture. The total operating cost is evaluated for the operating lifetime of the PSA and for the feedstock price. The maintenance cost are assumed to be 2% of the installed equipment cost per year.

The feedstock price is predominantly determined by the natural gas price. The price of the hydrogen added to the mixture is determined by the production method of the hydrogen. In the case of a 10 vol% addition of hydrogen to the natural gas mixtures, the energy content of the hydrogen is equal to 3.2% in the mixture. Therefore, the following equation is used to calculate the feedstock price,

$$Feedstock = \$NG \cdot 0.968 + \$NG \cdot 0.032 \cdot F_{production} \quad (3.1)$$

Where $\$NG$ represents the natural gas price in \$/GJ and $F_{production}$ represents the production factor for the hydrogen produced through various methods. This equation was obtained from the industrial partners of the Future Fuels CRC. The production factors used are tabulated in Table 3.6. A factor 1 implies the hydrogen price is equal to the natural gas price in \$/GJ. Accordingly, hydrogen produced through electrolysis is estimated to be 3.5 times the natural gas price, hydrogen produced by coal gasification with CCS is 1.7 times the natural gas price, etc. It must be noted that this estimation is only correct for current hydrogen production prices. With increased development, the hydrogen cost price is likely to reduce, whereas the natural gas price, contrarily, is expected to increase.

TABLE 3.6: Production factors used for the feedstock price calculation of the natural gas and hydrogen mixture.

| Hydrogen production method | Production factor |
|----------------------------|-------------------|
| Electrolysis | 3.5 |
| Coal gasification with CCS | 1.7 |
| SMR with CCS | 2.2 |
| SMR without CCS | 1.5 |

A sensitivity analysis is performed for the natural gas price and the electricity price. The natural gas price is evaluated for a range of \$9.50/GJ to \$15.00/GJ [99]. The electricity price is evaluated for a range of 5 c/kWh to 25 c/kWh.

3.6 Comparison of Different Hydrogen Supply Methods

The last part of the economic analysis is to compare the final production cost of hydrogen for different types of hydrogen supply methods to a refuelling station. There are three cases considered, which are presented in Figure 3.3. Case A represents the refuelling station presented in this thesis. Hydrogen is produced at a central location, then injected and transported as a mixture in the natural gas pipeline network to a refuelling station, where it is separated by a PSA process. Finally, the hydrogen is compressed, stored, and dispensed into a fuel cell vehicle.

Case B considers a refuelling station at which the hydrogen is directly produced on-site by electrolysis. The electricity required for the electrolysis can be taken directly from the grid or from a direct renewable energy source, such as PV cells or wind mills. No transport of the hydrogen is required, therefore the produced hydrogen can be directly compressed, stored, and then dispensed.

The last case, case C, considers a refuelling station where hydrogen is again produced at a centralised hydrogen plant, then transported as a compressed gas by a tube-trailer to the refuelling station, where it is further compressed, stored, and dispensed. The distance the hydrogen has to travel is a dominating factor in the final hydrogen price.

For all three cases sensitivity analyses are conducted, focusing on the electricity price, natural gas price, and tube-trailer distance travelled.

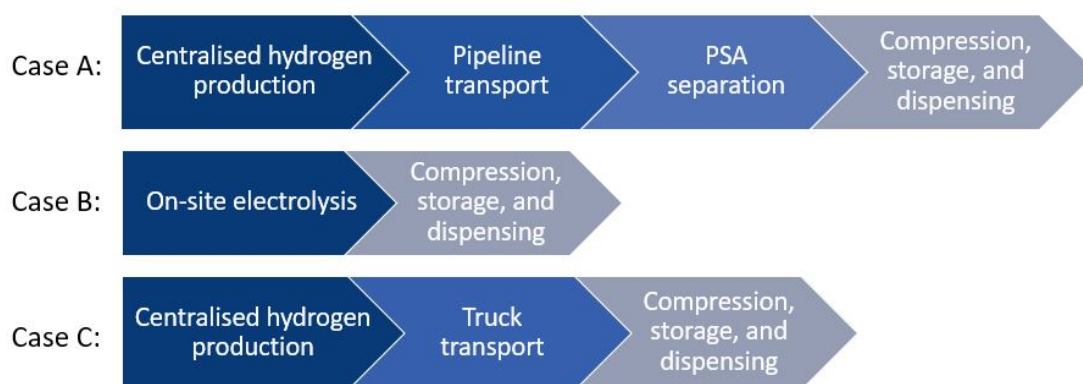


FIGURE 3.3: Overview of the three different hydrogen supply methods considered in the comparison.

3.7 Summary

This chapter covered the methodology used for the research in this project. The adsorbent screening is based on literature data, where a high working capacity and working selectivity are the main selection criteria. The PSA process that will be used for the separation is explained in detail. The simulations that will be performed using the process simulator MINSA are based on a lab scale, which defines the dimensions and flowrate used. The simulations focus on the analysis for the thickness of the pre-layer.

The design for a refuelling station with hydrogen supplied by a PSA system is made for three different demand sizes of hydrogen per day, representing a small, medium, and large refuelling station. The PSA system is scaled accordingly, using the process simulation results. The design and economic analysis for the compression and storage required at a refuelling station is optimised using the HRSAM model. The economics of the PSA is analysed separately, for the capital cost and the operating cost. Finally, an economic analysis for different hydrogen supply methods at a refuelling station is performed, focusing on hydrogen supplied by a PSA system, by on-site electrolysis, and by tube-trailer as compressed gas.

Chapter 4

Process Analysis

4.1 Introduction

This chapter provides the results of the PSA process analysis. First of all, the adsorbent material screening and selection is presented. Secondly, the simulation results are analysed for both the 5 vol% and 10 vol% of hydrogen added to the natural gas. The optimum pre-layer thickness is evaluated, as well as the adsorption characteristics of the various gas components.

4.2 Results Adsorbents Screening

The main component of the gas mixture to be separated by the PSA process is methane. Therefore, the adsorption of methane on various materials is considered first and the main layer of the bed will consist of an adsorbent material with a large working capacity for methane. Then, the pre-layer is examined, focusing on the adsorption of heavy hydrocarbons. Lastly, the adsorption of nitrogen on various adsorbent materials is considered.

4.2.1 Methane Adsorption

Methane can be adsorbed by activated carbons, zeolites, and MOFs, of which a high surface area and high micropores volume are generally favourable for an increased adsorption [49]. In Figure B.1 the adsorption isotherms of a selected number of materials reviewed for the adsorption of methane is presented. The working capacities are calculated for the partial pressure range and listed in Table B.1. COF-102 and COF-103 show the highest working capacity of 7.40 and 6.72 mol/kg, respectively. Depending on the type of activated carbon, different working capacities can be achieved. Activated carbon NC100 shows the highest working capacity of 6.08 mol/kg, whereas activated carbon Norit R1 shows a slightly lower working capacity, which is very similar to the working capacity of CuBTC. The material properties of the most promising adsorbents

are presented in Table 4.1, together with their respective working capacities. A relation between the working capacity and BET surface area and pore volume is observed, where a large surface area and pore volume results in a larger working capacity.

TABLE 4.1: Working capacity and material properties of selected materials for methane adsorption.

| Material | Working capacity [mol/kg] | Total pore volume [cm³/g] | BET surface area [m²/g] | Reference |
|-----------------|--------------------------------------|-------------------------------------------------|-----------------------------------------------|------------------|
| COF-102 | 7.40 | 1.55 | 3620 | [100] |
| AC NC100 | 6.08 | 0.67 | 1493 | [101] |
| CuBTC | 4.56 | 0.82 | 1522 | [102, 103] |
| AC Norit R1 | 4.39 | 0.61 | 1328 | [103, 104] |

Covalent organic frameworks (COFs) are a relatively new type of material, firstly demonstrated in 2005, and create a porous structure by linking light-weight elements by covalent bonds [105]. This provides a low mass density and high thermal stability. COF-102 and COF-103 are both promising methane adsorbents, but their performance does not significantly exceed that of activated carbon NC100. Furthermore, the development of COFs is still in the research phase. Therefore, this material will not be selected as the adsorbent for methane. It is, however, an interesting material to consider as developments progress.

CuBTC is a benzene-1,3,5-tricarboxylate MOF, which is also known as BasoliteTM C300 as trademark name of Sigma Aldrich. The structure of the material consists of two types of pores: main channels with a square cross-section and tetrahedral side pockets [106]. Figure 4.1 shows the adsorption of the different gases present in the natural gas mixture on CuBTC at 298 K. The solid lines represent the isotherms. Not all literature used provided the isotherm data with the experimental data, therefore some gases are represented only with an isotherm, whereas for others experimental data points are shown as well. A very strong adsorption of the heavy hydrocarbons, C₃H₈, C₄H₁₀, and C₅H₁₂, and CO₂ is observed by the steep initial line of the isotherms. The partial pressure operating range of these heavy hydrocarbons is within this steep initial line, which implies these gases will not easily desorb at the desorption pressure.

TABLE 4.2: Selectivity of methane on CuBTC and activated carbon.

| Selectivity | AC | CuBTC |
|------------------------------------------------|-----------|--------------|
| CH ₄ /CO ₂ | 0.49 | 0.23 |
| CH ₄ /N ₂ | 2.87 | 3.30 |
| CH ₄ /H ₂ | 10.25 | 8.26 |
| CH ₄ /C ₂ H ₆ | 0.23 | 0.13 |

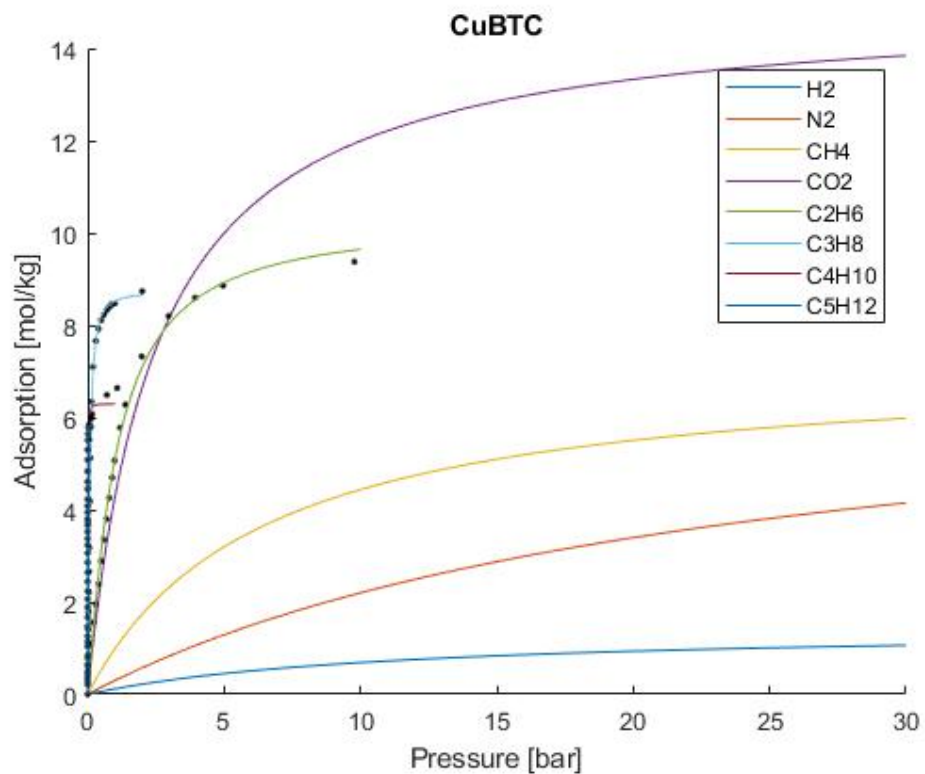


FIGURE 4.1: Adsorption isotherms of different gases on CuBTC at 298 K. Based on data from [102, 107–110].

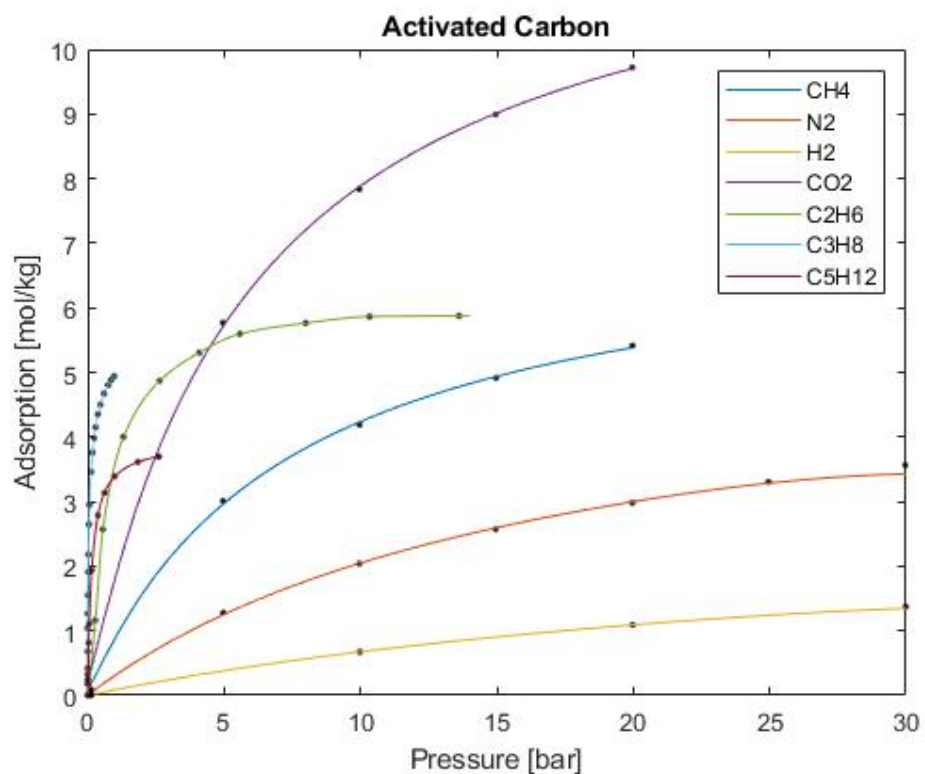


FIGURE 4.2: Adsorption isotherms of different gases on activated carbon at 298K. Based on data from [47, 103, 111, 112].

The selectivity of the different gases on CuBTC is calculated for a pressure range from 0.001 bar to 1 bar, and is presented in Table 4.2. A high selectivity of methane over nitrogen and methane over hydrogen is observed. However, ethane and CO₂ have a higher selectivity on CuBTC than methane. The heat of adsorption of methane on CuBTC at an adsorption is calculated to be 15 kJ/mol [113].

In Figure 4.2 the single gas isotherms for the different gases in the mixture are plotted for activated carbon. Similarly to the adsorption isotherms for CuBTC, activated carbon adsorbs heavy hydrocarbons very strongly, shown by the steep initial slope. The selectivity measured of the same pressure range (0.001 - 1 bar) for the different gases on activated carbon is presented in Table 4.2. The selectivity of methane over hydrogen is significantly larger for activated carbon than CuBTC. However, the selectivity of methane over nitrogen is slightly lower. Both CO₂ and C₂H₆ have a higher selectivity than methane on activated carbon. The heat of adsorption of methane on activated carbon is calculated to be around 15 kJ/mol as well [47].

Furthermore, in Figure 4.3 the working capacity and working selectivity of several gases on activated carbon is presented as a function of the feed pressure. The working capacity is calculated for a single gas component with a desorption pressure of 1 bar. Clearly, as the feed pressure increases, the total amount adsorbed for all gases increases and thus the working capacity. The working selectivity is calculated, assuming a 50-50 concentration of the gases. The working selectivity of methane over hydrogen and

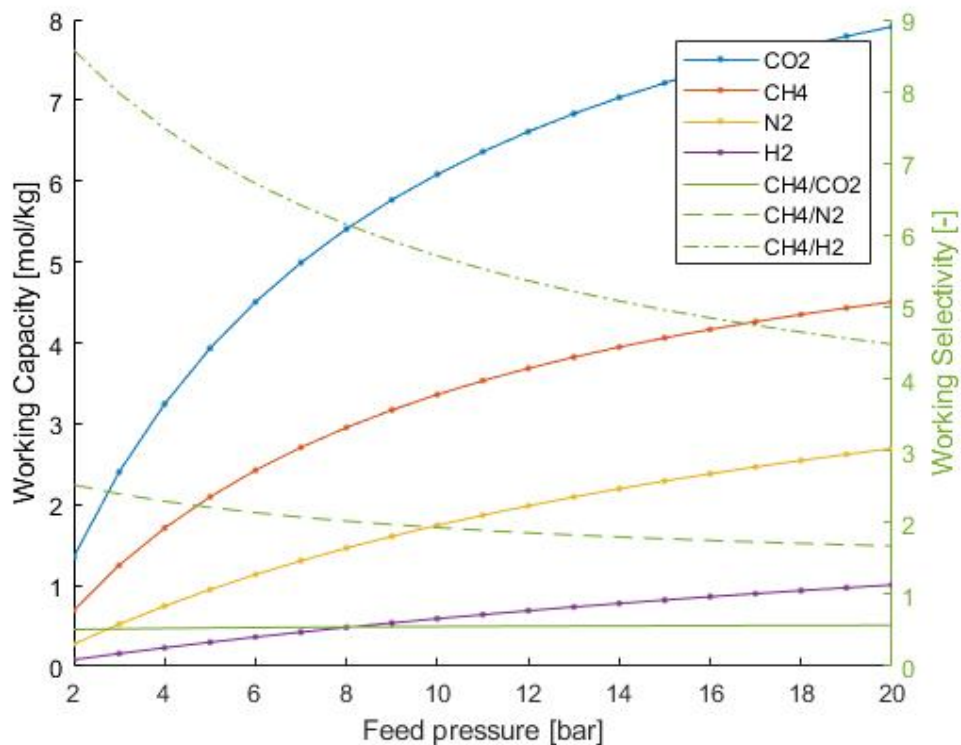


FIGURE 4.3: Working capacity and selectivity for selected gases on activated carbon represented as function of the feed pressure, assuming blow down to atmospheric pressure. Based on data from [103].

methane over nitrogen drops as the feed pressure increases. The difference in working capacity at low pressure is larger than at higher pressures. Moreover, the selectivity of methane over CO₂ is relatively constant as their working capacities increase similarly with increasing feed pressure.

It can be concluded that both CuBTC and activated carbon require a removal of the heavy hydrocarbons before the gas mixture reaches the methane adsorbent layer, such that the gases do not accumulate and a high selectivity of methane is ensured. CuBTC shows a stronger adsorption of the heavy hydrocarbons. If these gas components are not completely adsorbed in a pre-layer, they will cause accumulation in the main layer, hence decrease the performance of the bed. CuBTC is not yet available at a commercial scale, whereas activated carbon is. The price for activated carbon is thus significantly lower than the price for CuBTC. Therefore, in this study, activated carbon is chosen as the adsorbent for the main layer in the adsorbent bed. There are many different types of activated carbon, which have to be investigated experimentally to find the most suitable adsorbent. Currently in the simulation, data from Norit activated carbon will be used, which is previously measured in the lab at the University of Melbourne.

4.2.2 Heavy Hydrocarbon Adsorption

Before the gas mixture reaches the main adsorbent layer where methane is adsorbed, strongly adsorbing gases on activated carbon must be removed. Therefore, a material is sought that can adsorb them all sufficiently in a so called adsorption pre-layer. In Figure 4.2, a very steep initial line in the adsorption isotherm for heavy hydrocarbons was observed on activated carbon. This indicates that at the desorption pressure, these gases will not desorb from the activated carbon and thus accumulate the material. The pre-layer adsorbent material must therefore have a linear isotherm profile, such that regeneration at the desorption pressure is possible.

The adsorption isotherms of ethane for a selected number of materials is presented in Figure B.2, for propane in Figure B.3, and for CO₂ in Figure B.4 in Appendix B. The working capacities are calculated for the respective partial pressure ranges. In this case, however, it is crucial to look at the adsorption isotherms. The concentrations and operating partial pressure ranges of the heavy hydrocarbons and CO₂ are low. It is therefore preferred to have a material with a linear isotherm, such that accumulation of the gas components can be prevented.

It is common practice in industry to use silica gel as a pre-layer in PSA processes for the adsorption of heavy hydrocarbons and CO₂ [69]. The adsorption isotherm of silica gel for the different gases in the mixture is presented in Figure 4.4. A linear isotherm behaviour is observed for all gases except for pentane and hexane, which show a more steep initial curve. The isotherm provides a good understanding of the adsorption characteristics, and shows desorption is possible within the pressure range of the heavy hydrocarbons and CO₂. The heat of adsorption is calculated to be 21, 23, and 26 kJ/mol, respectively, for ethane, propane, and CO₂ [114].

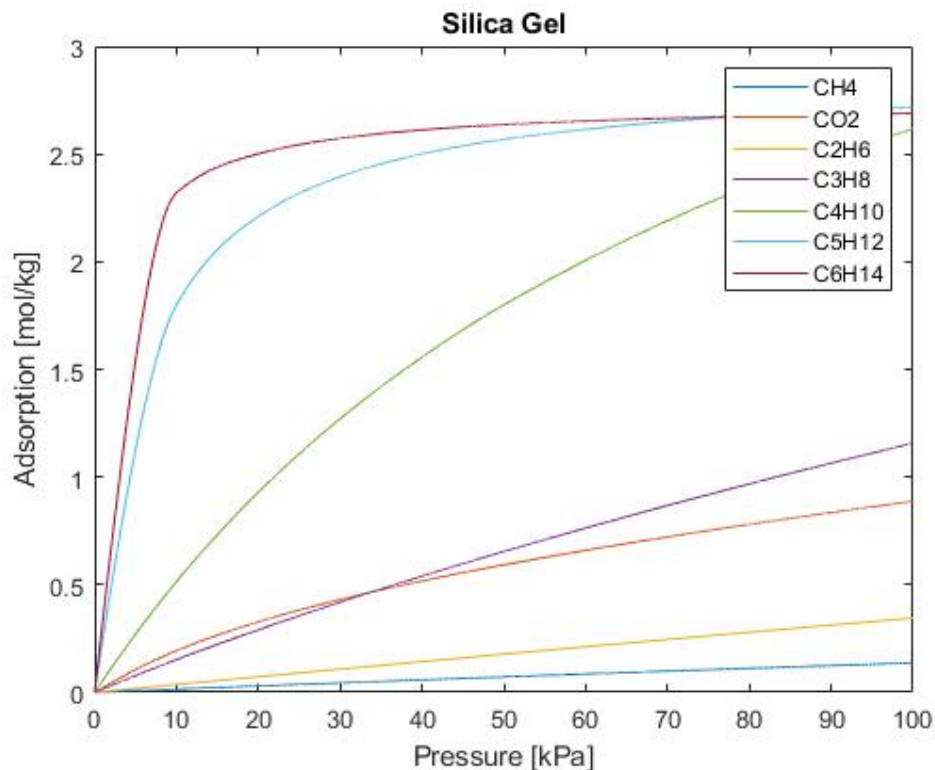


FIGURE 4.4: Adsorption isotherms of different gases on silica gel at 298K. Dual site Langmuir curves plotted. Based on data from [114].

It is therefore concluded that, based on the linear isotherms, silica gel is best suitable as pre-layer in the adsorption bed. The heavy hydrocarbons and CO₂ will be adsorbed, protecting the main activated carbon layer. At the desorption pressure, the pre-layer of silica gel will be regenerated, which ensures a clean bed at the start of the next cycle and thus a high purity hydrogen can be produced.

4.2.3 Nitrogen Adsorption

Lastly, the adsorption of nitrogen is evaluated. Nitrogen is not strongly adsorbed in either the silica gel pre-layer or in the activated carbon main layer. This results in a mixture of mainly hydrogen, nitrogen, and some methane left at the end of the adsorbent bed. Therefore, the last layer in the bed should have a high working capacity for nitrogen. The adsorption isotherms for the adsorption of nitrogen is presented in Figure B.5 in Appendix B for a selected number of adsorbent materials. All working capacities are listed in Table B.1.

Initially, zeolite 5A was frequently used in industry for the production of pure O₂. It is made up of A-type crystalline structures with a pore size of 5 Å. Since the 1990s, lithium-based zeolites gained more interest due to the increased adsorption capacity for N₂ which is evaluated by Shen et al. [115]. The Li⁺ cations cause a larger adsorption of N₂, but a lower adsorption capacity for O₂, compared to zeolite 5A. Zeolite LiLSX has a pore diameter of 7.4 Å [116]. Currently, LiLSX zeolite is the favoured adsorbent for

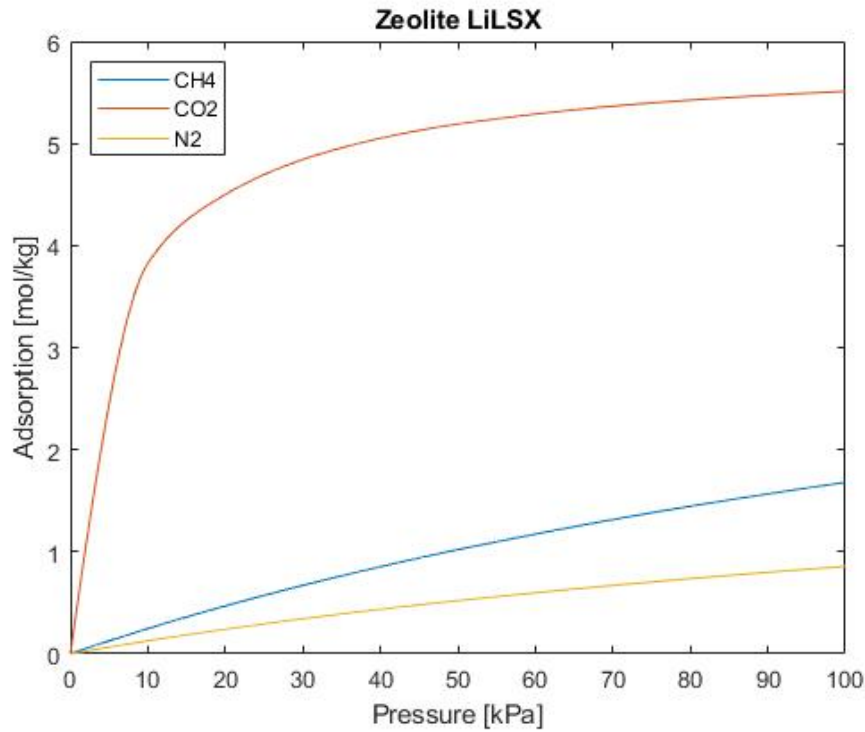


FIGURE 4.5: Adsorption isotherms of nitrogen on various types of zeolite at 298 K. Based on the data from [118, 120].

nitrogen adsorption, because of the large working capacity [117]. The material properties of zeolite LiLSX and zeolite 5A are listed in Table 4.3.

TABLE 4.3: Working capacity and material properties of selected materials for nitrogen adsorption.

| Material | Working capacity [mol/kg] | Total pore volume [cm ³ /g] | BET surface area [m ² /g] | Reference |
|---------------|---------------------------|----------------------------------------|--------------------------------------|------------|
| Zeolite LiLSX | 1.16 | 0.32 | 640 | [117, 118] |
| Zeolite 5A | 0.60 | 0.22 | 613 | [106, 119] |

In Figure 4.5 the adsorption isotherms for various gases on zeolite LiLSX are presented. A strong adsorption of CO₂ is observed. This is not very concerning, as most CO₂ will already be adsorbed in either the silica gel pre-layer or in the main activated carbon layer. The selectivity of nitrogen over CO₂ and nitrogen over methane is calculated over a pressure range of 10 to 200 kPa and tabulated in Table 4.4. The adsorption of methane and CO₂ is stronger than for N₂, but this will not have a significant influence, since most methane and CO₂ will be adsorbed in the main adsorbent layer of the bed and thus the partial pressure of these gas components will be a lot smaller. The heat of adsorption on zeolite LiLSX for the adsorption of nitrogen is 18 kJ/mol [117].

It is concluded, based on the high working capacity, that zeolite LiLSX is best suitable for the adsorption of N₂. Any trace elements of ethane and CO₂ remaining in the mixture will adsorbed in the zeolite layer as well.

TABLE 4.4: Selectivity of N₂ over various gases on zeolite LiLSX.

| Selectivity | Zeolite LiLSX |
|---------------------------------|---------------|
| N ₂ /CO ₂ | 0.62 |
| N ₂ /CH ₄ | 0.52 |

The screening analysis presented above is solely based on literature data. For a first selection of the materials this is sufficient, but lab experiments are required to find the optimum materials. For example, there are many different types of activated carbons, with each a different working capacity for the different gases. This could be clearly seen from the data presented in Table 4.1, where the AC NC100 and the AC Norit R1 show a difference of almost 2 mol/kg for the working capacity of methane. At the moment, several different activated carbons are being tested in the lab already.

Furthermore, the isothermal working capacity and working selectivity are used to evaluate the different materials. This does not take into account the heat generated during adsorption. Ideally, adiabatic working capacity and working selectivity provide a better understanding of the adsorption characteristics for the different gases on the materials. It should therefore be noticed that the total amount adsorbed is therefore lower than calculated in the the screening performed in this study.

4.2.4 Adsorption of Trace Gases

In the natural gas mixture other trace elements can be present as well, which cannot be incorporated in the simulations due to the restricted number of components possible in MINSA (maximum of 5 components, see Section 3.3). However, it is important to consider the adsorption characteristics of these elements for a good understanding of their influence in a real system, for both the PSA itself and the fuel cell when the hydrogen is supplied as fuel to a vehicle. The main component to consider are sulphur components, including mercaptans and hydrogen sulphide. Furthermore, potentially small traces of water (40-70 mg/m³) can be present in the natural gas.

Mercaptans

Mercaptans are organic gases which are naturally found in living organisms. It is composed of carbon, hydrogen, and sulphur and is added to gas mixtures for safety, typically 200 ppb, as mercaptans have a strong odour of rotting cabbage [121, 122]. In the New South Wales gas network odorant is added in Longford for the EGP and in Young for the Moomba to Sydney pipeline. A concentration of 12 mg/m³ is injected, of which 70% is tetrahydrothiophene (C₄H₈S) and 30% tertiary butyl mercaptan (C₄H₁₀S). Mercaptans are polar gases, which are therefore strongly adsorbed by hydrophilic surfaces. Extensive literature is available on the adsorption of mercaptans on activated carbons, zeolites, and silica gel.

TABLE 4.5: Molecular dipole moments of various components [126].

| Component | Dipole moment [D] |
|-------------------|-------------------|
| Water | 1.84 |
| Propyl mercaptan | 1.60 |
| Ethyl mercaptan | 1.58 |
| Methyl mercaptan | 1.52 |
| Hydrogen sulphide | 0.98 |
| Carbon dioxide | 0 |

Activated carbon is mostly utilised to remove mercaptans from air. The adsorption of mercaptans strongly depends on the surface chemistry and the pore structure [123]. Bashkova et al. [124] reported that methyl mercaptans can oxidize to dimethyl disulphide on the surface of activated carbons, which forms a stronger adsorption due to the increased size and boiling point of the molecule. Furthermore, it is concluded that the adsorption properties are strongly affected by the surface oxygen groups. Lee et al. [125] studied the adsorption characteristics of activated carbon for acid and base treatments and concludes that the acid treatment increases the amount of functional groups, without altering the pore structure, which positively effects the adsorption capacity of methyl mercaptans on activated carbon. The chemisorptive bonding utilized in the adsorption of mercaptans on activated carbons makes regeneration challenging and utilizing activated carbons for removal of mercaptans not suitable for a cyclic process. Zeolites and silica gel form physisorptive bonds and are therefore easier regenerated [126, 127].

The adsorption of mercaptans on zeolites and silica gel increases with an increased polarity of the adsorbing gas [126]. Both materials are polar, which means that the materials have a higher affinity with molecules with a larger dipole moment. In Table 4.5 the dipole moments of the various components discussed in this section are listed. On silica gel, therefore, heavier mercaptans are more strongly adsorbed than light mercaptans. The adsorption of mercaptans on zeolites is also influenced by the pore size. As heavier mercaptans grow in critical diameter, the available adsorption sites in the zeolite decrease [126].

On the surface of an amorphous silica-alumina gel, mainly polar silanol groups (Si-OH) and siloxane groups (Si-O-Si) are present. Polar adsorptives form dipole interactions with the silanol by hydrogen bridges. Sulphur groups, such as mercaptans, form hydrogen bridges between the SH group and the silanol OH group. Furthermore, donor-acceptor interactions between the free electrons of the S atom in the sulphur component and the aluminum sites can be formed, where the free electrons are the donors [127].

It can be concluded from the analysis above that the pre-layer of silica gel will be sufficient to remove the mercaptans present in the natural gas mixture.

Hydrogen sulphide

Another sulphur component that is naturally present in the natural gas is hydrogen sulphide [128]. It is corrosive and toxic and removed from the natural gas as it may

damage the pipelines. Trace elements are extremely harmful for the catalyst of the fuel cell as well, just like the mercaptans. The adsorption properties are similar to that of the mercaptans as explained above. It has a smaller dipole moment, which relates to a less strong adsorption on the surface of both silica gel and zeolites. However, again the silica gel pre-layer selected for the adsorbent column will be able to deal with the adsorption of any trace elements of hydrogen sulphide.

Water

In natural gas, small amounts of water can be present as well, which decreases the heating value of the gas while increasing the volume [129]. It is not directly harmful for the fuel cell, but it does lower the efficiency [35]. Water is, however, a very strong adsorbent which makes it harmful for the adsorption process. Therefore, it is important to understand the adsorption characteristics of water on different adsorbents. The average water content in the natural gas mixture in Australia is 40-70 mg/m³. The adsorption of water on activated carbons primarily happens on the hydrophilic surface sites, forming strong chemisorptive bonds between the functional groups and the water [130]. The surface functional groups form hydrogen bonds with the water and when adsorption increases, clusters of water molecules will form around the adsorption site. Water can further adsorb into the micropores as the clusters grow. Desorption of water is achieved easily by decreasing the partial pressure, as the bonds are sufficiently weak [131].

Due to the large dipole moment, water is known to be a very strong adsorbing gas on silica gel and zeolites. Water mainly adsorbs on the silanol groups of the silica gel, which are present in large numbers and thus creates a high adsorption capacity for water. Hydrogen bridges are formed between the OH groups of water and the silanol groups on the silica-alumina gel surface. Donor-acceptor interactions with the aluminum sites are formed as well, with the free electrons of the oxygen atoms as donors. The oxygen atom is a harder base with a higher electronegativity, which makes the hydrogen bridges formed stronger, compared to sulphur components, but the donor-acceptor interactions weaker [127]. Water is more easily regenerated from silica gel than from zeolites, which is why this is the preferred material for water removal in PSA processes [52]. Concluding, any small amount of water present in the mixture can be adsorbed by the silica gel pre-layer, protecting the main activated carbon bed.

4.3 Simulation Results

The simulations are performed with a 5 vol% and 10 vol% hydrogen feed content. The results presented in this section focus on the thickness of the silica gel pre-layer, which is varied from 0 to 0.4 m for both cases. The results obtained at cyclic steady state (see Section 3.3) are compared for the different feed conditions and their adsorption profiles presented.

The simulation results for a 5 vol% hydrogen input feed are presented in Table 4.6 and for a 10 vol% hydrogen input feed in Table 4.7. Figure 4.6 through Figure 4.13 show

the solid loading and gas concentration profiles of the grouped heavy hydrocarbons and methane at the end of the adsorption step as a function of the length of the bed, for a feed input of 5 vol% and 10 vol% of hydrogen. The solid loading and gas concentration profiles for ethane, nitrogen, and hydrogen are summarised in Appendix C. In all graphs, the markers represent the data points as calculated by MINSA, and a smooth line is plotted through the points using Matlab to clearly show the trend.

The results show that the hydrogen product purity is above 99% for a pre-layer of 0.1, 0.2, and 0.3 meter for both a 5 vol% and 10 vol% hydrogen input feed. Without a pre-layer of silica gel, the hydrogen purity drops significantly to around 20% hydrogen purity. The solid loading adsorption of the grouped heavy hydrocarbons at the end of the adsorption step show a steep initial adsorption directly at the start of the bed. This can be seen for both cases in Figure 4.6 and Figure 4.10. Furthermore, along the rest of the bed, the heavy hydrocarbon adsorption resumes high. In the case of using a pre-layer, the steep adsorption loading is delayed, depending on the thickness of the pre-layer. This ensures a protection of the main activated carbon layer performed by the silica gel. The total amount adsorbed on the silica gel layer is relatively low, because the adsorption of the heavy hydrocarbons is less strong on silica gel compared to the adsorption on activated carbon. It is however beneficial to have a less strong adsorption of the heavy hydrocarbons in the pre-layer, such that desorption of the gases can be ensured.

Due to the strong adsorption of the grouped heavy hydrocarbons when no pre-layer is used, the total amount of methane adsorbed in the bed is significantly reduced, as can

TABLE 4.6: Overview of the simulation results for a hydrogen input feed of 5 vol%, for a varying silica gel pre-layer thickness.

| Pre-layer [m] | Top Output [%] | | Bottom Output [%] | | Total H ₂ product output [kg/day] |
|---------------|-----------------------|-------------------------|------------------------|------------------------------|----------------------------------------------|
| | H ₂ purity | H ₂ recovery | CH ₄ purity | H ₂ concentration | |
| 0.0 | 20.55 | 91.07 | 95.27 | 0.58 | 9.84 |
| 0.1 | 99.35 | 99.68 | 95.58 | 0.32 | 10.77 |
| 0.2 | 99.31 | 93.48 | 95.32 | 0.34 | 10.10 |
| 0.3 | 99.26 | 92.43 | 95.23 | 0.45 | 9.99 |
| 0.4 | 26.72 | 93.85 | 94.66 | 0.41 | 10.14 |

TABLE 4.7: Overview of the simulation results for a hydrogen input feed of 10 vol%, for a varying silica gel pre-layer thickness.

| Pre-layer [m] | Top Output [%] | | Bottom Output [%] | | Total H ₂ product output [kg/day] |
|---------------|-----------------------|-------------------------|------------------------|------------------------------|----------------------------------------------|
| | H ₂ purity | H ₂ recovery | CH ₄ purity | H ₂ concentration | |
| 0.0 | 16.47 | 95.06 | 93.71 | 1.28 | 20.60 |
| 0.1 | 99.70 | 95.72 | 95.33 | 0.41 | 20.74 |
| 0.2 | 99.78 | 94.98 | 95.26 | 0.52 | 20.58 |
| 0.3 | 99.77 | 94.06 | 95.08 | 0.64 | 20.38 |
| 0.4 | 23.72 | 97.02 | 93.24 | 0.58 | 21.02 |

be seen for both cases in Figure 4.8 and Figure 4.12. The heavy hydrocarbons occupy all the sites in the activated carbon, leaving not enough sites available for the adsorption of the methane. Due to the strong adsorption of the heavy hydrocarbons on the activated carbon, at the desorption pressure, the heavy hydrocarbons will not desorb. Therefore, as the process is continued for more and more cycles, the amount of available sites will continue decreasing. This accumulation of the heavy hydrocarbons can be prevented with a pre-layer. The gas concentration profiles confirm the high methane concentration left at the end of the bed for both a 5 vol% and 10 vol% hydrogen feed input, as can be seen in Figure 4.9 and Figure 4.13. It must be noted that for a system with no pre-layer, cyclic steady state cannot be achieved, as the accumulation of the heavy hydrocarbons and CO₂ continue with each cycle. The purity of the hydrogen product will therefore continue to decrease.

When the pre-layer is increased to 0.4 meter, the hydrogen purity drops as well to around 25% purity. Due to the length of the pre-layer, the adsorption of the heavy hydrocarbons is strongly delayed. The total length of the activated carbon in the scenario where a pre-layer of 0.4 meter is used, is reduced to 0.7 meter. In the adsorption profile of methane, the solid loading is delayed, similarly to the heavy hydrocarbons. The adsorption loading stays very high nearing the end of the bed, whereas in the other scenarios where a shorter pre-layer is used, the methane adsorption drops. This suggests that the methane concentration in the gas mixture is still very high. In Figure 4.9 and Figure 4.13 the gas concentration of methane is plotted as a function of the bed length for the case where 5 vol% and 10 vol% of hydrogen is used in the feed gas. This clearly illustrates the methane concentration is still very high at the end of the bed, resulting in a low purity hydrogen product.

Due to the increased pre-layer, the length of the main layer is decreased as such that there is not enough activated carbon to adsorb all the methane present. In the case where a 5 vol% of hydrogen is used as the feed gas, the methane is adsorbed in the last zeolite layer as well. For the 10 vol% hydrogen feed, this is not the case. This difference is caused by the total amount of natural gas in the input mixture. When only 5 vol% of hydrogen is added, there is around 90% methane present. When 10 vol% of hydrogen is added, only 86% of methane has to be adsorbed, which causes the difference in the profiles. The gas concentration of the grouped heavy hydrocarbons is still high at the end of the bed. Adsorption is competitive, therefore the large amount of methane still present due to the long pre-layer is preferably adsorbed in the main layer compared to the heavy hydrocarbons. This decreases the adsorption of heavy hydrocarbons at the end of the bed, which did happen in the simulations with a shorter pre-layer, as all methane was already adsorbed at that point in the bed.

The hydrogen recovery achieved is for all cases >90%. The methane purity in the bottom product is for all simulations around 95%. Only for the simulation results for a 10 vol% hydrogen input feed with no pre-layer and with a pre-layer of 0.4 meter, the methane purity is around 93%. The amount of hydrogen in the bottom product is always below 1% except for the simulation with a 10 vol% hydrogen feed input and no pre-layer. Then the hydrogen concentration in the bottom product is 1.28%. The total amount of hydrogen produced during a full day is around 10 kg for a feed input of 5

vol% hydrogen and doubled to 20 kg of hydrogen when the feed input concentration is doubled as well to 10 vol%.

The simulations are optimised for a high hydrogen purity product and a high recovery. Therefore, the hydrogen purity achieved in the simulations performed for both cases of hydrogen in the feed stream are around 99.5%, with a recovery of >90%. In the design of the PSA process, a trade off must always be made between a high purity and a high recovery. The simulations performed during this study focused on the optimisation of the PSA process for a high purity hydrogen (of >99%) and a high recovery. A high recovery is economically beneficial, however, in this case it means that the purity of the hydrogen achieved does not meet the fuel cell quality requirements (see Table 1.1).

The purity requirements can be achieved with the proposed PSA system by decreasing the adsorption time. This, however, does significantly reduce the recovery of the system, which is an economical trade off that must be made. Another option to meet the hydrogen purity requirement, is to add an additional purifying unit. Different options can be considered. An additional simple two bed PSA can be used, which focuses on the adsorption of the hydrocarbons left in the hydrogen product. Furthermore, the use of a membrane to enrich the hydrogen input stream before the gas enters the PSA process can be considered, as proposed by Liemberger et al. [38]. The hydrogen product can also be purified by a membrane after the PSA process. A further feasibility study is required to fully investigate the different options.

It can be concluded that to ensure high purity hydrogen, a pre-layer of at least 0.1 meter is required and a maximum of 0.3 meter. No pre-layer causes the heavy hydrocarbons to accumulate on the activated carbon and thus reducing the sites available for methane adsorption, resulting in a low purity hydrogen product. Using a pre-layer which is too long, reduces the total amount of activated carbon left and leaving not enough adsorbent to adsorb the methane present in the mixture. This effect is stronger in the case of 5 vol% of hydrogen used in the feed stream, as more methane is initially present. The ideal pre-layer therefore has a thickness of 0.2 meter, ensuring enough activated carbon present to adsorb all the methane and enough silica gel pre-layer to prevent accumulation of the heavy hydrocarbons.

The temperature profiles as a function of the bed length are presented in Appendix C for both a 5 vol% and 10 vol% hydrogen feed input. An increase in the temperature is observed at the beginning of the bed, which peaks around the start of the main layer, in the case of 0.1, 0.2 and 0.3 meter pre-layer. If no pre-layer is used, the temperature profile is relatively steady. This is caused by the accumulated heavy hydrocarbons, which occupy the adsorption sites and thus not much adsorption is able to happen. The temperature profile for a pre-layer of 0.4 meter is also relatively flat, but higher temperatures are achieved due to the larger amount of methane adsorption possible in the main layer. The maximum temperature reached for a 5 vol% hydrogen feed input is 308 K, and for a 10 vol% hydrogen input feed 315 K. In both cases, the pre-layer thickness is 0.2 meter, which confirms that this is the ideal pre-layer thickness, as most adsorption happens. Furthermore, for all simulations the pressure drop is within 5 kPa from the feed pressure of 20 bar.

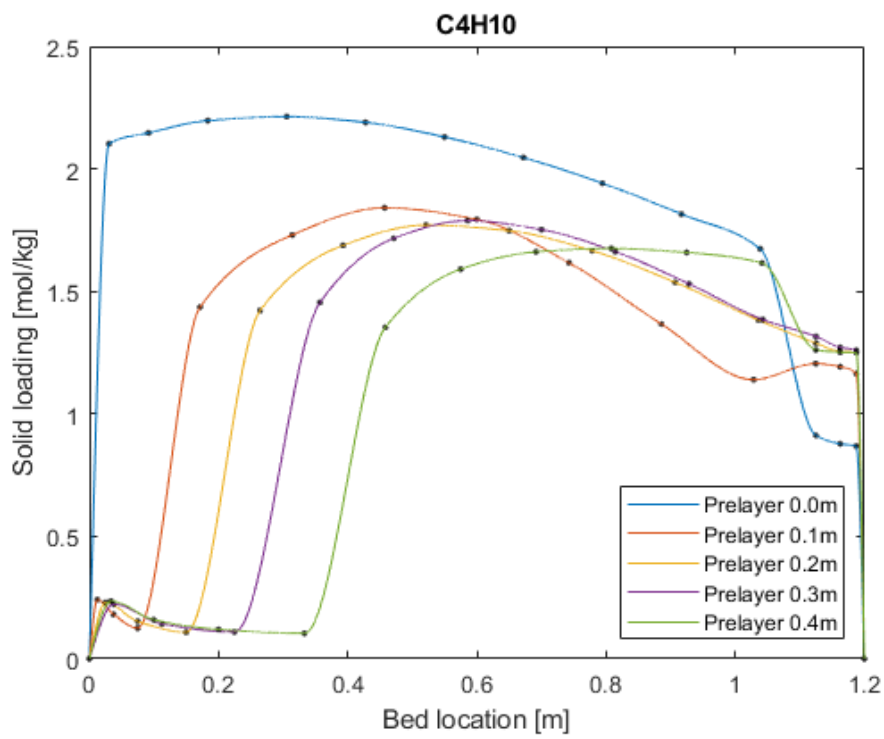


FIGURE 4.6: Solid loading of the heavy hydrocarbons at the end of the adsorption step for a 5 vol% hydrogen feed input.

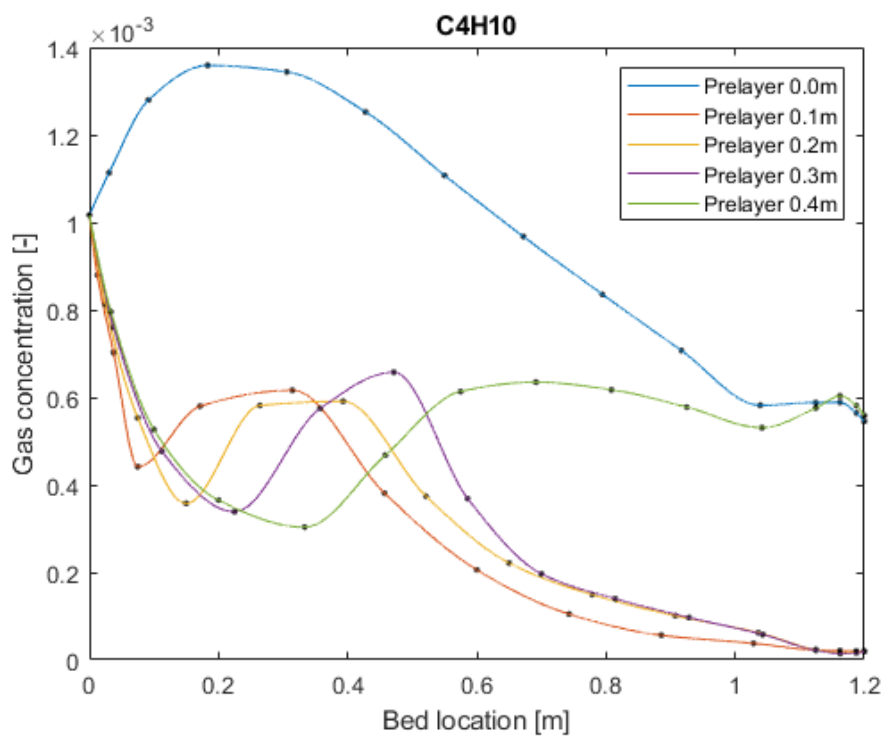


FIGURE 4.7: Gas concentration of the heavy hydrocarbons at the end of the adsorption step for a 5 vol% hydrogen feed input.

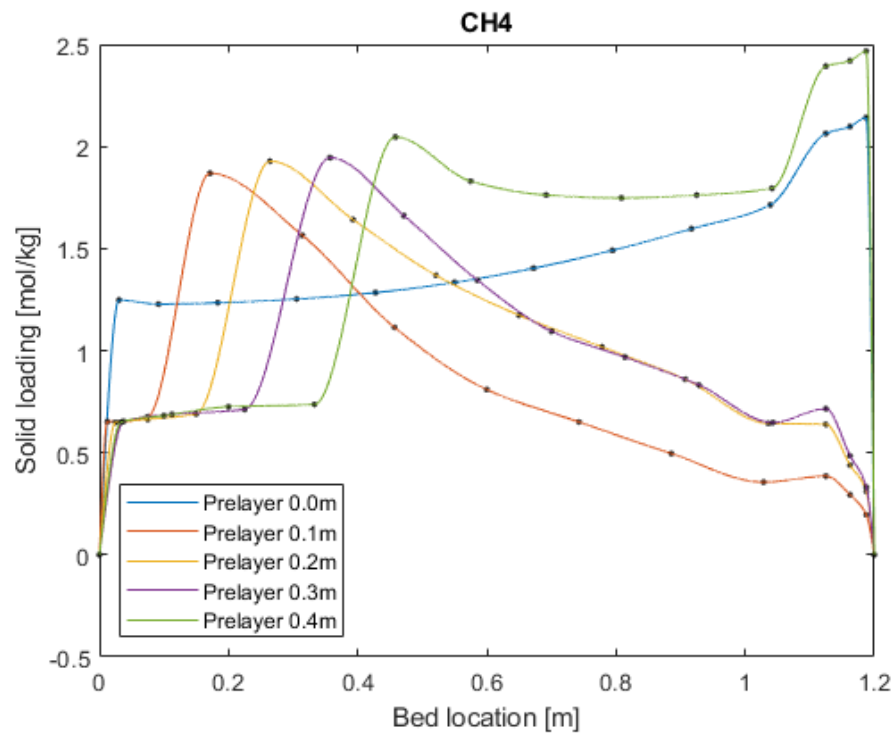


FIGURE 4.8: Solid loading of the methane at the end of the adsorption step for a 5 vol% hydrogen feed input.

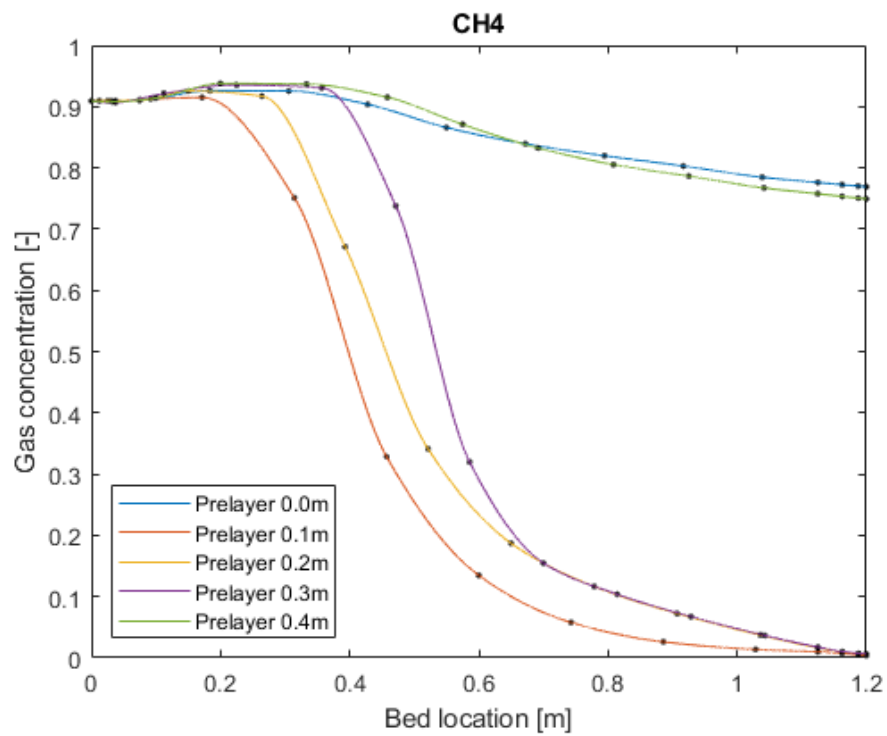


FIGURE 4.9: Gas concentration of the methane at the end of the adsorption step for a 5 vol% hydrogen feed input.

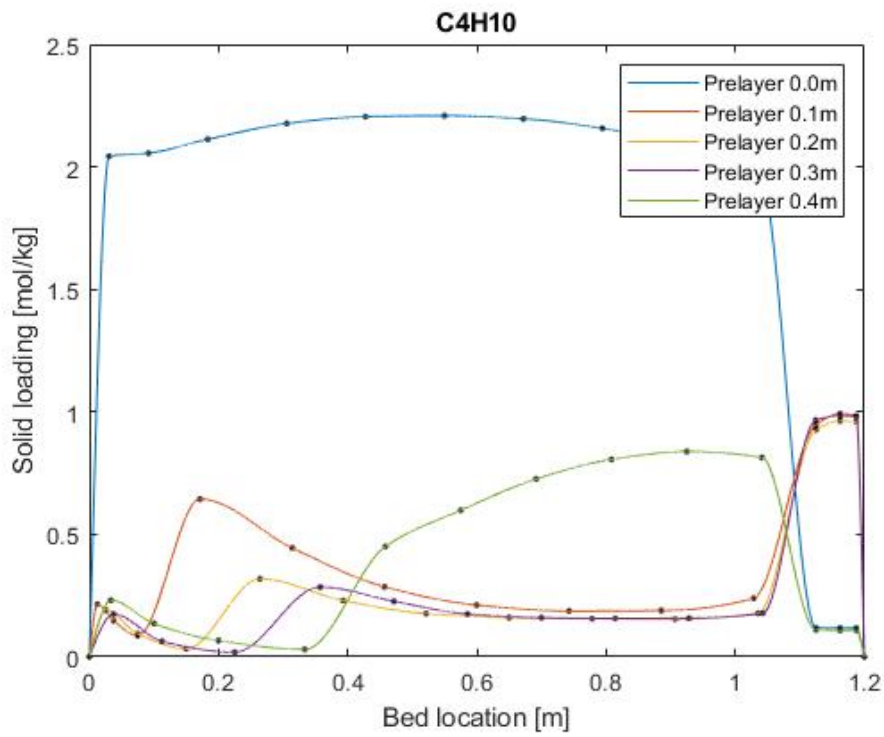


FIGURE 4.10: Solid loading of the heavy hydrocarbons at the end of the adsorption step for a 10 vol% hydrogen feed input.

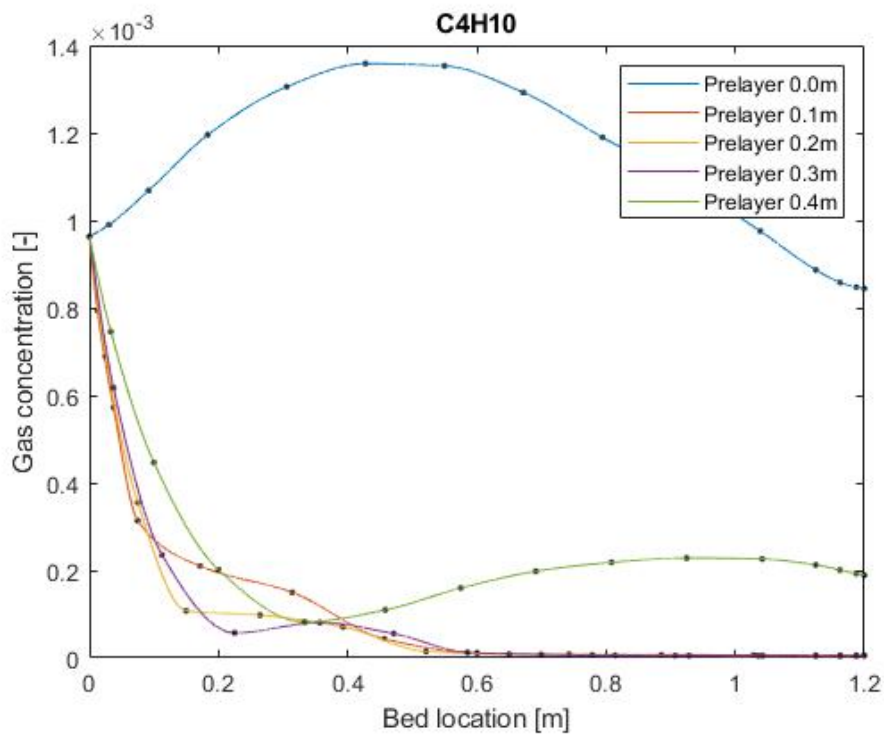


FIGURE 4.11: Gas concentration of the heavy hydrocarbons at the end of the adsorption step for a 10 vol% hydrogen feed input.

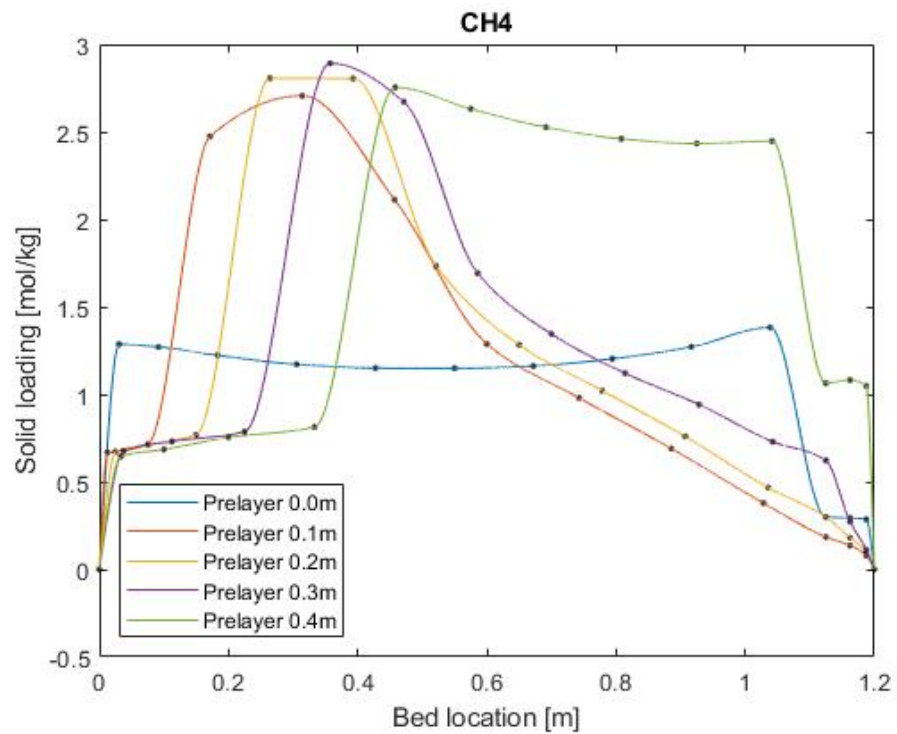


FIGURE 4.12: Solid loading of the methane at the end of the adsorption step for a 10 vol% hydrogen feed input.

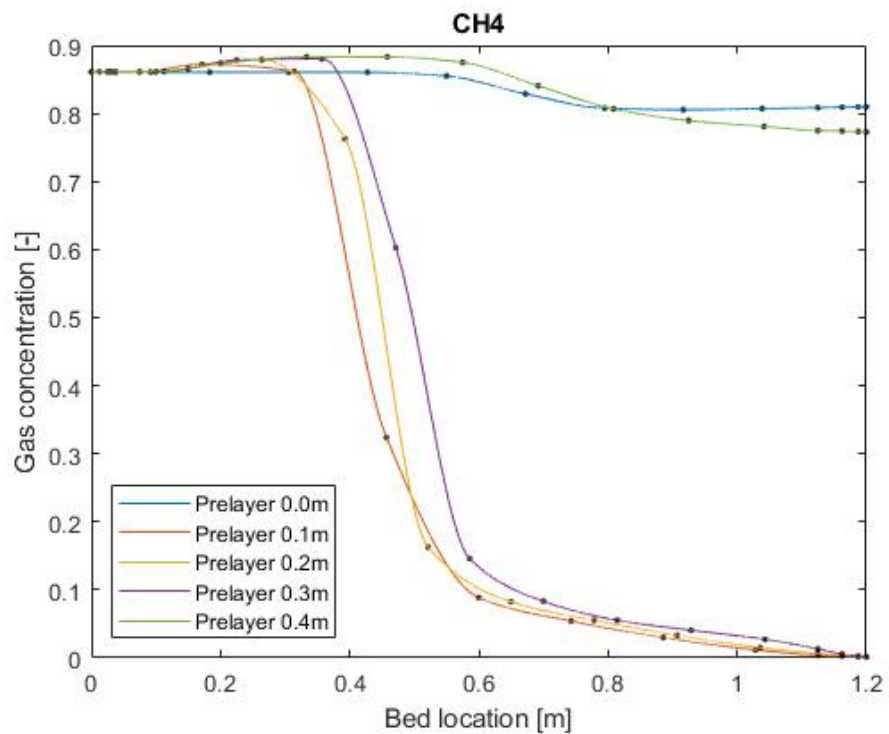


FIGURE 4.13: Gas concentration of the methane at the end of the adsorption step for a 10 vol% hydrogen feed input.

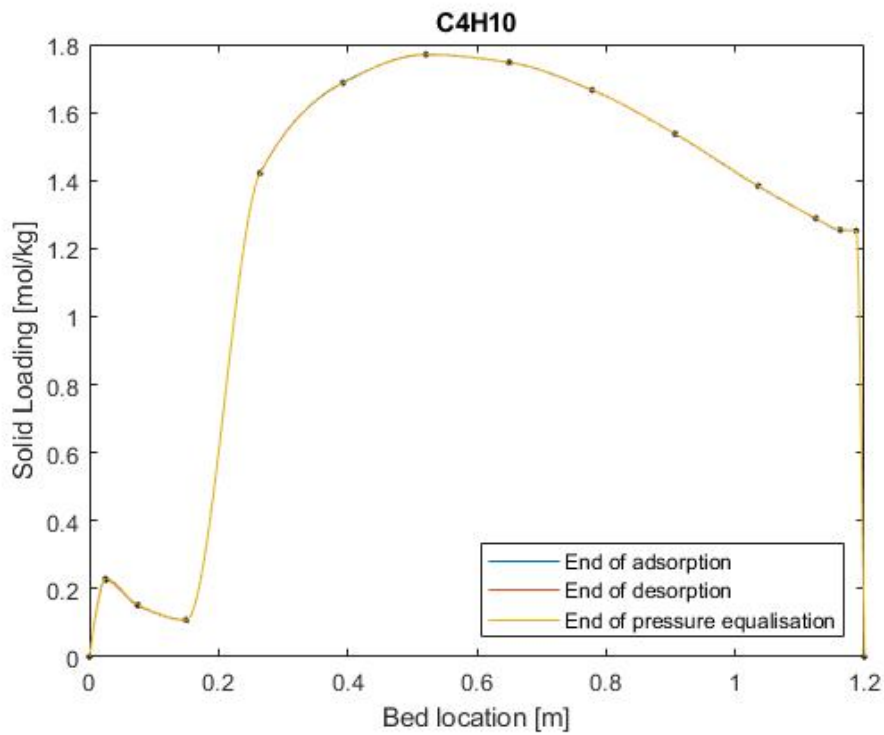


FIGURE 4.14: Solid loading of the heavy hydrocarbons at the end of the adsorption step, end of desorption step, and the end of the pressure equalisation steps for a 5 vol% hydrogen feed input.

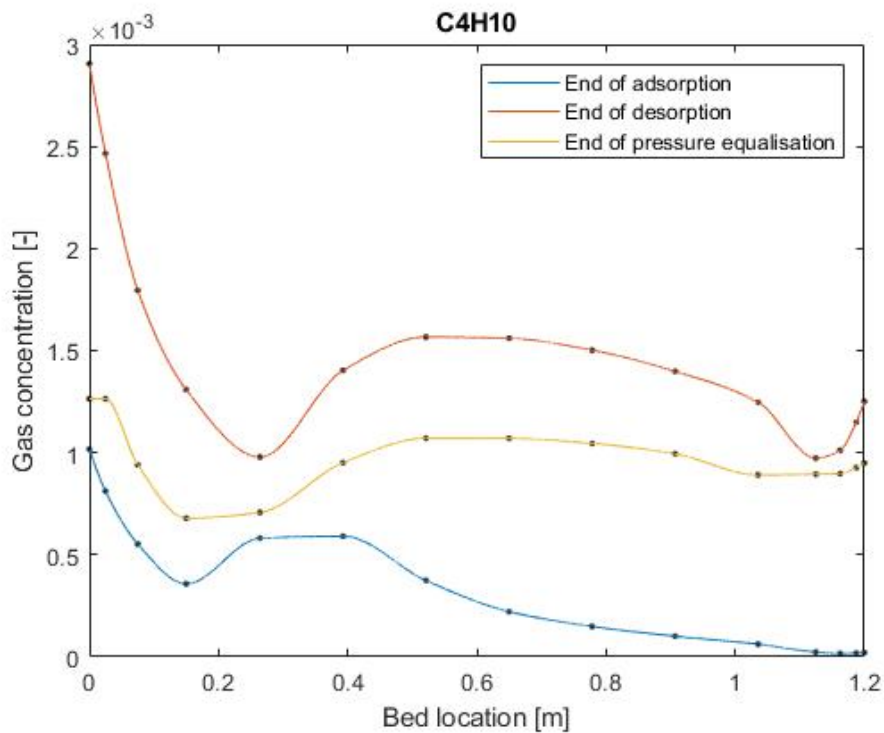


FIGURE 4.15: Gas concentration of the heavy hydrocarbons at the end of the adsorption step, end of desorption step, and the end of the pressure equalisation steps for a 5 vol% hydrogen feed input.

TABLE 4.8: Gas concentrations and adsorption amount of heavy hydrocarbons at different location in the bed, at the end of the adsorption, pressure equalisation, and desorption step.

| Bed location | Gas concentration [-] | | | Solid loading [mol/kg] | | |
|--------------|-----------------------|----------|------------|------------------------|-----------|------------|
| | Adsorption | PE | Desorption | Adsorption | PE | Desorption |
| Bottom | 8.12E-04 | 1.26E-03 | 2.47E-03 | 2.293E-01 | 2.289E-01 | 2.251E-01 |
| Pre-layer | 3.57E-04 | 6.79E-04 | 1.31E-03 | 1.089E-01 | 1.087E-01 | 1.082E-01 |
| Main layer | 2.21E-04 | 1.07E-03 | 1.56E-03 | 1.747E+00 | 1.747E+00 | 1.746E+00 |
| Top layer | 1.77E-05 | 9.26E-04 | 1.15E-03 | 1.252E+00 | 1.252E+00 | 1.251E+00 |

To get a better understanding of what happens during the entire cycle, not only the adsorption characteristics at the end of the adsorption step are interesting to consider, but also the adsorption at the end of the pressure equalisation and desorption steps. In Figure 4.14 and Figure 4.15 the solid loading and gas concentration of the grouped heavy hydrocarbons at the end of the adsorption, desorption, and pressure equalisation steps are presented.

The heavy hydrocarbons present overlapping lines at the end of the adsorption, desorption, and pressure equalisation steps. From the adsorption data tabulated in Table 4.8 it can be seen that the heavy hydrocarbons desorb during the pressure equalisation step and the desorption step. Only a small amount of heavy hydrocarbons is supplied to the system, so the amount of gas desorbed is relative to this feed input. In the gas concentration profile of the heavy hydrocarbons there is a strong increase in the concentration at the end of the desorption step. This proves that the pre-layer is very important for the desorption of the heavy hydrocarbons in the cycle.

To illustrate the separation process simulated, a flow diagram of the gas flows going in and coming out of the PSA system is represented in Figure 4.16. A feed stream of 10 vol% of hydrogen is used, which results in a mixture of 86.1 vol% of methane, 2.62 vol% of ethane and CO₂, 1.15 vol% of nitrogen and only 0.096 vol% of the heavy hydrocarbons.

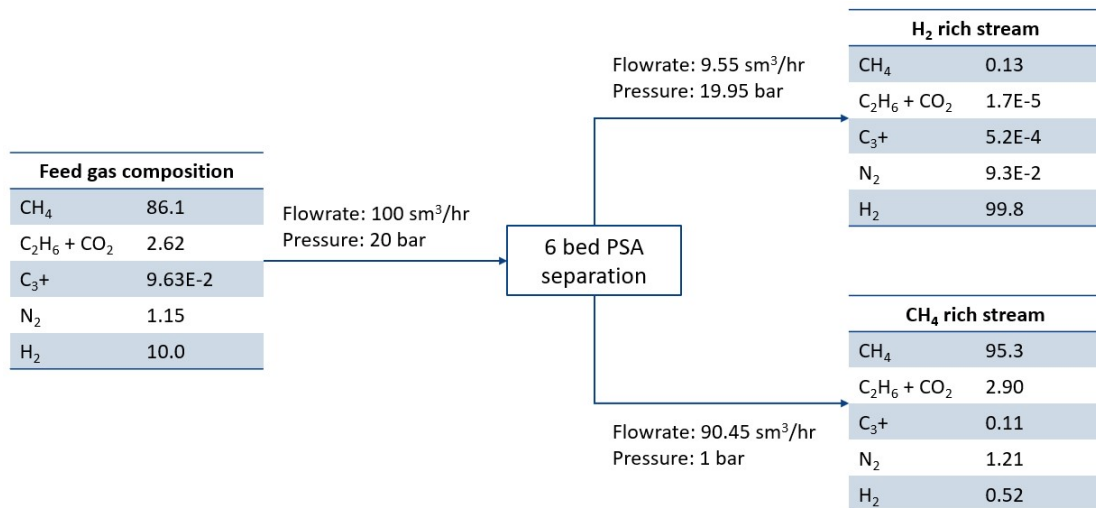


FIGURE 4.16: Gas flows in the separation of hydrogen and natural gas by a PSA process using a 10 vol% hydrogen input feed and a pre-layer of 0.2 meter.

Due to the maximum number of gas components in the MINSA simulator, ethane and CO₂ are combined, so are the heavy hydrocarbons (C₃+).

The feed gas enters the PSA system with a flow rate of 100 sm³/hr at a pressure of 20 bar. The PSA separates the mixture, producing a hydrogen rich stream at the top and a methane rich stream at the bottom. The top stream leaves the PSA system at a slightly reduced pressure of 19.95 bar and a flow rate of 9.55 sm³/hr during the adsorption step. The hydrogen purity of this stream is 99.8 vol%, with methane as the main contaminating gas left in the mixture. The methane rich stream leaves the bottom of the PSA system at atmospheric pressure during the blowdown step with a flow rate of 90.45 sm³/hr. A total of 95.3 vol% of methane is present in this mixture, and just 0.52 vol% of hydrogen.

The performed simulations are based on isotherm data from literature, which gives a good insight in the adsorption characteristics. However, to optimise the simulation results, the isotherm data should be measured in the lab for each material and each gas. Currently, these experiments are being performed for silica gel, different types of activated carbon, and zeolite LiLSX. These data will replace the literature data currently used in the simulations, providing more representative results of the PSA process.

Furthermore, breakthrough experiments must be performed in order to get a better understanding of the kinetics in the bed. Currently the mass transfer is calculated according to the Gleuckauf equation (see Equation 2.17), in which the diffusion coefficients are calculated by MINSA. With the results obtained from break through experiments, the Gleuckauf equation will be replaced by the measured data representing the mass transfer and thus the mass transfer can be represented more accurately.

The focus of this work is on the PSA process at 20 bar and 298 K. The pressure is indicative for the place in the gas distribution network where the PSA will be operating. This will be in the secondary transmission pipeline which transports the natural gas at pressures between 10 to 70 bar. Currently, the operation of the PSA process is simulated for a pressure of 30 bar and 50 bar as well, by other members of the research group. It is considered unlikely for the PSA to operate at much higher pressures, as this will significantly drive the capital cost of the PSA process. At higher pressures the valves that can be used are significantly more expensive than at lower pressures. A typical operating pressure of a PSA in industry is between 10 - 40 bar [132], therefore no other pressures are considered in the simulations.

Furthermore, the temperature at which the system operates is assumed 298 K. In Australia, the temperature at different times a year and at different location in the country, can vary greatly. With increasing temperature, the total amount of gas adsorbed decreases. It is therefore interesting to simulate the PSA process at different operating temperatures relevant to the conditions applicable in Australia, to see how big the influence of this can be.

The process analysis in this study focused on the thickness of the pre-layer. The thickness of the post-layer, zeolite LiLSX, has been fixed to 0.1 meter. The influence of the thickness of this zeolite layer will be an interesting process analysis to perform in

future work. The gas mixture of natural gas from different sources varies, which might lead to a conclusion that for some areas a different thickness of each layer is required to optimise the separation of hydrogen from natural gas.

4.4 Summary

A screening analysis is performed for the selection of the adsorbent materials in the beds. Activated carbon is selected as the adsorbent for the main layer in the bed, as it has a high working capacity and selectivity for methane, which is the main component in the gas mixture. It is a commercial material, and therefore available at low cost. To prevent the heavy hydrocarbons from accumulating in the main layer, a pre-layer is required. Silica gel is selected as the pre-layer material, because it has a linear isotherm profile for the heavy hydrocarbons and CO₂, meaning that the gas components can be desorbed during the blowdown step, and thus regenerating the bed. Lastly, nitrogen is not adsorbed well on activated carbon or silica gel, therefore a final layer of zeolite is used. Zeolite LiLSX showed the highest working capacity for nitrogen, and is therefore selected.

The simulations performed in this study assumed a hydrogen input feed of 5 vol% and 10 vol% and operating conditions of 20 bar, 298 K. The thickness of the pre-layer is evaluated, looking at a thickness of 0 to 0.4 meter, with the goal to produce high purity hydrogen (>99%). The final zeolite layer is fixed at 0.1 meter and the total height of the column is 1.2 meter. When using no pre-layer, the heavy hydrocarbons accumulate in the activated carbon main layer. This reduces the number of sites available in the activated carbon for the methane to adsorb. Therefore, the hydrogen purity is not achieved. When a pre-layer of 0.4 meter is used, the total amount of activated carbon left is reduced to only 0.7 meter. This is not enough to adsorb all the methane in the gas mixture, and therefore the hydrogen purity is not achieved either. The optimum pre-layer thickness is therefore 0.2 meter in a bed of 1.2 meter height.

Chapter 5

Techno-Economic Analysis

5.1 Introduction

This chapter discusses the economic feasibility of hydrogen supplied by a PSA system at a refuelling station. The main components required at such a refuelling station are presented in Figure 5.1. The natural gas and hydrogen mixture is drawn from the gas pipeline at a pressure of 20 bar and used as input feed stream for the PSA system. A pure hydrogen product is obtained at the top of the PSA system and initially stored in a low pressure vessel at 20 bar. Next, the hydrogen must be compressed and stored such that a dispenser can fill up a fuel cell vehicle. The maximum pressure in the vehicle tank is 700 bar. Therefore, hydrogen is stored at higher pressures, which can be done in different ways. In this schematic, part of the hydrogen is compressed to a medium pressure (200-500 bar) and part is stored at a high pressure (900-1000 bar).

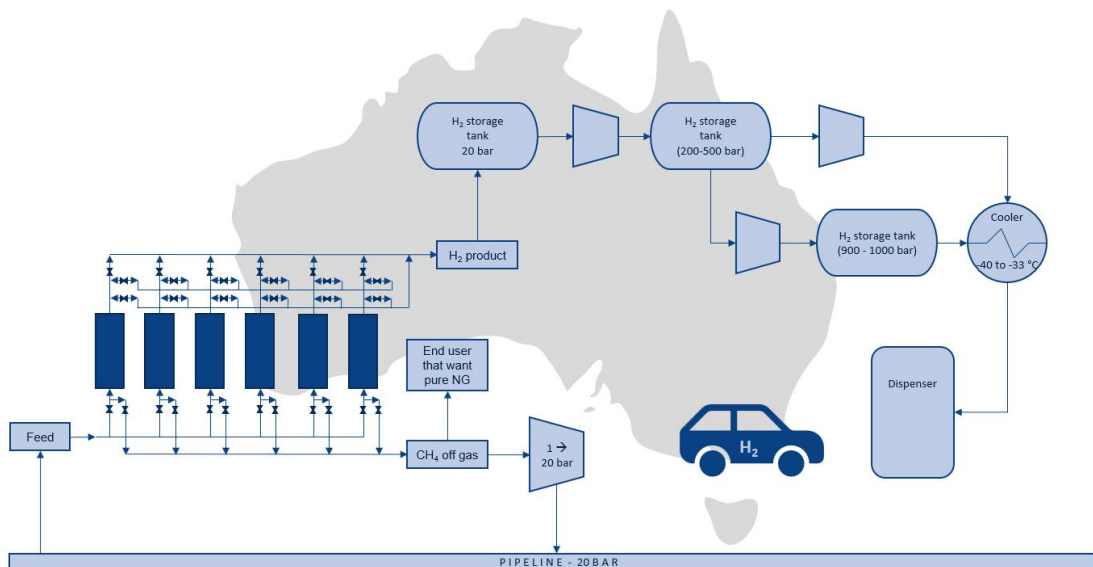


FIGURE 5.1: Schematic overview of a hydrogen refuelling station where a PSA process is used to separate the hydrogen from the natural gas mixture, transported in the natural gas pipeline network.

When dispensing, hydrogen can either directly be drawn from the high pressure storage tank, or first from the medium pressure tank and then from the high pressure tank. A cooler is always required to cool the gas down to at least $-33\text{ }^{\circ}\text{C}$ before a vehicle can be filled by the dispenser. Furthermore, the methane rich stream can either be supplied back into the natural gas pipeline network or directly supplied to other end users, which require a pure natural gas. If the downstream product is supplied back to the pipeline network, the gas must be compressed to the required pressure in the pipeline. This is not necessarily the same pipeline at 20 bar as the gas was drawn from, but can be another nearby pipeline at lower pressures. This significantly reduces the pressure ratio of the compressor and will therefore be less costly.

5.2 Design Hydrogen Refuelling Station

This section presents the detailed design of the hydrogen refuelling station at which the PSA system separates the hydrogen and natural gas, delivered by a pipeline. The design focuses on a 10 vol% of hydrogen in the natural gas mixture. Three different scenario's are considered, where the hydrogen demand per day is varied as presented in Table 3.5.

5.2.1 Design PSA system

The sizing of the PSA process is based on the scaling of the flowrate with the height and the inner diameter of the adsorption bed. The results are presented in Table 5.1. The first row represents the dimensions and flowrates used for the simulation, as presented in Chapter 4. For a 10 vol% hydrogen in the gas mixture, a product of 20 kg of hydrogen is produced. With this, the flowrate for a production of 350, 700, and 1000 kg of hydrogen can be scaled accordingly. The inner diameter and the height of the column are scaled with the flowrate, keeping the ratio of the height over the diameter around 4. As discussed in Section 3.4.1, this is not an ideal scaling, where the column height is kept constant to ensure the pressure drop does not increase. Due to the operating pressure and the heat generation insight the bed, this is not a feasible design option and thus the height and the inner diameter are scaled with the flowrate.

TABLE 5.1: Dimensions PSA columns for a different hydrogen product demand, representing different sizes of hydrogen refuelling station.

| Output product [kg H ₂ /day] | Input volume flow [m ³ /hr] | Inner Diameter [m] | Height [m] | Ratio H:ID | Velocity [m/s] |
|--------------------------------------------|-------------------------------------------|-----------------------|------------|------------|----------------|
| 20 | 100 | 0.30 | 1.20 | 4.00 | 0.40 |
| 350 | 1750 | 0.80 | 2.95 | 3.69 | 0.97 |
| 700 | 3500 | 1.00 | 3.78 | 3.78 | 1.24 |
| 1000 | 5000 | 1.10 | 4.46 | 4.06 | 1.23 |

A continuous operation of the PSA is assumed, as this results in the smallest columns for the PSA process. The PSA cycle is easily paused and continued, therefore the operation time of the PSA is controlled by the hydrogen demand. A pressure based

system, in which the PSA is switched on as soon as the pressure in the hydrogen storage tank drops below a certain threshold, is utilised. If necessary the PSA runs 24 hours on a day, to meet the hydrogen fuelling demand. If the demand is lower at a given day, the PSA operation is limited to what is required, saving energy for the separation process and for the compression as well.

Furthermore, to ensure a continuous operation of the PSA process, the installation of two additional adsorption columns should be considered at the refuelling station. This is both convenient when something happens in the system and when maintenance is required. The additional columns can then be utilised to keep providing a hydrogen production flow, such that the refuelling station does not have to shut down.

One of the scale up PSA processes is simulated, representing a small refuelling station producing 350 kg of hydrogen per day. The operating conditions are summarised in Table 5.2. A total height of the column of 3.5 meters is used with a diameter of 0.85 meter. Simulation results obtained showed that a product of around 350 kg of hydrogen can be produced per day. Further research is required to optimise the simulation further.

TABLE 5.2: Input values for scale up PSA process, producing 350 kg of hydrogen per day.

| Component | Value | Unit |
|------------------|-------|---------------------|
| Silica gel | 0.6 | m |
| Activated carbon | 2.6 | m |
| Zeolite LiLSX | 0.3 | m |
| Height bed | 3.5 | m |
| Inner diameter | 0.85 | m |
| Flowrate | 1500 | sm ³ /hr |
| Hydrogen input | 10 | vol% |

Lastly, the compressor for the waste stream at the bottom of the PSA is designed. This is done using Aspen HYSYS. Depending on the location of the refuelling station, this gas stream can be supplied to another distribution pipe than it was extracted from (see Figure 2.15). If the refuelling station is located in a domestic area, it is very likely a low pressure distribution pipeline is available at 2 to 4 bar. In this case, the methane rich stream requires a compression of only 1 to 3 bar. The compressors are designed for the three different refuelling station scenario's, and the results are presented in Table 5.3.

TABLE 5.3: Results of the Aspen HYSYS compressor design for the compressor of the waste stream. The three flowrates represent the streams of a small, medium, and large refuelling station, respectively. Cost for compressor and cooler are equipment cost.

| Flowrate [gmol/s] | Duty [kW] | Compressor costs [\$] | Cooler costs [\$] |
|-------------------|-----------|-----------------------|-------------------|
| 23 | 78 | 285,500.00 | 23,600.00 |
| 47 | 158 | 470,500.00 | 36,300.00 |
| 67 | 256 | 600,000.00 | 45,900.00 |

The compressors are reciprocating integral gas engine compressors and an efficiency of 55% is assumed. To ensure a safe compression a cooler is added.

5.2.2 Design Compression and Storage

For the compression and storage of hydrogen at a hydrogen refuelling station a balance must be found between the pressure at which what amount of hydrogen is stored, the total amount of hydrogen that is stored on-site, and the size and total number of storage tanks.

The total storage capacity at the refuelling station must meet the hydrogen demand at any time of the day. This demand fluctuates hourly during the day, but also fluctuates daily during a week. Figure 5.2 represents the fluctuation in demand at a gasoline station in the US during a day. The average hourly demand is 4.2% of the total daily demand [20]. In order to meet the demand during the peak hours at a refuelling station, the storage capacity must be the sum of the above average demand during a full day. This is about 30% of the total daily demand and is used as an estimation of the total storage capacity required at a hydrogen refuelling station. Therefore, a minimum storage capacity of 105, 210, and 300 kg of hydrogen is required, respectively, for a small, medium, and large refuelling station.

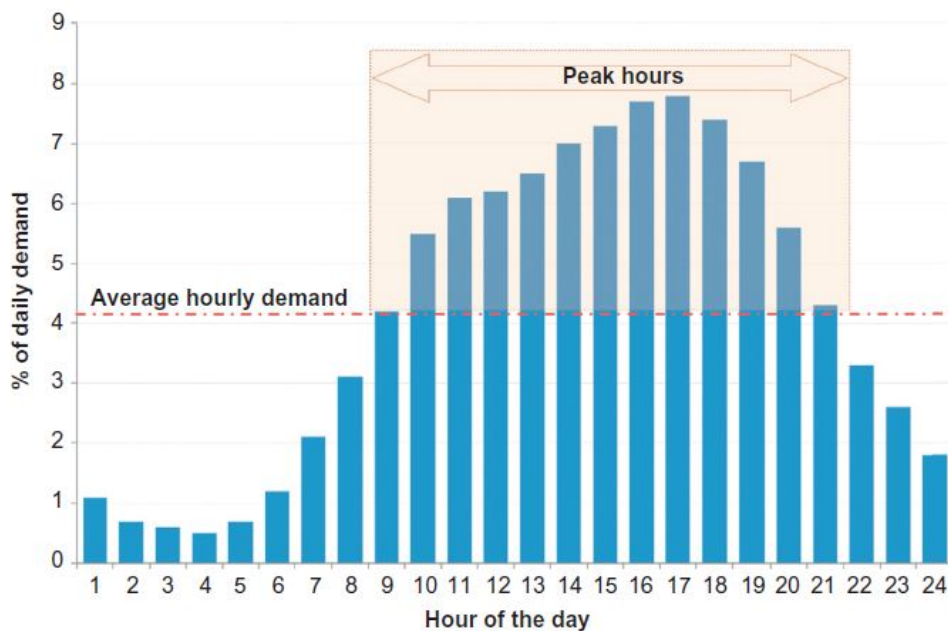


FIGURE 5.2: Variations in the demand per hour during a day for a gasoline station in the US [20].

For the sizing of the storage tanks and the compression, the HRSAM model is used. A total overview of the simulation results is presented in Appendix D. The main design parameters are presented in Table 5.4. The number of dispensers required is based on the total hydrogen demand per day. The capacity of one dispenser estimated to be 500

kg of hydrogen per day, hence the small refuelling station requires only one dispenser and the larger two stations require 2. For a larger demand, the land area of the station increases as well, as the number of dispensers and storage capacity increases. It must be noted that this area does not include the area required for the PSA system.

The cascade system consists of various hydrogen storage tanks at different pressures. Each cascade system consists of 3 tanks of the same size, with a different minimum pressure. For the low, medium, and high pressure vessels the minimum pressure is 330, 613, and 802 bar, respectively. When refuelling, hydrogen is first drawn from the low pressure vessel, followed by the medium, and then the high pressure vessel. The size of the vessels in the cascade system is fixed, therefore the number of cascade systems increases for a larger hydrogen demand. The optimum number of cascade systems for a small refuelling station is 4, and for a medium and larger refuelling station, respectively, 6 and 8.

The low pressure storage has a capacity of approximately 30% of the daily demand, storing the hydrogen at 20 bar. The model assumes pure hydrogen delivered by a pipeline at 20 bar. When using a PSA, the hydrogen rich stream leaving the system is at around 20 bar as well, therefore the same low pressure storage tank can be used.

The compressor supplies hydrogen from the low pressure storage tank to the cascade system to ensure the appropriate pressures in the different tanks is continuously maintained. Evidently, the minimum compressor flowrate increases as the cascade system increases as well. During the peak hours, as most hydrogen is dispensed, the compressor has to fill the cascade system accordingly, therefore a larger flowrate is required. Furthermore, an additional back up compressor is considered in the design by the HRSAM model.

There are different ways in which a hydrogen refuelling station can be designed. Another common way of compressing the hydrogen to the required pressures at a refuelling

TABLE 5.4: Main variables in HRSAM model design for a hydrogen refuelling station.

| Variable | Small HRS | Medium HRS | Large HRS | Unit |
|------------------------------------------------------------------------------|-----------|------------|-----------|----------------|
| Number of dispensers | 1 | 2 | 2 | - |
| Average Hourly Demand During a Day | 15 | 29 | 42 | kg/hr |
| Station land area | 198 | 396 | 402 | m ² |
| Cascade system | | | | |
| Cascade size required at refuelling station | 161 | 241 | 322 | kg |
| Low Pressure Storage Needed Amount at Refueling Station for Peak Hours Surge | 112 | 224 | 311 | kg |
| Optimum Number of Cascade Systems | 4 | 6 | 8 | - |
| Maximum Dispensable Amount from Cascade | 47.3 | 71 | 94.7 | kg |
| Compressor | | | | |
| Minimum Compressor Capacity | 15 | 29 | 42 | kg/hr |
| Average Compressor Demand During a Day | 0.243 | 0.486 | 0.694 | kg/min |
| Required Compressor Flowrate for Peak and Adjacent Hour | 21.3 | 47.4 | 62.8 | kg/hr |
| Required Compressor Flowrate Above Average for Peak Hour | 0.111 | 0.305 | 0.353 | kg/min |

station is by an ionic compressor. This compressor is capable of compressing the hydrogen from pressures as low as 5 bar up to 1000 bar [133]. TFA Project Group are fuel industry specialists in Australia, which is also engaged in hydrogen refuelling stations [134]. Their hydrogen station design also utilises an ionic compressor. In Australia, several sites are under development, but non are at commercial scale yet.

5.3 Techno-Economic Analysis

The following section presents the economics of the designed refuelling station as discussed above. All prices are provided in Australian dollars. First, the capital cost and the operating cost of the PSA system are discussed, followed by the economics of the storage and compression.

5.3.1 Economics PSA system

The equipment costs of the major components for the PSA process are presented in Table 5.5. The sizes of the pressure vessels are indicative for a medium sized refuelling station, at which 700 kg of hydrogen is produced per day, with an input feed of 10 vol% of hydrogen. The adsorbent material prices are obtained by online research, the cost for the pressure vessels, storage tank, and valves are based on quotations of various companies. The compressor cost is calculated using the build in economic analysis tool in Aspen HYSYS.

The PSA process requires a lot of valves for operating the process. All beds must be connected by pipelines, where valves control the flowrates from and to the different beds during the cycles. The accurate operation of the valves is crucial in the PSA process, therefore commonly butterfly valves are chosen for a PSA system [135]. These valves can operate at a high accuracy and can handle fast cycling well. This comes at a cost, therefore valves are considered as a main cost component in the capital cost analysis of the PSA.

TABLE 5.5: Equipment cost for the pressure swing adsorption process.

| Component | | Amount | Unit price | Uninstalled | Reference |
|--------------------------------------|-------------------------------------------------|--------------------|---------------|-----------------|------------|
| Adsorbent material | Silica gel | 3.0 m ³ | \$ 3000.00 | \$ 9,000.00 | [136] |
| | AC | 13 m ³ | \$ 700.00 | \$ 9,100.00 | [137] |
| | Zeolite LiLSX | 1.5 m ³ | \$ 26,000.00 | \$ 39,000.00 | [138] |
| Pressure vessel | Stainless steel (volume: 3 m ³) | 6 | \$ 14,500.00 | \$ 87,000.00 | [139, 140] |
| Compressor waste stream | Centrifugal integral gear compressor | 1 | \$ 500,000.00 | \$ 500,000.00 | Aspen |
| Valves | Butterfly | 35 | \$ 500.00 | \$ 17,500.00 | [141] |
| Storage tanks | Stainless steel (volume: 50 m ³) | 2 | \$ 140,000.00 | \$ 280,000.00 | [139, 140] |
| Total Equipment Cost | | | | \$ 941,600.00 | |
| Total Capital Investment Cost | | | | \$ 1,883,200.00 | |

In order to estimate the total capital investment cost of a PSA process, the Lang factors are commonly used in industry. However, since the PSA process designed for the separation of hydrogen and natural gas at a refuelling station is significantly smaller than an industrial scale PSA, these Lang factors are not suitable. The system will be placed as a skid on a refuelling station, thus for example all piping is already connected and the control panel installed. Therefore, after elaborate discussion with and based on previous experience of Prof. Paul Webley with building small scale PSA units, it is concluded that the capital cost for the PSA can be assumed twice the equipment cost. This results in a total of around \$1.9 million for the designed PSA system.

The operation costs of the PSA process consist of the maintenance cost of the PSA, the operation cost of the compressor, the capital investment cost spread out over the lifetime of the PSA system, and the feedstock price of the natural gas with 10 vol% hydrogen mixture. To calculate the operating cost of the PSA, the hydrogen demand of a medium sized refuelling station is considered only, which is 700 kg of hydrogen per day.

The maintenance cost are calculated as 2% of the total installed cost of the PSA system per year. The cost of the compressor are calculated using the compressor duty, obtained from the Aspen HYSYS calculation presented in Table 5.3. The electricity price is varied between 5 and 25 c/kWh. The feedstock price of the natural gas blended with 10 vol% hydrogen is calculated according to Equation 3.1. A price range for the natural gas of \$9.50/GJ to \$15.00/GJ is assumed. The price range for the electricity

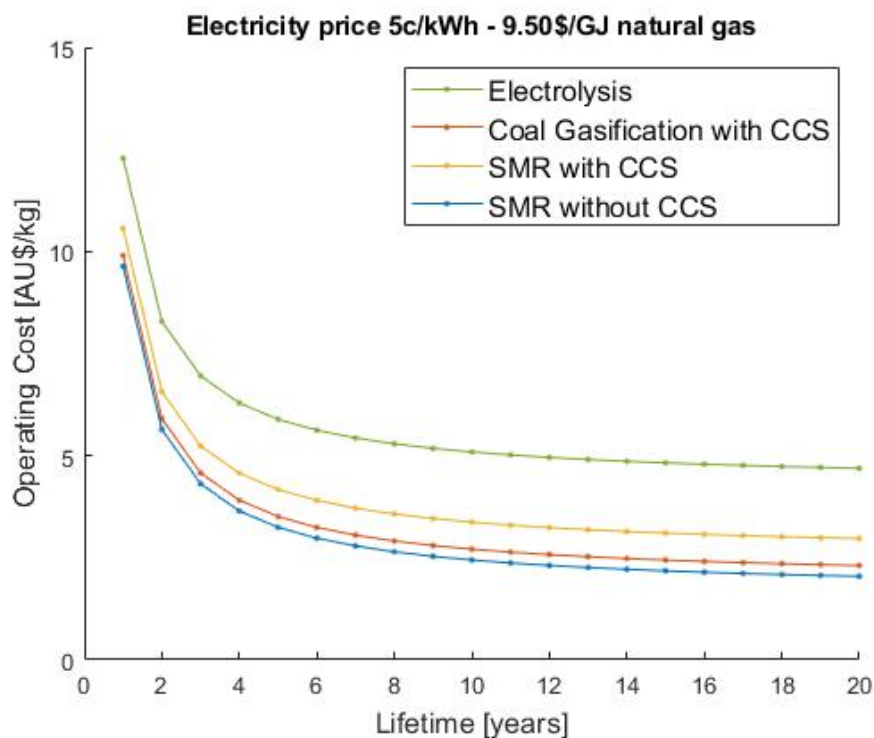


FIGURE 5.3: Best case operating cost of the PSA as a function of the lifetime, for different production methods of hydrogen assuming an electricity price of 5c/kWh and a natural gas price of \$9.50/GJ.

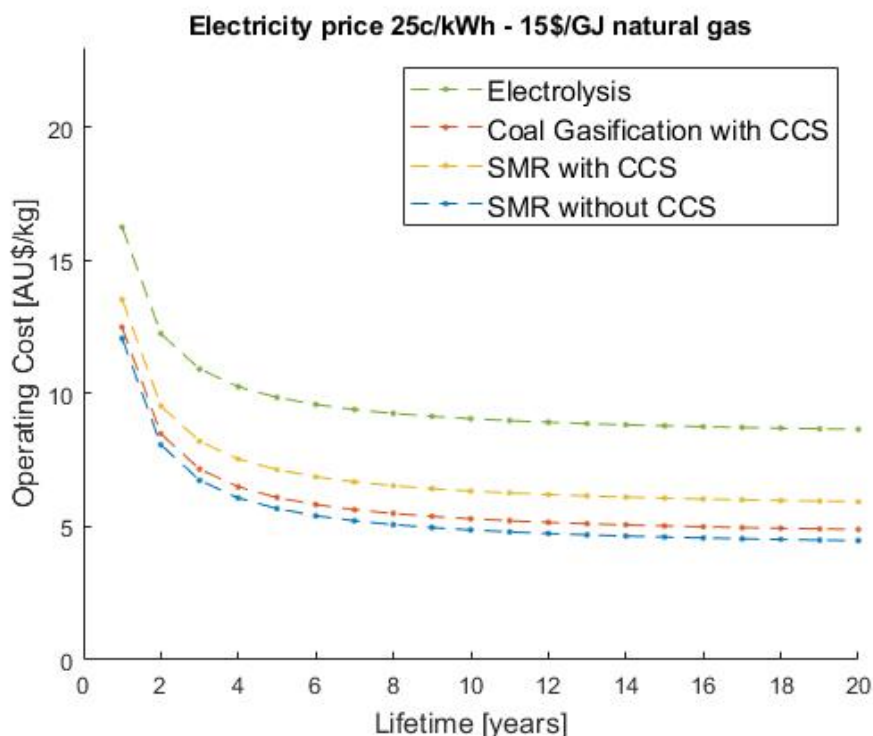


FIGURE 5.4: Worst case operating cost of the PSA as a function of the lifetime, for different production methods of hydrogen assuming an electricity price of 25c/kWh and a natural gas price of \$15.00/GJ.

price and the natural gas price are chosen after discussion with the industrial partners within the Future Fuels CRC project. It is assumed that the methane rich product stream is supplied back to the gas grid. It must be noted that currently no regulations are in place yet for supplying natural gas back to the grid in Australia. Further research on how this can be implemented is therefore required at policy level. Some form of analysing the quality of the natural gas will also be required, before it can be re-injected in the gas grid. The quality of the gas will play a role in the price of the natural gas as well.

Figure 5.3 and Figure 5.4 present the operating cost of the PSA as a function of the lifetime of the PSA system, calculated for four different hydrogen production methods. Figure 5.3 represents the best case scenario where an electricity price of 5c/kWh and a natural gas price of \$9.50/GJ is assumed. Figure 5.4 represents the worst case scenario, with an electricity price of 25c/kWh and a natural gas price of \$15.00/GJ.

The centralised production of hydrogen through electrolysis is the most expensive method, whereas SMR hydrogen production without CCS is the least expensive. The influence of the lifetime on the operation cost reduces after 8 to 10 years. A more detailed overview of the different cost components for the PSA operation will be presented in Section 5.4.

5.3.2 Economics Compression and Storage

The capital and operating cost for the compression, storage and dispensing for the three sizes of refuelling station described previously (Table 3.5) are calculated with the HRSAM model and presented in Table 5.6. A detailed overview of all the cost components are presented in Appendix D. The initial capital investment costs include the installed equipment cost for the compressors, refrigerator, storage tanks, dispenser and the overall control and safety equipment. Other capital investment include cost for site preparation, engineering & design, project contingency, one-time licensing fees and up-front permitting costs, all calculated as a percentage of the initial capital investment cost. Lastly, the operational & maintenance (O&M) cost consist of labour cost, electricity costs and maintenance cost, calculated for each operating components. The electricity price is assumed to be 25c/kWh, and labour cost are estimated at \$25.40 per hour [142]. In the following section a sensitivity analysis on the electricity price is performed, assuming an electricity price range of 5c/kWh to 25c/kWh.

The cost price for the compression, storage, and dispensing of the hydrogen is presented in Table 5.7, for the three different scenario's of hydrogen demand at the refuelling station. An analysis period of 10 years is assumed, with a debt interest rate of 6%.

TABLE 5.6: Overview table of capital and operational and maintenance costs for a hydrogen refuelling station with varying daily demand.

| Component | Small HRS | Medium HRS | Large HRS |
|----------------------------|--------------|--------------|--------------|
| Initial capital investment | \$ 3,900,000 | \$ 6,400,000 | \$ 7,600,000 |
| Other capital investment | \$ 900,000 | \$ 1,500,000 | \$ 1,750,000 |
| O&M cost per year | \$ 290,000 | \$ 480,000 | \$ 595,000 |

TABLE 5.7: Cost breakdown for hydrogen compression, storage and dispensing (CS&D) at a refuelling station expressed in \$/kg H₂, assuming an electricity price of 25c/kWh.

| Component | Small HRS | Medium HRS | Large HRS |
|-----------------|-----------|------------|-----------|
| Total CS&D Cost | 13.32 | 10.88 | 9.20 |
| Capital | 9.03 | 7.31 | 6.11 |
| O&M less energy | 3.08 | 2.34 | 1.91 |
| Energy/fuel | 1.21 | 1.21 | 1.18 |

The HRSAM model is made based on the American market, and is therefore not completely representative for the Australian market. The electricity price and labour costs are in range with the Australian prices, however equipment costs for example were not further compared with the Australian market. There is currently no hydrogen refuelling station operational yet in Australia, which makes it very difficult to compare any of the prices calculated. The model does provide a good insight in the compression and storage design required at the refuelling station.

5.4 Comparison of Different Hydrogen Supply Methods

The final hydrogen price at a refuelling station, which includes compression, storage, and dispensing (CS&D), can now be compared for different hydrogen supply methods. The first case is the one studied in this thesis, where a PSA system is used to separate the pipeline transported hydrogen from the natural gas. The second case assumed on-site hydrogen production through electrolysis. The last case considers centrally produced hydrogen transported by tube-trailer to the station. All methods require on-site compression, storage, and dispensing.

5.4.1 Case A: PSA separation

The final cost price of hydrogen for Case A includes the operational cost of the PSA and the cost for compression, storage, and dispensing. Four different centralised hydrogen production methods are considered, which are electrolysis, coal gasification with CCS, and SMR with and without CCS. The cost for the pipeline transport of the natural gas and hydrogen mixture is assumed to be incorporated in the natural gas price. Furthermore, the PSA lifetime is fixed at 10 years to match the analysis period used in the HRSAM model to calculate the cost for CS&D. A sensitivity analysis on the electricity price (5-25c/kWh) and natural gas price (\$9.50-15.00/GJ) is performed and the best case and worst case scenario are presented in Figure 5.5 and Figure 5.6. A break down of the cost is provided in Table 5.8 and Table 5.9.

TABLE 5.8: Best case scenario, hydrogen production price assuming electricity price of 5c/kWh and a natural gas price of \$9.50/GJ. The fixed PSA costs include the capital cost for a 10 year lifetime and the maintenance cost.

| H ₂ production | Electrolysis | Coal with CCS | SMR with CCS | SMR without CCS |
|-------------------------------------|--------------|---------------|--------------|-----------------|
| PSA compressor | \$ 0.27 | \$ 0.27 | \$ 0.27 | \$ 0.27 |
| PSA fixed | \$ 0.90 | \$ 0.90 | \$ 0.90 | \$ 0.90 |
| PSA feedstock | \$ 3.74 | \$ 1.36 | \$ 2.02 | \$ 1.09 |
| CS&D (20-1000 bar) | \$ 9.88 | \$ 9.88 | \$ 9.88 | \$ 9.88 |
| Total [A\$/kg H₂] | \$ 14.79 | \$ 12.41 | \$ 13.07 | \$ 12.14 |

TABLE 5.9: Worst case scenario, hydrogen production price assuming electricity price of 25c/kWh and a natural gas price of \$15.00/GJ. The fixed PSA costs include the capital cost for a 10 year lifetime and the maintenance cost.

| H ₂ production | Electrolysis | Coal with CCS | SMR with CCS | SMR without CCS |
|-------------------------------------|--------------|---------------|--------------|-----------------|
| PSA compressor | \$ 1.36 | \$ 1.36 | \$ 1.36 | \$ 1.36 |
| PSA fixed | \$ 0.90 | \$ 0.90 | \$ 0.90 | \$ 0.90 |
| PSA feedstock | \$ 5.90 | \$ 2.14 | \$ 3.19 | \$ 1.72 |
| CS&D (20-1000 bar) | \$ 10.88 | \$ 10.88 | \$ 10.88 | \$ 10.88 |
| Total [A\$/kg H₂] | \$ 19.04 | \$ 15.27 | \$ 16.33 | \$ 14.86 |

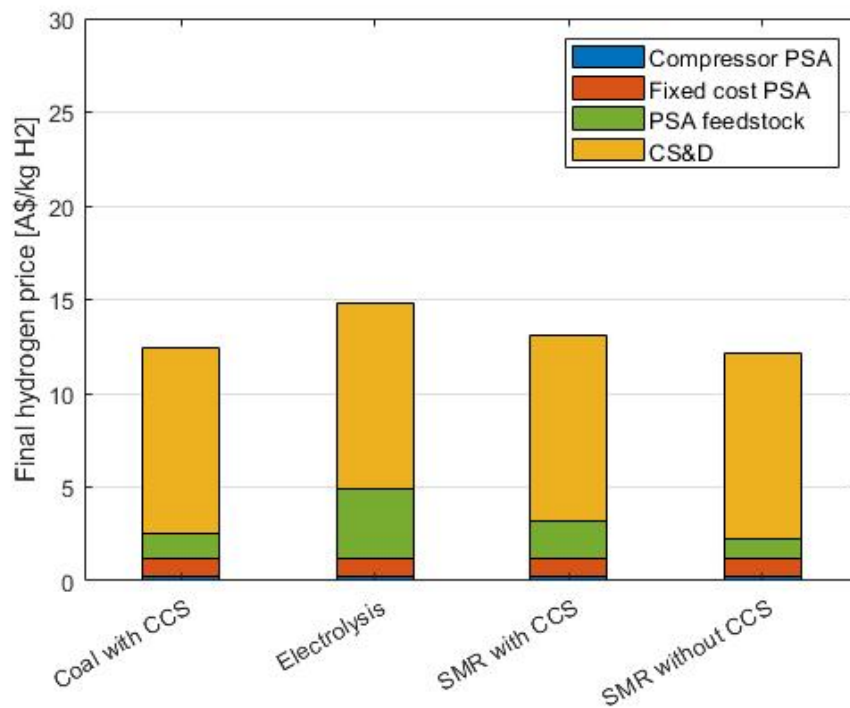


FIGURE 5.5: Best case scenario for PSA separated hydrogen assuming a natural gas price of \$9.50/GJ and an electricity price of 5c/kWh.

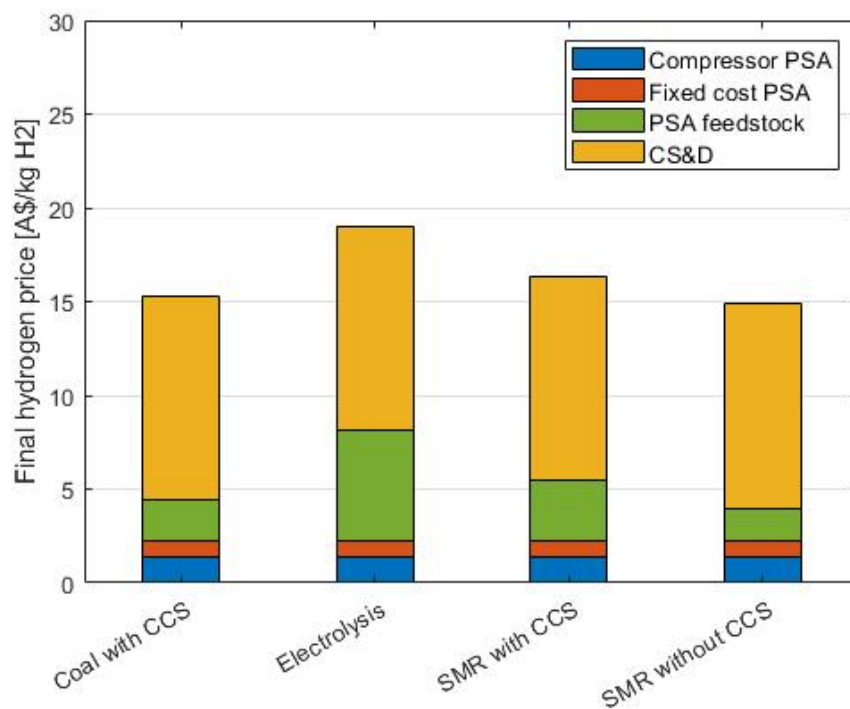


FIGURE 5.6: Worst case scenario for PSA separated hydrogen assuming a natural gas price of \$15.00/GJ and an electricity price of 25c/kWh.

In all cases, the compression, storage, and dispensing is the major cost component in the final hydrogen price. The electricity price has a major influence on the compressor used to compressed the methane rich stream back into the pipeline. Just a slide increase is seen in the cost for the compression, storage, and dispensing is observed. In the best case scenario, the final hydrogen cost price for green hydrogen is \$14.79, which can be reduced to \$12.14 when grey hydrogen is supplied.

When the natural gas price is increased, the cost price for hydrogen also increases as a result of the equation used to calculate the price for the feedstock mixture (see Equation 3.1). This is not representative for a real scenario, therefore the results of the worst case scenario are not as realistic as the prices for the best case scenario. In a further study, a more detailed calculation on the PSA operating cost for future prospect is recommended.

5.4.2 Case B: On-site Electrolysis

The production of hydrogen on-site through electrolysis significantly reduces the amount of steps to be taken before the hydrogen can be dispensed into the car, as no transport is required. An electrolyser can be connected to the grid, providing a continuous supply of electricity, or it can be connected to a direct renewable energy source such as solar PV or wind. This reduces the capacity factor and thus increases the cost of the hydrogen produced. According to the National Hydrogen Roadmap, published by Bruce et al. [30], currently the hydrogen price in Australia made from grid connected electricity is around \$6.60/kg and \$11/kg for hydrogen produced from direct renewables. A capacity factor 85% is considered for a grid connected electrolyser, whereas for direct renewables a capacity factor of only 35% can be assumed.

Table 5.10 provides an overview of the efficiency, capital cost, and calculated levelised cost of hydrogen of two different types of electrolysers, a proton exchange membrane (PEM) electrolyser and an alkaline electrolyser (AE), for a 2018 and 2025 prospect in Australia [30]. The final price of hydrogen is strongly influenced by the electricity price. This is illustrated in Figure 5.7, where the hydrogen production cost for hydrogen produced by a PEM or AE electrolyser cells is presented as a function of the electricity price.

TABLE 5.10: Constants used for the different electrolyser cells [30].

| | | PEM electrolyser | AE electrolyser |
|-------------------------------------------|------|------------------|-----------------|
| Efficiency [kWh/kg H₂] | 2018 | 54 | 58 |
| | 2025 | 45 | 49 |
| Capital cost [\$/kW] | 2018 | 3496 | 1347 |
| | 2025 | 968 | 1012 |
| Levelised cost of hydrogen [\$/kg] | 2018 | 6.08-7.43 | 4.78-5.84 |
| | 2025 | 2.29-2.79 | 2.54-3.10 |

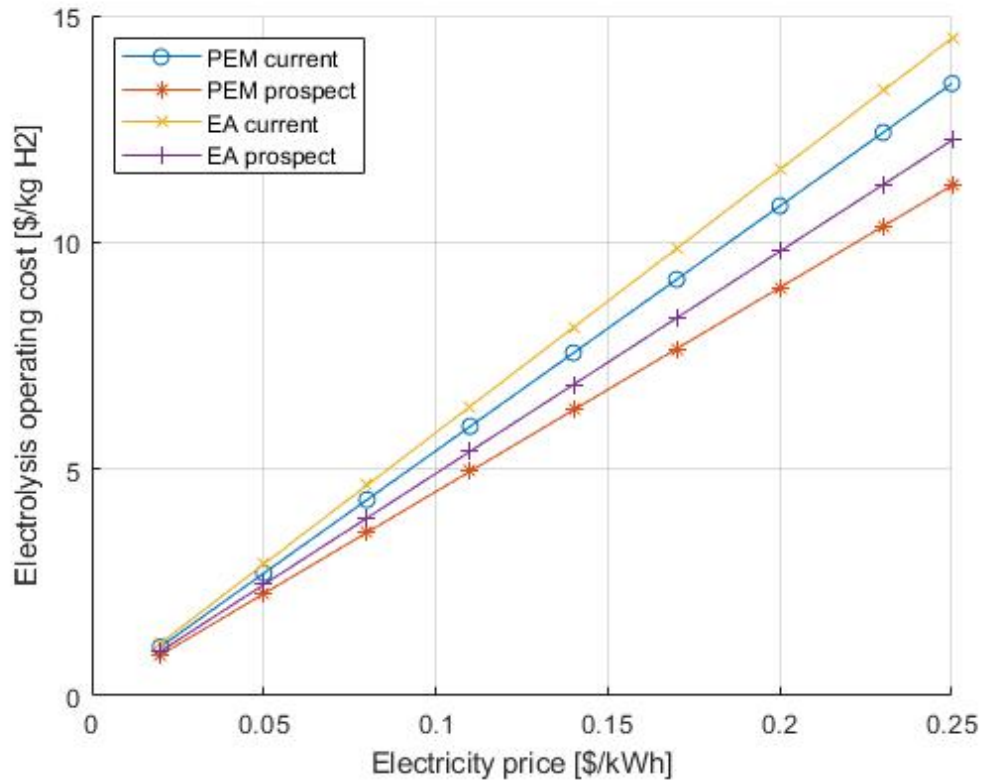


FIGURE 5.7: Hydrogen production cost by electrolysis as a function the electricity price, assuming electrolyser efficiencies as tabulated in Table 5.10.

TABLE 5.11: Final hydrogen price for on-site electrolysis with a PEM cell and an AE cell. Prices are calculated for 5c/kWh and 25c/kWh and for varying capital cost based on [30].

| Electricity Price [c/kWh] | | PEM | AE |
|---------------------------|------|----------|----------|
| 5 | 2018 | \$ 16.77 | \$ 15.14 |
| | 2025 | \$ 13.12 | \$ 13.47 |
| 25 | 2018 | \$ 28.57 | \$ 27.74 |
| | 2025 | \$ 23.12 | \$ 24.27 |

To compare the final hydrogen price at a refuelling station where the hydrogen is produced on-site by electrolysis with case A, where a PSA is used, the compression, storage, and dispensing must be included. The pressure of hydrogen produced by electrolysis is around 30 to 35 bar for a PEM cell and around 10 bar for an AE cell, therefore the same cost for CS&D is assumed as in case A. The pressure difference (20 to 1000 bar, or 10-30 to 1000 bar) is assumed negligible in the final CS&D price.

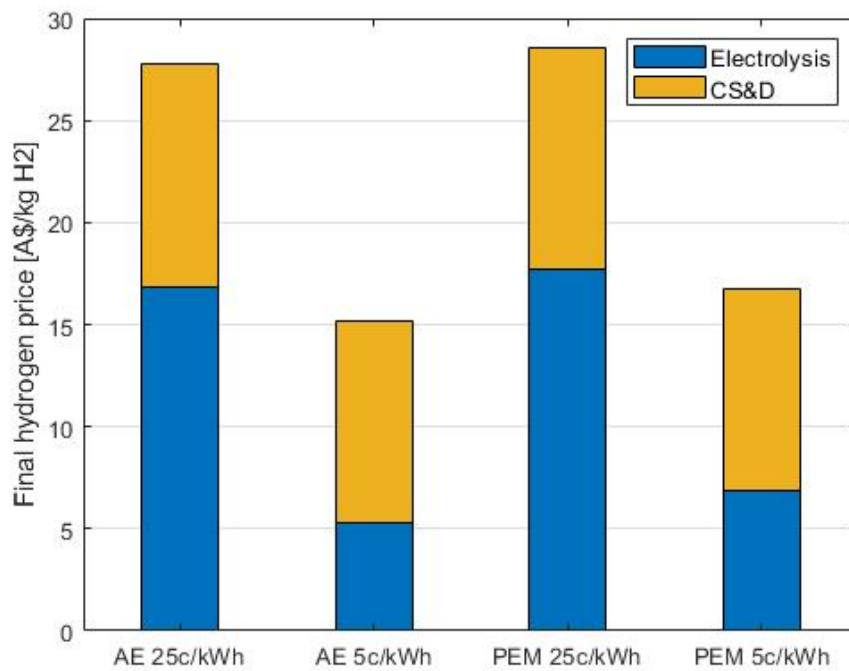


FIGURE 5.8: Current hydrogen price for on-site electrolysis, assuming various electricity prices for both PEM and AE electrolyser cells [30].

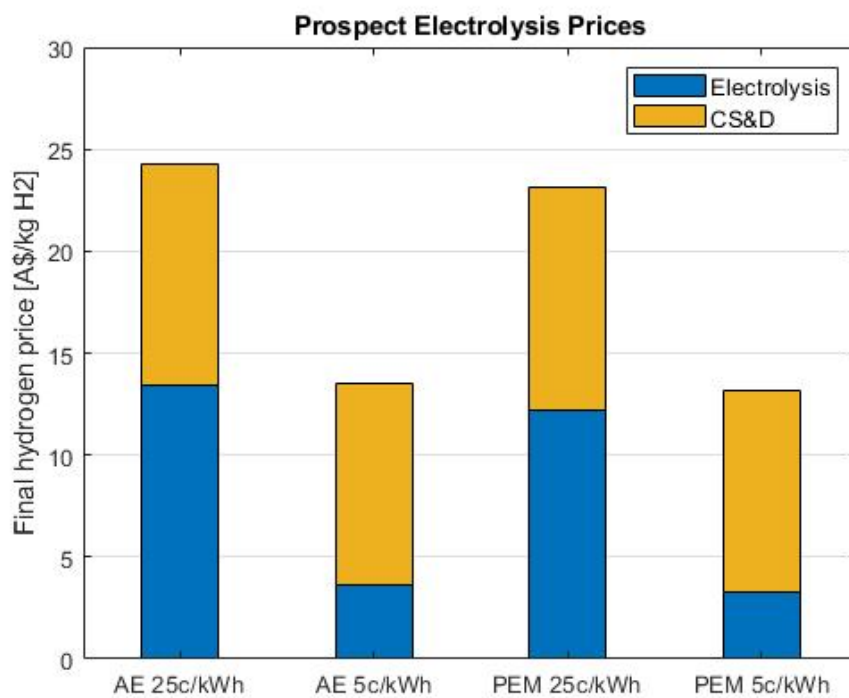


FIGURE 5.9: Prospect of hydrogen price for on-site electrolysis, assuming various electricity prices for both PEM and AE electrolyser cells [30].

In Figure 5.8 the final hydrogen price is plotted for a current PEM and AE cell, for an electricity price of 5c/kWh and 25c/kWh. Figure 5.9 represents the prospect hydrogen price produced by a PEM or AE cell for varying electricity price. In Table 5.11, all final hydrogen prices are tabulated. For an electricity price of 25c/kWh the final hydrogen price is very expensive, even considering the electrolyser prospect for 2025. For 5c/kWh electricity price, currently hydrogen can be produced for \$15.14. Comparing this to the hydrogen cost price in Case A for hydrogen produced by electrolysis, which was estimated to be \$14.97, the hydrogen price is very comparable. Considering the development of electrolysers in the future, the cost of hydrogen produced on-site by an electrolyser will be less expensive than for a refuelling station of Case A.

However, if the hydrogen is produced as blue or grey hydrogen in Case A, the final hydrogen price will be significantly lower than in Case B. The prospected hydrogen price in 2025 for electrolysers will be slightly above the estimated hydrogen price in the best case scenario for fossil fuel based hydrogen separated by a PSA system in Case A. It is therefore concluded that on-site hydrogen production by electrolysis is strongly influenced by the electricity price and the development of the electrolyser cells will influence the cost estimates for the future.

5.4.3 Case C: Tube-Trailer Transportation

The last case considered is a refuelling station where centralised hydrogen is transported over the road by a tube-trailer as compressed gas. A compression of 350 bar is assumed, with the cost for compression from 35 to 350 bar estimated at \$0.42 per kg hydrogen [30]. The influence of the distance travelled by the tube-trailer is analysed, varying from 200 to 1000 km travelled. Bruce et al. [30] estimated the average distance travelled by a tube-trailer in Australia annually to be 166,330 km, which is around 455 km daily, therefore this distance is calculated as well. The cost for transportation are estimated at \$2.98 per travelled km [30].

Furthermore, the influence of the electricity price is analysed, varying between 5c/kWh and 25c/kWh. This will influence the CS&D only. The HRSAM model is used to estimate the CS&D cost for a refuelling station where tube-trailer is supplied with hydrogen at a pressure of 350 bar. The detailed design is presented in Appendix D. The cost for CS&D is estimated to be \$8.12 and \$8.52, respectively, for an electricity price of 5c/kWh and 25c/kWh. It must be noted that the cost price for hydrogen produced through electrolysis is fixed at \$6.60 for this analysis, as this is the currently estimated price in Australia according to Bruce et al. [30]. The influence of the electricity price was evaluated in case B. As case C focuses on the transport of hydrogen, the influence of the electricity price on the hydrogen cost price produced by electrolysis is not considered.

Table 5.12 and Table 5.13 represent all final hydrogen prices calculated for Case C. In Figure 5.10, the best case scenario for tube-trailer transported hydrogen over a distance of 200 km is depicted for different hydrogen production methods, assuming an electricity price of 5c/kWh. The CS&D dominates the final hydrogen price for all four results. If hydrogen produced through coal gasification without CCS is used, the final hydrogen

price is lowest, which is as expected. Figure 5.11 represents the worst case scenario, where hydrogen is transported over a distance of 1000 km, again for different hydrogen production methods, and this time assuming an electricity price of 25c/kWh.

TABLE 5.12: Best case scenario for tube-trailer transported hydrogen for varying distances travelled, assuming an electricity price of 5c/kWh.

| tube-trailer distance travelled [km] | Electrolysis | Coal with CCS | SMR with CCS | Coal without CCS |
|--------------------------------------|--------------|---------------|--------------|------------------|
| 200 | \$ 15.89 | \$ 12.43 | \$ 12.06 | \$ 11.13 |
| 455 | \$ 16.84 | \$ 13.38 | \$ 13.01 | \$ 12.08 |
| 1000 | \$ 18.87 | \$ 15.41 | \$ 15.04 | \$ 14.11 |

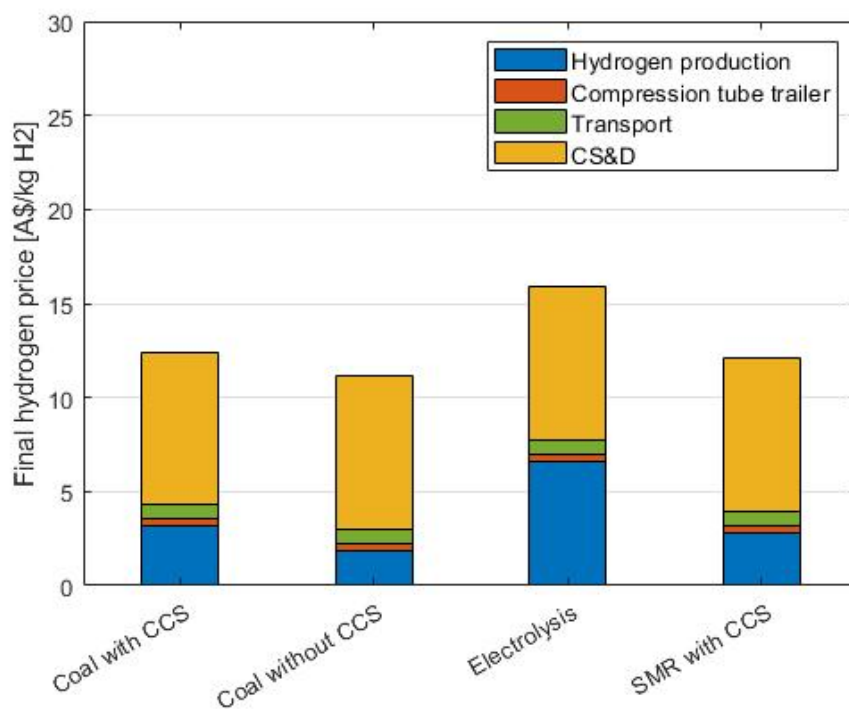


FIGURE 5.10: Best case scenario for tube-trailer transported hydrogen over a distance of 200 km, assuming an electricity price of 5c/kWh.

TABLE 5.13: Worst case scenario for tube-trailer transported hydrogen for varying distances travelled, assuming an electricity price of 25c/kWh.

| Distance travelled [km] | Electrolysis | Coal with CCS | SMR with CCS | Coal without CCS |
|-------------------------|--------------|---------------|--------------|------------------|
| 200 | \$ 16.29 | \$ 12.83 | \$ 12.46 | \$ 11.53 |
| 455 | \$ 17.24 | \$ 13.78 | \$ 13.41 | \$ 12.48 |
| 1000 | \$ 19.27 | \$ 15.81 | \$ 15.44 | \$ 14.51 |

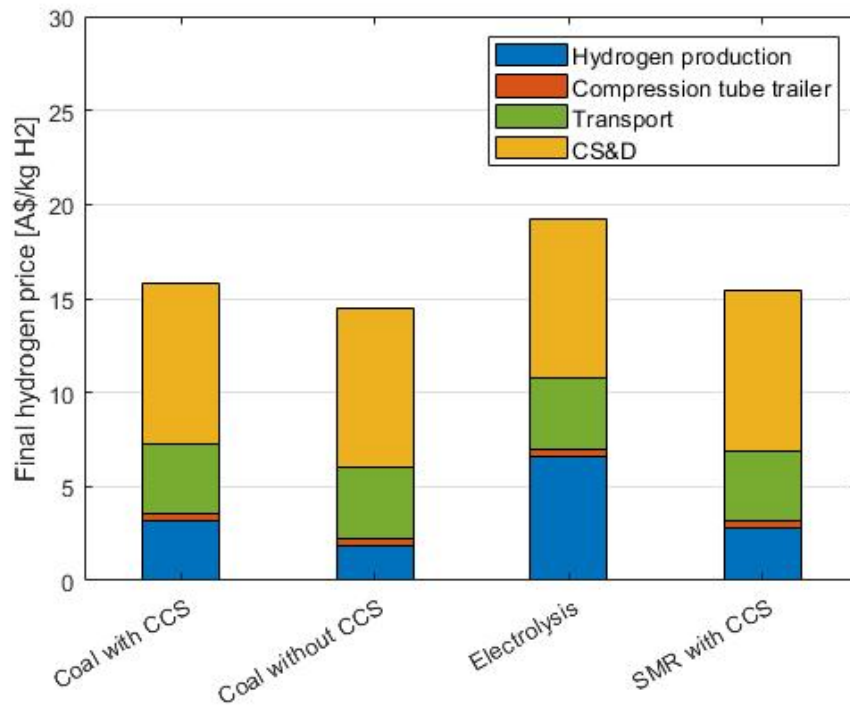


FIGURE 5.11: Worst case scenario for tube-trailer transported hydrogen over a distance of 1000 km, assuming an electricity price of 25c/kWh.

To compare the hydrogen price for Case A and Case C, a break-even distance is calculated and tabulated in Table 5.14. This is calculated for the best case and worst case scenarios, resulting in a break-even distance travelled by the tube-trailer for which the final hydrogen price is equal. The final hydrogen price for transported hydrogen made by electrolysis, will always be more expensive than PSA separated hydrogen with hydrogen originating from electrolysis in the best case scenario. For hydrogen produced through coal gasification with CCS, the break-even distance is lowest, namely 245 km only. After 245 km travelled by the tube-trailer, the final hydrogen price will always be more expensive than using a PSA at the refuelling station to separate the hydrogen from the natural gas. With decreasing hydrogen production cost, the break-even distance of the tube-trailer increases. In the worst case scenario of the PSA where hydrogen originates from electrolysis, the break-even distance is 750 km. Again, this increases further when the cost for the hydrogen production method decreases.

In the analysis of tube-trailer transported hydrogen, a fixed pressure in the tube-trailer is assumed. As development continues, compressed hydrogen is expected to be transported at higher pressures and thus increasing the amount of hydrogen which can

TABLE 5.14: Break-even distance with hydrogen cost price compared to PSA refuelling station, for the best case and worst case scenario.

| | Electrolysis | Coal with CCS | SMR with CCS |
|----------------------------------------------|--------------|---------------|--------------|
| Break-even distance best case scenario [km] | - | 245 | 520 |
| Break-even distance worst case scenario [km] | 750 | 2760 | 2330 |

be transported by tube-trailer. In this analysis the carbon footprint of each hydrogen supply chain is not considered, but the transportation of hydrogen will clearly have a large impact on the total carbon footprint. This could play a role in the final decision for the hydrogen supply method used at a refuelling station and is therefore recommended for future research.

It is very interesting to investigate the possibilities of developing a system in which hydrogen is transported as a mixture with natural gas over the long distances, separated at a central location just outside a city, and then transported by tube-trailers to the refuelling stations. In that way the two transportation methods can be combined and used in their advantages. The pure methane separated during the PSA process can then for example also be directly supplied to an end user close by, which will reduce any further cost for compression and/or transport. Strategic locations for such a node system must be identified in further studies to effectively transition to a hydrogen economy in Australia.

To transition to a hydrogen economy in Australia, blending the hydrogen in the already existing natural gas pipeline network is a logical first step. It is hard to set a time estimate of when this will actually be feasible and for how long this will be used. It is expected that eventually all natural gas will be replaced by hydrogen, and thus the need for a separation is no longer present either. The PSA separation at a hydrogen refuelling station will therefore only be relevant in the early stage of the transition to a hydrogen economy.

Also, with continuing development of electrolysis cells, the efficiency can be improved and the capital cost will reduce. This can result in lower cost of hydrogen supplied by electrolysis than by a PSA system. It is, however, important to investigate how the costs scale up when total hydrogen supplied increases. Fuel cells scale up linearly, as more and more stacks are required to produce more hydrogen. When scaling a PSA system, the overall cost do not increase linearly, and thus a PSA system at large scale can be more economical than an electrolyser at large scale. These issues will be key in the decision to make what hydrogen supply method should be used at a refuelling station and are recommended to be further investigated in future work.

5.5 Summary

In the first part of this chapter, the actual design of a refuelling station where hydrogen is supplied by a PSA separation is presented. The design is focused on a 10 vol% hydrogen in the feed gas mixture alone. The main component present is the PSA system, which was analysed in Chapter 4, and the compressor and storage tanks. The PSA system and the compression and storage is scaled for three different hydrogen demands, representing a small, medium, and large refuelling station respectively. The PSA is designed according to a scaling analysis, which is confirmed by a simulation done for a hydrogen production of 350 kg/day. The HRSAM model is used to optimise the compressor and storage design, which uses a cascade storage tank system for hydrogen storage. The storage tanks capacity required is equal to 30% of the total daily demand of hydrogen.

The second part of this chapter focuses on the economic analysis of all the components required at the proposed refuelling station, focusing on a medium sized station with a demand of 700 kg/day of hydrogen. The total capital investment cost for the PSA system is estimated at approximately \$1.9 million. Operating cost of the PSA consist of the compressor, for compressing the natural gas waste stream back into the pipeline at 2 bar, the capital investment cost spread out over the lifetime of the PSA system, the maintenance cost, and the feedstock price of the natural gas and hydrogen mixture. A sensitivity analysis for the electricity price, natural gas price, and the production method of hydrogen has been performed. In the best case scenario, where hydrogen in the feedstock is produced through electrolysis, the PSA operating cost is estimated at \$4.91/kg of hydrogen.

The final hydrogen price, including compression, storage, and dispensing at the refuelling station, has been compared for two other hydrogen supply methods: on-site electrolysis and tube-trailer transported hydrogen. In the best case scenario, where hydrogen is supplied by a PSA system, the final hydrogen price is \$14.79/kg of hydrogen. For hydrogen supplied by on-site electrolysis, the final hydrogen price is strongly influenced by the electricity price. In the best case scenario, where an electricity price of 5c/kWh is assumed, hydrogen can be produced by on-site electrolysis (AE cell) for \$15.14/kg of hydrogen, with the prospect of \$13.47/kg of hydrogen in 2025. A PEM cell is currently more expensive (\$16.77/kg of hydrogen), but is expected to produce hydrogen for \$13.12/kg of hydrogen by 2025. Lastly, tube-trailer transported hydrogen is strongly influenced by the distance travelled. For a minimum of 200 km, hydrogen can be dispensed at \$15.89 in the best case scenario, assuming hydrogen produced by electrolysis.

Chapter 6

Conclusion and Recommendations

6.1 Conclusion

The object of this master thesis is: to design a PSA system to separate a feed stream of natural gas and 5 vol% or 10 vol% of hydrogen at 20 bar, such that the pure hydrogen product can be used as a fuel for fuel cell vehicles at a hydrogen refuelling station; and to assess the economic feasibility of a refuelling station where hydrogen is supplied by a PSA system. This last chapter covers the main findings of this study. First the main conclusion will be given. Then, a more detailed conclusion on the process analysis, performed in Chapter 4, and the economic analysis, described in Chapter 5, is provided.

Main conclusion The designed PSA system has been proven both technically feasible to produce a high purity hydrogen product and economically feasible to implement at a hydrogen refuelling station. An optimum PSA separation is achieved with a 6 bed PSA system, where each column contains a pre-layer of silica gel for the adsorption of heavy hydrocarbons and CO₂, a main layer of activated carbon for methane adsorption, and a post-layer of zeolite LiLSX for nitrogen adsorption. The ideal pre-layer thickness is analysed to be 0.2 meter for a column of 1.2 meter total height. With this design, hydrogen supplied by a PSA system is economically feasible at a refuelling station. The final hydrogen price, after dispensing, is dominated by the cost for compression and storage. Compared to hydrogen supplied by on-site electrolysis, PSA supplied hydrogen is currently a more economical option. On-site electrolysis can become a more economical option in the future with improved cell efficiencies and reduced electricity prices. Tube-trailer transported hydrogen is highly influenced by the distance travelled. If the hydrogen originates from electrolysis, tube-trailer transported hydrogen will always be more expensive. For different fossil fuel based hydrogen technologies, a break-even distance is calculated.

6.1.1 PSA Process Analysis

The first part of this study analysed the PSA separation process. The proposed PSA design is a 6 bed system, with a 12 step cycle. The cycle consists of 4 pressure equalisation steps, ensuring a high hydrogen recovery, and a repressurisation step with the pure hydrogen product. This ensures a cleaner bed at the end of the cycles, as all remaining gas components adsorbed in the void space are desorbed. The adsorbent material is the main part of the PSA influencing the separation. Therefore, an adsorbent screening analysis has been performed based on the single component isotherm data found in literature.

Activated carbon is selected as the main adsorbent material, because it has a large working capacity for methane, which is the main component in the gas mixture, and it is available at low cost. Heavy hydrocarbons present in the natural gas mixture adsorb very strongly to activated carbon, shown by the steep initial curve in the isotherm. This means that the gas components do not desorb at the desorption pressure, causing accumulation. To prevent this, a pre-layer is required, which adsorbs the contaminating gas components before reaching the main layer. This material requires a linear isotherm for the contaminating gases, such that the pre-layer can be sustained. Silica gel has linear isotherms for all heavy hydrocarbons and CO₂, and is therefore selected as the pre-layer adsorbent. Lastly, an adsorbent material is required for the adsorption of nitrogen, as this gas is not adsorbed well on either silica gel or activated carbon. Zeolite LiLSX showed the best working capacity for nitrogen adsorption, and is therefore selected as the post-layer adsorbent material.

A process analysis has been performed using the adsorption simulator MINSA. The aim of the analysis was to determine the optimal thickness of the different adsorbent layers for a hydrogen input feed of 5 vol% and 10 vol%, whilst producing a high purity hydrogen product and a high recovery. The total height of the column is kept constant at 1.2 meter, with an inner diameter of 0.3 meter. The thickness of the pre-layer is varied from 0 to 0.4 meter. The thickness of the post-layer is not evaluated in this analysis, and therefore kept constant at 0.1 meter.

It is concluded that a high purity hydrogen product (>99%) can be achieved for a pre-layer of 0.1 to 0.3 meter. When no pre-layer is used, the contaminating gases (heavy hydrocarbons and CO₂) accumulate on the activated carbon layer, occupying all the available adsorption site. Therefore, the methane is not able to adsorb and thus ends up in the hydrogen product stream. If a pre-layer of 0.4 meter is used, the total length of the activated carbon remaining in the bed is insufficient to adsorb all the methane, and thus no high purity hydrogen product can be achieved. The same results were obtained for both a 5 vol% and 10 vol% hydrogen in the input feed. Therefore, a pre-layer of 0.2 meter in a column of 1.2 meter is the ideal thickness, ensuring enough activated carbon is present to adsorb all the methane and enough silica gel to prevent the heavy hydrocarbons from accumulating into the main bed.

6.1.2 Techno-Economic Analysis

The second part of this study investigated the economic feasibility of a PSA at refuelling stations with hydrogen supplied by a PSA system. This was done for three different hydrogen demands per day, representing a small, medium, and large refuelling station of respectively, 350, 700, and 1000 kg of hydrogen per day. The analysis focused on a 10 vol% hydrogen in the input feed only. For this, the PSA system was scaled accordingly to meet the hydrogen demand. An optimisation tool (HRSAM) was used to design the compressor and storage tanks. The storage consists of a low pressure tank, storing 30% of the total daily demand at 20 bar, and multiple cascade storage tanks. Hydrogen is drawn from the low pressure storage to supply the compressor, which in turn supplies the hydrogen to the cascade storage tanks. The cascade system consist of 3 tanks of equal size, at three different pressures. When dispensing hydrogen into a vehicle, hydrogen from the low pressure storage tank is used first, followed by the medium pressure storage, and lastly the high pressure storage tank. A total of 4 cascade systems is required for a small refuelling station, 6 cascade system for a medium station, and 8 cascade system for large refuelling station.

The capital cost and operating cost for the compression and storage designed for the three sizes of hydrogen demand per station are calculated by the HRSAM tool. Initial capital costs for the small, medium, and large station are estimated, respectively, at around \$3.9 million, \$6.4 million, and \$7.6 million. Operating cost per year are estimated at \$290,000, \$480,000, and \$595,000 for the respective refuelling station, assuming an electricity price of 25c/kWh.

The equipment cost for the main components in the PSA system are determined by quotations and online research. The compressor is design using Aspen. The total capital cost for the PSA system is estimated to be twice the equipment cost, resulting in an initial capital investment of approximately \$1.9 million. The operating cost of the PSA are predominantly influenced by the feedstock price of the natural gas and hydrogen mixture. Different hydrogen production methods, natural gas prices, and electricity prices are considered. In the best case scenario, where an electricity of 5c/kWh and a natural gas price of \$9.50/GJ is assumed, the PSA operating costs are \$7.91/kg of hydrogen, when hydrogen originates from electrolysis, and \$2.26/kg of hydrogen, for hydrogen originating from SMR without CCS.

The final hydrogen price, including hydrogen compression, storage, and dispensing, is compared for three different hydrogen supply methods at a refuelling station assuming a total hydrogen demand of 700 kg/day. For all cases, the price for compression, storage, and dispensing takes up a major part of the final price. In the first case, hydrogen is supplied by a PSA system. For the best case scenario, hydrogen can be dispensed for \$14.79/kg of hydrogen, with hydrogen originating from electrolysis, and for \$12.14, when hydrogen originates from SMR without CCS.

In the second case, the hydrogen is directly produced on-site by electrolysis. It is concluded that for current PEM and AE cells, hydrogen produced by electrolysis at an electricity price of 5c/kWh is slightly more expensive than PSA supplied hydrogen, with

hydrogen originally produced by electrolysis as well. When the production of hydrogen is by fossil fuel based resources, PSA supplied hydrogen is significantly less expensive. The prospect for PEM and AE cells is that the efficiency and total capital cost will reduce. Therefore, the final hydrogen price in 2025, produced by PEM or AE cells, is expected to compete with the the PSA supplied hydrogen, with hydrogen originally produced from fossil fuels (with or without CCS).

Finally, tube-trailer transported hydrogen is compared with PSA supplied hydrogen. The final hydrogen price is strongly influenced by the distance travelled by tube-trailer and the production method of the hydrogen. When hydrogen is produced by electrolysis for both tube-trailer transported and PSA supplied hydrogen, assuming an electricity price of 5c/kWh, PSA supplied hydrogen will always be more economical (even if the distance travelled is 0 km). This changes if the hydrogen is produced through coal gasification or SMR with or without CCS. The cheaper the production method of hydrogen, the larger the break-even distance the tube-trailer can travel before PSA supplied hydrogen becomes more economical.

6.2 Recommendations

The recommendations for future work can be divided into two parts. The first part focuses on the process analysis and the second part on the economic analysis.

- The literature based study for the adsorption materials provides a good first insight in the materials to be used. For the final selection of the activated carbon, isotherm measurements are required to find the most suitable activated carbon. Currently, this is being researched by another member of the research group. Also, break through experiments are required to estimate the mass transfer for the gases in the different materials. This is now calculated with the LDF model, which provides a good first estimation.
- In the process simulations performed in this work, the thickness of the pre-layer was investigated. The post-layer of zeolite LiLSX was fixed at 0.1 meter. In further research, it is recommended to evaluate this layer as well, such that an optimal separation can be achieved.
- The hydrogen purity required for a fuel cell are not yet met with the simulations performed. This can be achieved by decreasing the adsorption time, but therefore also decreasing the recovery. In a further study an economic analysis must be performed, which considers purity, recovery, and potentially a hybrid system. This could include a second PSA with only two beds, which further purifies the hydrogen product. Or a membrane, before or after the PSA separation.
- The operating conditions analysed in this study were 20 bar and 298 K. In further studies different pressures should be evaluated to investigate the potential locations at the natural gas grid where the PSA system can be operated. Currently,

other members of the research group are investigating 30 bar and 50 bar. Temperatures in Australia vary widely as well, therefore it will be good to simulate the PSA process at temperatures that represent the temperature range experienced in Australia to investigate the influence of temperature on the PSA system.

- Lastly, it will be important to validate the process simulations with actual experiments to confirm the simulation results presented in this study.

The recommendations for future work, focusing on the economic analysis of a refuelling station with hydrogen supplied by a PSA system are outlined next.

- The model used to calculate the cost for a refuelling station is based on a US market, as the developers are based in the US. This gives a good initial representation of the costs, but a more detailed study on the Australian market is recommended to get a better idea of the prices domestically.
- It is very difficult to predict the future, therefore it will be important to consider the different possibilities in the future with respect to the then most recent data available. It is therefore recommended that the parameters used in the sensitivity analysis for the three hydrogen supply methods (electricity price, natural gas price, electrolyser cost price, and hydrogen pressure in tube-trailers) are regularly monitor when evaluating the cost for a refuelling station.
- The pressure at which hydrogen is transported in the tube-trailer is assumed to be 350 bar in this study. With improving technology, the storage tank pressures can be increased to higher pressures and thus increasing the amount hydrogen that can be transported per tube-trailer load. In a further study, it is recommended that this is incorporated in the evaluation of the different hydrogen supply methods.
- Furthermore, the carbon footprint of the three hydrogen supply methods discussed (PSA, electrolysis, and tube-trailer) is not considered in this study. Especially in tube-trailer transported hydrogen, the carbon emitted is an important aspect to consider. This should be further investigated and taken into consideration when making a final decision on the hydrogen supply method at a refuelling station.
- Currently, no regulations or policies are in place for supplying natural gas back into the grid. It is highly recommended to investigate the possibilities and discuss the options with the industrial partners of the Future Fuel CRC to get a clear picture of what could and what could not be possible.
- It is recommended to perform a study on the possibilities of a node system, in which hydrogen is transported over the long distances in a pipeline, then separated at a central PSA plant and then further transported by tube-trailers to the respective refuelling stations within the maximum radius of the tube-trailer. In this way, the both hydrogen transportation methods can be used, exploiting the advantageous of both. Strategic locations of where the PSA systems and where the refuelling stations should be place require further investigation. This will be crucial in effectively transitioning to a hydrogen economy in Australia.

-
- Lastly, the economics of scale should be further investigated for the different hydrogen supply methods. On-site electrolysis scales linearly, as more stacks have to be added to produce more hydrogen. PSA system do not scale linearly, therefore the choice of the hydrogen supply method at different station sizes will be very much influenced by the capital cost of the supply method. It is recommended to investigate what the trade-off is to have a better idea of the possibilities.

Appendix A

Natural Gas composition

TABLE A.1: Composition of natural gas for all states in Australia in mol% [31].

| Component | SA/NSW Moomba | QLD Gladstone | VIC/TAS Longford | WA W LPG Plant | NT Typical |
|------------------|--------------------------|--------------------------|-----------------------------|---------------------------|-----------------------|
| Methane | 95.709 | 98.56 | 94.103 | 93.019 | 86.591 |
| Ethane | 2.369 | 0 | 3.965 | 2.349 | 2.215 |
| Propane | 0.071 | 0 | 0.444 | 0.016 | 0.712 |
| i-Butane | 0.004 | 0 | 0.03 | 0 | 0.11 |
| n-Butane | 0.008 | 0 | 0.027 | 0 | 0.18 |
| i-Pentane | 0.002 | 0 | 0.006 | 0 | 0.07 |
| n-Pentane | 0.006 | 0 | 0.001 | 0 | 0.06 |
| n-Hexane | 0.016 | 0 | 0.004 | 0 | 0.05 |
| n-Heptane | 0 | 0 | 0 | 0 | 0.02 |
| n-Octane | 0 | 0 | 0 | 0 | 0.01 |
| n-Nonane | 0 | 0 | 0.002 | 0 | 0 |
| Nitrogen | 1.274 | 1.32 | 1.017 | 3.572 | 9.19 |
| Carbon Dioxide | 0.541 | 0.12 | 0.402 | 1.043 | 0.792 |

TABLE A.2: Moomba natural gas composition with 5% and 10% hydrogen added [31].

| Component | Concentration [mol%] | | |
|------------------|-----------------------------|-------|-------|
| Methane | 95.709 | 90.92 | 86.14 |
| Ethane | 2.369 | 2.25 | 2.13 |
| Propane | 0.071 | 0.067 | 0.064 |
| i-Butane | 0.004 | 0.004 | 0.004 |
| n-Butane | 0.008 | 0.008 | 0.007 |
| i-Pentane | 0.002 | 0.002 | 0.002 |
| n-Pentane | 0.006 | 0.006 | 0.005 |
| n-Hexane | 0.016 | 0.015 | 0.014 |
| n-Heptane | 0 | 0 | 0 |
| n-Octane | 0 | 0 | 0 |
| n-Nonane | 0 | 0 | 0 |
| Nitrogen | 1.274 | 1.21 | 1.15 |
| Carbon Dioxide | 0.541 | 0.51 | 0.49 |
| Hydrogen | 0 | 5 | 10 |

Appendix B

Material Isotherms

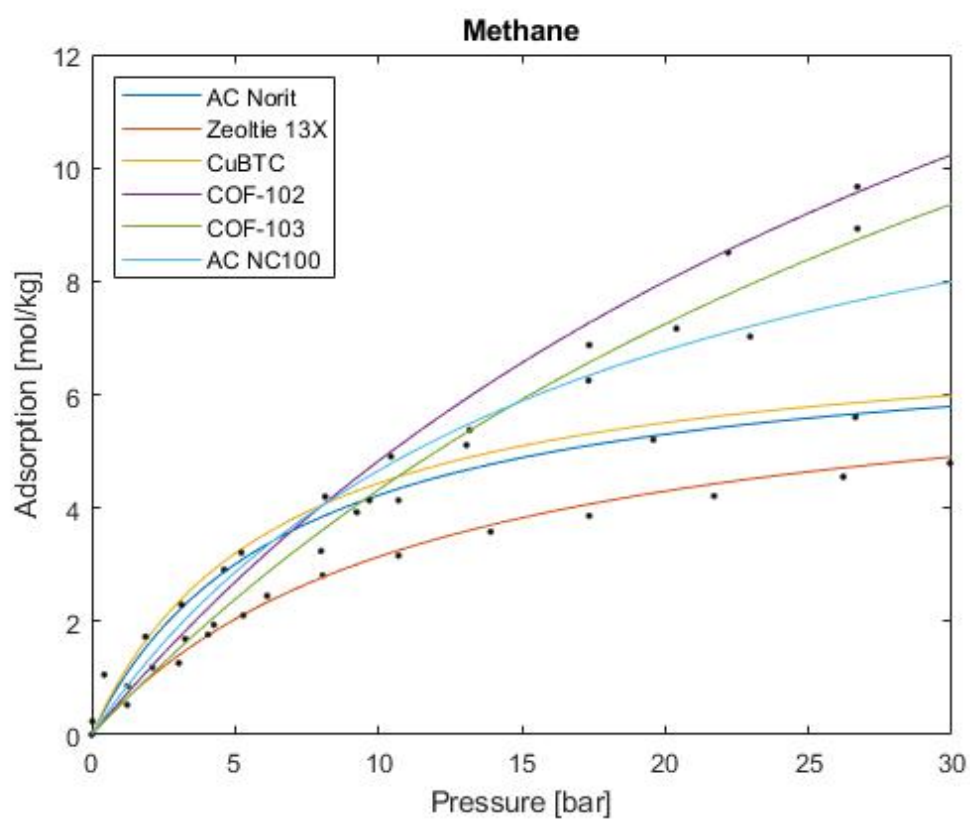


FIGURE B.1: Methane adsorption isotherms for different materials at 298 K. Lines are Langmuir isotherms.

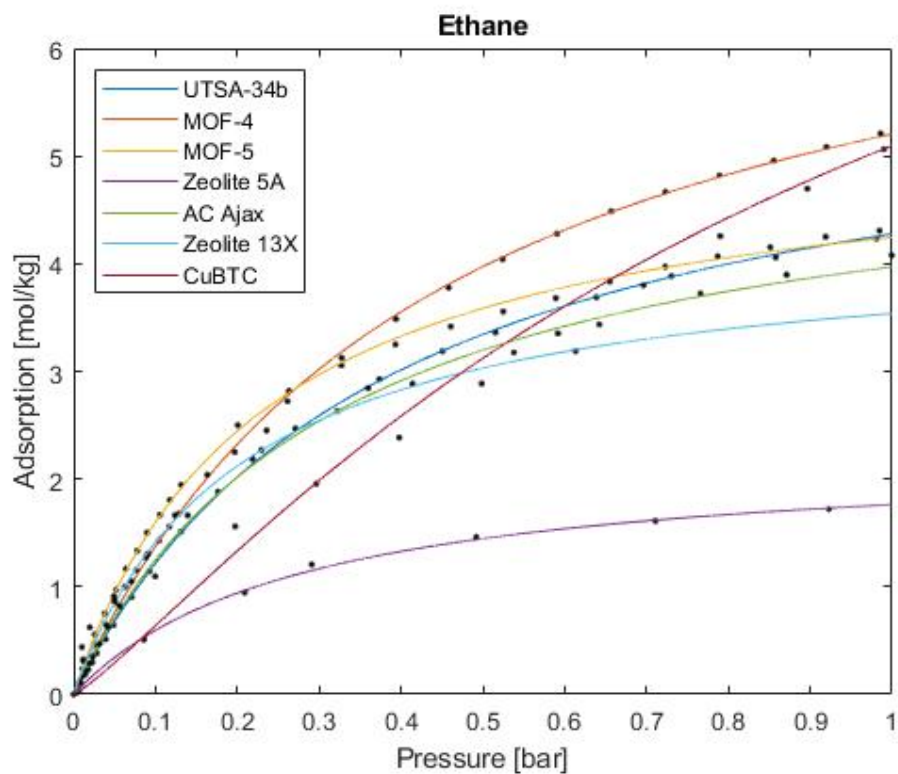


FIGURE B.2: Ethane adsorption isotherms for different materials at 298 K.

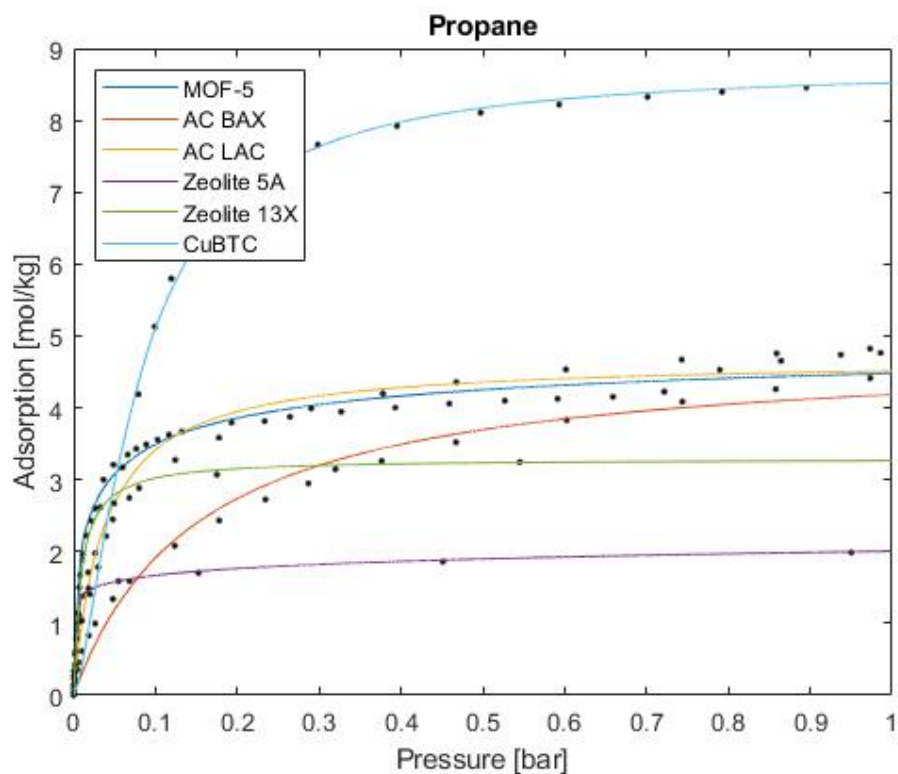


FIGURE B.3: Propane adsorption isotherms for different materials at 298 K.

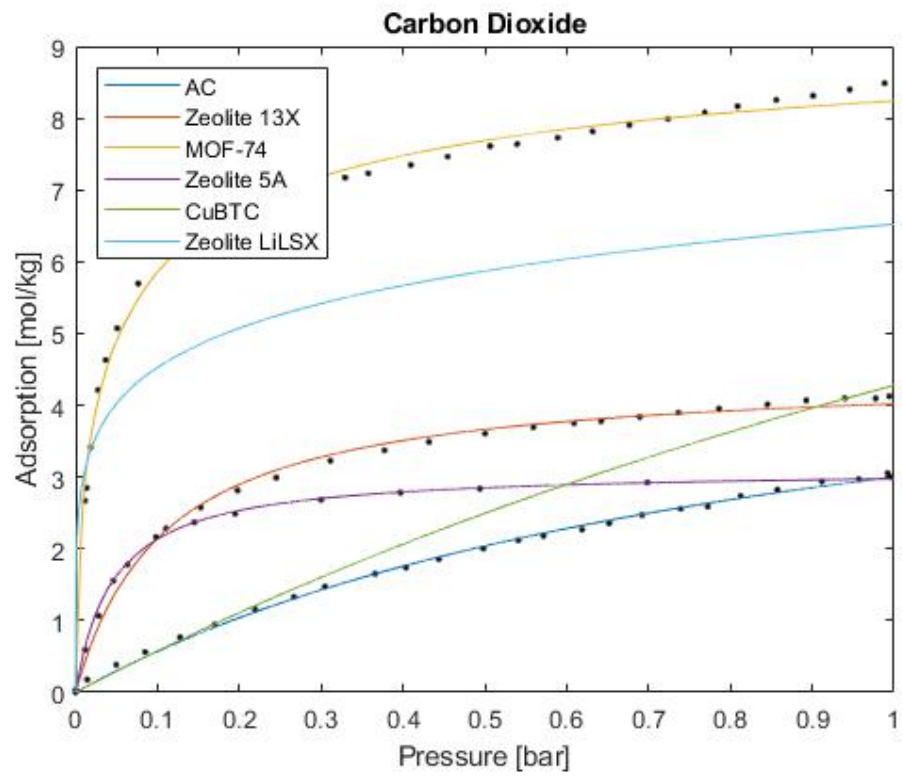


FIGURE B.4: Carbon dioxide adsorption isotherms for different materials at 298 K.

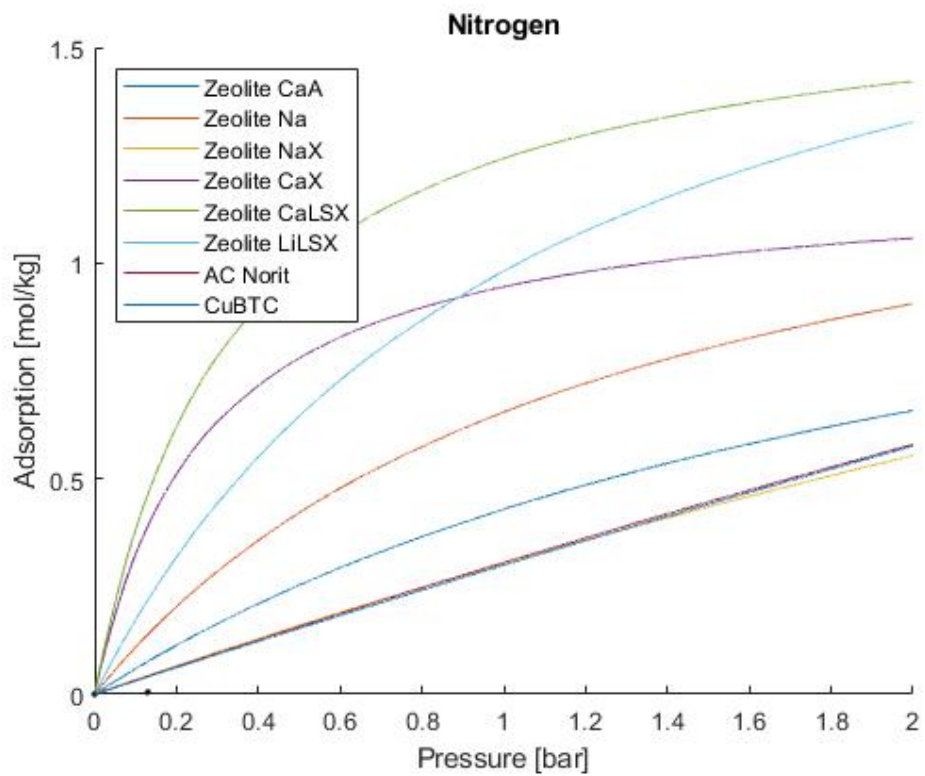


FIGURE B.5: Nitrogen adsorption isotherms for different materials at 298 K.

TABLE B.1: Overview table with all working capacities of the adsorbent materials for each isotherm presented in Appendix B.

| Adsorbent | Working capacity [mol/kg] | Reference |
|-----------------------|----------------------------------|------------------|
| Methane | 1-20 bar | Figure B.1 |
| COF-102 | 7.400 | [100] |
| COF-103 | 6.724 | [100] |
| AC NC100 | 6.078 | [101] |
| AC RB2 | 4.555 | [143] |
| CuBTC | 4.517 | [102] |
| AC Norit | 4.392 | [104] |
| Zeolite 13X | 3.761 | [144] |
| Ethane | 0.03-0.8 bar | Figure B.2 |
| MOF-4 | 4.358 | [145] |
| UTSA-34b | 3.572 | [146] |
| MOF-5 | 3.446 | [145] |
| AC Ajax | 3.294 | [147] |
| Zeolite 13X | 2.842 | [148] |
| CuBTC | 2.599 | [108] |
| Zeolite 5A | 1.452 | [149] |
| Propane | 0.003-0.8 bar | Figure B.3 |
| CuBTC | 4.330 | [108] |
| AC LAC | 2.848 | [111] |
| Zeolite 13X | 2.134 | [148] |
| MOF-5 | 2.005 | [145] |
| AC BAX | 1.568 | [111] |
| Zeolite 5A | 0.377 | [150] |
| Carbon Dioxide | 0.003-0.8 bar | Figure B.4 |
| MOF-74 | 3.937 | [46] |
| Zeolite 5A | 1.790 | [119] |
| Zeolite 13X | 1.779 | [46] |
| AC | 0.448 | [46] |
| CuBTC | 0.446 | [102] |
| Nitrogen | 0.1-2 bar | Figure B.5 |
| Zeolite LiLSX | 1.155 | [117] |
| Zeolite CaLSX | 1.040 | [117] |
| Zeolite Na | 0.796 | [117] |
| Zeolite CaX | 0.733 | [117] |
| Zeolite CaA | 0.599 | [117] |
| AC Norit | 0.547 | [103] |
| CuBTC | 0.545 | [102] |
| Zeolite NaX | 0.520 | [117] |

Appendix C

Simulation Results

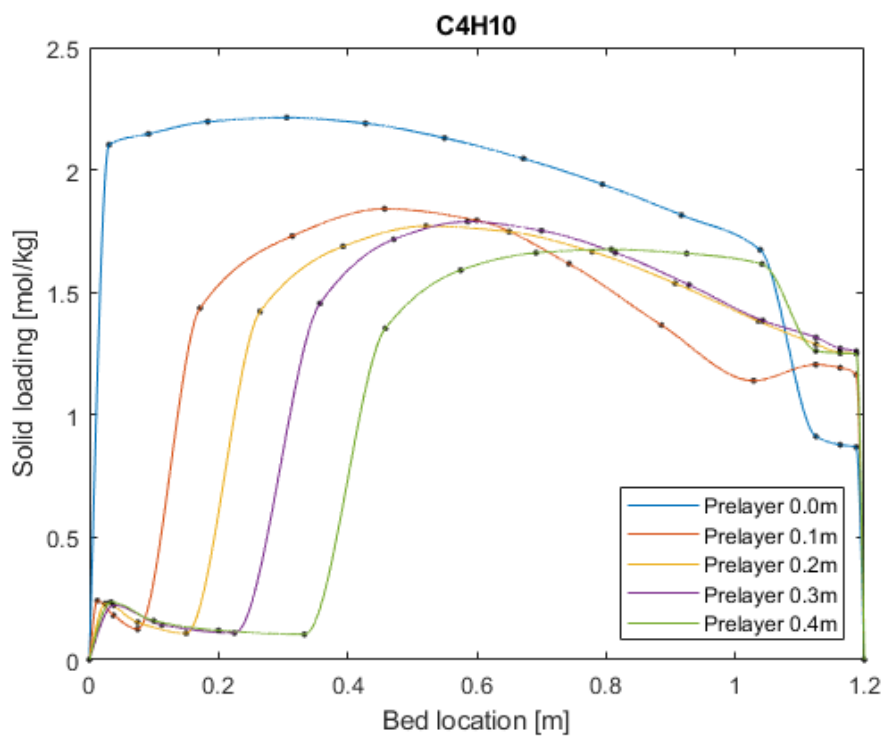


FIGURE C.1: Solid loading of the heavy hydrocarbons at the end of the adsorption step for a 5 vol% hydrogen feed input.

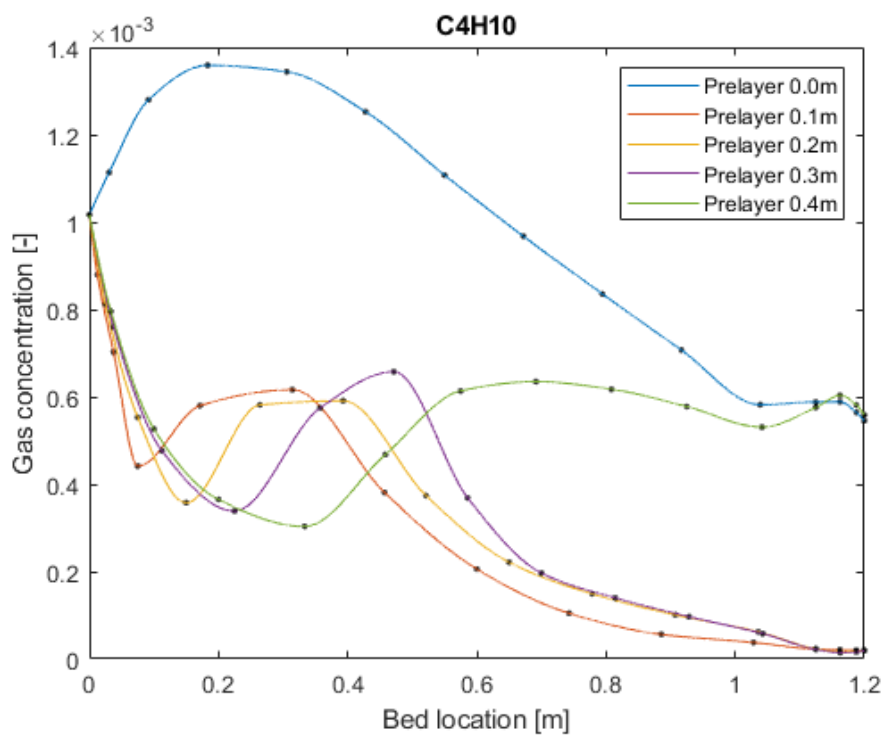


FIGURE C.2: Gas concentration of the heavy hydrocarbons at the end of the adsorption step for a 5 vol% hydrogen feed input.

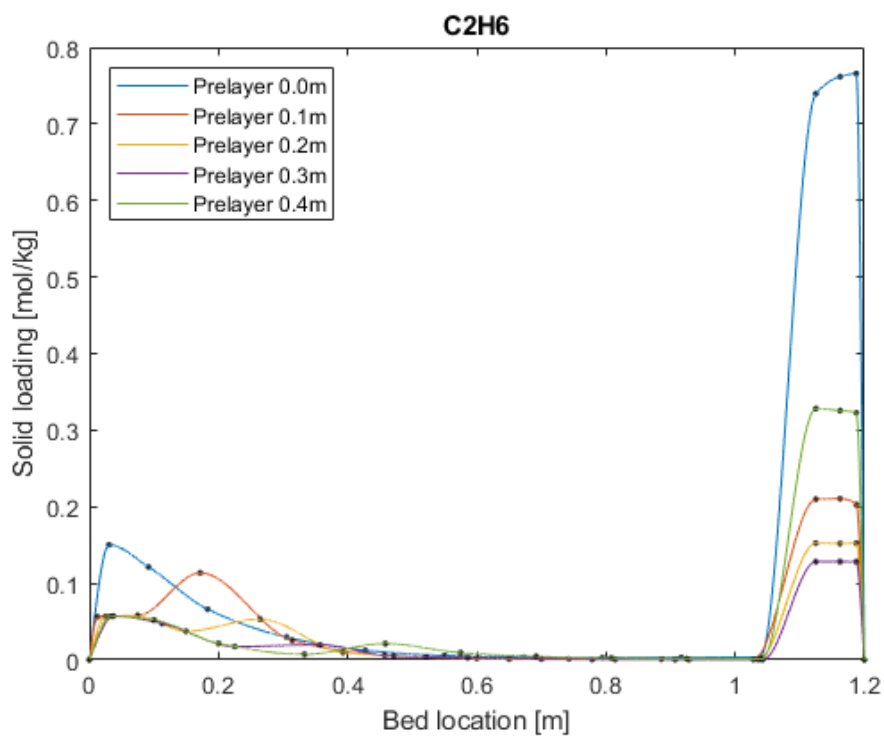


FIGURE C.3: Solid loading of ethane and CO₂ at the end of the adsorption step for a 5 vol% hydrogen feed input.

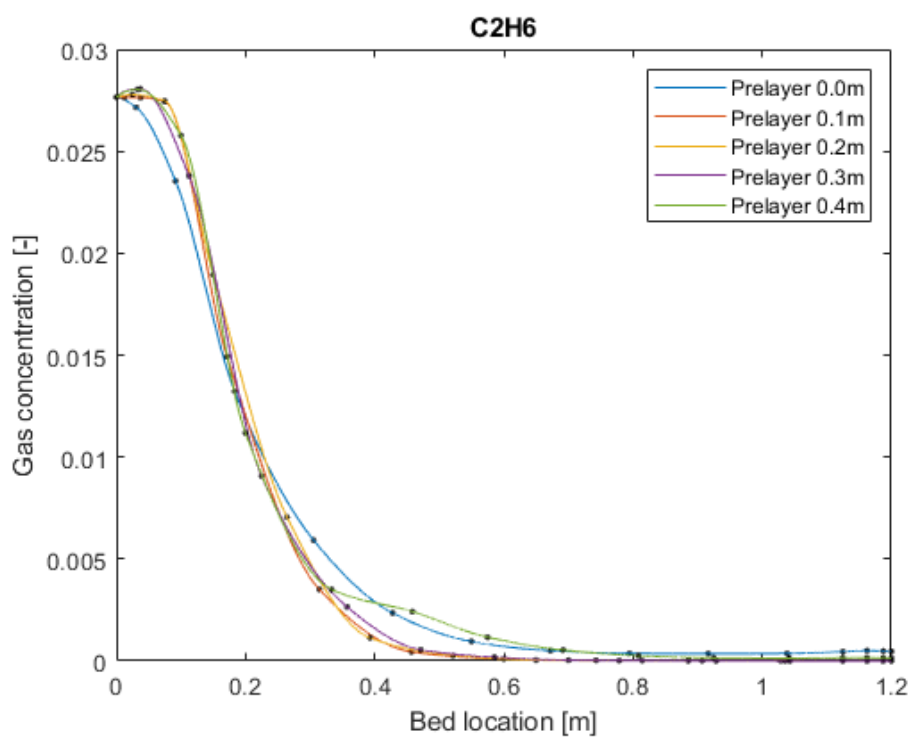


FIGURE C.4: Gas concentration of ethane and CO₂ at the end of the adsorption step for a 5 vol% hydrogen feed input.

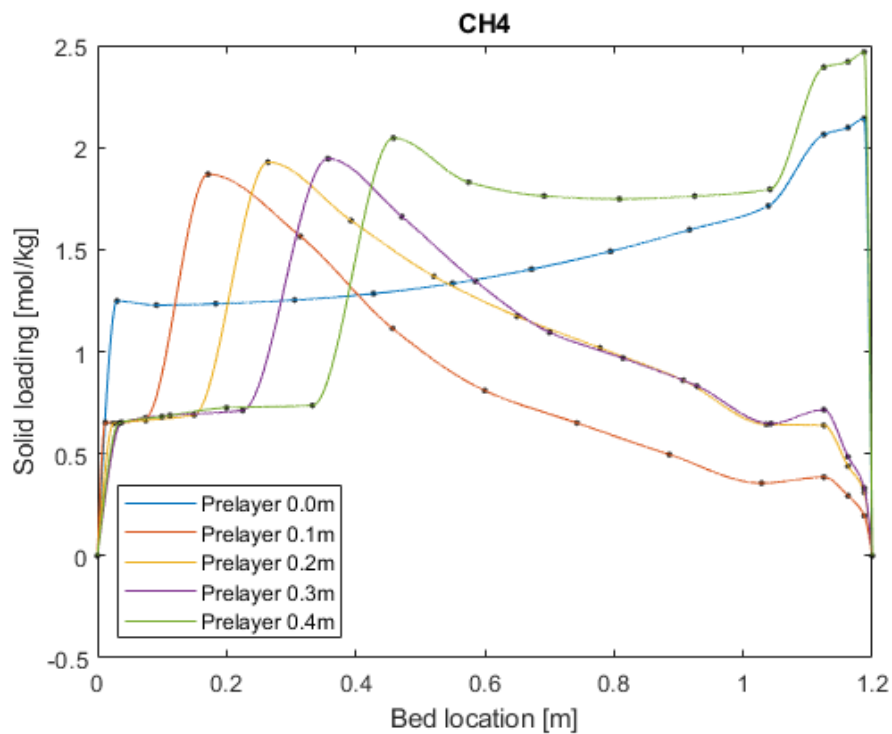


FIGURE C.5: Solid loading of methane at the end of the adsorption step for a 5 vol% hydrogen feed input.

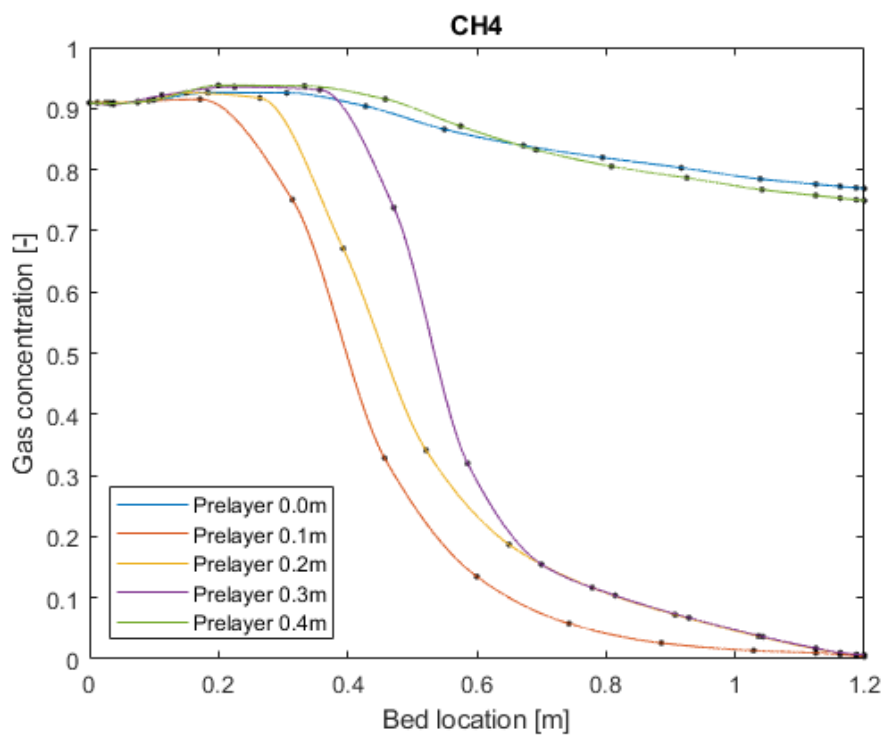


FIGURE C.6: Gas concentration of methane at the end of the adsorption step for a 5 vol% hydrogen feed input.

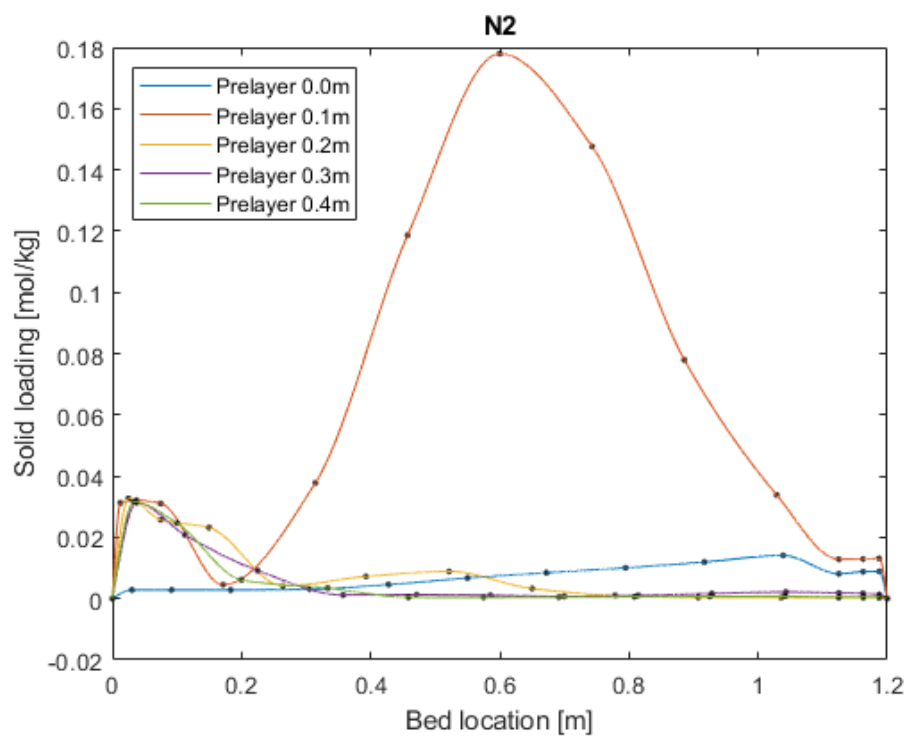


FIGURE C.7: Solid loading of nitrogen at the end of the adsorption step for a 5 vol% hydrogen feed input.

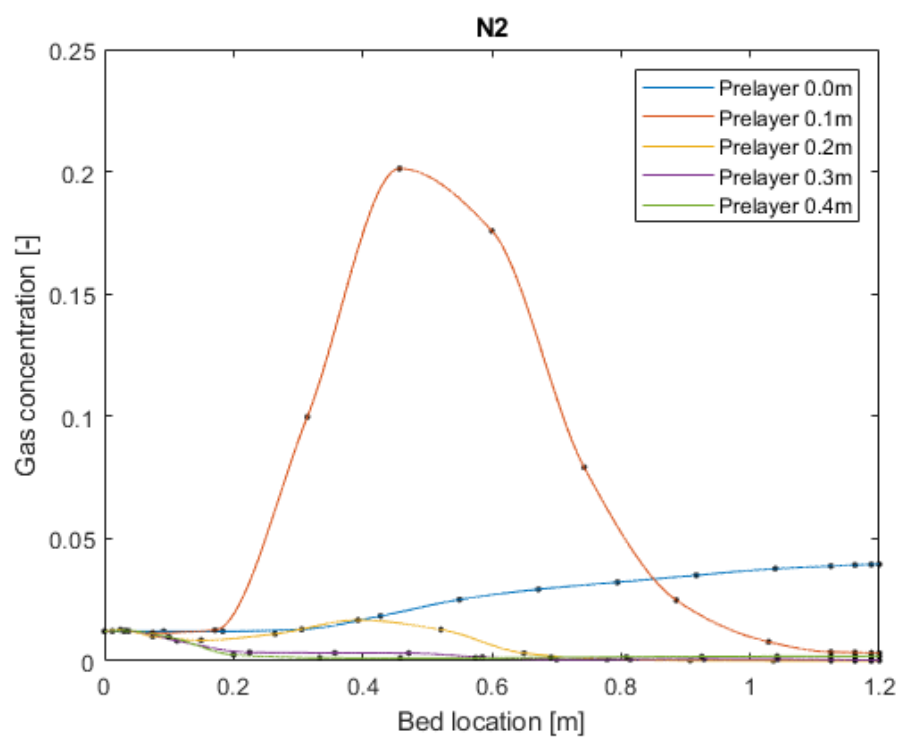


FIGURE C.8: Gas concentration of nitrogen at the end of the adsorption step for a 5 vol% hydrogen feed input.

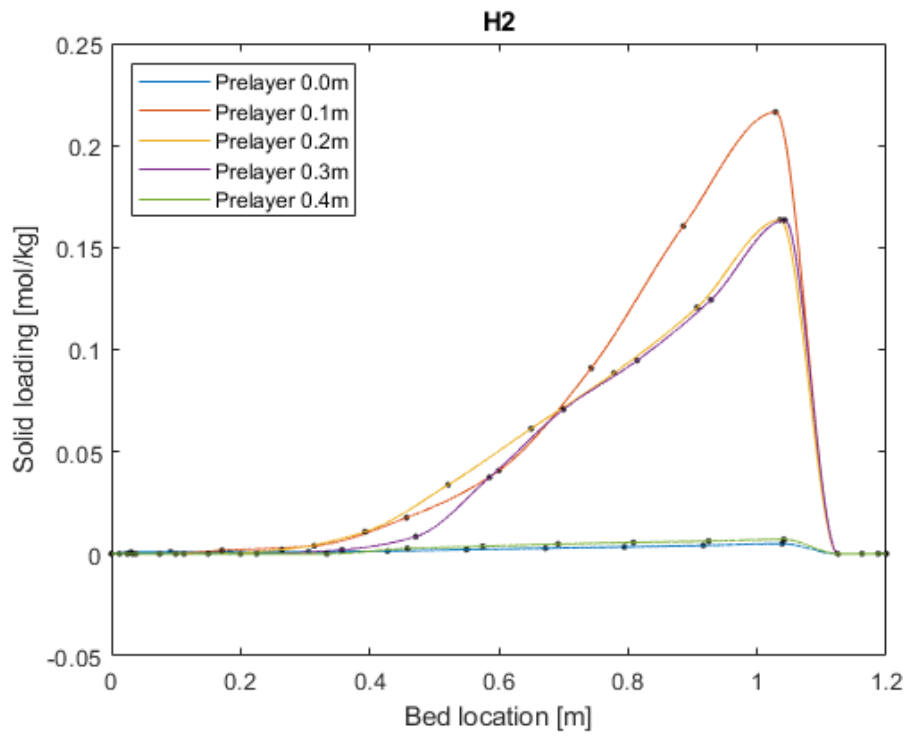


FIGURE C.9: Solid loading of hydrogen at the end of the adsorption step for a 5 vol% hydrogen feed input.

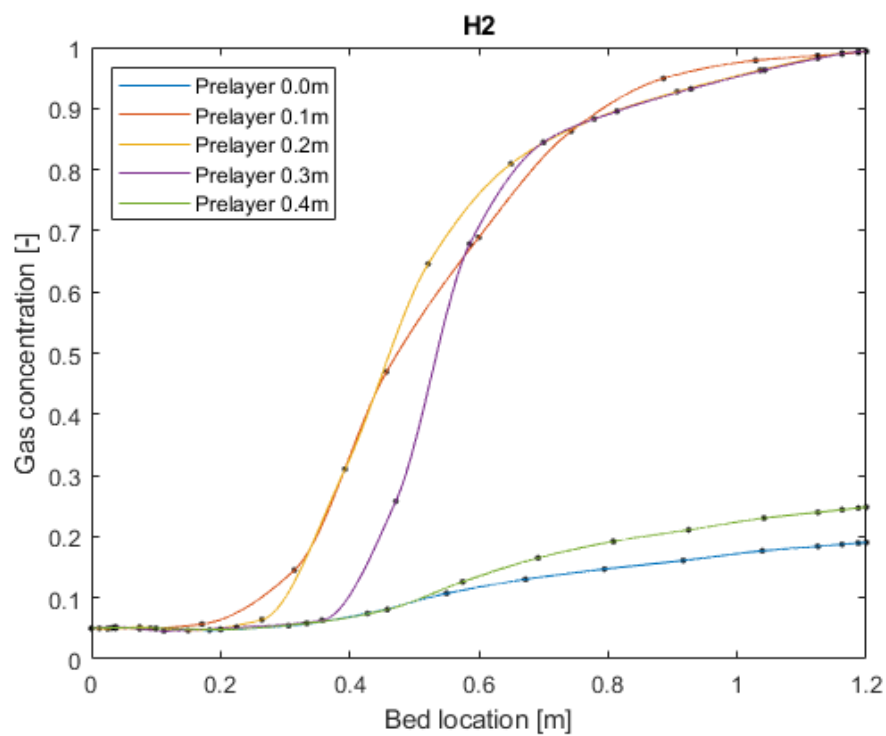


FIGURE C.10: Gas concentration of hydrogen at the end of the adsorption step for a 5 vol% hydrogen feed input.

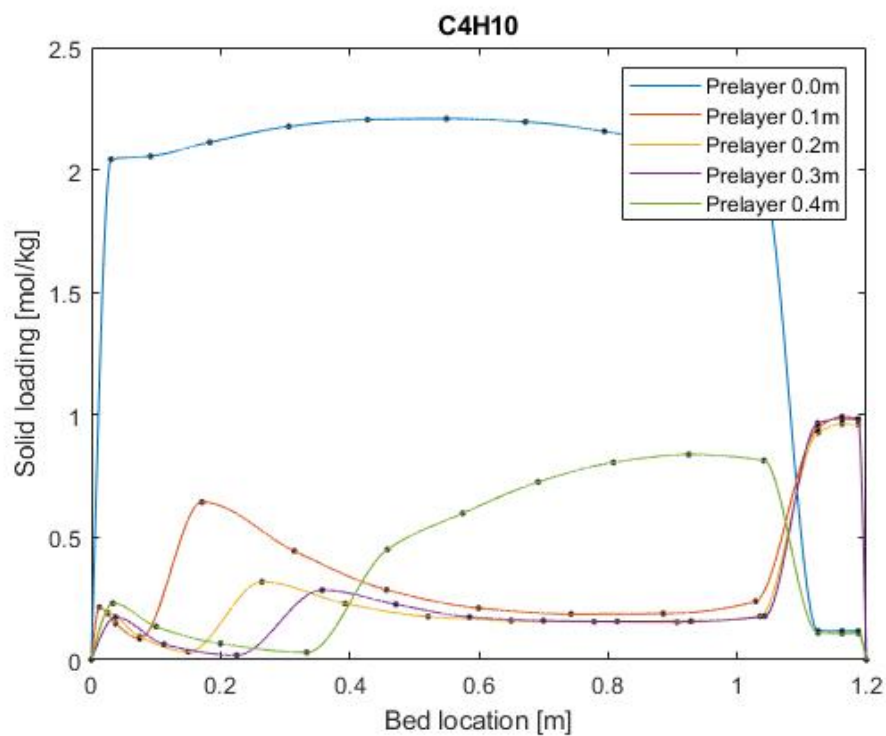


FIGURE C.11: Solid loading of the heavy hydrocarbons at the end of the adsorption step for a 10 vol% hydrogen feed input.

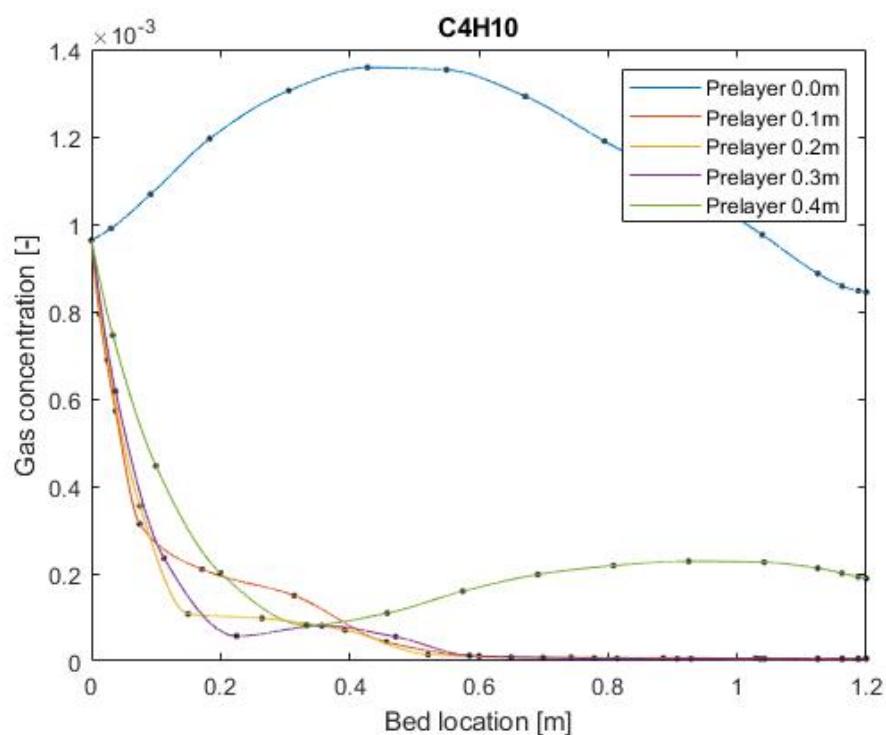


FIGURE C.12: Gas concentration of the heavy hydrocarbons at the end of the adsorption step for a 10 vol% hydrogen feed input.

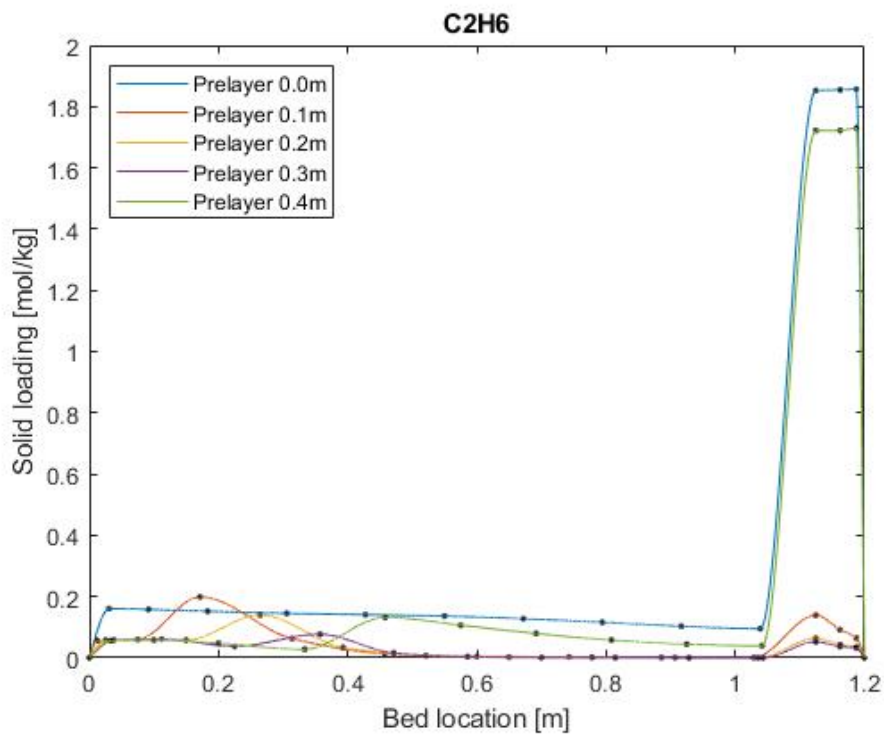


FIGURE C.13: Solid loading of ethane and CO₂ at the end of the adsorption step for a 10 vol% hydrogen feed input.

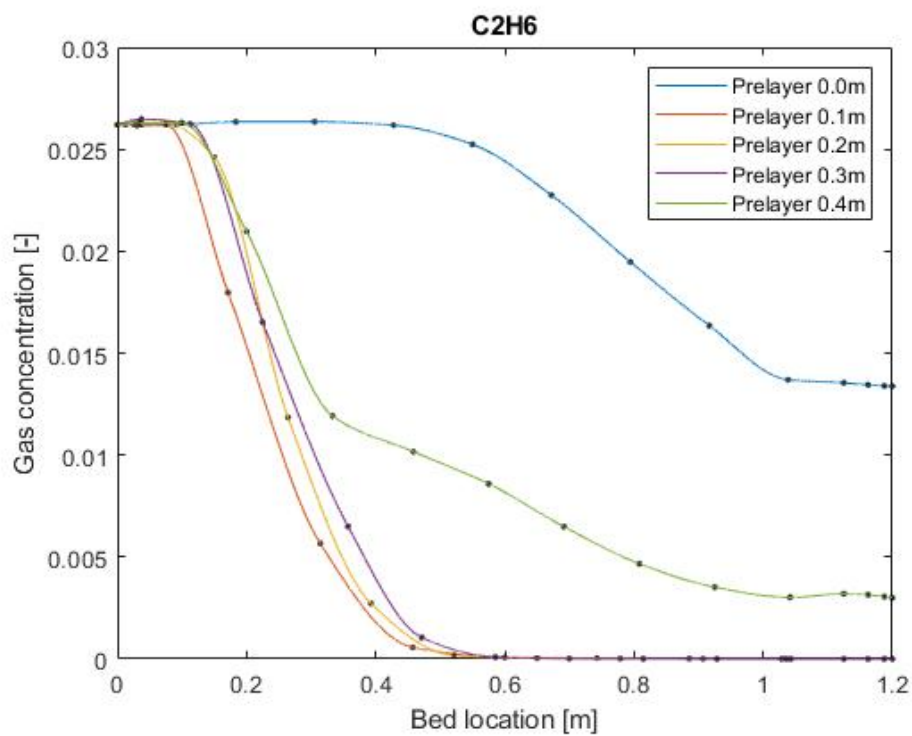


FIGURE C.14: Gas concentration of ethane and CO₂ at the end of the adsorption step for a 10 vol% hydrogen feed input.

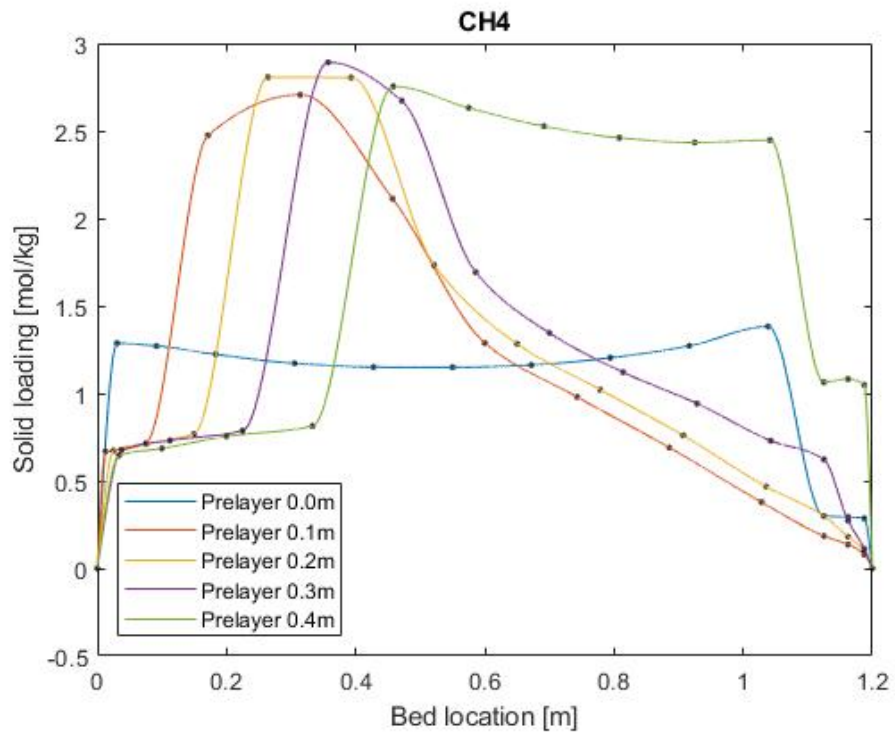


FIGURE C.15: Solid loading of methane at the end of the adsorption step for a 10 vol% hydrogen feed input.

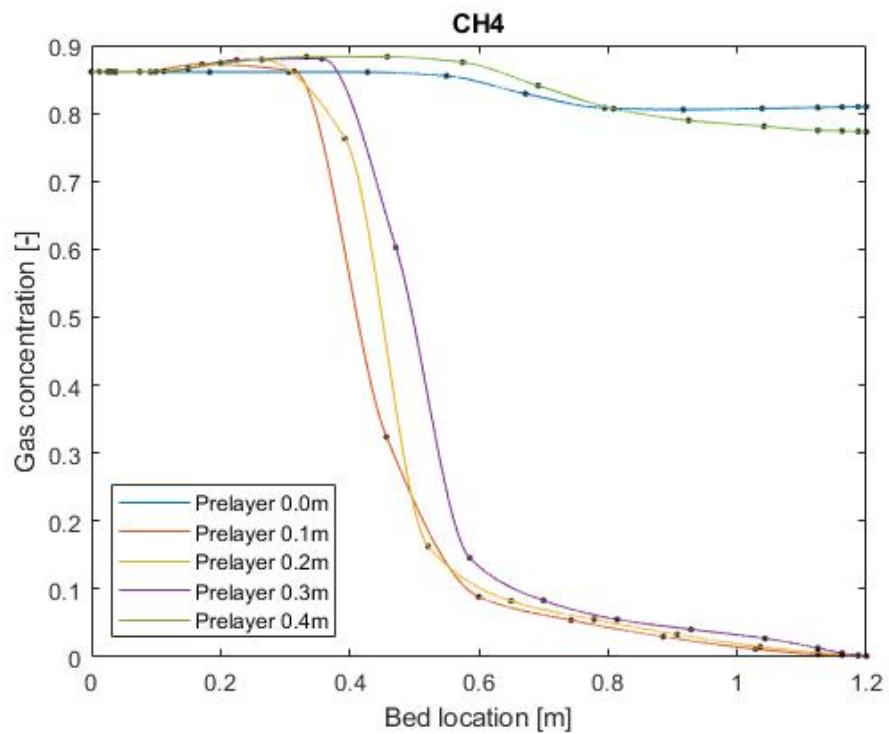


FIGURE C.16: Gas concentration of methane at the end of the adsorption step for a 10 vol% hydrogen feed input.

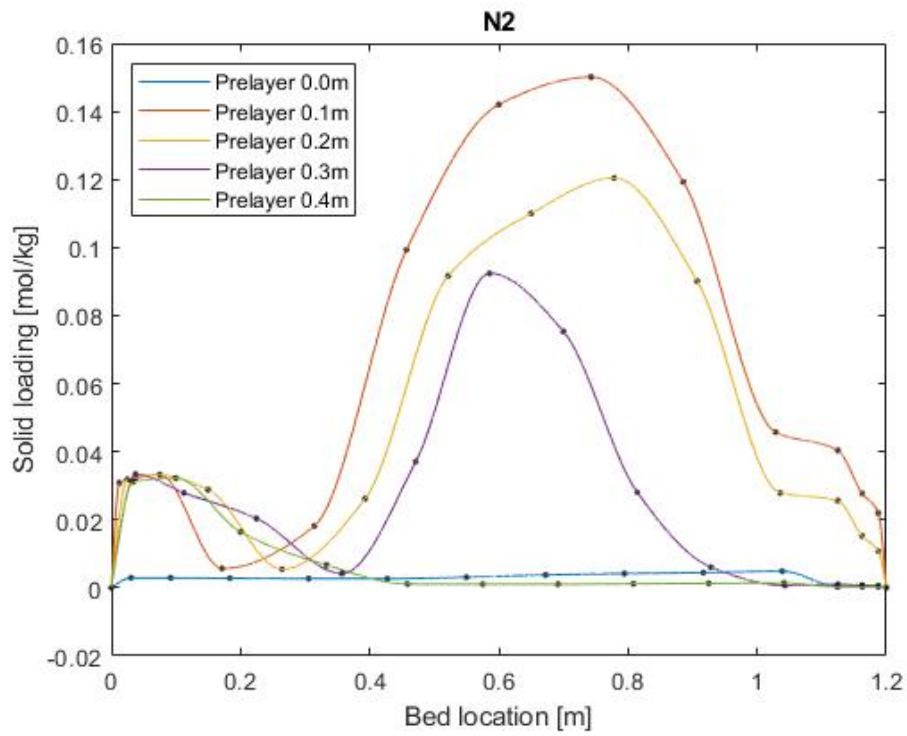


FIGURE C.17: Solid loading of nitrogen at the end of the adsorption step for a 10 vol% hydrogen feed input.

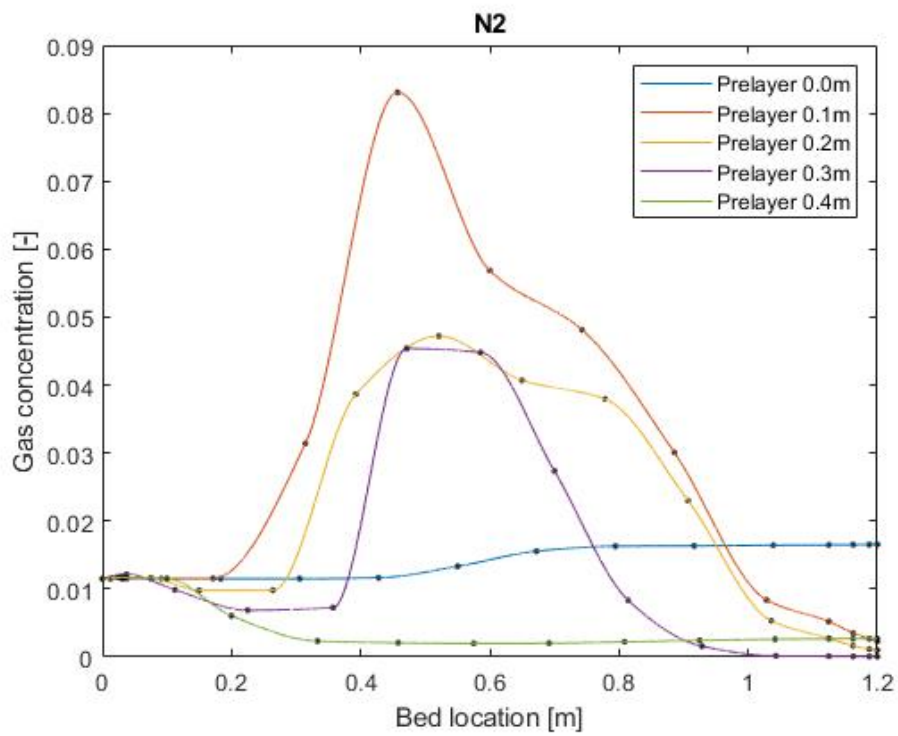


FIGURE C.18: Gas concentration of nitrogen at the end of the adsorption step for a 10 vol% hydrogen feed input.

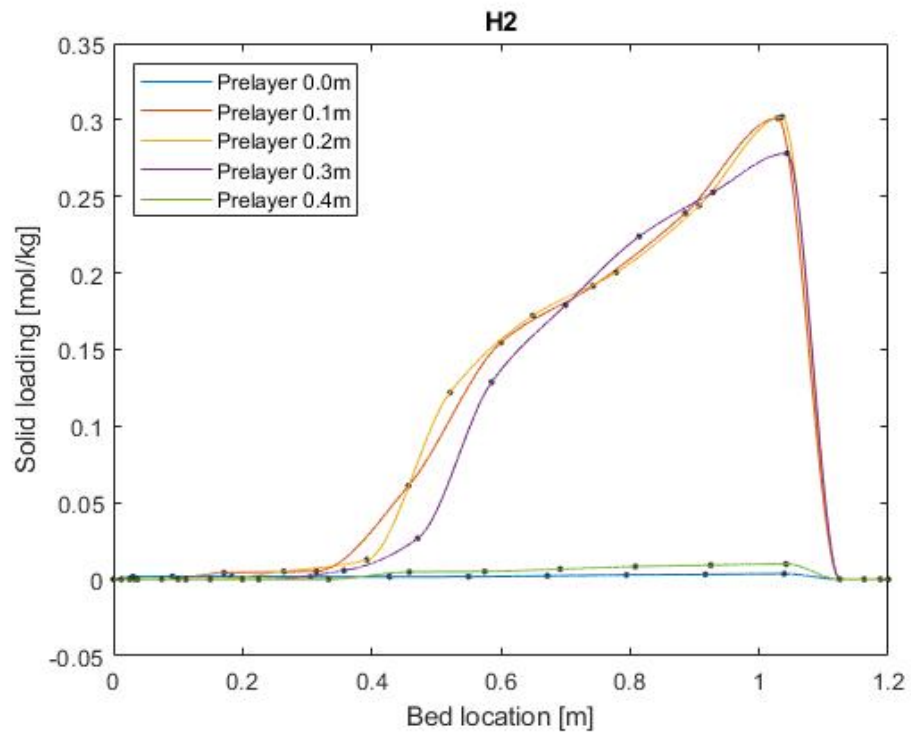


FIGURE C.19: Solid loading of hydrogen at the end of the adsorption step for a 10 vol% hydrogen feed input.

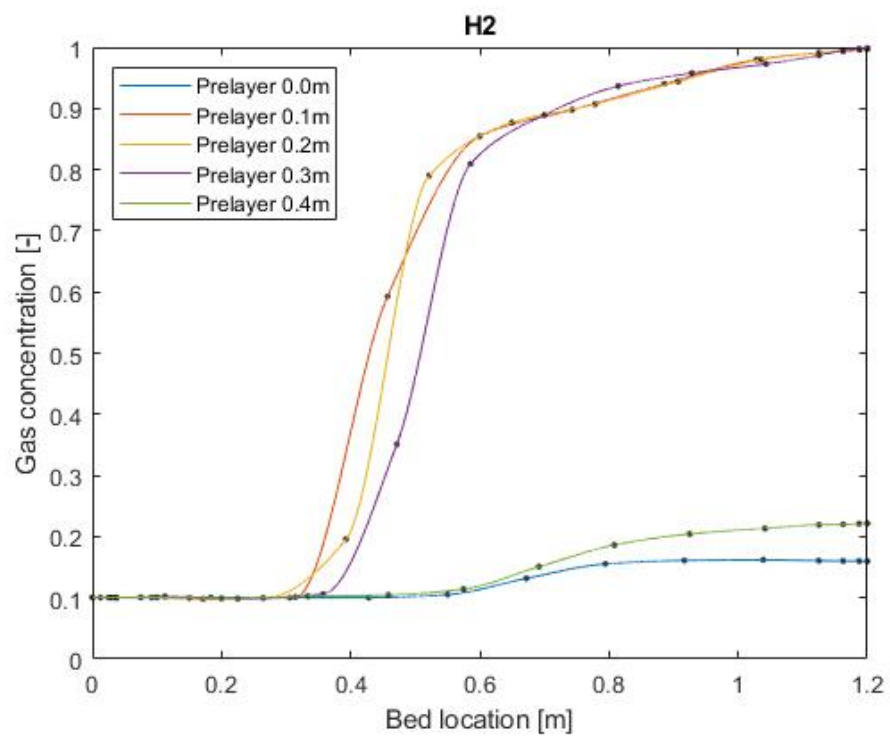


FIGURE C.20: Gas concentration of hydrogen at the end of the adsorption step for a 10 vol% hydrogen feed input.

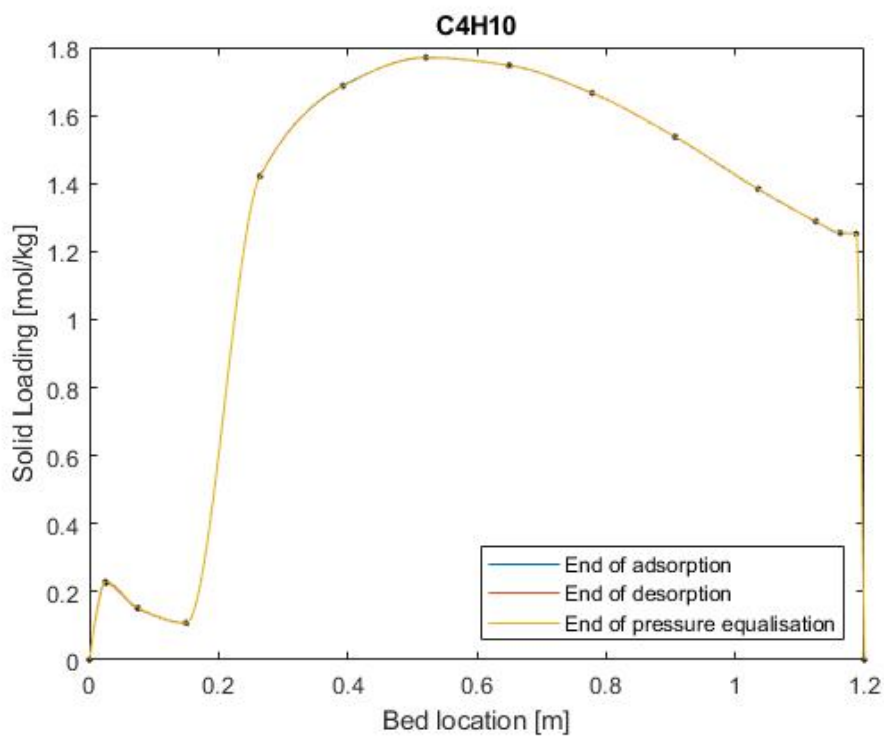


FIGURE C.21: Solid loading of the heavy hydrocarbons at the end of the adsorption, desorption, and pressure equalisation step for a 5 vol% hydrogen feed input, with a pre-layer of 0.2 meter.

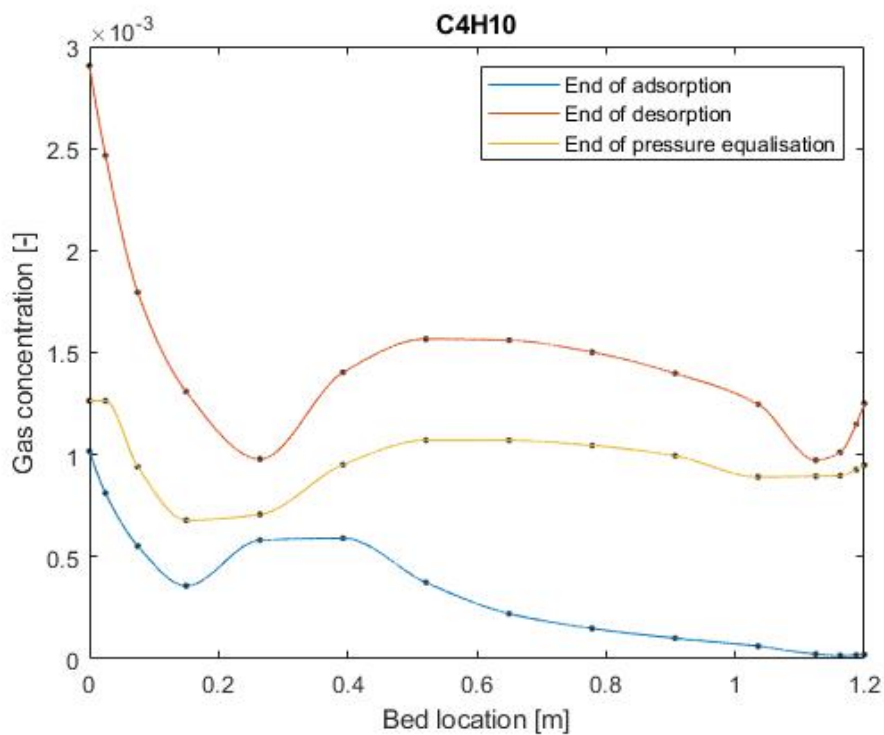


FIGURE C.22: Gas concentration of the heavy hydrocarbons at the end of the adsorption, desorption, and pressure equalisation step for a 5 vol% hydrogen feed input, with a pre-layer of 0.2 meter.

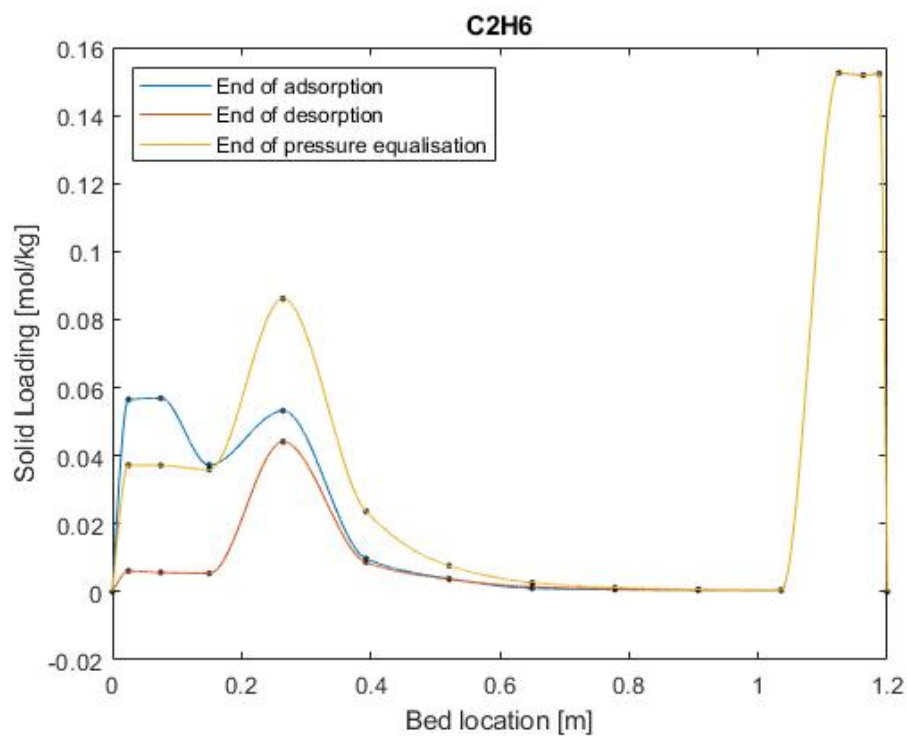


FIGURE C.23: Solid loading of ethane and CO₂ at the end of the adsorption, desorption, and pressure equalisation step for a 5 vol% hydrogen feed input, with a pre-layer of 0.2 meter.

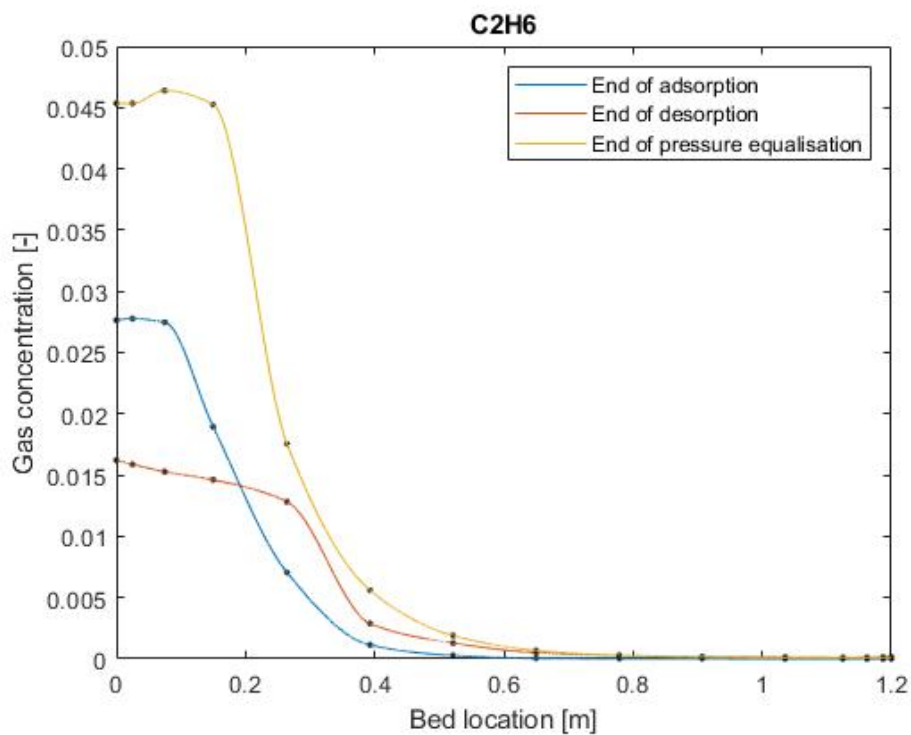


FIGURE C.24: Gas concentration of ethane and CO₂ at the end of the adsorption, desorption, and pressure equalisation step for a 5 vol% hydrogen feed input, with a pre-layer of 0.2 meter.

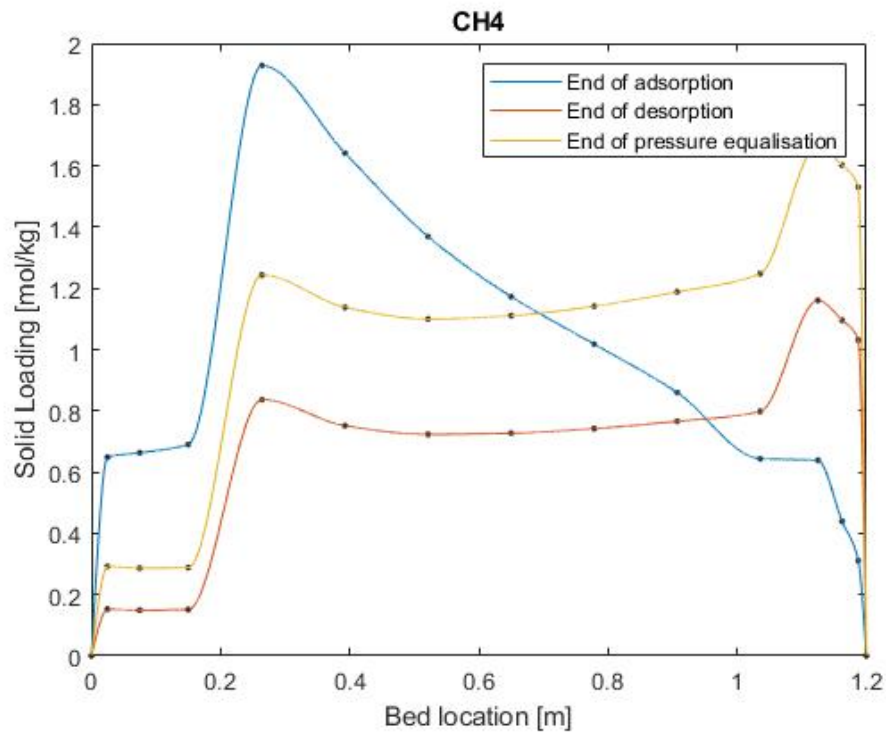


FIGURE C.25: Solid loading of methane at the end of the adsorption, desorption, and pressure equalisation step for a 5 vol% hydrogen feed input, with a pre-layer of 0.2 meter.

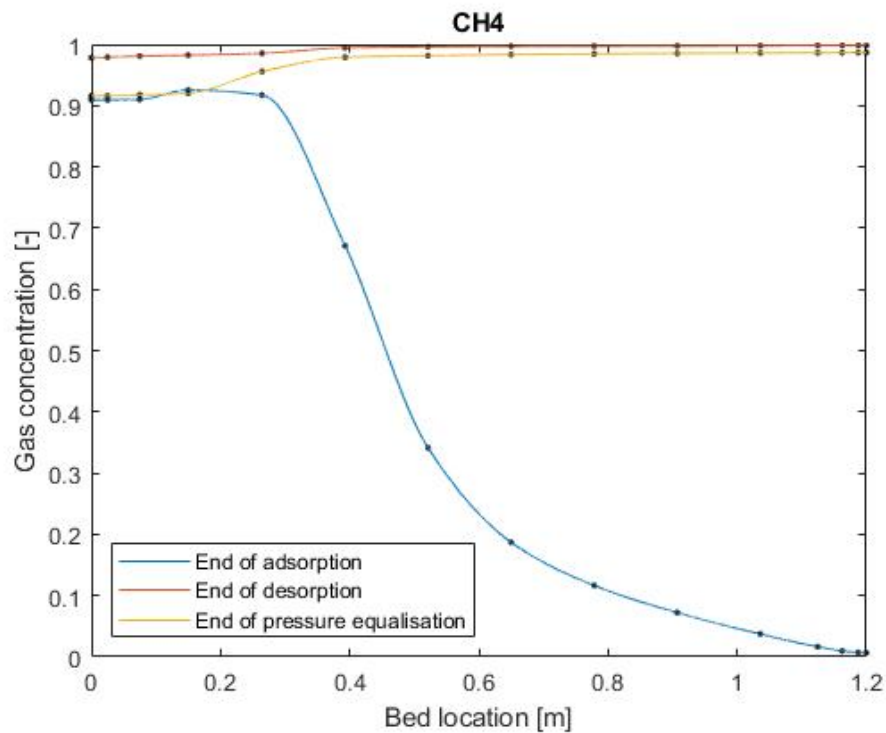


FIGURE C.26: Gas concentration of methane at the end of the adsorption, desorption, and pressure equalisation step for a 5 vol% hydrogen feed input, with a pre-layer of 0.2 meter.

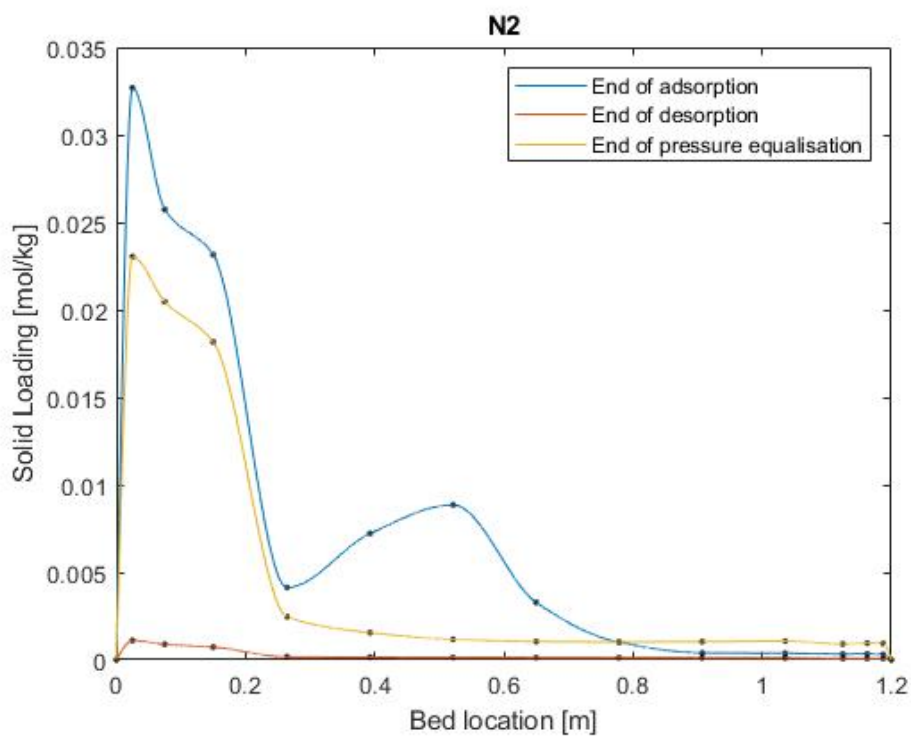


FIGURE C.27: Solid loading of nitrogen at the end of the adsorption, desorption, and pressure equalisation step for a 5 vol% hydrogen feed input, with a pre-layer of 0.2 meter.

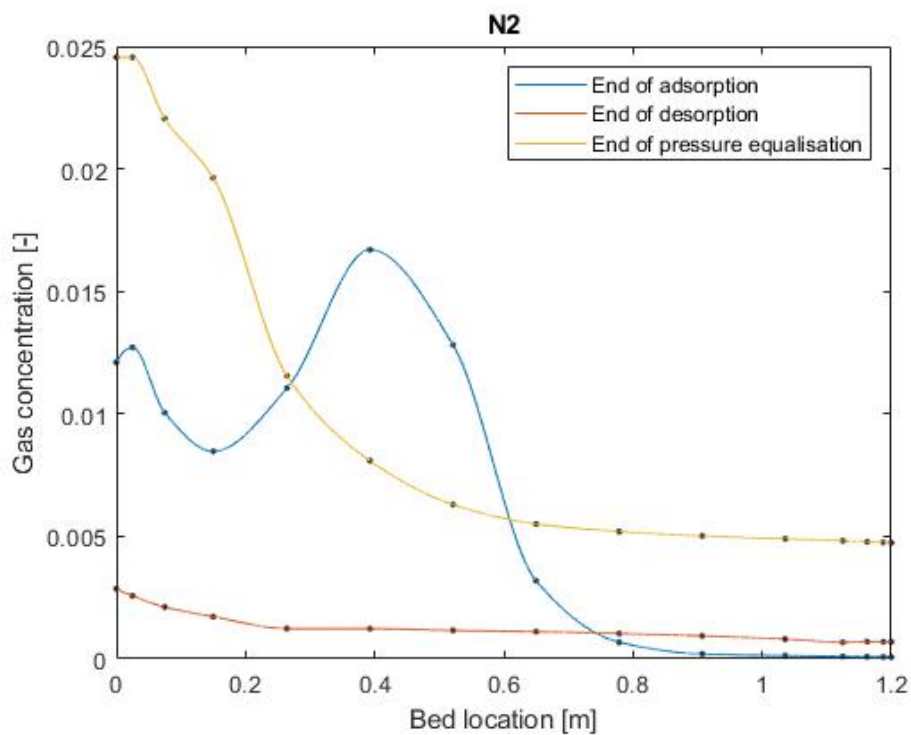


FIGURE C.28: Gas concentration of nitrogen at the end of the adsorption, desorption, and pressure equalisation step for a 5 vol% hydrogen feed input, with a pre-layer of 0.2 meter.

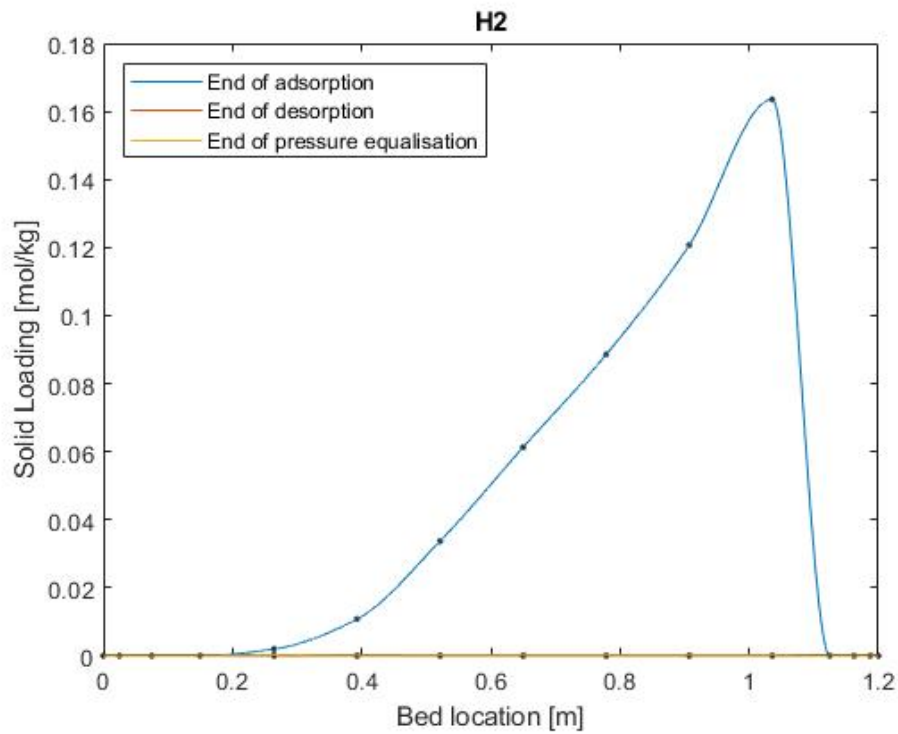


FIGURE C.29: Solid loading of hydrogen at the end of the adsorption, desorption, and pressure equalisation step for a 5 vol% hydrogen feed input, with a pre-layer of 0.2 meter.

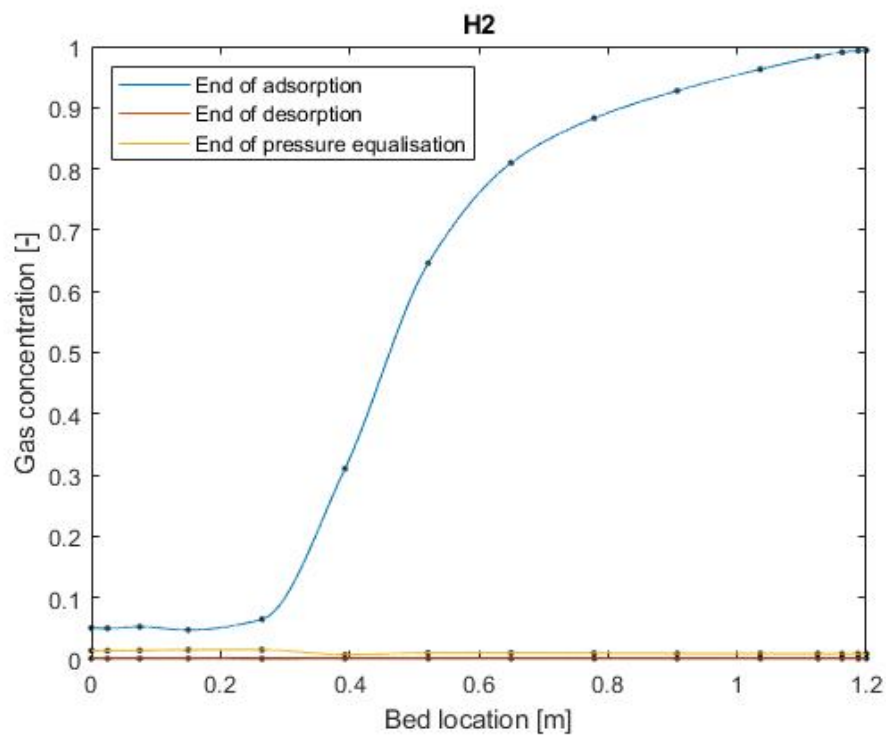


FIGURE C.30: Gas concentration of hydrogen at the end of the adsorption, desorption, and pressure equalisation step for a 5 vol% hydrogen feed input, with a pre-layer of 0.2 meter.

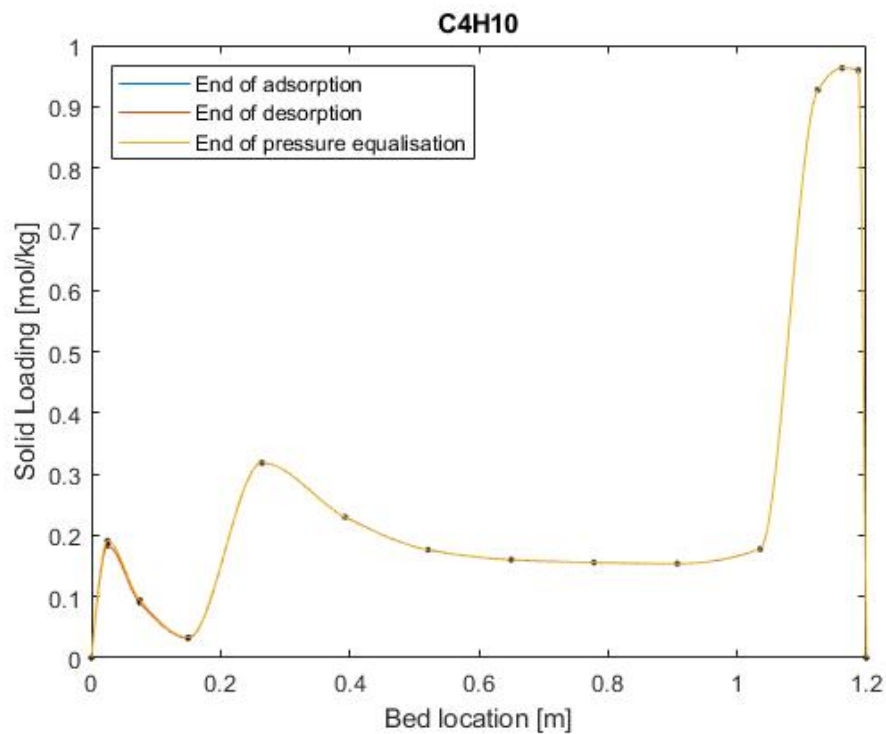


FIGURE C.31: Solid loading of the heavy hydrocarbons at the end of the adsorption, desorption, and pressure equalisation step for a 10 vol% hydrogen feed input, with a pre-layer of 0.2 meter.

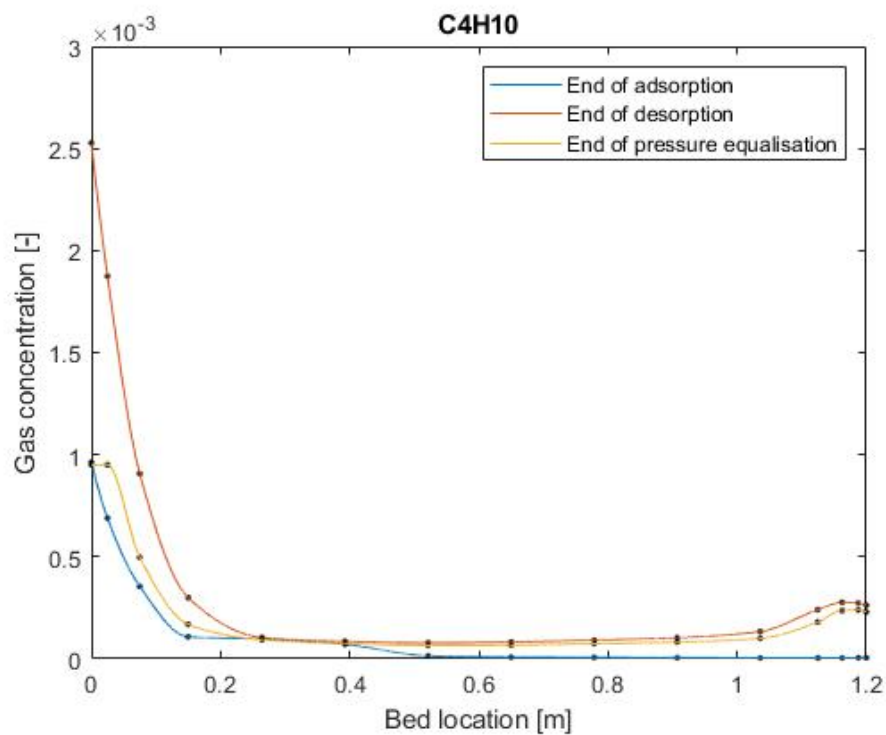


FIGURE C.32: Gas concentration of the heavy hydrocarbons at the end of the adsorption, desorption, and pressure equalisation step for a 10 vol% hydrogen feed input, with a pre-layer of 0.2 meter.

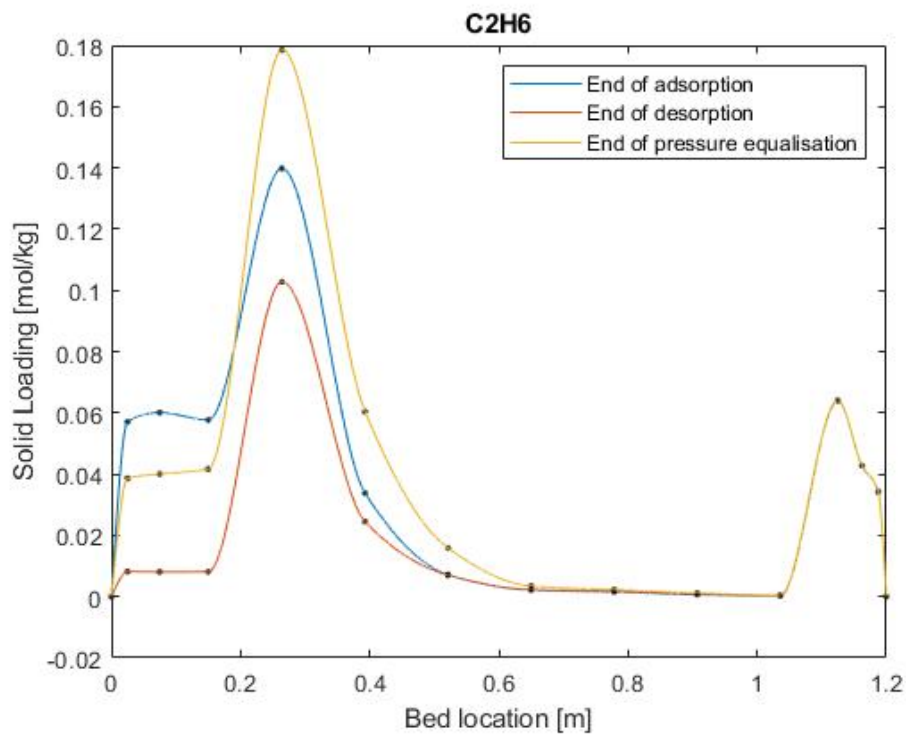


FIGURE C.33: Solid loading of ethane and CO_2 at the end of the adsorption, desorption, and pressure equalisation step for a 10 vol% hydrogen feed input, with a pre-layer of 0.2 meter.

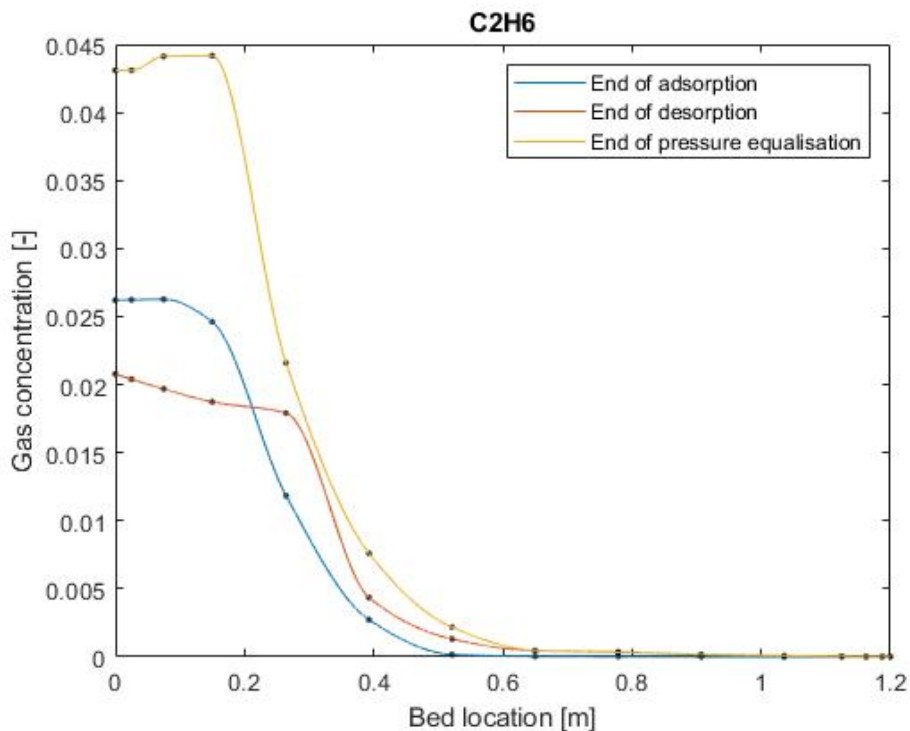


FIGURE C.34: Gas concentration of ethane and CO_2 at the end of the adsorption, desorption, and pressure equalisation step for a 10 vol% hydrogen feed input, with a pre-layer of 0.2 meter.

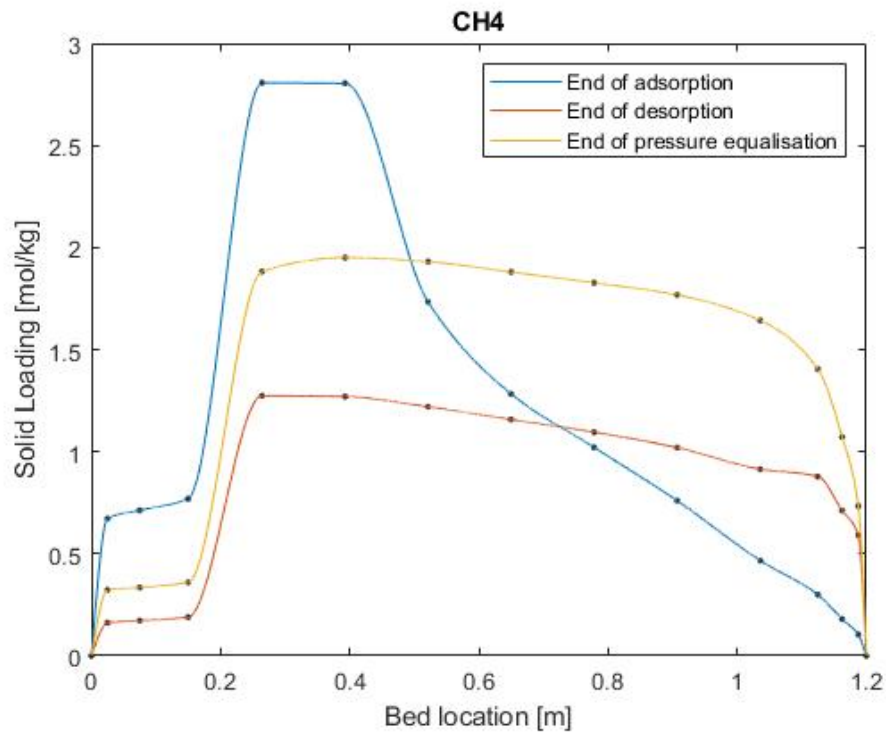


FIGURE C.35: Solid loading of methane at the end of the adsorption, desorption, and pressure equalisation step for a 10 vol% hydrogen feed input, with a pre-layer of 0.2 meter.

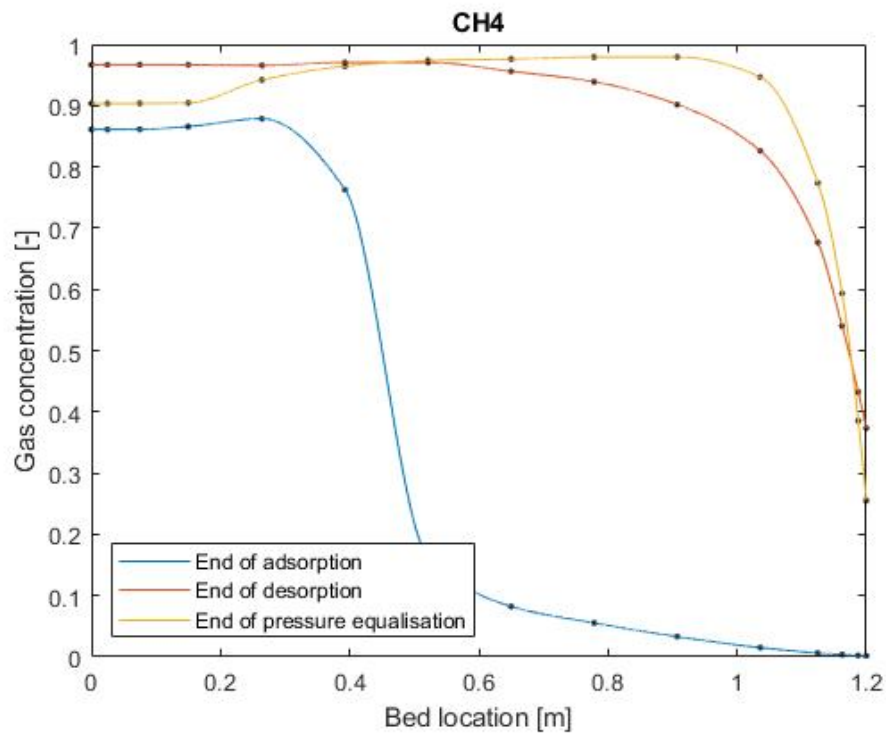


FIGURE C.36: Gas concentration of methane at the end of the adsorption, desorption, and pressure equalisation step for a 10 vol% hydrogen feed input, with a pre-layer of 0.2 meter.

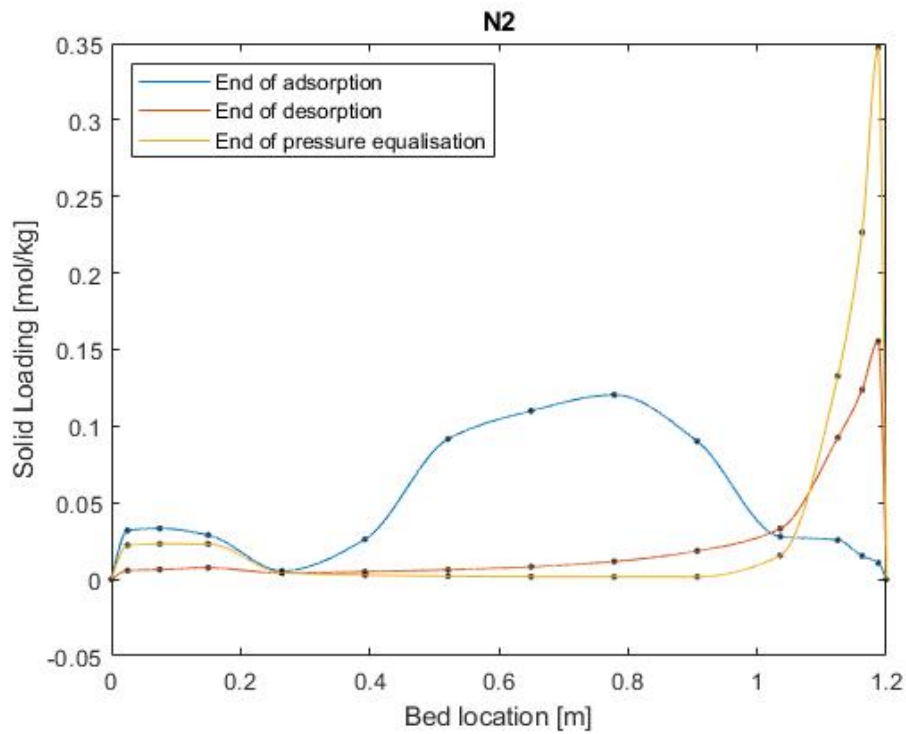


FIGURE C.37: Solid loading of nitrogen at the end of the adsorption, desorption, and pressure equalisation step for a 10 vol% hydrogen feed input, with a pre-layer of 0.2 meter.

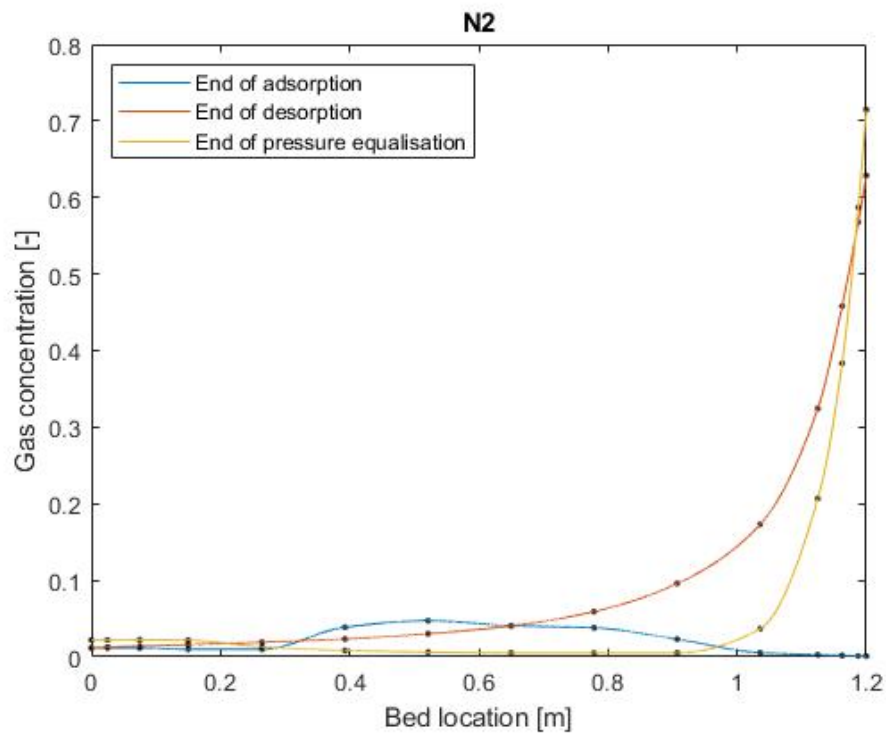


FIGURE C.38: Gas concentration of nitrogen at the end of the adsorption, desorption, and pressure equalisation step for a 10 vol% hydrogen feed input, with a pre-layer of 0.2 meter.

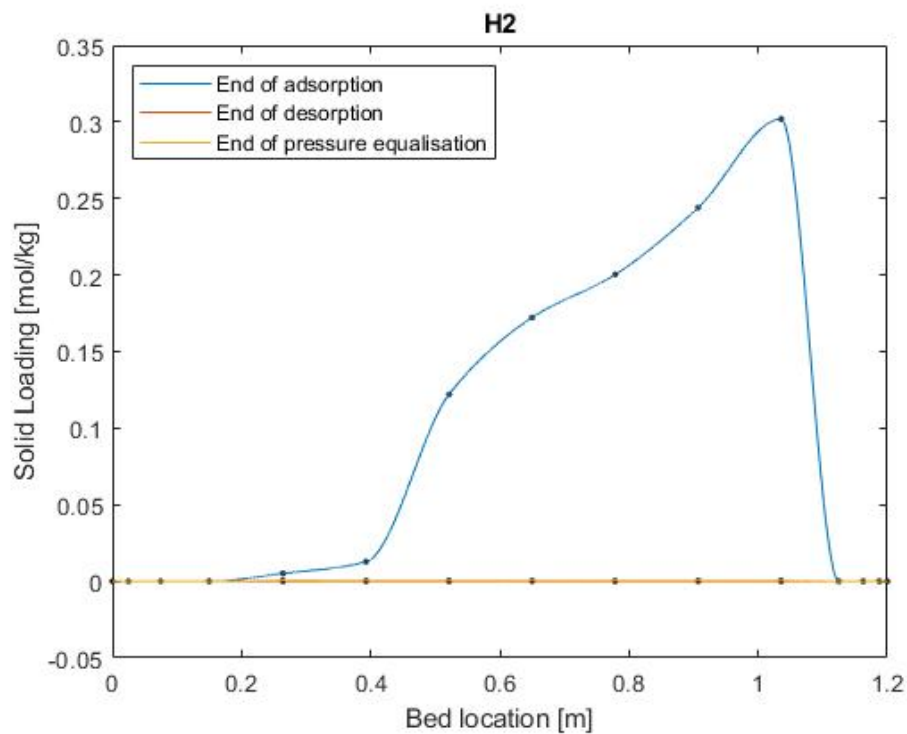


FIGURE C.39: Solid loading of hydrogen at the end of the adsorption, desorption, and pressure equalisation step for a 10 vol% hydrogen feed input, with a pre-layer of 0.2 meter.

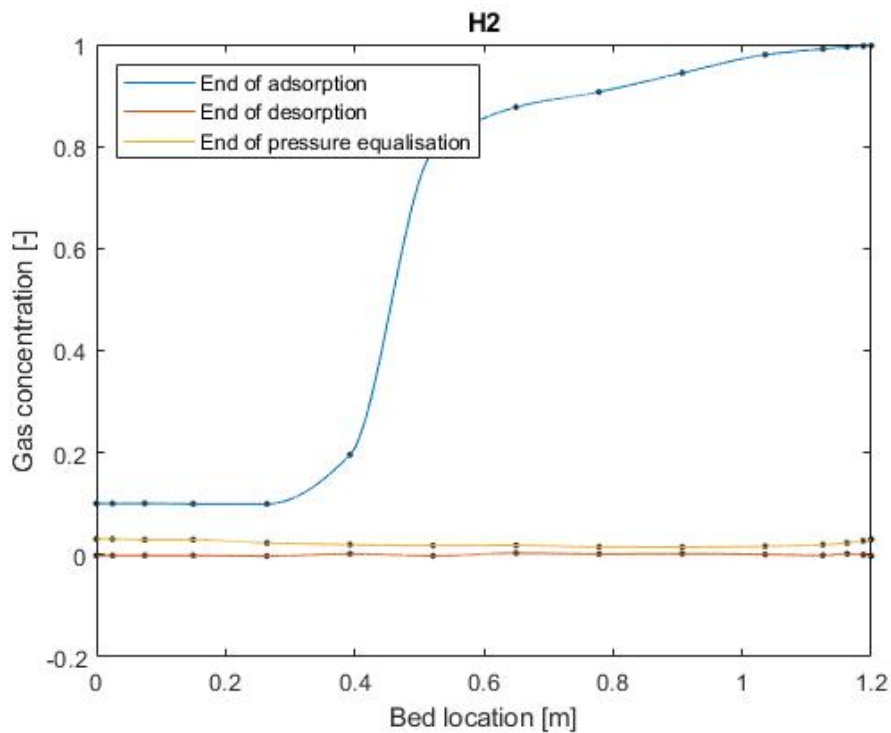


FIGURE C.40: Gas concentration of hydrogen at the end of the adsorption, desorption, and pressure equalisation step for a 10 vol% hydrogen feed input, with a pre-layer of 0.2 meter.

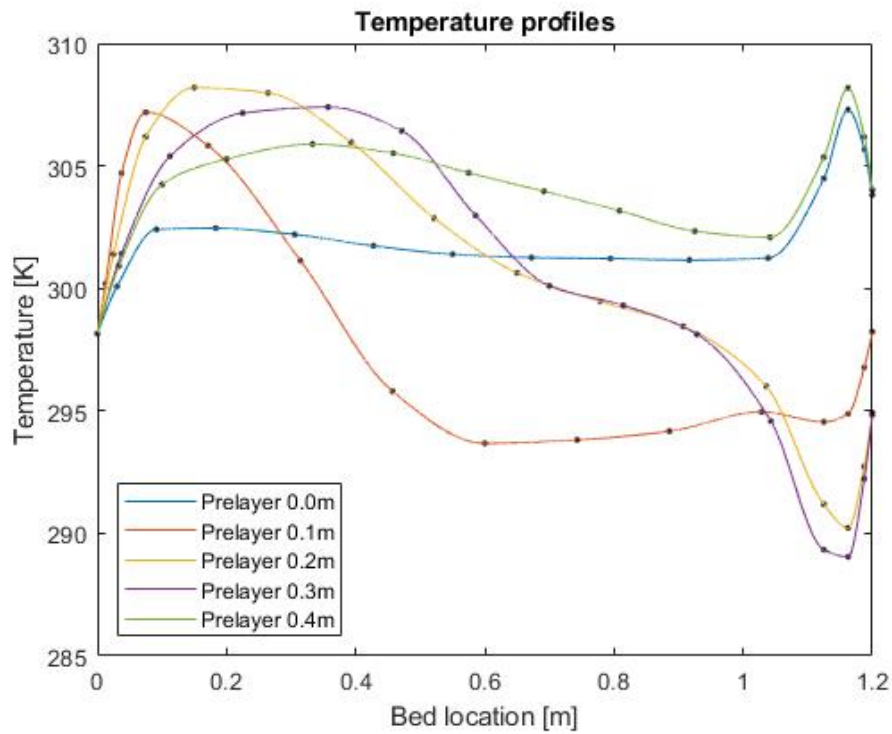


FIGURE C.41: Temperature profiles at the end of the adsorption step for 5 vol% hydrogen feed input.

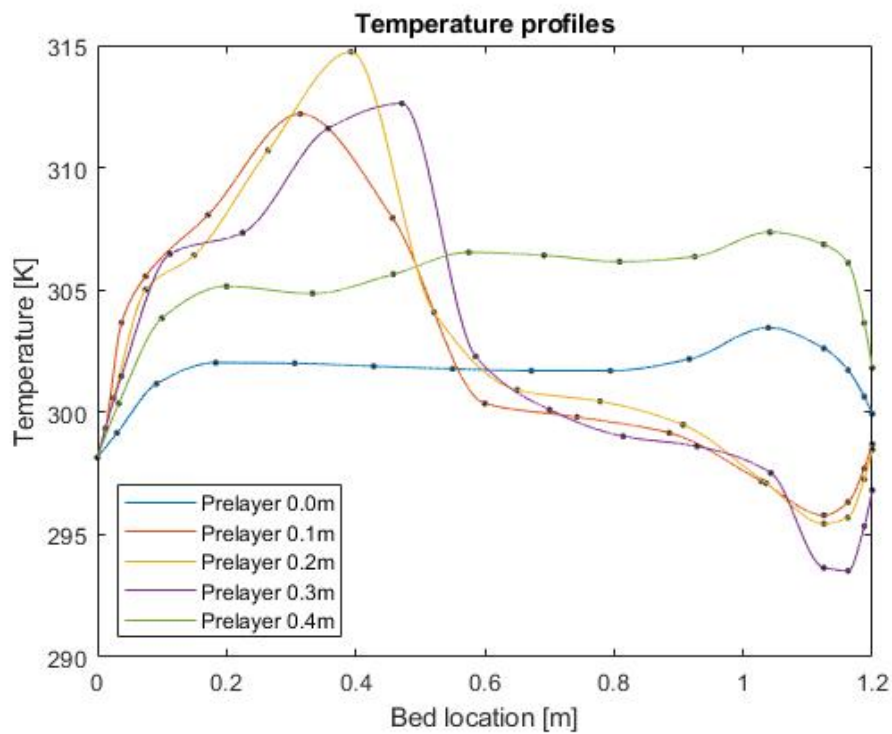


FIGURE C.42: Temperature profiles at the end of the adsorption step for 10 vol% hydrogen feed input.

Appendix D

HRSAM Model Results

TABLE D.1: Constant values used by the HRSAM model to calculate the optimum compression and storage design for a hydrogen refuelling station.

| Constant | Value | Unit |
|-----------------------------------------------------------|--------------|----------------|
| Maximum number of vehicles back-to-back during peak hours | 4 | - |
| Average Hourly Demand as a % of daily demand | 4.2 | % |
| Compressor | | |
| Pressure Ratio | 6.9 | - |
| Number of Stages | 2 | - |
| Motor Efficiency | 91 | % |
| Electrical Voltage Supply Requirement | 480 | V |
| Refrigeration unit | | |
| Maximum Capacity of Refrigeration Unit | 10 | ton |
| Minimum Capacity of Refrigeration Unit | 1.74 | ton |
| Cascade | | |
| High-Pressure vessel Useable Capacity at Peak Demand | 9.8 | % |
| Mid-Pressure vessel Useable Capacity at Peak Demand | 25 | % |
| Low-Pressure vessel Useable Capacity at Peak Demand | 53.5 | % |
| Cascade Vessel Capacity/Unit | 40 | kg |
| Average cascade Useable Capacity at Peak Demand | 29.4 | % |
| Cascade Vessel Outside Diameter | 0.40 | m |
| Cascade Vessel Length | 4.60 | m |
| Cascade Vessel Wall Thickness | 0.06 | m |
| High Pressure Cascade Storage Vessel | | |
| Volume | 0.28 | m ³ |
| Maximum Pressure | 944 | bar |

TABLE D.1: Constant values used by the HRSAM model to calculate the optimum compression and storage design for a hydrogen refuelling station.

| Constant | Value | Unit |
|-----------------------------------------------|--------------|----------------|
| Minimum Pressure | 802 | bar |
| Number of vessels in high-pressure bank | 1 | - |
| Medium Pressure Cascade Storage Vessel | | |
| Volume | 0.28 | m ³ |
| Maximum Pressure | 944 | bar |
| Minimum Pressure | 613 | bar |
| Number of vessels in med-pressure bank | 1 | - |
| Low Pressure Cascade Storage Vessel | | |
| Volume | 0.28 | m ³ |
| Maximum Pressure | 944 | bar |
| Minimum Pressure | 330 | bar |
| Number of vessels in low-pressure bank | 1 | - |
| Low pressure storage vessel | | |
| Low Pressure Storage Vessel Diameter | 1.2 | m |
| Low Pressure Storage Vessel Length | 7.6 | m |
| Low Pressure Storage Vessel Wall Thickness | 0.064 | m |
| Low Pressure Storage Vessel Capacity | 123.6 | kg |
| Tube-trailer storage vessel | | |
| Width | 4.6 | m |
| Maximum pressure in tube trailer | 350 | bar |
| Minimum pressure in tube trailer | 50 | bar |

TABLE D.2: Design variables for a hydrogen refuelling station with different hydrogen demand, representing a small, medium, and large refuelling station.

| Variables | Pipeline | | | Truck | | Unit |
|----------------------------------------------------------|-----------|------------|-----------|------------|-------|----------------|
| | Small HRS | Medium HRS | Large HRS | Medium HRS | HRS | |
| Number of dispensers | 1 | 2 | 2 | 2 | 2 | - |
| Number of hoses | 2 | 4 | 4 | 4 | 4 | - |
| Maximum Number of Fills During Peak Hour | 8 | 16 | 16 | 16 | 16 | - |
| Average Hourly Demand During a Day | 15 | 29 | 42 | 29 | 29 | kg/hr |
| Station land area | 198 | 396 | 402 | 601 | 601 | m ² |
| Cascade system | | | | | | |
| Cascade size required at refuelling station | 161 | 241 | 322 | 241 | 241 | kg |
| Low Pressure Storage | 112 | 224 | 311 | - | - | kg |
| Optimum Number of Cascade Systems | 4 | 6 | 8 | 6 | 6 | - |
| Maximum Dispensable Amount from Cascade | 47.3 | 71 | 94.7 | 71 | 71 | kg |
| Cascade Size as a Percent of Average Daily Demand | 45.9 | 34.5 | 32.2 | 34.5 | 34.5 | % |
| Mass Flow Cascade Must Sustain | 10 | 20 | 20 | 20 | 20 | kg/min |
| Compressor | | | | | | |
| Minimum Compressor Capacity | 15 | 29 | 42 | 29 | 29 | kg/hr |
| Total Compressor Capacity to Meet Demand Requirements | 21 | 47 | 63 | 47 | 47 | kg/hr |
| Actual Shaft Power Requirement for Each Compressor | 65 | 144 | 191 | 106 | 106 | kW |
| Motor Rating per Compressor | 78 | 173 | 227 | 129 | 129 | kW |
| Average Compressor Demand During a Day | 0.243 | 0.486 | 0.694 | 0.486 | 0.486 | kg/min |
| Required Compressor Flowrate for Peak and Adjacent Hour | 21.3 | 47.4 | 62.8 | 47.4 | 47.4 | kg/hr |
| Required Compressor Flowrate Above Average for Peak Hour | 0.111 | 0.305 | 0.353 | 0.305 | 0.305 | kg/min |
| Tube-trailer | | | | | | |
| Number of tube trailers at station at any time | - | - | - | - | 2 | - |

TABLE D.3: Initial capital investment overview for a small refuelling station, with hydrogen supplied by a pipeline at 20 bar, and a demand of 350 kg of hydrogen per day.

| Component | Value | Uninstalled costs | Installation factor | Installed cost |
|----------------------------------------------|--------|-------------------|---------------------|------------------------|
| Refrigeration Equipment | | | | |
| Number of condensing/HX units | 2.00 | | | |
| Refrigeration capacity per unit (tons) | 3.39 | \$ 53,909.63 | 2 | \$ 232,545.83 |
| Number of Heat Exchanger | 1.00 | \$ 62,363.28 | 2 | |
| Compressor | | | | |
| Number of Compressors | 2.00 | | | |
| Main Compressor Power per unit (kW) | 77.78 | \$ 1,915,889.05 | 1.3 | \$ 2,490,655.77 |
| Dispenser | | | | |
| Number of Dispensers | 1.00 | \$ 144,704.67 | 1.3 | \$ 188,116.08 |
| Electrical | | | | |
| Electrical Voltage Supplied (Volts) | 480.00 | \$ 51,658.76 | 2.24 | \$ 115,715.61 |
| Cascade | | | | |
| Capacity (kg of Hydrogen) | 160.82 | \$ 383,012.61 | 1.3 | \$ 497,916.39 |
| Low-Pressure Storage for Hourly Surge | | | | |
| Number of Units | 1.00 | | | |
| Unit Size (kg of Hydrogen) | 123.61 | \$ 204,462.56 | 1.3 | \$ 265,801.33 |
| Remainder of Station | | | | |
| Overall Control and Safety Equipment | | | 1 | \$ 147,960.00 |
| Total Initial Capital Investment | | | | \$ 3,938,711.01 |

TABLE D.4: Initial capital investment overview for a medium refuelling station, with hydrogen supplied by a pipeline at 20 bar, and a demand of 700 kg of hydrogen per day.

| Component | Value | Uninstalled costs | Installation factor | Installed cost |
|----------------------------------------------|--------|-------------------|---------------------|------------------------|
| Refrigeration Equipment | | | | |
| Number of condensing/HX units | 4.00 | | | |
| Refrigeration capacity per unit (tons) | 3.39 | \$ 97,705.72 | 2 | \$ 444,864.58 |
| Number of Heat Exchanger | 2.00 | \$ 124,726.57 | 2 | |
| Compressor | | | | |
| Number of Compressors | 3.00 | | | |
| Main Compressor Power per unit (kW) | 86.50 | \$ 3,064,354.83 | 1.3 | \$ 3,983,661.28 |
| Dispenser | | | | |
| Number of Dispensers | 2.00 | \$ 289,409.35 | 1.3 | \$ 376,232.15 |
| Electrical | | | | |
| Electrical Voltage Supplied (Volts) | 480.00 | \$ 63,232.39 | 2.24 | \$ 141,640.54 |
| Cascade | | | | |
| Capacity (kg of Hydrogen) | 241.24 | \$ 574,518.91 | 1.3 | \$ 746,874.59 |
| Low-Pressure Storage for Hourly Surge | | | | |
| Number of Units | 2.00 | | | |
| Unit Size (kg of Hydrogen) | 123.61 | \$ 408,925.13 | 1.3 | \$ 531,602.67 |
| Remainder of Station | | | | |
| Overall Control and Safety Equipment | | | 1 | \$ 147,960.00 |
| Total Initial Capital Investment | | | | \$ 6,372,835.80 |

TABLE D.5: Initial capital investment overview for a large refuelling station, with hydrogen supplied by a pipeline at 20 bar, and a demand of 1000 kg of hydrogen per day.

| Component | Value | Uninstalled costs | Installation factor | Installed cost |
|----------------------------------------------|--------|-------------------|---------------------|------------------------|
| Refrigeration Equipment | | | | |
| Number of condensing/HX units | 4.00 | | | |
| Refrigeration capacity per unit (tons) | 3.39 | \$ 97,705.72 | 2.00 | \$ 444,864.58 |
| Number of Heat Exchanger | 2.00 | \$ 124,726.57 | 2.00 | |
| Compressor | | | | |
| Number of Compressors | 3.00 | | | |
| Main Compressor Power per unit (kW) | 113.69 | \$ 3,614,144.12 | 1.30 | \$ 4,698,387.36 |
| Dispenser | | | | |
| Number of Dispensers | 2.00 | \$ 289,409.35 | 1.30 | \$ 376,232.15 |
| Electrical | | | | |
| Electrical Voltage Supplied (Volts) | 480.00 | \$ 69,712.93 | 2.24 | \$ 156,156.96 |
| Cascade | | | | |
| Capacity (kg of Hydrogen) | 321.65 | \$ 766,025.22 | 1.30 | \$ 995,832.78 |
| Low-Pressure Storage for Hourly Surge | | | | |
| Number of Units | 3.00 | | | |
| Unit Size (kg of Hydrogen) | 123.61 | \$ 613,387.69 | 1.30 | \$ 797,404.00 |
| Remainder of Station | | | | |
| Overall Control and Safety Equipment | | \$ 147,960.00 | 1.00 | \$ 147,960.00 |
| Total Initial Capital Investment | | | | \$ 7,616,837.84 |

TABLE D.6: Initial capital investment overview for a medium refuelling station, with hydrogen supplied by a tube-trailer at 350 bar, and a demand of 700 kg of hydrogen per day.

| Component | Value | Uninstalled costs | Installation factor | Installed cost |
|-----------------------------------------|--------|-------------------|---------------------|------------------------|
| Refrigeration Equipment | | | | |
| Number of condensing/HX units | 4.00 | | | |
| Refrigeration capacity per unit (tons) | 3.39 | \$ 97,705.72 | 2 | \$ 444,864.58 |
| Number of Heat Exchanger | 2.00 | \$ 124,726.57 | 2 | |
| Compressor | | | | |
| Number of Compressors | 3.00 | | | |
| Main Compressor Power per unit (kW) | 64.33 | \$ 2,562,677.70 | 1.3 | \$ 3,331,481.01 |
| Dispenser | | | | |
| Number of Dispensers | 2.00 | \$ 289,409.35 | 1.3 | \$ 376,232.15 |
| Electrical | | | | |
| Electrical Voltage Supplied (Volts) | 480.00 | \$ 57,879.06 | 2.24 | \$ 129,649.09 |
| Cascade | | | | |
| Capacity (kg of Hydrogen) | 241.24 | \$ 574,518.91 | 1.3 | \$ 746,874.59 |
| Remainder of Station | | | | |
| Overall Control and Safety Equipment | | | 1 | \$ 147,960.00 |
| Total Initial Capital Investment | | | | \$ 5,177,061.42 |

TABLE D.7: Total operational costs for three different sizes of hydrogen refuelling stations.

| Components | Unit | Pipeline | | | Truck | | |
|---------------------------------------------|----------------|----------------------|----------------------|----------------------|----------------------|----------------------|------------|
| | | Small HRS | Medium HRS | Large HRS | Medium HRS | Medium HRS | Medium HRS |
| Labour | | | | | | | |
| Labor required | hrs/year | 2337 | 2779 | 3038 | 2779 | 2779 | |
| Total labour cost | \$/year | \$ 58,887.31 | \$ 70,029.21 | \$ 76,560.49 | \$ 70,029.21 | \$ 70,029.21 | |
| Utility Costs | | | | | | | |
| Main Compressors Electricity Consumption | kWh | 450795 | 898735 | 1265436 | 286809 | 286809 | |
| Booster Compressors Electricity Consumption | kWh | 0 | 0 | 0 | 0 | 0 | |
| Refrigeration Electricity Consumption | kWh | 55157 | 110315 | 138612 | 110315 | 110315 | |
| Total Electricity Consumption | kWh | 505952 | 1009050 | 1404047 | 397123 | 397123 | |
| Total Electricity Cost | \$/year | \$ 123,033.47 | \$ 245,372.92 | \$ 341,425.37 | \$ 70,510.04 | \$ 70,510.04 | |
| Fixed Costs | | | | | | | |
| Insurance | - | \$ 48,446.15 | \$ 78,385.88 | \$ 93,687.11 | \$ 63,677.86 | \$ 63,677.86 | |
| Property Taxes | - | \$ 48,446.15 | \$ 78,385.88 | \$ 93,687.11 | \$ 63,677.86 | \$ 63,677.86 | |
| Licensing and permits | - | \$ 4,844.61 | \$ 7,838.59 | \$ 9,368.71 | \$ 6,367.79 | \$ 6,367.79 | |
| Operating, Maintenance and Repairs | - | \$ 116,432.24 | \$ 187,686.84 | \$ 221,568.64 | \$ 156,163.69 | \$ 156,163.69 | |
| Overhead and G&A | - | \$ 11,777.46 | \$ 14,005.84 | \$ 15,312.10 | \$ 14,005.84 | \$ 14,005.84 | |
| Other Fixed Operating Costs | | | | | | | |
| Refuelling station area | m ² | 198 | 396 | 402 | 601 | 601 | |
| Rent and H2 area based on site plan | | \$ 13,881.57 | \$ 27,763.14 | \$ 28,122.34 | \$ 42,067.24 | \$ 42,067.24 | |
| Total O&M costs | \$/year | \$ 425,748.96 | \$ 709,468.30 | \$ 879,731.86 | \$ 879,731.86 | \$ 486,499.51 | |

TABLE D.8: Other capital costs for a hydrogen refuelling station, as percentage of the initial capital investment costs.

| Other Capital Costs | Value | | | Truck | | |
|-------------------------------------------------------------|-----------|----------------------|------------------------|------------------------|------------------------|-------|
| | Small HRS | Medium HRS | Large HRS | Small HRS | Medium HRS | Truck |
| Site Preparation (% of Initial Capital Investment) | 5% | \$ 196,935.55 | \$ 318,641.79 | \$ 380,841.89 | \$ 258,853.07 | |
| Engineering & Design (% of Initial Capital Investment) | 10% | \$ 393,871.10 | \$ 637,283.58 | \$ 761,683.78 | \$ 517,706.14 | |
| Project Contingency (% of Initial Capital Investment) | 5% | \$ 196,935.55 | \$ 318,641.79 | \$ 380,841.89 | \$ 258,853.07 | |
| One-time Licensing Fees (% of Initial Capital Investment) | 0% | \$ - | \$ - | \$ - | \$ - | |
| Up-Front Permitting Costs (% of Initial Capital Investment) | 3% | \$ 118,161.33 | \$ 191,185.07 | \$ 228,505.14 | \$ 155,311.84 | |
| Total Other Capital Costs | | \$ 905,903.53 | \$ 1,465,752.23 | \$ 1,751,872.70 | \$ 1,190,724.13 | |

TABLE D.9: Assumptions for operational and maintenance costs for a hydrogen refuelling station.

| Constants | Unit | Value |
|------------------------------------------------------|--------------------------------------|-------|
| Operating Labor cost | \$/man-hour | 25.40 |
| Electricity Price | \$/kWh | 0.25 |
| Insurance | % of total capital investment | 1.0 |
| Property Taxes | % of total capital investment | 1.0 |
| Licensing and Permits | % of total capital investment | 0.1 |
| Operating, Maintenance and Repairs for Compressors | % of compressor installed capital | 4.0 |
| Operating, Maintenance and Repairs for Refrigeration | % of refrigeration installed capital | 2.0 |
| Operating, Maintenance and Repairs for Storage | % of storage installed capital | 1.0 |
| Operating, Maintenance and Repairs for Electrical | % of electrical installed capital | 1.0 |
| Operating, Maintenance and Repairs for Dispensers | % of dispenser installed capital | 1.0 |
| Operating, Maintenance and Repairs for Remainder | % of remainder installed capital | 1.0 |
| Overhead and G&A | % of total labour cost | 20.0 |
| Rent | \$/m ² per month | 3.23 |
| GDP Deflator Price Index | - | 1.36 |

TABLE D.10: HRSAM model assumptions.

| Assumptions | Value | Unit |
|----------------------------------|--------------|-------------|
| Refrigeration Equipment Lifetime | 15 | years |
| Compressors Lifetime | 10 | years |
| Storage Lifetime | 30 | years |
| Electrical Lifetime | 30 | years |
| Dispenser Lifetime | 10 | years |
| Remainder of Station Lifetime | 30 | years |
| Inflation Rate | 2 | % |
| State Taxes | 6 | % |
| Federal Taxes | 35 | % |

Appendix E

Final Hydrogen Cost Calculations

TABLE E.1: Hydrogen production price assuming electricity price of 5c/kWh and a natural gas price of \$15.00/GJ. The fixed PSA costs include the capital cost for a 10 year lifetime and the maintenance cost.

| H ₂ production | Electrolysis | Coal with CCS | SMR with CCS | SMR without CCS |
|-------------------------------------|-----------------|-----------------|-----------------|-----------------|
| PSA compressor | \$ 0.27 | \$ 0.27 | \$ 0.27 | \$ 0.27 |
| PSA fixed | \$ 0.80 | \$ 0.80 | \$ 0.80 | \$ 0.80 |
| PSA feedstock | \$ 5.90 | \$ 2.14 | \$ 3.19 | \$ 1.72 |
| CS&D (20-1000 bar) | \$ 9.88 | \$ 9.88 | \$ 9.88 | \$ 9.88 |
| Total [A\$/kg H₂] | \$ 16.95 | \$ 13.19 | \$ 14.24 | \$ 12.77 |

TABLE E.2: Hydrogen production price assuming electricity price of 25c/kWh and a natural gas price of \$9.50/GJ. The fixed PSA costs include the capital cost for a 10 year lifetime and the maintenance cost.

| H ₂ production | Electrolysis | Coal with CCS | SMR with CCS | SMR without CCS |
|-------------------------------------|-----------------|-----------------|-----------------|-----------------|
| PSA compressor | \$ 1.36 | \$ 1.36 | \$ 1.36 | \$ 1.36 |
| PSA fixed | \$ 0.80 | \$ 0.80 | \$ 0.80 | \$ 0.80 |
| PSA feedstock | \$ 3.74 | \$ 1.36 | \$ 2.02 | \$ 1.09 |
| CS&D (20-1000 bar) | \$ 10.88 | \$ 10.88 | \$ 10.88 | \$ 10.88 |
| Total [A\$/kg H₂] | \$ 16.88 | \$ 14.50 | \$ 15.16 | \$ 14.23 |

TABLE E.3: Final hydrogen price for on-site electrolysis, assuming an electricity price of 5c/kWh.

| | PEM | | AE | |
|----------------------------------------|----------|----------|----------|----------|
| | 2018 | 2025 | 2018 | 2025 |
| Electrolysis operational cost | \$ 2.70 | \$ 2.25 | \$ 2.90 | \$ 2.45 |
| Electrolyser fixed capital cost | \$ 4.19 | \$ 0.99 | \$ 2.36 | \$ 1.14 |
| CS&D (20-1000 bar) | \$ 9.88 | \$ 9.88 | \$ 9.88 | \$ 9.88 |
| Total [A\$/kg H₂] | \$ 16.77 | \$ 13.12 | \$ 15.14 | \$ 13.47 |

TABLE E.4: Final hydrogen price for on-site electrolysis, assuming an electricity price of 25c/kWh.

| | PEM | | AE | |
|----------------------------------------|----------|----------|----------|----------|
| | 2018 | 2025 | 2018 | 2025 |
| Electrolysis operational cost | \$ 13.50 | \$ 11.25 | \$ 14.50 | \$ 12.25 |
| Electrolyser fixed capital cost | \$ 4.19 | \$ 0.99 | \$ 2.36 | \$ 1.14 |
| CS&D (20-1000 bar) | \$ 10.88 | \$ 10.88 | \$ 10.88 | \$ 10.88 |
| Total [A\$/kg H₂] | \$ 28.57 | \$ 23.12 | \$ 27.74 | \$ 24.27 |

TABLE E.5: Final hydrogen price for truck transported hydrogen, assuming an electricity price of 5c/kWh and a distance travelled of 200 km.

| | Electrolysis | Coal + CCS | SMR + CCS | Coal without CCS |
|------------------------------------------|--------------|------------|-----------|------------------|
| Hydrogen production cost | \$ 6.60 | \$ 3.14 | \$ 2.77 | \$ 1.84 |
| Compression truck to 35 - 350 bar | \$ 0.42 | \$ 0.42 | \$ 0.42 | \$ 0.42 |
| Truck transport (200 km) | \$ 0.75 | \$ 0.75 | \$ 0.75 | \$ 0.75 |
| CS&D (350-1000 bar) | \$ 8.12 | \$ 8.12 | \$ 8.12 | \$ 8.12 |
| Total [A\$/kg H₂] | \$ 15.89 | \$ 12.43 | \$ 12.06 | \$ 11.13 |

TABLE E.6: Final hydrogen price for truck transported hydrogen, assuming an electricity price of 25c/kWh and a distance travelled of 200 km.

| | Electrolysis | Coal + CCS | SMR + CCS | Coal without CCS |
|------------------------------------------|--------------|------------|-----------|------------------|
| Hydrogen production cost | \$ 6.60 | \$ 3.14 | \$ 2.77 | \$ 1.84 |
| Compression truck to 35 - 350 bar | \$ 0.42 | \$ 0.42 | \$ 0.42 | \$ 0.42 |
| Truck transport (200 km) | \$ 0.75 | \$ 0.75 | \$ 0.75 | \$ 0.75 |
| CS&D (350-1000 bar) | \$ 8.52 | \$ 8.52 | \$ 8.52 | \$ 8.52 |
| Total [A\$/kg H₂] | \$ 16.29 | \$ 12.83 | \$ 12.46 | \$ 11.53 |

TABLE E.7: Final hydrogen price for truck transported hydrogen, assuming an electricity price of 5c/kWh and a distance travelled of 455 km.

| | Electrolysis | Coal + CCS | SMR + CCS | Coal without CCS |
|------------------------------------------|--------------|------------|-----------|------------------|
| Hydrogen production cost | \$ 6.60 | \$ 3.14 | \$ 2.77 | \$ 1.84 |
| Compression truck to 35 - 350 bar | \$ 0.42 | \$ 0.42 | \$ 0.42 | \$ 0.42 |
| Truck transport (455 km) | \$ 1.70 | \$ 1.70 | \$ 1.70 | \$ 1.70 |
| CS&D (350-1000 bar) | \$ 8.12 | \$ 8.12 | \$ 8.12 | \$ 8.12 |
| Total [A\$/kg H₂] | \$ 16.84 | \$ 13.38 | \$ 13.01 | \$ 12.08 |

TABLE E.8: Final hydrogen price for truck transported hydrogen, assuming an electricity price of 25c/kWh and a distance travelled of 455 km.

| | Electrolysis | Coal + CCS | SMR + CCS | Coal without CCS |
|-------------------------------------|-----------------|-----------------|-----------------|------------------|
| Hydrogen production cost | \$ 6.60 | \$ 3.14 | \$ 2.77 | \$ 1.84 |
| Compression truck to 35 - 350 bar | \$ 0.42 | \$ 0.42 | \$ 0.42 | \$ 0.42 |
| Truck transport (455 km) | \$ 1.70 | \$ 1.70 | \$ 1.70 | \$ 1.70 |
| CS&D (350-1000 bar) | \$ 8.52 | \$ 8.52 | \$ 8.52 | \$ 8.52 |
| Total [A\$/kg H₂] | \$ 17.24 | \$ 13.78 | \$ 13.41 | \$ 12.48 |

TABLE E.9: Final hydrogen price for truck transported hydrogen, assuming an electricity price of 5c/kWh and a distance travelled of 1000 km.

| | Electrolysis | Coal + CCS | SMR + CCS | Coal without CCS |
|-------------------------------------|-----------------|-----------------|-----------------|------------------|
| Hydrogen production cost | \$ 6.60 | \$ 3.14 | \$ 2.77 | \$ 1.84 |
| Compression truck to 35 - 350 bar | \$ 0.42 | \$ 0.42 | \$ 0.42 | \$ 0.42 |
| Truck transport (455 km) | \$ 3.73 | \$ 3.73 | \$ 3.73 | \$ 3.73 |
| CS&D (350-1000 bar) | \$ 8.12 | \$ 8.12 | \$ 8.12 | \$ 8.12 |
| Total [A\$/kg H₂] | \$ 18.87 | \$ 15.41 | \$ 15.04 | \$ 14.11 |

TABLE E.10: Final hydrogen price for truck transported hydrogen, assuming an electricity price of 25c/kWh and a distance travelled of 1000 km.

| | Electrolysis | Coal + CCS | SMR + CCS | Coal without CCS |
|-------------------------------------|-----------------|-----------------|-----------------|------------------|
| Hydrogen production cost | \$ 6.60 | \$ 3.14 | \$ 2.77 | \$ 1.84 |
| Compression truck to 35 - 350 bar | \$ 0.42 | \$ 0.42 | \$ 0.42 | \$ 0.42 |
| Truck transport (455 km) | \$ 3.73 | \$ 3.73 | \$ 3.73 | \$ 3.73 |
| CS&D (350-1000 bar) | \$ 8.52 | \$ 8.52 | \$ 8.52 | \$ 8.52 |
| Total [A\$/kg H₂] | \$ 19.27 | \$ 15.81 | \$ 15.44 | \$ 14.51 |

Bibliography

- [1] COAG Energy Council Hydrogen Working Group. Australia's National Hydrogen Strategy. Technical report, COAG Energy Council Hydrogen Working Group, 2019.
- [2] Adeel Ahmed, Abul Quasem Al-Amin, Angelina F. Ambrose, and R. Saidur. Hydrogen fuel and transport system: A sustainable and environmental future. *International Journal of Hydrogen Energy*, 41(3):1369–1380, 2016. ISSN 03603199. doi: 10.1016/j.ijhydene.2015.11.084. URL <http://dx.doi.org/10.1016/j.ijhydene.2015.11.084>.
- [3] Tatiane da Silva Veras, Thiago Simonato Mozer, Danielle da Costa Rubim Messeder dos Santos, and Aldara da Silva César. Hydrogen: Trends, production and characterization of the main process worldwide. *International Journal of Hydrogen Energy*, 42(4):2018–2033, 2017. ISSN 03603199. doi: 10.1016/j.ijhydene.2016.08.219.
- [4] Oliver Ehret and Klaus Bonhoff. Hydrogen as a fuel and energy storage: Success factors for the German energiewende. *International Journal of Hydrogen Energy*, 40(15):5526–5533, 2015. ISSN 03603199. doi: 10.1016/j.ijhydene.2015.01.176. URL <http://dx.doi.org/10.1016/j.ijhydene.2015.01.176>.
- [5] M. Melaina, B. Bush, M. Muratori, J. Zuboy, and S. Ellis. National Hydrogen Scenarios: How Many Stations, Where, and When? Technical Report October, National Renewable Energy Laboratory, 2017. URL http://h2usa.org/sites/default/files/H2USA_LRWG_NationalScenarios2017.pdf.
- [6] Sean B. Walker, Ushnik Mukherjee, Michael Fowler, and Ali Elkamel. Benchmarking and selection of Power-to-Gas utilizing electrolytic hydrogen as an energy storage alternative. *International Journal of Hydrogen Energy*, 41(19):7717–7731, 2016. ISSN 03603199. doi: 10.1016/j.ijhydene.2015.09.008. URL <http://dx.doi.org/10.1016/j.ijhydene.2015.09.008>.
- [7] Sean B. Walker, Daniel van Lanen, Ushnik Mukherjee, and Michael Fowler. Greenhouse gas emissions reductions from applications of Power-to-Gas in power generation. *Sustainable Energy Technologies and Assessments*, 20:25–32, 2017. ISSN 22131388. doi: 10.1016/j.seta.2017.02.003. URL <http://dx.doi.org/10.1016/j.seta.2017.02.003>.

- [8] Geoscience Australia. Australian energy resource assessment, 2019. URL <https://aera.ga.gov.au/#!/>. Accessed on: 30-03-2020.
- [9] Clean Energy Council. Renewable energy target, 2018. URL <https://www.cleanenergycouncil.org.au/advocacy-initiatives/renewable-energy-target>. Accessed on: 01-04-2020.
- [10] Gordon Weiss, Marina Lou, Miheka Patel, Helen Wetherell, and Peter Holt. Renewable gas for the future. Technical Report June, Energetics, 2019.
- [11] Clean Energy Council. Clean Energy Australia REPORT 2019. Technical report, 2019. URL <https://assets.cleanenergycouncil.org.au/documents/resources/reports/clean-energy-australia/clean-energy-australia-report-2019.pdf>.
- [12] Australian Energy Statistics. Australian Energy Update 2019. Technical Report September, Department of the Environment and Energy, Canberra, 2019.
- [13] Jemena. Greening Australia’s Gas Network, 2020.
- [14] Australian Renewable Energy Agency. About arena, 2020. URL <https://arena.gov.au/about/>. Accessed on: 01-04-2020.
- [15] Australian Renewable Energy Agency. Jemena power to gas demonstration, 2020. URL <https://arena.gov.au/projects/jemena-power-to-gas-demonstration/>. Accessed on: 01-04-2020.
- [16] Joan Ogden, Christopher Yang, Michael Nicholas, and Lew Fulton. Hydrogen Transition. Technical report, 2014.
- [17] Matteo Muratori, Brian Bush, Chad Hunter, and Marc W. Melaina. Modeling hydrogen refueling infrastructure to support passenger vehicles. *Energies*, 11(5), 2018. ISSN 19961073. doi: 10.3390/en11051171.
- [18] Brian Bush, Matteo Muratori, Chad Hunter, Jarett Zuboy, Marc Melaina, Brian Bush, Matteo Muratori, Chad Hunter, Jarett Zuboy, and Marc Melaina. Scenario Evaluation and Regionalization Analysis (SERA) Model: Demand Side and Refueling Infrastructure Buildout. Technical Report June, 2019.
- [19] US Department of Energy. Hydrogen fueling station locations, 2020. URL https://afdc.energy.gov/fuels/hydrogen_locations.html#/find/nearest?fuel=HY&country=US. Accessed on: 01-05-2020.
- [20] K. Reddi, M. Mintz, A. Elgowainy, and E. Sutherland. Building a hydrogen infrastructure in the United States. In *Compendium of Hydrogen Energy*, chapter 13, pages 293–319. Elsevier Ltd., 1 edition, 2016. ISBN 9781782423645. doi: 10.1016/b978-1-78242-364-5.00013-0. URL <http://dx.doi.org/10.1016/B978-1-78242-364-5.00013-0>.
- [21] Sofoklis S. Makridis. Hydrogen storage and compression. *Methane and Hydrogen for Energy Storage*, (June):1–28, 2016. doi: 10.1049/pbpo101e{\-}ch1.

- [22] R. Gerboni. Introduction to hydrogen transportation. In *Compendium of Hydrogen Energy*, chapter 11, pages 283–299. Elsevier Ltd., 2016. ISBN 9781782423621. doi: 10.1016/b978-1-78242-362-1.00011-0.
- [23] Fan Zhang, Pengcheng Zhao, Meng Niu, and Jon Maddy. The survey of key technologies in hydrogen energy storage. *International Journal of Hydrogen Energy*, 41(33):14535–14552, 2016. ISSN 03603199. doi: 10.1016/j.ijhydene.2016.05.293. URL <http://dx.doi.org/10.1016/j.ijhydene.2016.05.293>.
- [24] Zine labidine Messaoudani, Fotis Rigas, Mahar Diana Binti Hamid, and Che Rosmani Che Hassan. Hazards, safety and knowledge gaps on hydrogen transmission via natural gas grid: A critical review. *International Journal of Hydrogen Energy*, 41(39):17511–17525, 2016. ISSN 03603199. doi: 10.1016/j.ijhydene.2016.07.171. URL <http://dx.doi.org/10.1016/j.ijhydene.2016.07.171>.
- [25] Neil Smith and Mark Coates. Identifying the commercial, technical and regulatory issues for injecting renewable gas in Australian distribution gas networks. Technical Report July, Energy Networks Australia, 2017.
- [26] M.W Melaina, O. Antonia, and M. Penev. Blending Hydrogen into Natural Gas Pipeline Networks: A Review of Key Issues. Technical Report March, NREL, 2013.
- [27] Dries Haeseldonckx and D William. The use of the natural-gas pipeline infrastructure for hydrogen transport in a changing market structure. 32:1381–1386, 2007. doi: 10.1016/j.ijhydene.2006.10.018.
- [28] Harmen de Vries, Anatoli V. Mokhov, and Howard B. Levinsky. The impact of natural gas/hydrogen mixtures on the performance of end-use equipment: Interchangeability analysis for domestic appliances. *Applied Energy*, 208(August): 1007–1019, 2017. ISSN 03062619. doi: 10.1016/j.apenergy.2017.09.049. URL <https://doi.org/10.1016/j.apenergy.2017.09.049>.
- [29] Young Do Jo and Bum Jong Ahn. Analysis of hazard area associated with hydrogen gas transmission pipelines. *International Journal of Hydrogen Energy*, 31(14): 2122–2130, 2006. ISSN 03603199. doi: 10.1016/j.ijhydene.2006.01.008.
- [30] S Bruce, M Temminghoff, J Hayward, E Schmidt, D Palfreyman, and P Hartley. National Hydrogen Roadmap. Technical report, CSIRO, 2019.
- [31] GPA Engineering. Hydrogen in the gas distribution networks. Technical report, 2019.
- [32] Maha Rhandi, Marine Trégaro, Florence Druart, Jonathan Deseure, and Marian Chatenet. Electrochemical hydrogen compression and purification versus competing technologies: Part I. Pros and cons. *Chinese Journal of Catalysis*, 41(5): 756–769, 2020. ISSN 18722067. doi: 10.1016/S1872-2067(19)63404-2.
- [33] Brian M. Besancon, Vladimir Hasanov, Raphaëlle Imbault-Lastapis, Robert Benesch, Maria Barrio, and Mona J. Mølnvik. Hydrogen quality from decarbonized

- fossil fuels to fuel cells. *International Journal of Hydrogen Energy*, 34(5):2350–2360, 2009. ISSN 03603199. doi: 10.1016/j.ijhydene.2008.12.071.
- [34] Xuan Cheng, Zheng Shi, Nancy Glass, Lu Zhang, Jiujun Zhang, Datong Song, Zhong Sheng Liu, Haijiang Wang, and Jun Shen. A review of PEM hydrogen fuel cell contamination: Impacts, mechanisms, and mitigation. *Journal of Power Sources*, 165(2):739–756, 2007. ISSN 03787753. doi: 10.1016/j.jpowsour.2006.12.012.
- [35] Arul Murugan and Andrew S. Brown. Review of purity analysis methods for performing quality assurance of fuel cell hydrogen. *International Journal of Hydrogen Energy*, 40(11):4219–4233, 2015. ISSN 03603199. doi: 10.1016/j.ijhydene.2015.01.041. URL <http://dx.doi.org/10.1016/j.ijhydene.2015.01.041>.
- [36] Gabriel Bernardo, Tiago Araújo, Telmo Silva Lopes, José Sousa, and Adélio Mendes. Recent advances in membrane technologies for hydrogen purification. *International journal of hydrogen energy*, 5, 2019. doi: 10.1016/j.ijhydene.2019.06.162.
- [37] André B de Haan and Hans Bosch. Absorption and stripping. In *Industrial Separation Processes*. 2013. doi: 10.1515/9783110306729.53.
- [38] Werner Liemberger, Markus Groß, Martin Miltner, and Michael Harasek. Experimental analysis of membrane and pressure swing adsorption (PSA) for the hydrogen separation from natural gas. *Journal of Cleaner Production*, 167:896–907, 2017. ISSN 0959-6526. doi: 10.1016/j.jclepro.2017.08.012. URL <http://dx.doi.org/10.1016/j.jclepro.2017.08.012>.
- [39] Sunghoon Kim, Daeho Ko, Sung Wook Row, and Jiyong Kim. Techno-economic evaluation of hybrid systems of pressure swing adsorption and membrane processes for coalbed methane separation. *Chemical Engineering Research and Design*, 115: 230–240, 2016. ISSN 02638762. doi: 10.1016/j.cherd.2016.09.036.
- [40] André de Haan and Hans Bosch. Adsorption and ion exchange. In *Industrial Separation Processes*, chapter 6, pages 143 – 176. De Gruyter, 2013.
- [41] Douglas M Ruthven, Shamsuzzaman Farooq, and Kent S Knaebel. *Pressure Swing Adsorption*. 1994. ISBN 1560815175.
- [42] Dragan D Nikolic and Eustathios S Kikkinides. Modelling and optimization of hybrid PSA/membrane separation processes. pages 283–305, 2015. doi: 10.1007/s10450-015-9670-z.
- [43] Baojun Li, Gaohong He, Xiaobin Jiang, Yan Dai, and Xuehua Ruan. Pressure swing adsorption/membrane hybrid processes for hydrogen purification with a high recovery. *Frontiers of Chemical Science and Engineering*, 10(2):255–264, 2016. ISSN 20950187. doi: 10.1007/s11705-016-1567-1.
- [44] Isabel A.A.C. Esteves and José P.B. Mota. Gas separation by a novel hybrid membrane/pressure swing adsorption process. *Industrial and Engineering Chemistry Research*, 46(17):5723–5733, 2007. ISSN 08885885. doi: 10.1021/ie070139j.

- [45] Yan Sun, Congmin Liu, Wei Su, Yaping Zhou, and Li Zhou. Principles of methane adsorption and natural gas storage. *Adsorption*, 15(2):133–137, 2009. ISSN 09295607. doi: 10.1007/s10450-009-9157-x.
- [46] Brian Joseph Maring and Paul A Webley. A new simplified pressure/vacuum swing adsorption model for rapid adsorbent screening for CO₂ capture applications. *International Journal of Greenhouse Gas Control*, 15:16–31, 2013. ISSN 1750-5836. doi: 10.1016/j.ijggc.2013.01.009. URL <http://dx.doi.org/10.1016/j.ijggc.2013.01.009>.
- [47] Byoung Uk Choi, Dae Ki Choi, Young Whan Lee, Byung Kwon Lee, and Sung Hyun Kim. Adsorption equilibria of methane, ethane, ethylene, nitrogen, and hydrogen onto activated carbon. *Journal of Chemical and Engineering Data*, 48(3):603–607, 2003. ISSN 00219568. doi: 10.1021/je020161d.
- [48] P. González-García. Activated carbon from lignocellulosics precursors: A review of the synthesis methods, characterization techniques and applications. *Renewable and Sustainable Energy Reviews*, 82(August 2017):1393–1414, 2018. ISSN 18790690. doi: 10.1016/j.rser.2017.04.117.
- [49] Arash Arami-Niya, Wan Mohd Ashri Wan Daud, Farouq S. Mjalli, Faisal Abnisa, and Mohammad Saleh Shafeeyan. Production of microporous palm shell based activated carbon for methane adsorption: Modeling and optimization using response surface methodology. *Chemical Engineering Research and Design*, 90(6):776–784, 2012. ISSN 02638762. doi: 10.1016/j.cherd.2011.10.001.
- [50] Marco Tagliabue, David Farrusseng, Susana Valencia, Sonia Aguado, Ugo Ravon, Caterina Rizzo, Avelino Corma, and Claude Mirodatos. Natural gas treating by selective adsorption: Material science and chemical engineering interplay. *Chemical Engineering Journal*, 155(3):553–566, 2009. ISSN 13858947. doi: 10.1016/j.cej.2009.09.010.
- [51] Mark W. Ackley, Salil U. Rege, and Himanshu Saxena. Application of natural zeolites in the purification and separation of gases. *Microporous and Mesoporous Materials*, 61(1-3):25–42, 2003. ISSN 13871811. doi: 10.1016/S1387-1811(03)00353-6.
- [52] Yu Wang and M. Douglas LeVan. Adsorption equilibrium of carbon dioxide and water vapor on zeolites 5a and 13X and silica gel: Pure components. *Journal of Chemical and Engineering Data*, 54(10):2839–2844, 2009. ISSN 00219568. doi: 10.1021/je800900a.
- [53] Ralph T Yang. *Gas Separation by Adsorption Processes*. 1987. ISBN 0409900044.
- [54] C W Skarstrom. Method and apparatus for fractionating gaseous mixtures by adsorption, 1960. URL <https://patentimages.storage.googleapis.com/6d/25/43/2bc6fbdf971e28/US2944627.pdf>.
- [55] Douglas M. Ruthven. *Principles of Adsorption and Adsorption Processes*. 1984. ISBN 0471866067.

- [56] Carlos A. Grande. Advances in Pressure Swing Adsorption for Gas Separation. *ISRN Chemical Engineering*, 2012:1–13, 2012. ISSN 2090-861X. doi: 10.5402/2012/982934.
- [57] M. Chlendi and D. Tondeur. Dynamic behaviour of layered columns in pressure swing adsorption. *Gas Separation and Purification*, 9(4):231–242, 1995. ISSN 09504214. doi: 10.1016/0950-4214(95)00005-V.
- [58] Jong Ho Park, Jong Nam Kim, Soon Haeng Cho, Jong Duk Kim, and Ralph T. Yang. Adsorber dynamics and optimal design of layered beds for multicomponent gas adsorption. *Chemical Engineering Science*, 53(23):3951–3963, 1998. ISSN 00092509. doi: 10.1016/S0009-2509(98)00196-1.
- [59] Gang Li, Penny Xiao, Dong Xu, and Paul A. Webley. Dual mode roll-up effect in multicomponent non-isothermal adsorption processes with multilayered bed packing. *Chemical Engineering Science*, 66(9):1825–1834, 2011. ISSN 00092509. doi: 10.1016/j.ces.2011.01.023. URL <http://dx.doi.org/10.1016/j.ces.2011.01.023>.
- [60] Jocelyn Bonjour, Jean Bertrand Chalfen, and Francis Meunier. Temperature swing adsorption process with indirect cooling and heating. *Industrial and Engineering Chemistry Research*, 41(23):5802–5811, 2002. ISSN 08885885. doi: 10.1021/ie011011j.
- [61] Paul A. Webley. Adsorption technology for CO₂ separation and capture: A perspective. *Adsorption*, 20(2-3):225–231, 2014. ISSN 09295607. doi: 10.1007/s10450-014-9603-2.
- [62] Zhen Liu, Carlos A. Grande, Ping Li, Jianguo Yu, and Alirio E. Rodrigues. Multi-bed vacuum pressure swing adsorption for carbon dioxide capture from flue gas. *Separation and Purification Technology*, 81(3):307–317, 2011. ISSN 13835866. doi: 10.1016/j.seppur.2011.07.037.
- [63] Jun Zhang, Paul A. Webley, and Penny Xiao. Effect of process parameters on power requirements of vacuum swing adsorption technology for CO₂ capture from flue gas. *Energy Conversion and Management*, 49(2):346–356, 2008. ISSN 01968904. doi: 10.1016/j.enconman.2007.06.007.
- [64] Filipe V S Lopes, Carlos A Grande, and Alirio E Rodrigues. Fast-cycling VPSA for hydrogen purification. *Fuel*, 93:510–523, 2012. ISSN 0016-2361. doi: 10.1016/j.fuel.2011.07.005. URL <http://dx.doi.org/10.1016/j.fuel.2011.07.005>.
- [65] Shivaji Sircar. Pressure Swing Adsorption. pages 1389–1392, 2002. doi: 10.1021/ie0109758.
- [66] Yechun Zhang, Thomas L.H. Saleman, Gang (Kevin) Li, Gongkui Xiao, Brent R. Young, and Eric F. May. Non-isothermal numerical simulations of dual reflux pressure swing adsorption cycles for separating N₂ + CH₄. *Chemical Engineering Journal*, 292:366–381, 2016. ISSN 13858947. doi: 10.1016/j.cej.2016.02.018. URL <http://dx.doi.org/10.1016/j.cej.2016.02.018>.

- [67] Tushar S. Bhatt, Giuseppe Storti, and Renato Rota. Detailed simulation of dual-reflux pressure swing adsorption process. *Chemical Engineering Science*, 122:34–52, 2015. ISSN 00092509. doi: 10.1016/j.ces.2014.09.013. URL <http://dx.doi.org/10.1016/j.ces.2014.09.013>.
- [68] David T. Kearns and Paul A. Webley. Modelling and evaluation of dual-reflux pressure swing adsorption cycles: Part I. Mathematical models. *Chemical Engineering Science*, 61(22):7223–7233, 2006. ISSN 00092509. doi: 10.1016/j.ces.2006.07.040.
- [69] S. Sircar and T. C. Golden. Purification of hydrogen by pressure swing adsorption. *Separation Science and Technology*, 35(5):667–687, 2000. ISSN 01496395. doi: 10.1081/SS-100100183.
- [70] Niklas Hedin, Linnéa Andersson, Lennart Bergström, and Jinyue Yan. Adsorbents for the post-combustion capture of CO₂ using rapid temperature swing or vacuum swing adsorption. *Applied Energy*, 104:418–433, 2013. ISSN 03062619. doi: 10.1016/j.apenergy.2012.11.034.
- [71] Narges Bagheri and Jalal Abedi. Adsorption of methane on corn cobs based activated carbon. *Chemical Engineering Research and Design*, 89(10):2038–2043, 2011. ISSN 02638762. doi: 10.1016/j.cherd.2011.02.002.
- [72] Simone Cavenati, Carlos A. Grande, and Alírio E. Rodrigues. Upgrade of methane from landfill gas by pressure swing adsorption. *Energy and Fuels*, 19(6):2545–2555, 2005. ISSN 08870624. doi: 10.1021/ef050072h.
- [73] David Grainger, Jon Arvid Lie, and May-britt Hägg. Hydrogen recovery in a combined natural gas-hydrogen distribution network using carbon molecular sieve membranes 550–750 °C. (x):1–5, 2006.
- [74] Shahrouz Nayeboossadri, John D. Speight, and David Book. Hydrogen separation from blended natural gas and hydrogen by Pd-based membranes. *International Journal of Hydrogen Energy*, 44(55):29092–29099, 2019. ISSN 03603199. doi: 10.1016/j.ijhydene.2019.03.044. URL <https://doi.org/10.1016/j.ijhydene.2019.03.044>.
- [75] Maria Nordio, Solomon Assefa, Martin Van Sint, Viviente Sole, Fausto Gallucci, and D Alfredo Pacheco. ScienceDirect Techno-economic evaluation on a hybrid technology for low hydrogen concentration separation and purification from natural gas grid. (xxxx), 2020. doi: 10.1016/j.ijhydene.2020.05.009.
- [76] David Grainger and May Britt Hägg. The recovery by carbon molecular sieve membranes of hydrogen transmitted in natural gas networks. *International Journal of Hydrogen Energy*, 33(9):2379–2388, 2008. ISSN 03603199. doi: 10.1016/j.ijhydene.2008.03.001.
- [77] Werner Liemberger, Markus Groß, Martin Miltner, Helga Prazak-Reisinger, and Michael Harasek. Extraction of green hydrogen at fuel cell quality from mixtures with natural gas. *Chemical Engineering Transactions*, 52:427–432, 2016. ISSN 22839216. doi: 10.3303/CET1652072.

- [78] Werner Liemberger, Daniel Halmschlager, Martin Miltner, and Michael Harasek. Efficient extraction of hydrogen transported as co-stream in the natural gas grid – The importance of process design. *Applied Energy*, 233-234(November 2017): 747–763, 2019. ISSN 03062619. doi: 10.1016/j.apenergy.2018.10.047.
- [79] Richard S Todd and Paul A Webley. Limitations of the LDF/equimolar counterdiffusion assumption for mass transport within porous adsorbent pellets. 57: 4227–4242, 2002.
- [80] S. Sircar and J. R. Hufton. Why does the linear driving force model for adsorption kinetics work? *Adsorption*, 6(2):137–147, 2000. ISSN 09295607. doi: 10.1023/A:1008965317983.
- [81] E. Glueckauf and JI Coates. Theory of chromatography. part iv. the influence of incomplete equilibrium on the front boundary of chromatograms and on the effectiveness of separation. *Journal of the Chemical Society (Resumed)*, pages 1315–1321, 1947.
- [82] Paul A. Webley and Jianming He. Fast solution-adaptive finite volume method for PSA/VSA cycle simulation; 1 single step simulation. *Computers and Chemical Engineering*, 23(11-12):1701–1712, 2000. ISSN 00981354. doi: 10.1016/S0098-1354(99)00320-8.
- [83] Richard S Todd, Jianming He, Paul A Webley, Christopher Beh, Simon Wilson, and Matthew A Lloyd. Fast Finite-Volume Method for PSA/VSA Cycle Simulations - Experimental Validation. M:3217–3224, 2001. doi: 10.1021/ie0008070.
- [84] Tan-Ping Chen. Hydrogen Delivery Infrastructure Options Analysis. Technical report, 2008. URL <http://internal-pdf//Tan-PingChen,Nexantetal.-FinalReport.pdf%0Ahttp://49893a80-2ac2-4a8c-bf30-c05466bf5150.jpg>.
- [85] Jim Simnick, Erika Sutherland, Tim Barckholtz, Al Burgunder, Dan Casey, Sara Dillich, Amgad Elgowainy, Jim Merritt, George Parks, Steve Pawel, and Herie Soto. Hydrogen Delivery Technical Team Roadmap. Technical Report June, 2013.
- [86] Jinsong Zhang, Timothy S Fisher, P. Veeraraghavan Ramachandran, Jay P Gore, and Issam Mudawar. A Review of Heat Transfer Issues in Hydrogen Storage Technologies. *Journal of Heat Transfer*, 127(December):1391–1399, 2005. doi: 10.1115/1.2098875.
- [87] G Parks, R Boyd, J Cornish, and R Remick. Hydrogen Station Compression, Storage, and Dispensing Technical Status and Costs: Systems Integration. Technical Report May 2014, 2014. URL <http://www.osti.gov/scitech//servlets/purl/1130621/>.
- [88] Hervé Barthélémy. Hydrogen storage - Industrial perspectives. *International Journal of Hydrogen Energy*, 37(22):17364–17372, 2012. ISSN 03603199. doi: 10.1016/j.ijhydene.2012.04.121.
- [89] SAE International. Surface Vehicle Standard. Technical report, 2014.

- [90] R. Wurster. *Hydrogen safety*. Elsevier Ltd., 1 edition, 2012. ISBN 9781439862322. doi: 10.1201/b13046-17. URL <http://dx.doi.org/10.1016/B978-1-78242-364-5.00009-9>.
- [91] J. W. Sheffield, K. B. Martin, and R. Folkson. Electricity and hydrogen as energy vectors for transportation vehicles. *Alternative Fuels and Advanced Vehicle Technologies for Improved Environmental Performance: Towards Zero Carbon Transportation*, pages 117–137, 2014. doi: 10.1533/9780857097422.1.117.
- [92] Krishna Reddi, Amgad Elgowainy, and Erika Sutherland. Hydrogen refueling station compression and storage optimization with tube-trailer deliveries. *International Journal of Hydrogen Energy*, 39(33):19169–19181, 2014. ISSN 03603199. doi: 10.1016/j.ijhydene.2014.09.099.
- [93] R. Judd and D. Pinchbeck. *Hydrogen admixture to the natural gas grid*. Elsevier Ltd., 1 edition, 2016. ISBN 9781782423645. doi: 10.1016/b978-1-78242-364-5.00008-7. URL <http://dx.doi.org/10.1016/B978-1-78242-364-5.00008-7>.
- [94] D.W. Siderius, V.K. Shen, R.D. Johnson III, and R.D. van Zee. Nist/arpa-e database of novel and emerging adsorbent materials. *National Institute of Standards and Technology: Gaithersburg MD, 20899*. URL <http://adsorbents.nist.gov>. Accessed on 27-04-2020.
- [95] Frank G. Wiessner. Basics and industrial applications of pressure swing adsorption (PSA), the modern way to separate gas. *Gas Separation and Purification*, 2(3): 115–119, 1988. ISSN 09504214. doi: 10.1016/0950-4214(88)80026-4.
- [96] Matt Nathal and Lauren Burke. Equipment sizing. URL https://processdesign.mccormick.northwestern.edu/index.php/Equipment_sizing. Accessed on: 31-08-2020.
- [97] E. Sutherland, A. Elgowainy, and S. Dillich. H2 Delivery Cost Projections – 2013. *DOE Hydrogen and Fuel Cells Program Record*, pages 1–4, 2013.
- [98] EIA. Engineering Economic Analysis Guide: Liquid Fuels Technologies. (December):50, 2015. URL www.eia.gov.
- [99] Core Energy & Resources Pty Limitedcore. Delivered Wholesale Gas Price Outlook 2019-2050. (January), 2019. URL https://www.aemo.com.au/-/media/Files/Gas/National_Planning_and_Forecasting/GS00/2019/CORE-Eastern-Australia-Gas-Price-Projections-Report-16-January-2019.pdf.
- [100] Hiroyasu Furukawa and Omar M. Yaghi. Storage of hydrogen, methane, and carbon dioxide in highly porous covalent organic frameworks for clean energy applications. *Journal of the American Chemical Society*, 131(25):8875–8883, 2009. ISSN 00027863. doi: 10.1021/ja9015765.
- [101] L. Hamon, L. Chenoy, and G. De Weireld. Determination of absolute gas adsorption isotherms: Simple method based on the potential theory for buoyancy effect

- correction of pure gas and gas mixtures adsorption. *Adsorption*, 20(2-3):397–408, 2014. ISSN 09295607. doi: 10.1007/s10450-013-9579-3.
- [102] Bruna Silva, Ioan Solomon, Ana M. Ribeiro, U. Hwang Lee, Young Kyu Hwang, Jong San Chang, José M. Loureiro, and Alírio E. Rodrigues. H₂ purification by pressure swing adsorption using CuBTC. *Separation and Purification Technology*, 118:744–756, 2013. ISSN 13835866. doi: 10.1016/j.seppur.2013.08.024.
- [103] J. Rother and T. Fieback. Multicomponent adsorption measurements on activated carbon, zeolite molecular sieve and metal-organic framework. *Adsorption*, 19(5): 1065–1074, 2013. ISSN 09295607. doi: 10.1007/s10450-013-9527-2.
- [104] E. Dundar, R. Zacharia, R. Chahine, and P. Bénard. Potential theory for prediction of high-pressure gas mixture adsorption on activated carbon and MOFs. *Separation and Purification Technology*, 135(1):229–242, 2014. ISSN 18733794. doi: 10.1016/j.seppur.2014.08.021. URL <http://dx.doi.org/10.1016/j.seppur.2014.08.021>.
- [105] Xiao Feng, Xuesong Ding, and Donglin Jiang. Covalent organic frameworks. *Chemical Society Reviews*, 41(18):6010–6022, 2012. ISSN 14604744. doi: 10.1039/c2cs35157a.
- [106] Andrés A. García Blanco, Andrea F. Vallone, Sophia A. Korili, Antonio Gil, and Karim Sapag. A comparative study of several microporous materials to store methane by adsorption. *Microporous and Mesoporous Materials*, 224:323–331, 2016. ISSN 13871811. doi: 10.1016/j.micromeso.2016.01.002.
- [107] Ambarish R. Kulkarni and David S. Sholl. Screening of Copper Open Metal Site MOFs for Olefin/Paraffin Separations Using DFT-Derived Force Fields. *Journal of Physical Chemistry C*, 120(40):23044–23054, 2016. ISSN 19327455. doi: 10.1021/acs.jpcc.6b07493.
- [108] Ana Martín-Calvo, Elena García-Pérez, Juan Manuel Castillo, and Sofia Calero. Molecular simulations for adsorption and separation of natural gas in IRMOF-1 and Cu-BTC metal-organic frameworks. *Physical Chemistry Chemical Physics*, 10(47):7085–7091, 2008. ISSN 14639076. doi: 10.1039/b807470d.
- [109] A. Luna-Triguero, J. M. Vicent-Luna, P. Gómez-Álvarez, and S. Calero. Olefin/Paraffin Separation in Open Metal Site Cu-BTC Metal-Organic Framework. *Journal of Physical Chemistry C*, 121(5):3126–3132, 2017. ISSN 19327455. doi: 10.1021/acs.jpcc.6b11808.
- [110] Ying Wu, Dai Tang, Ross J. Verploegh, Hongxia Xi, and David S. Sholl. Impacts of Gas Impurities from Pipeline Natural Gas on Methane Storage in Metal-Organic Frameworks during Long-Term Cycling. *Journal of Physical Chemistry C*, 121(29):15735–15745, 2017. ISSN 19327455. doi: 10.1021/acs.jpcc.7b03459.
- [111] Masoud Mofarahi, Mojtaba Sadrameli, and Jafar Towfighi. Characterization of activated carbon by propane and propylene adsorption. *Journal of Chemical and Engineering Data*, 48(5):1256–1261, 2003. ISSN 00219568. doi: 10.1021/je0340553.

- [112] P.L.J. Mayfield and D D Do. Measurement of the Single Component Adsorption Kinetics of Ethane , Butane , and Pentane onto Activated Carbon Using a Differential Adsorption Bed. pages 1262–1270, 1991.
- [113] T. Asadi, M. R. Ehsani, A. M. Ribeiro, J. M. Loureiro, and A. E. Rodrigues. CO₂/CH₄ Separation by Adsorption using Nanoporous Metal organic Framework Copper-Benzene-1,3,5-tricarboxylate Tablet. *Chemical Engineering and Technology*, 36(7):1231–1239, 2013. ISSN 09307516. doi: 10.1002/ceat.201300046.
- [114] Marie Georges Olivier and Roger Jadot. Adsorption of light hydrocarbons and carbon dioxide on silica gel. *Journal of Chemical and Engineering Data*, 42(2): 230–233, 1997. ISSN 00219568. doi: 10.1021/je960200j.
- [115] Dongmin Shen, Martin Bülow, Sudhakar R. Jale, Frank R. Fitch, and Adeola F. Ojo. Thermodynamics of nitrogen and oxygen sorption on zeolites LiLSX and CaA. *Microporous and Mesoporous Materials*, 48(1-3):211–217, 2001. ISSN 13871811. doi: 10.1016/S1387-1811(01)00355-9.
- [116] N. A. Sokolova and V. B. Kazanskii. Diffusion of ethane-hydrogen mixtures in LiLSX and CaA zeolites studied by diffuse reflectance IR spectroscopy. *Kinetics and Catalysis*, 46(6):879–883, 2005. ISSN 00231584. doi: 10.1007/s10975-005-0151-3.
- [117] Shivaji Sircar and Alan L. Myers. Gas Separation by Zeolites. In *Handbook of Zeolite Science and Technology*, chapter 22. 2003. doi: 10.1201/9780203911167.ch22.
- [118] Caixia Tian, Qiang Fu, Zhaoyang Ding, Zhiyang Han, and Donghui Zhang. Experiment and simulation study of a dual-reflux pressure swing adsorption process for separating N₂/O₂. *Separation and Purification Technology*, 189:54–65, 2017. ISSN 18733794. doi: 10.1016/j.seppur.2017.06.041. URL <http://dx.doi.org/10.1016/j.seppur.2017.06.041>.
- [119] Nabil Tlili, Georges Grévilot, and Cécile Vallières. Carbon dioxide capture and recovery by means of TSA and/or VSA. *International Journal of Greenhouse Gas Control*, 3(5):519–527, 2009. ISSN 17505836. doi: 10.1016/j.ijggc.2009.04.005.
- [120] Franklin E. Epietang, Jianbo Li, Yingshu Liu, and Ralph T. Yang. Low-pressure performance evaluation of CO₂, H₂O and CH₄ on Li-LSX as a superior adsorbent for air prepurification. *Chemical Engineering Science*, 147:100–108, 2016. ISSN 00092509. doi: 10.1016/j.ces.2016.03.022.
- [121] Jason Donev, Kailyn Stenhouse, Jordan Hania, and Bethel Afework. Energy education - mercaptan. URL <https://energyeducation.ca/encyclopedia/Mercaptan>. Accessed on: 30-06-2020.
- [122] Monika Golebiowska, Michael Roth, Lucyna Firlej, Bogdan Kuchta, and Carlos Wexler. The reversibility of the adsorption of methane-methyl mercaptan mixtures in nanoporous carbon. *Carbon*, 50(1):225–234, 2012. ISSN 00086223. doi: 10.1016/j.carbon.2011.08.039. URL <http://dx.doi.org/10.1016/j.carbon.2011.08.039>.

- [123] Dae Jung Kim, Hyung Ik Lee, Jae Eui Yie, Seung Jai Kim, and Ji Man Kim. Ordered mesoporous carbons: Implication of surface chemistry, pore structure and adsorption of methyl mercaptan. *Carbon*, 43(9):1868–1873, 2005. ISSN 00086223. doi: 10.1016/j.carbon.2005.02.035.
- [124] Svetlana Bashkova, Andrey Bagreev, and Teresa J. Bandosz. Adsorption/oxidation of CH₃SH on activated carbons containing nitrogen. *Langmuir*, 19(15):6115–6121, 2003. ISSN 07437463. doi: 10.1021/la0300030.
- [125] Song Woo Lee, Wan Mohd Ashri Wan Daud, and Min Gyu Lee. Adsorption characteristics of methyl mercaptan, dimethyl disulfide, and trimethylamine on coconut-based activated carbons modified with acid and base. *Journal of Industrial and Engineering Chemistry*, 16(6):973–977, 2010. ISSN 1226086X. doi: 10.1016/j.jiec.2010.04.002. URL <http://dx.doi.org/10.1016/j.jiec.2010.04.002>.
- [126] Bastian Steuten, Christoph Pasel, Michael Luckas, and Dieter Bathen. Trace level adsorption of toxic sulfur compounds, carbon dioxide, and water from methane. *Journal of Chemical and Engineering Data*, 58(9):2465–2473, 2013. ISSN 00219568. doi: 10.1021/je400298r.
- [127] Volkmar Chowanietz, Christoph Pasel, Michael Luckas, and Dieter Bathen. Temperature Dependent Adsorption of Sulfur Components, Water, and Carbon Dioxide on a Silica-Alumina Gel Used in Natural Gas Processing. *Journal of Chemical and Engineering Data*, 61(9):3208–3216, 2016. ISSN 15205134. doi: 10.1021/acs.jced.6b00301.
- [128] Frederik Berg, Christoph Pasel, Tobias Eckardt, and Dieter Bathen. Temperature Swing Adsorption in Natural Gas Processing: A Concise Overview. *ChemBioEng Reviews*, 6(3):59–71, 2019. ISSN 21969744. doi: 10.1002/cben.201900005.
- [129] S. Faramawy, T. Zaki, and A. A.E. Sakr. Natural gas origin, composition, and processing: A review. *Journal of Natural Gas Science and Engineering*, 34:34–54, 2016. ISSN 18755100. doi: 10.1016/j.jngse.2016.06.030.
- [130] D. D. Do and H. D. Do. A model for water adsorption in activated carbon. *Carbon*, 38(6):767–773, 1999. ISSN 00086223. doi: 10.1016/j.carbon.2009.01.039.
- [131] Dong Xu, Penny Xiao, Jun Zhang, Gang Li, Gongkui Xiao, Paul A. Webley, and Yuchun Zhai. Effects of water vapour on CO₂ capture with vacuum swing adsorption using activated carbon. *Chemical Engineering Journal*, 230:64–72, 2013. ISSN 13858947. doi: 10.1016/j.cej.2013.06.080. URL <http://dx.doi.org/10.1016/j.cej.2013.06.080>.
- [132] Raymond Hadden. Hydrogen production. In *Hydrocarbon Engineering*, volume 8, pages 71–72. 2003. ISBN 9780128130254. doi: 10.1002/9781119707875.ch12.
- [133] H₂ fueling technologies. URL http://www.linde-gas.com/en/processes/hydrogen_energy_h2/h2_one_stop_shop/h2_fuelling_technologies/index.html. Accessed on: 13-11-2020.

- [134] Tfa project group hydrogen consultants. URL <https://www.tfa.com.au/projects/renewable-fuels/hydrogen-consultants/>. Accessed on: 12-11-2020.
- [135] Michael Stinn and Jonathan Vance. Selecting valves for pressure swing adsorption, 2018. URL www.eptq.com.
- [136] Water resistant silica alumina gel. URL https://www.alibaba.com/product-detail/Water-Resistant-Silica-Alumina-gel-SILICA_1600053244973.html?spm=a2700.galleryofferlist.0.0.73854221IUUQEQ. Accessed on: 29-09-2020.
- [137] Water filter treatment chemicals coconut activated carbon 8x30 mesh. URL https://www.alibaba.com/product-detail/Water-Filter-Treatment-Chemicals-Coconut-Activated_62572500177.html?spm=a2700.galleryofferlist.0.0.55da5a4avp9N03&s=p. Accessed on: 29-09-2020.
- [138] Li-lsx molecular sieve. URL https://www.alibaba.com/product-detail/0-4-0-8mm-Oxygen-Concentrator_1600072729852.html?spm=a2700.galleryofferlist.normal_offer.d_title.470799a2bBwLRT. Accessed on: 29-09-2020.
- [139] Anne Qi. Quotation Sheet of Hydrogen Gas Tank, 2020.
- [140] Quotation Pressure Vessel, 2020.
- [141] Nickolas Fisher. Quotation butterfly valves, 2020.
- [142] Average chemical plant operator hourly pay in australia. URL https://www.payscale.com/research/AU/Job=Chemical_Plant_Operator/Hourly_Rate. Accessed on: 24-10-2020.
- [143] V. Goetz, O. Pupier, and A. Guillot. Carbon dioxide-methane mixture adsorption on activated carbon. *Adsorption*, 12(1):55–63, 2006. ISSN 09295607. doi: 10.1007/s10450-006-0138-z.
- [144] Simone Cavenati, Carlos A. Grande, and Alírio E. Rodrigues. Adsorption Equilibrium of Methane, Carbon Dioxide, and Nitrogen on Zeolite 13X at High Pressures. *Journal of Chemical and Engineering Data*, 49(4):1095–1101, 2004. ISSN 00219568. doi: 10.1021/je0498917.
- [145] Zhijie Chen, Karim Adil, Lukasz J. Weseliński, Youssef Belmabkhout, and Mohamed Eddaoudi. A supermolecular building layer approach for gas separation and storage applications: The eea and rtl MOF platforms for CO₂ capture and hydrocarbon separation. *Journal of Materials Chemistry A*, 3(12):6276–6281, 2015. ISSN 20507496. doi: 10.1039/c4ta07115h.
- [146] Yabing He, Zhangjing Zhang, Shengchang Xiang, Hui Wu, Frank R. Fronczek, Wei Zhou, Rajamani Krishna, Michael O’Keeffe, and Banglin Chen. High separation capacity and selectivity of C₂ hydrocarbons over methane within a microporous metal-organic framework at room temperature. *Chemistry - A European Journal*, 18(7):1901–1904, 2012. ISSN 09476539. doi: 10.1002/chem.201103927.

- [147] Xiaohu Dong, Huiqing Liu, Wei Guo, Jirui Hou, Zhangxin Chen, and Keliu Wu. Study of the confined behavior of hydrocarbons in organic nanopores by the potential theory. *Fluid Phase Equilibria*, 429:214–226, 2016. ISSN 03783812. doi: 10.1016/j.fluid.2016.09.008. URL <http://dx.doi.org/10.1016/j.fluid.2016.09.008>.
- [148] Flor R Siperstein and Alan L Myers. Mixed-Gas Adsorption. 47(5):1141–1159, 2001.
- [149] Masoud Mofarahi and Seyyed Milad Salehi. Pure and binary adsorption isotherms of ethylene and ethane on zeolite 5A. *Adsorption*, 19(1):101–110, 2013. ISSN 09295607. doi: 10.1007/s10450-012-9423-1.
- [150] Swapnil Divekar, Anshu Nanoti, Soumen Dasgupta, Aarti, Rekha Chauhan, Pushpa Gupta, Madhukar O. Garg, Surendra P. Singh, and Indra Mani Mishra. Adsorption equilibria of propylene and propane on zeolites and prediction of their binary adsorption with the ideal adsorbed solution theory. *Journal of Chemical and Engineering Data*, 61(7):2629–2637, 2016. ISSN 15205134. doi: 10.1021/acs.jced.6b00294.